DEVELOPMENT OF *IN VITRO* LIVER CULTURE TECHNIQUES TO INTEGRATE A PHYSIOLOGICALLY RELEVANT MICROENVIROMENT RECAPITULATING LIVER LOBULE ZONATION

Thomas Joseph DiProspero

A dissertation submitted to the faculty at the University of North Carolina at Chapel Hill in partial fulfillment of the requirements for the degree of Doctor of Philosophy in the Department of Chemistry in the School of Arts and Sciences.

Chapel Hill
2021

Approved by:

Matthew Lockett

Leslie Hicks

Frank Leibfarth

Jeffrey Dick

Stephen Ferguson

ABSTRACT

Thomas Joseph DiProspero: DEVELOPMENT OF *IN VITRO* LIVER CULTURE TECHNIQUES TO INTEGRATE A PHYSIOLOGICAL RELEVANT MICROENVIROMENT RECAPITULATING LIVER LOBULE ZONATION
(Under the direction of Matthew Ryen Lockett)

During drug-discovery, cell monolayers fail to accurately predict drug-induced liver injury– a common reason for discontinuation during clinical trials. One reason is that monolayer cultures lack many aspects of the tissue microenvironment. The liver is composed of subunits known as lobules. In the lobule, a sinusoid connects a portal triad and central vein and is surrounded by hepatocytes to maximize nutrient exchange. A unidirectional flow leads to extracellular gradients of oxygen, nutrients, hormones, and morphogens. These gradients in the lobule impact hepatocyte function through the differential expression of hepatocytic pathways in the periportal (PP) and perivenous (PV) regions.

To improve in vitro hepatocyte cultures, a platform that incorporates structural and microenvironmental factors is needed to recapitulate the liver. Factors include: coculturing liver-specific cells; inclusion of liver-specific extracellular gradients, specifically nutrients and morphogens; incorporating dynamic nutrient flow and distribution; and inclusion of appropriate three-dimensional hepatocyte organization, and a relevant extracellular matrix (ECM). In this work, I integrated physiological aspects– oxygen, morphogens, extracellular matrix stiffness, and a 3D paper scaffold culture– into in vitro cultures of different cell types with increasing hepatocyte-like functions: HepG2, HepaRG, and primary human hepatocytes (PHHs). I

evaluated cell health, liver-specific function, metabolic enzyme activity, and transcriptional regulation as each physiological condition was introduced individually, and in concert.

This work displayed that oxygen improves in vitro zonal patterning of SULT and UGT transcript, but oxygen alone could not achieve the drug metabolizing enzyme's zonal distribution. The inclusion of Wnt alone increases CYP, UGT and SULT activity, as compared to a control, while the magnitude of enzymatic activity increase is modulated by oxygen. Overall, the HepaRG cell's basal and inducible drug metabolizing enzyme activity is similar across a wide range of ECM stiffness suggesting that the HepaRG cells are adaptable to various ECMs, unlike PHHs. Lastly, direct comparisons of monolayers and paper-based cultured in PP and PV microenvironments, indicated zonation-like trends between the PP and PV conditions. The paper-based PV conditioned cells exhibited the highest drug metabolizing enzyme activity. This work developed a more representative in vitro liver models by incorporating tissue-specific features.

ACKNOWLEDGEMENTS

My doctoral work at UNC has been challenging but made easier with the support and guidance of many people. I want to start off by acknowledging and extending my deepest thanks to my advisor, Dr. Matthew Lockett. Your unwavering support in me to chase new ideas and your encouragement when science got hard was always appreciated. Matt your mentorship and ability to see my potential developed me into a splendid scientist and thinker. Thank you.

To my classmates of the incoming class of 2016 in the analytical division, thanks for the camaraderie throughout this experience. We faced the challenges together and everyone's mutual support is remembered fondly.

To the many members of the Lockett lab, thank you for sharing your knowledge and experience. I'm grateful for the various scientific discussions and collaborations to push this work forward. Each of you have shared your time and talents, lending your support, and asking for mine. I am grateful for each of you. I'm excited to see each of your successes.

And to my friends, new and old. Each of you provided unwavering support and believed in me every step of the way. I'm so glad I was able share the challenges and celebrations of graduate school with you and felt your support all along the way. A special thanks to the two lifelong friends I've met while in Chapel Hill- who would have thought that the bonds we made in the first week would transcend a lifetime. Five years later Jeff Ehrhardt and Josh Welfare, thank you both for being a part of my life; I'm happy to call you each family. I cannot wait for the many more game nights, beach trips, and last-minute calls to adventure as we grow.

Lastly, my family has been my inspiration and my drive. I love each of you so much no matter the distance. To Aunt Elaine, you've cheered me on for so long, a simple thank you isn't enough; thank you for the years of encouragement. To Nick, for keeping me grounded and believing in me every step of the way. To my Father, for being a fountain of advice and insight; for all the love and reminding me to keep my feet on the ground. To my Mom, thanks for being my inspiration, for your unconditional support, and for the desire to see me succeed. Thanks for answering the phone every time I called.

TABLE OF CONTENTS

LIST OF TABLES

LIST OF FIGURES

LIST OF ABBREVIATIONS

ΔΔCt	Delta delta cycle threshold
2D	Two-dimensional
3-MC	3-methylcholanthrene
3D	Three-dimensional
3PL	3-Parameter logistics fit
4PL	4-Parameter logistics fit
ABC	ATP-binding cassette
ACN	Acetonitrile
Acp	Adenomatous polyposis coli
ACTB	β-Actin
ADMET	Adsorption, distribution, metabolism, excretion, and toxicity
AFBO	Aflatoxin B1-8,9-epoxide
AhR	Aryl hydrocarbon receptor
APAP	Acetaminophen
ARNT	Aryl hydrocarbon receptor nuclear translocator
ATCC	American type cancer collection
ATP	Adenosine triphosphate
ATP	Adenosine triphosphate
BEH	Ethylene bridged hybrid
BSEP	Bile salt export pump
CaR	Constitutive androstane receptor
CCD	Charge-coupled device

CCP	Commercial collagen coated plate
cDNA	Complementary deoxyribonucleic acid
CITCO	O-[(3,4-dichlorophenyl)methyl]oxime 6-(4-chlorophenyl)-imidazo[2,1-b]thiazole-5-carboxaldehyde
CK-19	Cytokeratin-19
CO2	Carbon dioxide
CTG	CellTiter-Glo 2.0
CYP	Cytochrome P450
DAPI	4’,6-diamidino-2-phenylindole
DC	Direct current
DMEM	Dulbecco’s modified eagle medium
DMSO	Dimethyl sulfoxide
DNA	Deoxyribonucleic acid
DRAQ5	1, 5-bis{[2-(di-methylamino)ethyl]amino}-4, 8-dihydroxyanthracene-9, 10-dione
EC_{50}	Half maximal effective concentration, potency
ECM	Extracellular matrix
EDC	1-ethyl-3-(3-dimethylaminopropyl)carbodiimide hydrochloride
EROD	7-ethoxyresorufin-O-deethylase
Ex/Em	Excitation/emission
FBS	Fetal bovine serum
GLI	Glioma-associated oncogene
GLUT	Glucose transporters
GSH	Glutathione
GST	Glutathione S-transferases

HCM	Hepatocyte culture medium
hEGF	Guman epidermal growth factor
HEPES	4-(2-hydroxyethyl)-1-piperazineethanesulfonic acid
HESI	Geated electrospray ionization
Hh	Hedgehog
HIF	Hypoxia inducible factor
HIF-1α	Hypoxia inducible factor – 1 alpha
HNF4	Hepatocyte nuclear factor 4α
HPLC	High-performance liquid chromatography
IGFBP-1	Insulin-like growth factor- binding protein 1
IL-1β	Interleukins-1β
IL-6	Interleukin-6
K	Thousand
LC-MS/MS	Liquid chromatography- tandem mass spectrometry
LEF	Lymphoid enhancer factor
LGR	Leucine-rich repeat-containing g-protein coupled receptor
MES	2-(N-morpholino) ethanesulfonic acid
mg/mL	Milligram per milliliter
Midz	Midizolam
Min	Minute
miRNA	microRNA
mL	Milliliter
mL/min	Milliliter per minute

mm	Millimeter
mM	Millimolar
mmHg	Millimeters of mercury
MRP	Multidrug resistance-associated proteins
MRP2	Multidrug resistance-associated protein 2
MTS	3-(4,5-Dimethylthiazol-2-yl)-5-(3-carboxymethoxyphenyl)-2-(4-sulfophenyl)-2H-tetrazolium
N	Biological replicate
N	Neutralized collagen
n	Technical replicate
N/m	Newton per meter
NaOH	Sodium hydroxide
NAPQI	N-acetyl-p-benzoquinone imine
NAT	N-acetyltransferase
NHS	N-Hydroxysuccinimide
nM	Nanomolar
N/m	Newton per meter
nm/sec	Nanometer per second
Nx	Neutralized, Crosslinked Collagen
O_2	Oxygen
OAT	Organic anion transporters
OATP	Organic-anion-transporting polypeptides
°C	Degrees celcius
OCT	Organic cation transporters

P-gp	P-glycoprotein
Pa	Pascal
PBS	Phosphate-buffered saline
PDMS	Polydimethylsiloxane
PEPCK	Phosphoenolpyruvate carboxykinase
pH	Log scale of acidity
PHHs	Primary human hepatocytes
PI	Propidium iodide
PP	Periportal
psi	Pounds per square inch
PV	Perivenous
PVA	Polyvinyl alcohol
PxR	Pregnane X receptor
qPCR	Quantitative polymerase chain reaction
R^2	R-Squared
RNA	Ribonucleic acid
ROS	Reactive oxygen species
RT	Reverse transcription
RT-qPCR	Reverse transcription quantitative polymerase chain reaction
SEM	Standard error of the mean
SLC	Solute carrier transporter
Std	Standard culture condition
SULT	Sulfotransferase

TCDD	2,3,7,8-tetrachlorodibenzo-p-dioxin
TCF	T-cell factor
Test	Testosterone
TNF-a	Tumor necrosis factor-α
UGT	UDP-glucuronosyltransferase
UPLC	Ultra performance liquid chromatography
UV	Ultraviolet
V	Voltage
v/v	Volume per volume
WRN	Wnt, Rspondin, noggin
X	Bulk crosslinked collagen
xg	Times gravity
µg	Microgram
µL	Microliter
µm	Micrometer

CHAPTER 1: INTRODUCTION

1.1 The liver

The liver serves a multitude of functions in the body, maintaining homeostasis by regulating glucose and energy production, breaking down proteins and regulating amino acid stores, and detoxifying the blood of ammonia and xenobiotics.[1] Furthermore, the liver is responsible for synthesizing and metabolizing various bioactive molecules and proteins, including lipoproteins, albumin, bile acids, and various hormones. The liver removes xenobiotics (toxins such as drugs, environmental pollutants, or herbal constituents) via metabolism. Metabolism accomplishes two main functions: (1) the neutralization of a xenobiotic, by reducing the target molecule's biological activity and (2) increasing the overall hydrophilicity of the molecule to facilitate excretion resulting in reduction of the xenobiotic's systemic concentration. [2] Xenobiotic metabolism is broken down into two phases. In Phase I metabolism, a family of enzymes known as cytochrome P450s (CYPs) oxidize the target molecule through the addition of an oxygen-containing functional group. This functional group increases the molecules overall reactivity and can be a location for subsequent conjugation reactions.[3] In Phase II metabolism, a wide range of enzyme families conjugate hydrophilic groups (e.g., glucuronides, sulfates, sulfamates) onto the target molecule. These hydrophilic groups aid in the excretion of the metabolized xenobiotic via the urinary system.[3]

1.1.1 The liver lobule structure

Research into liver structure and function has been an area of interest for hundreds of years, pioneered by Wepfer and Malpighi who introduced the concept of lobule subunits within

mammalian liver in 1664 and 1666, rrespectively.[4] The liver is composed of hexagonal structural subunits, known as lobules. Each corner of the lobule contains a set of three vessels, known as the portal triad, which consists of a bile duct, a hepatic artery, and a portal vein (**Figure 1.1a**). The bile duct collects bile produced by the liver and shuttles it to the gallbladder. The hepatic artery supplies oxygen-rich blood. The portal vein supplies nutrient-, hormone-, and xenobiotic-rich blood from the gastrointestinal track, spleen, and pancreas. The portal triad is a unique structure of the body, receiving blood from both a hepatic artery and portal vein. This mixing reduces the overall oxygen concentration delivered to the cells contained in the lobules. The pooled blood from both the hepatic artery and portal vein travel across the lobule through a sinusoidal cavity to a central vein. The point of entry is referred to as the periportal (PP) region. Once the blood reaches the center of the lobule, it is collected into the central vein and then redistributed throughout the body. The area around the central vein is known as perivenous (PV) region.[5]

The sinusoid is lined with endothelial cells, which form a fenestrated capillary structure that allows exchange with neighboring tissues (**Figure 1.2**). This leaky barrier retains red blood cells in the sinusoid, but allow nutrients and waste to diffuse from the sinusoid to the space of Disse, a protein-rich region between the endothelial cells and hepatocytes; the space of Disse helps buffer the hepatocytes from shear stress and turbulent blood flow as well as provides the hepatocytes a region of diffusion-dominated nutrient and waste exchange.[5–7] The hepatocytes are organized into hepatic cords: sheets of cells (one to two cell lengths thick) that branch radially from the central vein.

1.1.2 Cells of the liver

The organ-specific cells that compose the liver are classified as either parenchymal or non-parenchymal. Hepatocytes are the parenchymal cells of the liver, which are responsible for carrying out the main functions of the organ. Non-parenchymal cells, including stellate cells, Kupffer cells, and endothelial cells, maintain liver health and ensure the hepatocytes function properly.

Hepatocytes comprise approximately 80% of the liver mass, as they perform most of the liver-specific function. Hepatocytes are highly polarized, containing multiple axes of polarization, and are highly metabolically active, evident by their elevated oxygen consumption rate.[8] The basal side of hepatocytes face the sinusoid, and have microvilli to increase the surface area available for uptake and excretion of nutrients and waste into the blood. The apical sides of the hepatocytes face the bile canaculi found between two adjacent hepatocytes. Therefore, hepatocyte polarity is more complex than simple cell polarity (apical and basal sides on opposite ends of the cell) because hepatocytes have bile canaculi and sinusoids on multiple faces (**Figure 1.3**).[9,10] This complex polarity facilitates the excretion of synthesized bile and some waste products into these apical facing canaculi while they secrete other waste products back in to the blood on the basal face. The average size of the hepatocytes increases from 7 μm near the periportal region to greater than 40 μm at the perivenous region. Furthermore, growth of new hepatocytes is hypothesized to originate from a stem cell-like cells located in the periportal region of the sinusoid As the cells grow, they begin to differentiate into bile duct cells (cholangiocytes) if they move towards the portal triad or differentiate into hepatocytes if they move towards the central vein.[11]

Nonparenchymal cells support the function of hepatocytes and functions of the liver. Stellate cells reside in the space of Disse between the endothelial cells and hepatocytes. Stellate cells store and regulate lipids and vitamin A. They also maintain and regulate the extracellular

matrix (ECM) in the space of Disse via production of collagen type I and III, sinusoidal blood flow, and hepatic tissue repair. Kupffer cells are phagocytes that reside in the sinusoid, removing aging red blood cells, microbes, and endotoxins from the blood.[5] Kupffer cells are responsible for secreting and regulating signaling molecules and mediators such as cytokines, oxygen radicals and proteases in response to liver injury, regeneration, or immune system defense. These secreted molecules signal to cells within the liver and from other parts of the body.[8]

1.2 Hepatocyte metabolic pathways

Xenobiotic metabolism is an important area of focus, as the rate of production and the metabolic products themselves determine pharmacokinetic properties and potential toxicity of a drug. Metabolism occurs in three phases. Phase I metabolism is mediated by a superfamily of enzymes known as cytochrome P450s (CYPs). In humans, there are 18 families and 44 subfamilies of CYPs.[12] These enzymes catalyze the oxidative transformation of drugs and other lipophilic compounds, increasing their water solubility through the addition of oxygen-containing functional groups. A subset of CYPs are responsible for the majority of drug metabolism, with five isoforms (CYP1A2, CYP2C9, CYP2D6, CYP3A4, and CYP2B6) metabolizing about 60% of all drugs on the market.[13] The CYP1A family catalyzes hydroxylation of (poly)aromatic hydrocarbons and heterocyclic amines. The CYP2 family targets neutral, weakly acidic, or weakly basic compounds with one to two hydrogen bond acceptors. Isozymes within the CYP2 family are more reactive to specific chemical structures, for example CYP2C9 metabolizes weakly acidic molecules with a hydrogen bond acceptor. Lastly the CYP3 family targets large, lipophilic molecules; CYP3A4 catalyzes about 50% of all clinically relevant drugs.[12]

The proposed mechanism of action of each of the CYPs in the superfamily is similar, each relying on a heme-containing active site that mediates the transfer of elemental oxygen to an organic molecule. A nine-step reaction mechanism has been proposed and summarized by Peter Guengerich (**Figure 1.4**). The first step of the catalytic cycle is the association of the substrate with the iron (III) core- the substrate remains associated with the active site while the cycle continues. An electron is transferred to the iron core by NADPH-P450 reductase resulting in iron (II). Then, elemental oxygen binds to the iron (II) core and is reduced again by NADPH-P450 reductase forming a negatively charged iron (II)- peroxo complex. The negatively charged oxygen is protonated forming an iron (II)- OOH complex, followed by dehydration, forming the reactive iron (III) oxide. Iron (III) oxide extracts a proton from the substrate, forming iron (III) hydroxide and a free-radical substrate. The catalytic reaction finishes when the radical substrate extracts the hydroxide from the iron (III), resulting in an oxidized product and regenerating the iron (III) core.[14–16]

Drugs that undergo Phase I metabolism are primed for Phase II metabolism, which further increases the hydrophilicity of the target for easy excretion and biological inactivation. Phase II metabolism is mediated by transferases, namely the UDP-glucuronosyltransferase (UGT), sulfotransferase (SULT), N-acetyltransferase (NAT), and glutathione S-transferases (GST) enzyme families. These enzyme families conjugate a glucuronide, a sulfate, an acetyl, or a glutathione group to the target molecule, respectively. These conjugation reactions target alcohol groups, which are sometimes added by Phase I metabolism.[3] The UGT and SULT families are the largest contributors to drug metabolism. UGTs catalyze the conjugation of a glucuronide via nucleophilic substitution on an -O, -S, -N or -C with a lone electron pair. SULTs catalyze the transfer of a sulfate group via 3'-phosphoadenosine 5'-phosphosulphate acting as a donor for a sulfonate group to be accepted by the target.[3]

Phase III metabolism involves various membrane transport proteins, which help shuttle drugs into and metabolites out of the hepatocyte. The phospholipid bilayer is semipermeable, allowing the cell to select what comes in and out (e.g., only small, nonpolar molecules can pass through the membrane without assistance). For other molecules, transmembrane transport proteins are needed to facilitate transport across the phospholipid bilayer. For drug and metabolite transport there are two main protein families: ATP-binding cassette (ABC), and solute carrier (SLC) transporters.[17] ABC transporters mediate efflux of drugs or metabolites into the blood or bile- the binding and hydrolysis of ATP drives the ABC transporters expelling the drug or metabolite from the hepatocyte.[18] Some notable ABC transporters are multidrug resistance-associated proteins (MRPs), P-glycoprotein (P-gp),and bile salt export pump (BSEP). SLC transporters can be uptake or bidirectional transporters where the transport is mediated by various energy coupling mechanisms such as secondary active transport (symporter and antiporter) and facilitative transport by taking advantage of electrochemical gradients.[19] Notable SLC transporters are glucose transporters (GLUT), organic cation transporters (OCT), and organic anion transporters (OAT).

In general metabolism of a drug or xenobiotic follows the path of Phase I to Phase II and finally Phase III, however there are exceptions depending on the molecule's chemical structure and affinity for a particular enzyme.

1.3 Liver gradients and zonation

Within the liver lobule, various extracellular gradients have been measured. Some gradients result from cellular consumption outpacing replenishment (e.g., oxygen and glucose gradients). Nutrient- and oxygen-rich blood is introduced to the lobule at the portal triad, with the highest concentration of oxygen and glucose residing in the periportal region (**Figure 1.1b)**. The

hepatocytes closer to the central vein, the perivenous region of the lobule, have less access to oxygen and glucose. Oxygen gradients have been measured using an oxygen electrode. The blood oxygen partial pressure decreases from 65-60 mmHg O_2 (11-8% O_2) in the periportal region to 35-30 mmHg O_2 (5-3% O_2) in the perivenous region.[20–23] For glucose, the exact concentration fluctuates due to feeding and fasting cycles, but in general the periportal region has higher concentrations than the perivenous region.[1]

Other gradients arise from the non-parenchymal cells, which secrete morphogens and signaling molecules. One such morphogen is Wnt. Wnt is secreted by venous endothelial cells in the perivenous region, which binds to cell-membrane receptors triggering a signal cascade. During this cascade, Wnt binds membrane receptors allowing β-catenin to translocate to the nucleus and activate nuclear factors in the T cell factor (TCF) and lymphoid enhancer factor (LEF) families. Wnt triggered β-catenin/TCF binding facilitates the expression of characteristic periportal genes and proteins such as glutamine synthase (a key enzyme in ammonia detoxification), CYP2C family, CYP2E1 and CYP1A2. Furthermore, the overactivation of the Wnt pathway, via adenomatous polyposis coli (Acp) gene deletion, leads to perivenous phenotypes throughout the lobule.[24–26] Another morphogen of interest is Hedgehog (Hh), which promotes proliferation and differentiation of stem cells. The Hh ligands are secreted by periportal endothelial cells, bile duct epithelial cells and stellate cells, resulting in high concentrations of Hh in the periportal region of the lobule.[26,27] Hh binding to surface membrane receptors also triggers a cascade event which allows for glioma-associated oncogene (GLI) transcription factors to be activated.[28] Hh activation/GLI transcription factors have been shown to regulate the expression of insulin-like growth factors and lipid associated factors.[29]

The changing microenvironment across the liver lobule impacts hepatocyte function, resulting in differential expression of various hepatocytic pathways known as liver zonation. The specific gradients that are theorized to account for zonation are morphogens (Wnt, Hh), hormones or growth factors, oxygen, nutrients, and cytokines.[21] Liver zonation is broken up into three zones. Zone 1 is the region around the portal triad (periportal region); zone 3 is the region round the central vein (perivenous region); and zone 2 is the intermediate zone between the periportal and perivenous regions. Unique zone 1 and zone 3 characteristics were identified by measuring the expression of key enzymes within various pathways.[21] Some key pathways that are predominant in zone 1 (periportal region) are oxygen uptake, glucose delivery and gluconeogenesis from lactate and amino acids, fatty acid oxidation, and sulfation of Phase II metabolism. Within zone 3 (perivenous region), glucose uptake and glycolysis, lipogenesis, glucuronidation of Phase II metabolism and the CYPs of Phase I metabolism are some of the active pathways. Two other pathways, urea and bile acid synthesis are found across all three zones.[21]

One theory of the formation of liver zonation is "post-differentiation patterning," well explained by Gebhardt and colleagues. The post-differentiation patterning describes the various gradients in a hierarchical system. On the lowest level, morphogens such as Wnt and Hh initiate the modulation of the hepatocytes at the periportal and perivenous region of the sinusoid to a discrete state. The next level in the hierarchy (nutrients, hormones, and oxygen gradients) act upon the discrete-state hepatocytes by further modulating and fine-tuning gene expression. The hierarchical stacking of gradients could result in different expression levels of the same gene depending on the specific combination of a level 1 and level 2 gradient. The overlapping gradients results in highly dynamic gene expression patterns across the sinusoid; however, it is unclear if the hepatocytes respond to every gradient in concert or if there are a handful of predominant factors that lead to discrete states.[25]

1.4 The structure-function relationship of the liver

One approach when developing an in vitro model of an organ or organ-on-chip device is to determine structure-function relationships by incorporating different aspects of the tissue architecture and extracellular environment to determine which conditions maximize the desired organ function. In the liver lobule, endothelial cells surrounding the sinusoid maximize diffusion of nutrients and waste to the hepatocytes.[4] This layer of endothelial cells minimizes the shear stresses associated with moving fluids. Also, parenchymal and nonparenchymal cellular organization correspond with extracellular gradients present across the lobule, each of which will impact hepatocyte function.[11,30] Evaluating our current knowledge of the liver, liver lobule, and metabolic zonation, there are four factors of the liver that need to be incorporated into in vitro cultures and experimental set ups to recapitulate the liver: coculturing various liver specific cells alongside hepatocytes; inclusion of liver specific gradients, both nutrient and morphogens; the incorporation of a dynamic culture through flow and diffusion; and inclusion of appropriate three-dimensional (3D) organization of hepatocytes within the lobule.

1.4.1 Inclusion of extracellular matrices in in vitro models

Monolayer cultures lack many aspects of the tissue microenvironment, which has profound effects on cellular function; specifically, cell-extracellular matrix interactions, cell polarization, and more physiological cell morphology. Placing PHHs in extracellular-rich environments such as a collagen sandwich maintains their polarization and metabolic function,[31,32] where monolayers on culture-compatible plasticware readily depolarize[33,34] and lose liver-specific function within days of plating.[35,36] Similar increases in functionality are observed when HepG2 cells, an immortalized hepatocarcinoma cell line, are cultured as spheroids. These multicellular aggregates have increased

expression of Phase I and II metabolic enzymes when compared to monolayers.[37–39] The spheroids also reacquire functions that are lost in monolayer cultures, including glycogen storage and the transport of bile salts. The analogous recovery of liver specific function in a 3D environment between PHHs and HepG2 cells supports the idea that HepG2s can be an attractive surrogate for PHHs during rapid culture-device prototyping and high throughput screening. The in vivo hepatocyte extracellular matrix (ECM) is made up of proteins and proteoglycans. Protein composition within the ECM is a mixture of collagens (type I, II, IV, and V) followed by glycoproteins such as fibronectin and laminin, and proteoglycans (heparin sulfate and chondroitin sulfate).[40] LeCluyse and colleagues cultured rat hepatocytes between collagen type I slabs and concluded that the collagen type I ECM promoted extensive bile canaliculi networks, morphology, and function similar to in vivo hepatocytes.[41]

1.4.2 Inclusion of non-parenchymal cells in in vitro models

One part of the post-differentiation patterning theory to liver zonation is that the source of various morphogens is the nonparenchymal cells found within the liver sinusoid. This type of cell-cell interaction is known as paracrine signaling in which secreted molecules from one cell modulate signaling, activity, or differentiation of nearby cells. These signaling molecule-induced changes typically initiate when the extracellular concentration reaches a particular threshold, thus allowing signaling to be localized by a concentration-dependent output. For example, the source of the hedgehog is postulated to be from endothelial cells in the portal triad; as the concentration of hedgehog passes a critical threshold, the hepatocytes in the periportal region begin to proliferate.[27]

Incorporating nonparenchymal cells into hepatocyte cultures supports the importance of paracrine signaling, as these cells enhance hepatocyte function in vitro. Koike *et al.* prepared both mono- and cocultures of fresh rat hepatocytes. These coculture setups were layered structures containing nonparenchymal cells isolated from the same rat. Both albumin and urea production were increased and this format also was able to sustain hepatocyte health and function for 14 days, 10 days longer than the monocultures.[42,43] Khetani and Bhatia showed that colonies of primary rat hepatocytes surrounded by stromal fibroblasts in a 4:1 ratio produced more urea and albumin, for a longer culture time, than their monoculture counterparts. The cocultured hepatocytes had more Phase I transcript activity than the monocultures, however, both culture formats had comparable Phase II transcript activity. The authors concluded that coculturing helps improves the longevity of primary hepatocyte cultures.[44]

1.4.3 Inclusion of liver-specific gradients in in vitro models

While the incorporation of extracellular matrices, non-parenchymal cell types, and even 3D formats have been explored in in vitro liver models, little effort has focused on establishing extracellular environments that define the periportal and perivenous regions. The oxygen gradient has been well characterized across the liver lobule and, in a healthy liver, is not perturbed by cycles of feeding and fasting. Oxygen is a key regulator of liver zonation due to oxygen sensitive transcription factors called hypoxia-inducible factors (HIFs). The active pathway for HIF is the HIF proteins which (HIF1α) dimerize with aryl hydrocarbon receptor nuclear translocator (ARNT) which can increase or decrease the transcription of various hypoxia responsive elements. The HIF pathway is regulated by oxygen. When oxygen is present, HIF1α is readily targeted for degradation by hydroxylation followed by ubiquitination. At lower oxygen tensions, HIF1α is

stabilized.[45] Physiological oxygen in the lobule is between 11-3% O_2, the lower oxygen ranges enables HIF stabilization and the activation of the HIF pathway. However, most in vitro hepatocyte cultures are at, atmospheric oxygen levels around 21% O_2. This is a hyperoxic environment in which HIF1α is degraded. The hyperoxic environment leads to the cells' generation of more reactive oxygen species (ROS), which can cause oxidative stress to organelles and disrupt intracellular signaling, resulting in downstream effects. Prolonged exposure to a hyperoxic environment will change baseline expression of oxygen-consuming enzymes away from an *in vivo* state.[46]

In one study, Scharf *et al.* compared primary hepatocytes cultured under normoxic (16% O_2) and mild hypoxic (8% O_2) conditions; the gaseous environment in both setups was balanced with 5% CO_2 and N_2. They quantified the transcript and protein levels of insulin-like growth factor-binding protein 1 (IGFBP-1) at 16 and 8% O_2; insulin-like growth factors are known to be highly expressed in the perivenous region. They also measured the relation between HIF1α and IGFBP-1. This work showed low oxygen tensions increase the expression of IGFBP-1 and that HIF1α protein is colocalized with the IFGBP-1.[47] These results suggest that the oxygen gradient in the liver mediates zonation through HIF1α stabilization; therefore, culturing hepatocytes at physiological oxygen, rather than atmospheric oxygen, will help promote more in vivo character.

Results by Kietzmann and colleagues further support the importance of HIFs in regulating hepatocyte function. By measuring the localization of the mRNA and proteins of HIF1α, HIF2α and HIF3α in rat lobules, they showed HIF mRNA was predominantly found in hepatocytes in the perivenous region. At the protein level, the hepatocytes closest to the central vein expressed significantly more HIF1α, HIF2α and HIF3α than other hepatocytes in the lobule.[48] Hepatocytes closest to the central vein are experiencing the lowest oxygen tension and measuring a notable

change in stabilizing HIF proteins; therefore, low physiological oxygen tensions are necessary to promote an environment similar to the lobule.

1.4.4 Impact of flow on hepatocyte function

The blood flowing through the liver sinusoid contributes to the dynamics of the liver gradients by replenishing nutrients and removing waste from the sinusoid. Nutrients are supplied to the hepatocytes through diffusion from the blood into the space of Disse. Flow has been introduced into hepatocyte cultures with bioreactor culture methods and microfluidics.

Allen and Bhatia developed and characterized an in vitro perfusion system in which fresh culture medium was introduced to a bioreactor to maintain oxygen and nutrient concentrations. The perfusion system incorporated both media flow and a physiological oxygen gradients across a culture of primary rat hepatocytes cultured as a monolayer on collagen I coated glass slides. The flow rate was regulated using a syringe pump and oxygen was regulated with a gas exchanger. Within the bioreactor, they measured zonally distributed proteins, phosphoenolpyruvate carboxykinase (PEPCK), an enzyme part of the gluconeogenesis pathway, and CYP2B with western blot analysis. Both proteins followed in vivo zonal patterning in which PEPCK decreased in abundance from the periportal region to the perivenous region while CYP2B increased from the periportal to perivenous region. When the same experiments were performed without implementing a physiological oxygen gradient, there wasn't zonal distribution of these proteins, suggesting that the oxygen gradient is a key factor in liver zonation.[49]

Tanaka and colleagues evaluated the effect of shear stress on hepatocyte function by altering fluid flow over monolayers of hepatocytes on collagen I coated microchannel in a microfluidic culture system.[50] HepG2 cells were cultured within the microfluidic chip and

flowrates ranging from 1 μL min^{-1} to 10 μL min^{-1} which ranges from 0.6 to 6.0 Pa of shear stress. Exposure of HepG2 cells to increasing shear stress up to 6.0 Pa decreased albumin production and negatively impacted cell morphology; however, HepG2 cells under low shear stress conditions had enhance albumin secretion.

1.5 Focus of this work

There are different methods to culture hepatocytes in vitro: as monolayers, implementing an extracellular matrix, as spheroids, in microfluidic devices, or using a paper-scaffold; each of these methods have benefits and drawbacks. The most popular cell culture method involves culturing cells as monolayers, on glass or plasticware, due to their ease of use and high throughput capabilities. A three-dimensional (3D) component can be implemented by culturing the cell monolayers on a biologically relevant extracellular matrix such as collagen or Matrigel. Monolayers-on-ECM were further improved by adding another layer of ECM on top of the cell monolayer, sandwiching the cell monolayer between two ECM slabs. The sandwich culture format mimics native tissue structure due to the layered cell-EMC interactions.[43] Spheroids are another popular 3D culture method. Spheroids are clumps of cells that have superior cell-cell interactions and very little cell-ECM/ cell-surface interactions. Spheroids offer a tumor-like 3D structure and nutrient gradients that form from the edge of the spheroid to the core where the gradients are dictated by cellular consumption and diffusion. However, the microenvironments within the spheroids are difficult to control. Microfluidic devices are another attractive 3D culture method because of excellent microenvironmental control but microfluidic design experience, fabrication expertise, and pumps are a barrier of entry for many researchers. An alternative method for 3D

cell culture is paper scaffold cultures, in which the cellulose paper fibers are a scaffold for cells and ECM.

Paper-based culturing of hepatocytes is an attractive 3D culture format. Paper-based 3D culturing utilizes the cellulose paper fiber network as scaffolding for a cell compatible ECM, like collagen type I, increasing the cultures mechanical stability. Furthermore, the paper fibers act as small capillaries throughout the culture allowing for nutrient transport via capillary action .[51–53] Briefly, Whatman 105 lens paper is wax patterned to define a hydrophilic culture region and hydrophobic boarder. Cells are suspended in ECM hydrogel and evenly distributed into the cell culture region of the scaffold where the cell-laden ECM gelates, holding the cells within the paper scaffold.[54]

To better understand structure-function relationships in in vitro liver cultures, this work probes various aspects of an ideal liver model in a stepwise fashion, focusing on (1) culture dimensionality and format, and (2) physiological conditions mimicking the periportal or perivenous regions. The work evaluates both monolayer and coculture formats of hepatocytes and hepatocyte-like immortalized lines with microscopic, molecular biology, and metabolomic readouts.

Chapter 2 evaluates physiologically relevant oxygen tensions found in the periportal and perivenous regions on the health, response to hepatotoxins, and the induction of metabolically important transcripts of HepG2 hepatoma cells. The HepG2 cell line served as a model system to develop an experimental workflow to evaluate single-point physiological oxygen tensions found in the periportal and perivenous regions. In this chapter, I focused specifically on the influence of physiological oxygen and 3D paper-based cultures and compared those results to traditionally used monolayer cultures.

Chapter 3 builds on the importance of the oxygen tensions of the periportal and perivenous microenvironment by including the morphogen Wnt into the perivenous condition and using differentiated HepaRG cells. The HepaRG cell line is an immortalized hepatocyte cell line that are more representative of PHHs due to the HepaRG cell's highly active Phase I and II metabolic enzymes, energy metabolism, and secretory activity.[55] The HepaRG hepatocyte character in response to the perivenous and periportal culture conditions were compared as monolayer culture formats.

Chapter 4 focuses on physiological stiffness and evaluating how changing the ECM's physical properties influenced the metabolic competency of the HepaRG cell line. Culturing hepatocytes on collagen slabs is common practice, as it is an easily accessible and commercialized format. Here HepaRG and primary human hepatocytes were evaluated on collagen slabs of different stiffness of a collagen type I substrate, generated by neutralization and chemical cross-linking. The chemical properties associated with changes in collagen density and structure (e.g., number of sites for integrin binding) were controlled, allowing for focused structure-function studies of ECM stiffness vs. metabolic activity.

Chapter 5 evaluates HepaRG cells cultured under physiologically relevant conditions and within a 3D paper-based format. The paper scaffolds float at the air-liquid interface minimizing diffusion limitations of oxygen to the bottom of a culture dish- this ensures the HepaRG cells are exposed to the percent oxygen in the gaseous culture environment. This combines to assess how single point physiologically relevant microenvironmental culture conditions and formats influence the hepatocyte function of HepaRG cells in 3D cultures.

1.6 Figures and Tables

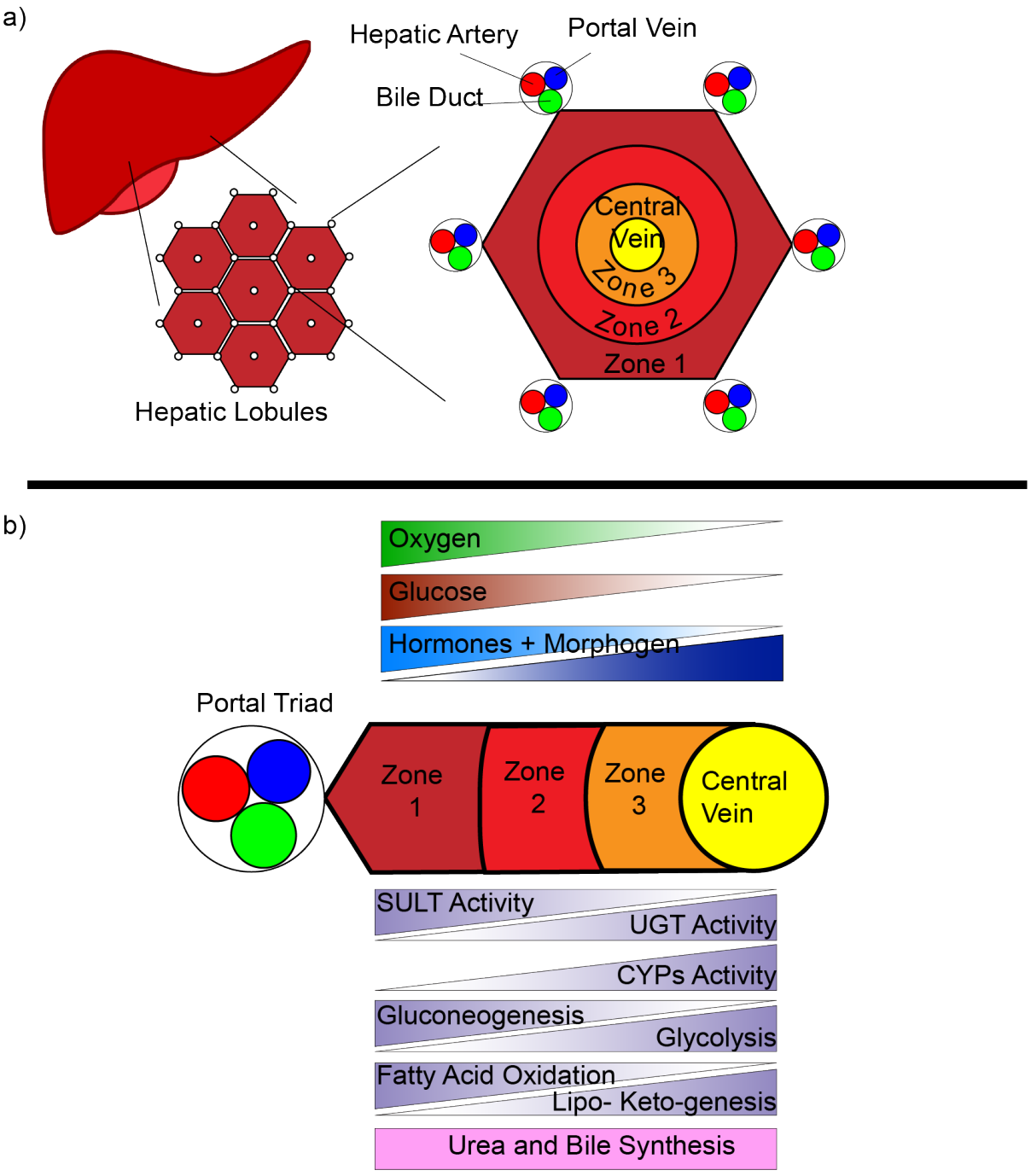

Figure 1.1 Diagram of the liver organization (a). The liver structural subunit is the lobule. At each corner of the hexagonal lobule is the portal triad consisting of the bile duct, portal vein and hepatic artery. At the center of the lobule is the central vein. As blood flows from the portal triad

to the central vein there are various gradients that form including oxygen, glucose, hormone, and morphogens (a). The extracellular gradients influence each hepatocyte's function resulting in differential expression of liver-specific function across the lobule. The distribution is known as liver zonation in which the hepatocytes in Zone 1, 2 and 3 exhibit distinct function.

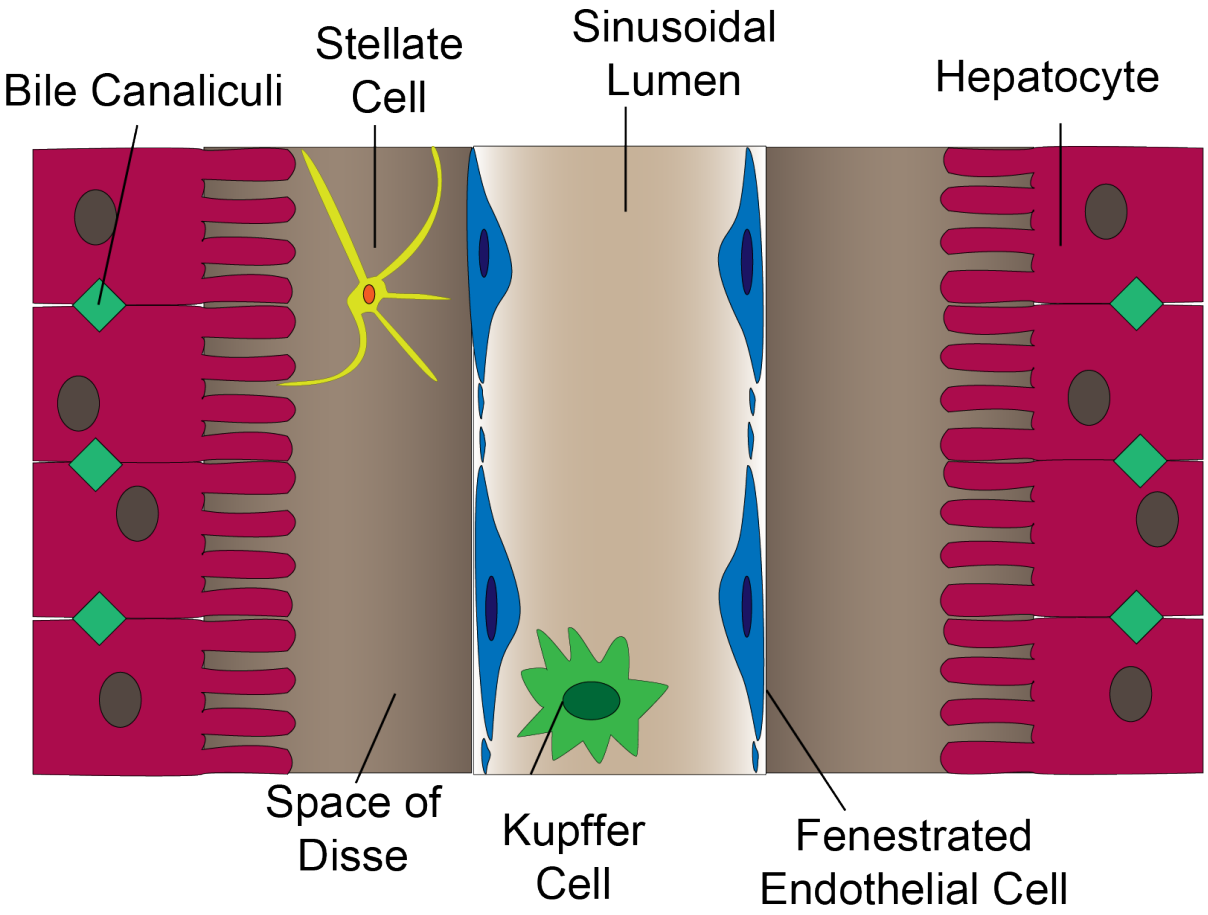

Figure 1.2 Diagram of the liver sinusoid and cellular organization. Blood flows through the sinusoidal lumen, fenestrated endothelial cells line the sinusoid to let molecules move in and out of the sinusoid while keeping red blood cells in the sinusoid. Nutrients diffuse from the lumen into the space of Disse, a protein dense space to facilitate hepatocyte nutrient uptake in a diffusion regime as well as buffers the hepatocytes from blood flow shear stress. Kupffer and stellate cells are nonparenchymal cells that support the function of the hepatocytes.

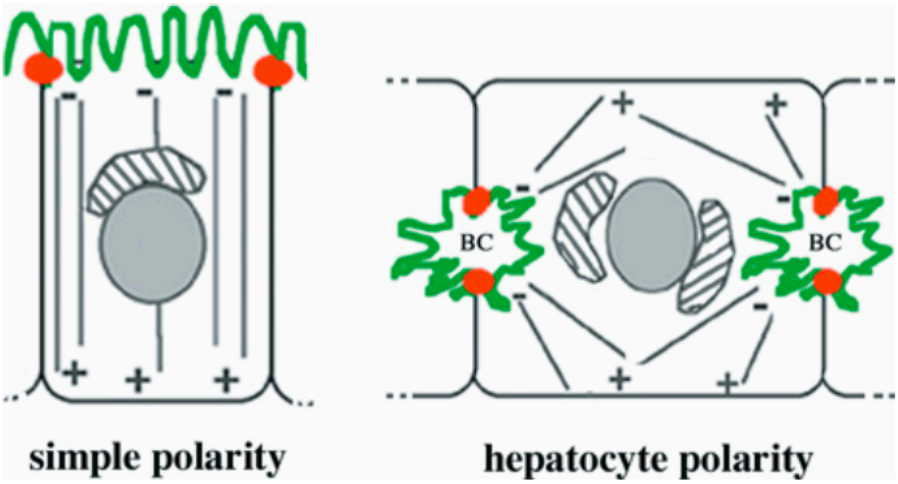

Figure 1.3. Diagram of simple vs hepatocyte polarity. The apical side (green) is separated from the basal side by tight junctions (red dots). Simple cell polarity has one axis of polarization with one basal and one apical side of the cell (+ to – end of the cell). Hepatocyte polarity has multiple axis of polarization due to bile canaculi in between neighboring hepatocytes and sinusoidal lumens flanking hepatocytes on multiple sides. Adapted from reference 10.

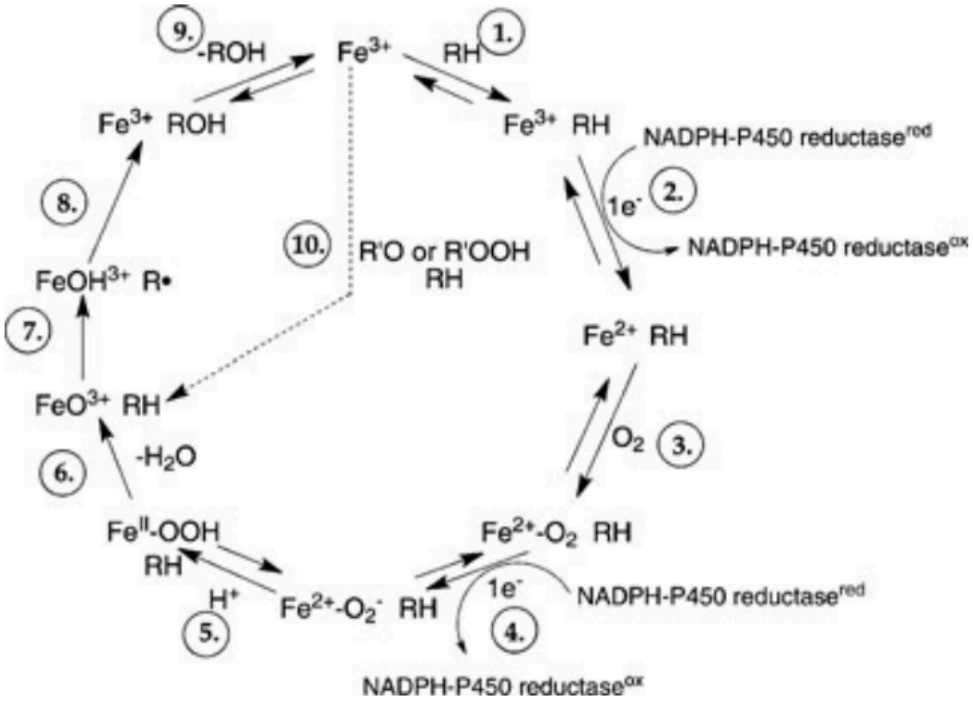

Figure 1.4 10-step CYP enzyme reaction mechanism. Adapted from reference 14.

REFERENCES

(1) Jungermann, K.; Katz, N. Functional Specialization of Different Hepatocyte Populations. *Physiol. Rev.* **1989**, *69* (3), 708–764. https://doi.org/10.1152/physrev.1989.69.3.708.

(2) Arjun, K.; Ekrem, Y.; Wehrle, C. J.; Tuma, F. *Liver Physiology*; StatPearls [Internet], 2021. https://doi.org/NBK535438.

(3) Jancova, P.; Anzenbacher, P.; Anzenbacherova, E. Phase II Drug Metabolizing Enzymes. *Biomed. Pap.* **2010**, *154* (2), 103–116. https://doi.org/10.5507/bp.2010.017.

(4) Jones, A. L.; Schmucker, D. L. Current Concepts of Liver Structure as Related to Function. *Gastroenterology* **1977**, *73* (4 I), 833–851. https://doi.org/10.1016/s0016-5085(19)31793-7.

(5) Wong, A.; Jennings, R. Hepatobiliary System. In *Veterinary Histology*; 2017; Vol. 53, pp 144–156.

(6) Lee-Montiel, F. T.; George, S. M.; Gough, A. H.; Sharma, A. D.; Wu, J.; DeBiasio, R.; Vernetti, L. A.; Taylor, D. L. Control of Oxygen Tension Recapitulates Zone-Specific Functions in Human Liver Microphysiology Systems. *Exp. Biol. Med.* **2017**, *242* (16), 1617–1632. https://doi.org/10.1177/1535370217703978.

(7) Kietzmann, T. Liver Zonation in Health and Disease: Hypoxia and Hypoxia-Inducible Transcription Factors as Concert Masters. *Int. J. Mol. Sci.* **2019**, *20* (9). https://doi.org/10.3390/ijms20092347.

(8) Usta, O. B.; McCarty, W. J.; Bale, S.; Hegde, M.; Jindal, R.; Bhushan, A.; Golberg, I.; Yarmush, M. L. Microengineered Cell and Tissue Systems for Drug Screening and Toxicology Applications: Evolution of in-Vitro Liver Technologies. *Technol. (Singap World Sci.)* **2015**, *3* (1), 1–26. https://doi.org/10.1142/S2339547815300012.

(9) Aleksandr, T.; Müsch, A. Hepatocyte Polarity. *Compr Physiol.* **2013**, 243–287. https://doi.org/10.1002/cphy.c120009.Hepatocyte.

(10) Decaens, C.; Durand, M.; Grosse, B.; Cassio, D. Which in Vitro Models Could Be Best Used to Study Hepatocyte Polarity? *Biol. Cell* **2008**, *100* (7), 387–398. https://doi.org/10.1042/bc20070127.

(11) Bhatia, S. N.; Toner, M.; Foy, B. D.; Rotem, A.; Tompkins, N. R. G.; Yarmush, M. L. Zonal Liver Cell Heterogeneity: Effects of Oxygen on Metabolic Functions of Hepatocytes. *Cell. Eng* **1996**, *1* (2), 125–135.

(12) Zanger, U. M.; Schwab, M. Cytochrome P450 Enzymes in Drug Metabolism: Regulation of Gene Expression, Enzyme Activities, and Impact of Genetic Variation. *Pharmacology and Therapeutics*. 2013. https://doi.org/10.1016/j.pharmthera.2012.12.007.

(13) Whitman, N. A.; McIntosh, J. C.; Penley, J. B.; Lockett, M. R. Microfabricated Devices

for Studying the Metabolism and Cytotoxicity of Drug Candidates. *Curr. Pharm. Biotechnol.* **2016**, *17*, 755–771.

(14) Guengerich, F. P. Mechanisms of Cytochrome P450 Substrate Oxidation: MiniReview. *J. Biochem. Mol. Toxicol.* **2007**, *21* (4), 163–168. https://doi.org/10.1002/jbt.20174.

(15) Guengerich, F. P. Mechanisms of Cytochrome P450-Catalyzed Oxidations. *ACS Catalacis* **2018**, *8* (12), 10964–10976. https://doi.org/10.1021/acscatal.8b03401.Mechanisms.

(16) Meunier, B.; de Visser, S. P.; Shaik, S. Mechanism of Oxidation Reactions Catalyzed by Cytochrome P450 Enzymes. *Chem. Rev.* **2004**, *104* (9), 3947–3980. https://doi.org/10.1021/cr020443g.

(17) Jetter, A.; Kullak-Ublick, G. A. Drugs and Hepatic Transporters: A Review. *Pharmacol. Res.* **2020**, *154* (January 2019). https://doi.org/10.1016/j.phrs.2019.04.018.

(18) Hollenstein, K.; Dawson, R. J.; Locher, K. P. Structure and Mechanism of ABC Transporter Proteins. *Curr. Opin. Struct. Biol.* **2007**, *17* (4), 412–418. https://doi.org/10.1016/j.sbi.2007.07.003.

(19) Colas, C.; Ung, P. M.-U.; Schlessinger, A. SLC Transporters: Structure, Function, and Drug Discovery. *RSC Med. Chem.* **2016**, *7* (6), 1069–1081. https://doi.org/10.1039/C6MD00005C.SLC.

(20) Oinonen, T.; Lindros, K. O. Zonation of Hepatic Cytochrome P-450 Expression and Regulation. *Biochem. J.* **1998**, *329*, 17–35. https://doi.org/10.1042/bj3290017.

(21) Kietzmann, T. Metabolic Zonation of the Liver: The Oxygen Gradient Revisited. *Redox Biol.* **2017**, *11* (January), 622–630. https://doi.org/10.1016/j.redox.2017.01.012.

(22) Braeuning, A.; Ittrich, C.; Köhle, C.; Hailfinger, S.; Bonin, M.; Buchmann, A.; Schwarz, M. Differential Gene Expression in Periportal and Perivenous Mouse Hepatocytes. *FEBS J.* **2006**, *273* (22), 5051–5061. https://doi.org/10.1111/j.1742-4658.2006.05503.x.

(23) Ji, S.; Lemasters, J. J.; Christenson, V.; Thurman, R. G. Periportal and Pericentral Pyridine Nucleotide Fluorescence from the Surface of the Perfused Liver: Evaluation of the Hypothesis That Chronic Treatment with Ethanol Produces Pericentral Hypoxia. *Proc. Natl. Acad. Sci. U. S. A.* **1982**, *79* (17 I), 5415–5419. https://doi.org/10.1073/pnas.79.17.5415.

(24) Benhamouche, S.; Decaens, T.; Godard, C.; Chambrey, R.; Rickman, D. S.; Moinard, C.; Vasseur-Cognet, M.; Kuo, C. J.; Kahn, A.; Perret, C.; Colnot, S. Apc Tumor Suppressor Gene Is the "Zonation-Keeper" of Mouse Liver. *Dev. Cell* **2006**, *10* (6), 759–770. https://doi.org/10.1016/j.devcel.2006.03.015.

(25) Gebhardt, R.; Baldysiak-Figiel, A.; Krügel, V.; Ueberham, E.; Gaunitz, F. Hepatocellular Expression of Glutamine Synthetase: An Indicator of Morphogen Actions as Master

Regulators of Zonation in Adult Liver. *Prog. Histochem. Cytochem.* **2007**, *41* (4), 201–266. https://doi.org/10.1016/j.proghi.2006.12.001.

(26) Wild, S. L.; Elghajiji, A.; Rodriguez, C. G.; Weston, S. D.; Burke, Z. D.; Tosh, D. The Canonical Wnt Pathway as a Key Regulator in Liver Development, Differentiation and Homeostatic Renewal. *Genes (Basel).* **2020**, *11* (10), 1–20. https://doi.org/10.3390/genes11101163.

(27) Matz-Soja, M.; Hovhannisyan, A.; Gebhardt, R. Hedgehog Signalling Pathway in Adult Liver: A Major New Player in Hepatocyte Metabolism and Zonation? *Med. Hypotheses* **2013**, *80* (5), 589–594. https://doi.org/10.1016/j.mehy.2013.01.032.

(28) Kolbe, E.; Aleithe, S.; Rennert, C.; Spormann, L.; Ott, F.; Meierhofer, D.; Gajowski, R.; Stöpel, C.; Hoehme, S.; Kücken, M.; Brusch, L.; Seifert, M.; von Schoenfels, W.; Schafmayer, C.; Brosch, M.; Hofmann, U.; Damm, G.; Seehofer, D.; Hampe, J.; Gebhardt, R.; Matz-Soja, M. Mutual Zonated Interactions of Wnt and Hh Signaling Are Orchestrating the Metabolism of the Adult Liver in Mice and Human. *Cell Rep.* **2019**, *29* (13), 4553-4567.e7. https://doi.org/10.1016/j.celrep.2019.11.104.

(29) Matz-Soja, M.; Rennert, C.; Schönefeld, K.; Aleithe, S.; Boettger, J.; Schmidt-Heck, W.; Weiss, T.; Hovhannisyan, A.; Zellmer, S.; Klöting, N.; Schulz, A.; Kratzsch, J.; Guthke, R.; Gebhardt, R. Hedgehog Signaling Is a Potent Regulator of Liver Lipid Metabolism and Reveals a GLI-Code Associated with Steatosis. *Elife* **2016**, *5* (MAY2016), 1–28. https://doi.org/10.7554/eLife.13308.

(30) Sigal, S. H.; Brill, S.; Fiorino, A. S.; Reid, L. M. The Liver as a Stem Cell and Lineage System. *Am. J. Physiol. - Gastrointest. Liver Physiol.* **1992**, *263* (2 26-2). https://doi.org/10.1152/ajpgi.1992.263.2.g139.

(31) Dunn, J. C. Y.; Tompkins, R. G.; Yarmush, M. L. Hepatocytes in Collagen Sandwich: Evidence for Transcriptional and Translational Regulation. *J. Cell Biol.* **1992**, *116* (4), 1043–1053. https://doi.org/10.1083/jcb.116.4.1043.

(32) Dunn, J. C. Y.; Yarmush, M. L.; Koebe, H. G.; Tompkins, R. G. Hepatocyte Function and Extracellular Matrix Geometry: Long-term Culture in a Sandwich Configuration. *FASEB J.* **1989**, *3* (2), 174–177. https://doi.org/10.1096/fasebj.3.2.2914628.

(33) Meyer, C.; Liebe, R.; Breitkopf-Heinlein, K.; Liu, Y.; Müller, A.; Rakoczy, P.; Thomas, M.; Weng, H.; Bachmann, A.; Ebert, M.; Dooley, S. Hepatocyte Fate Upon TGF-β Challenge Is Determined by the Matrix Environment. *Differentiation* **2015**, *89* (5), 105–116. https://doi.org/10.1016/j.diff.2015.04.001.

(34) Zeigerer, A.; Wuttke, A.; Marsico, G.; Seifert, S.; Kalaidzidis, Y.; Zerial, M. Functional Properties of Hepatocytes In Vitro Are Correlated With Cell Polarity Maintenance. *Exp. Cell Res.* **2017**, *350*, 242–252. https://doi.org/10.1016/j.yexcr.2016.11.027.

(35) Hewitt, N. J.; Lechón, M. J. G.; Houston, J. B.; Hallifax, D.; Brown, H. S.; Maurel, P.;

Kenna, J. G.; Gustavsson, L.; Lohmann, C.; Skonberg, C.; Guillouzo, A.; Tuschl, G.; Li, A. P.; Lecluyse, E.; Groothuis, G. M. M.; Hengstler, J. G. Primary Gepatocytes: Current Understanding of the Regulation of Metabolic Enzymes and Transporter Proteins, and Pharmaceutical Practice for the Use of Hepatocytes in Metabolism, Enzyme Induction, Transporter, Clearance, and Hepatotoxicity Studies. *Drug Metab. Rev.* **2007**, *39*, 159–234. https://doi.org/10.1080/03602530601093489.

(36) Guo, L.; Dial, S.; Shi, L.; Branham, W.; Liu, J.; Fang, J.-L.; Green, B.; Deng, H.; Kaput, J.; Ning, B. Similarities and Differences in the Expression of Drug-Metabolizing Enzymes Between Human Hepatic Cell Lines and Primary Human Hepatocytes. *Drug Metab. Dispos.* **2010**, *39* (3). https://doi.org/10.1124/dmd.110.035873.

(37) Chang, T. T.; Hughes-Fulford, M. Monolayer and Spheroid Culture of Human Liver Hepatocellular Carcinoma Cell Line Cells Demonstrate Distinct Global Gene Expression Patterns and Functional Phenotypes. *Tissue Eng. - Part A* **2009**, *15* (3), 559–567. https://doi.org/10.1089/ten.tea.2007.0434.

(38) Ramaiahgari, S. C.; Den Braver, M. W.; Herpers, B.; Terpstra, V.; Commandeur, J. N. M.; Van De Water, B.; Price, L. S. A 3D in Vitro Model of Differentiated HepG2 Cell Spheroids with Improved Liver-like Properties for Repeated Dose High-Throughput Toxicity Studies. *Arch. Toxicol.* **2014**, *88* (5), 1083–1095. https://doi.org/10.1007/s00204-014-1215-9.

(39) Gaskell, H.; Sharma, P.; Colley, H. E.; Murdoch, C.; Williams, D. P.; Webb, S. D. Characterization of a Functional C3A Liver Spheroid Model. *Toxicol. Res. (Camb).* **2016**, *5* (4), 1053–1065. https://doi.org/10.1039/c6tx00101g.

(40) Kim, Y.; Rajagopalan, P. 3D Hepatic Cultures Simultaneously Maintain Primary Hepatocyte and Liver Sinusoidal Endothelial Cell Phenotypes. *PLoS One* **2010**, *5* (11). https://doi.org/10.1371/journal.pone.0015456.

(41) LeCluyse, E. L.; Audus, K. L.; Hochman, J. H. Formation of Extensive Canalicular Networks by Rat Hepatocytes Cultured in Collagen-Sandwich Configuration. *Am. J. Physiol.* **1994**, *266* (6 Pt 1), C1764-74. https://doi.org/10.1152/ajpcell.1994.266.6.C1764.

(42) Koike, M.; Matsushita, M.; Taguchi, K.; Uchino, J. Function of Culturing Monolayer Hepatocytes by Collagen Gel Coating and Coculture with Nonparenchymal Cells. *Artif. Organs* **1996**, *20* (2), 186–192. https://doi.org/10.1111/j.1525-1594.1996.tb00725.x.

(43) Godoy, P.; Hewitt, N. J.; Albrecht, U.; Andersen, M. E.; Ansari, N.; Bhattacharya, S.; Bode, J. G.; Bolleyn, J.; Borner, C.; Böttger, J.; Braeuning, A.; Budinsky, R. A.; Burkhardt, B.; Cameron, N. R.; Camussi, G.; Cho, C. S.; Choi, Y. J.; Craig Rowlands, J.; Dahmen, U.; Damm, G.; Dirsch, O.; Donato, M. T.; Dong, J.; Dooley, S.; Drasdo, D.; Eakins, R.; Ferreira, K. S.; Fonsato, V.; Fraczek, J.; Gebhardt, R.; Gibson, A.; Glanemann, M.; Goldring, C. E. P. P.; Gómez-Lechón, M. J.; Groothuis, G. M. M. M.; Gustavsson, L.; Guyot, C.; Hallifax, D.; Hammad, S.; Hayward, A.; Häussinger, D.; Hellerbrand, C.; Hewitt, P.; Hoehme, S.; Holzhütter, H. G.; Houston, J. B.; Hrach, J.; Ito, K.; Jaeschke, H.;

Keitel, V.; Kelm, J. M.; Kevin Park, B.; Kordes, C.; Kullak-Ublick, G. A.; Lecluyse, E. L.; Lu, P.; Luebke-Wheeler, J.; Lutz, A.; Maltman, D. J.; Matz-Soja, M.; McMullen, P.; Merfort, I.; Messner, S.; Meyer, C.; Mwinyi, J.; Naisbitt, D. J.; Nussler, A. K.; Olinga, P.; Pampaloni, F.; Pi, J.; Pluta, L.; Przyborski, S. A.; Ramachandran, A.; Rogiers, V.; Rowe, C.; Schelcher, C.; Schmich, K.; Schwarz, M.; Singh, B.; Stelzer, E. H. K. K.; Stieger, B.; Stöber, R.; Sugiyama, Y.; Tetta, C.; Thasler, W. E.; Vanhaecke, T.; Vinken, M.; Weiss, T. S.; Widera, A.; Woods, C. G.; Xu, J. J.; Yarborough, K. M.; Hengstler, J. G. Recent Advances in 2D and 3D in Vitro Systems Using Primary Hepatocytes, Alternative Hepatocyte Sources and Non-Parenchymal Liver Cells and Their Use in Investigating Mechanisms of Hepatotoxicity, Cell Signaling and ADME. *Arch. Toxicol.* **2013**, *87* (8), 1315–1530. https://doi.org/10.1007/s00204-013-1078-5.

(44) Khetani, S. R.; Bhatia, S. N. Microscale Culture of Human Liver Cells for Drug Development. *Nat. Biotechnol.* **2008**, *26* (1), 120–126. https://doi.org/10.1038/nbt1361.

(45) Marxsen, J. H.; Stengel, P.; Doege, K.; Heikkinen, P.; Jokilehto, T.; Wagner, T.; Jelkmann, W.; Jaakkola, P.; Metzen, E. Hypoxia-Inducible Factor-1 (HIF-1) Promotes Its Degradation by Induction of HIF-α-Prolyl-4-Hydroxylases. *Biochem. J.* **2004**, *381* (3), 761–767. https://doi.org/10.1042/BJ20040620.

(46) Stuart, J. A.; Fonseca, J.; Moradi, F.; Cunningham, C.; Seliman, B.; Worsfold, C. R.; Dolan, S.; Abando, J.; Maddalena, L. A. How Supraphysiological Oxygen Levels in Standard Cell Culture Affect Oxygen-Consuming Reactions. *Oxid. Med. Cell. Longev.* **2018**, *2018*. https://doi.org/10.1155/2018/8238459.

(47) Scharf, J.-G.; Unterman, T. G.; Kietzmann, T. Oxygen-Dependent Modulation of Insulin-Like Growth Factor Binding Protein Biosynthesis in Primary Cultures of Rat Hepatocytes. *Endocrinology* **2005**, *146* (12), 5433–5443. https://doi.org/10.1210/en.2005-0948.

(48) Kietzmann, T.; Cornesse, Y.; Brechtel, K.; Modaressi, S.; Jungermann, K. Perivenous Expression of the MRNA of the Three Hypoxia-Inducible Factor α-Subunits, HIF1α, HIF2α and HIF3α, in Rat Liver. *CEUR Workshop Proc.* **2007**, *284* (March). https://doi.org/10.1042/0264-6021.

(49) Allen, J. W.; Bhatia, S. N. Formation of Steady-State Oxygen Gradients in Vitro: Application to Liver Zonation. *Biotechnol. Bioeng.* **2003**, *82* (3), 253–262. https://doi.org/10.1002/bit.10569.

(50) Tanaka, Y.; Yamato, M.; Okano, T.; Kitamori, T.; Sato, K. Evaluation of Effects of Shear Stress on Hepatocytes by a Microchip-Based System. *Meas. Sci. Technol.* **2006**, *17* (12), 3167–3170. https://doi.org/10.1088/0957-0233/17/12/S08.

(51) Songok, J.; Toivakka, M. Modelling of Capillary-Driven Flow for Closed Paper-Based Microfluidic Channels. *J. Micromechanics Microengineering* **2017**, *27* (6). https://doi.org/10.1088/1361-6439/aa6b40.

(52) Chen, Y. H.; Kuo, Z. K.; Cheng, C. M. Paper - a Potential Platform in Pharmaceutical Development. *Trends Biotechnol.* **2015**, *33* (1), 4–9. https://doi.org/10.1016/j.tibtech.2014.11.004.

(53) Liu, Z.; Hu, J.; Zhao, Y.; Qu, Z.; Xu, F. Experimental and Numerical Studies on Liquid Wicking into Filter Papers for Paper-Based Diagnostics. *Appl. Therm. Eng.* **2015**, *88*, 280–287. https://doi.org/10.1016/j.applthermaleng.2014.09.057.

(54) Lloyd, C. C.; Boyce, M. W.; Lockett, M. R. Paper-Based Invasion Assays for Quantifying Cellular Movement in Three-Dimensional Tissue-like Structures. *Curr. Protoc. Chem. Biol.* **2017**, *9* (2), 75–95. https://doi.org/10.1002/cpch.22.

(55) Tascher, G.; Burban, A.; Camus, S.; Plumel, M.; Chanon, S.; Le Guevel, R.; Shevchenko, V.; Van Dorsselaer, A.; Lefai, E.; Guguen-Guillouzo, C.; Bertile, F. In-Depth Proteome Analysis Highlights HepaRG Cells as a Versatile Cell System Surrogate for Primary Human Hepatocytes. *Cells* **2019**, *8* (2), 192. https://doi.org/10.3390/cells8020192.

CHAPTER 2: EVALUATING LIVER-SPECIFIC RESPONSES OF HEPG2 CELLS TO PHYSIOLOGICALLY RELEVANT OXYGEN TENSIONS[1]

2.1 Introduction

Current cell-based assays cannot accurately predict drug-induced liver injury or hepatotoxicity in patients, two factors which account for a significant number of late-stage drug failures.[1,2] Preclinical in vitro assays commonly use monolayers of primary human hepatocytes (PHHs) or cell lines presenting hepatocyte-like characteristics. The HepG2 liver hepatoma cell line displays liver-representative genotypes but has limited expression of cytochrome P450 (CYP) enzymes compared to PHHs.[3,4] Despite these limitations, HepG2 cells are commonly used in drug toxicity studies due to their availability and low genetic drift [5,6].

Monolayer cultures lack many aspects of the tissue microenvironment, which has profound effects on cellular function. Placing PHHs in extracellular-rich environments such as a collagen sandwich maintains their polarization and metabolic function,[7,8] where monolayers on culture-compatible plasticware readily depolarize [9,10] and lose liver-specific function within days of plating.[11,12] Similar increases in functionality are observed when HepG2 cells are cultures as spheroids. These multicellular aggregates have increased expression of phase I and II metabolic enzymes when compared to monolayers.[13–15] The spheroids also reacquire functions that are lost in monolayer cultures, including glycogen storage and the transport of bile salts. The analogous recovery of liver specific function in a 3D environment between PHHs and HepG2 cells supports

[1] This chapter previously appeared as an article in Toxicology in Vitro. The original citation is as follows: DiProspero T.J.; Dalrymple E..; Lockett, M. R. Physiologically relevant oxygen tensions differentially regulate hepatotoxic responses in HepG2 cells *Toxicol. in Vitro.* **2021**, *74*, *105156*.

the idea that HepG2 can be and attractive surrogate for PHHs during rapid prototyping and high throughput screens. We are not suggesting that HepG2 cells can replace PHHs, rather supplement the use of HepG2 to develop preliminary data for microenvironmental studies and high throughput toxicity studies.

While spheroids have clear advantages over monolayer cultures, the analysis of microenvironmental influences on cellular behavior is difficult to assess without histological slicing. The overlapping gradients of oxygen, nutrients, and soluble factors that extend across these structures also make it difficult to probe microenvironment-cellular function relationships, individually or in concert.[16] Oxygen is of particular interest, as it is a global regulator of cellular function in all tissues.[17] Within the liver, changes in oxygen availability correlates with liver zonation,[18,19] the distribution of metabolic activity in the hepatocytes that line each sinusoid. The blood oxygen partial pressure range from 65-60 mmHg O_2 (11-8% O_2) in the periportal region, to 35-30 mmHg O_2 (5-3% O_2) in the perivenous region.[19–21] Hepatocytes in the periportal region primarily express high densities of sulfotransferases (SULTs).[22] Hepatocytes in the perivenous region primarily express CYPs and UGP-glucuronosyltransferases (UGTs).

Given the significant drop in available oxygen from the periportal to the perivenous region, we probed the effect of three different oxygen partial pressures on HepG2 hepatoxicity as well as CYP expression and induction in monolayer and 3D culture formats. Cells cultured at 20% O_2 served as a comparison point with previous studies, as it is commonly used in tissue culture laboratories; cells cultured at 8% O_2 represented the periportal region; cells cultured at 3% O_2 represented the perivenous region. Our working hypothesis was the HepG2 metabolizing enzyme transcript profiles would better match those found in vivo when placed in an ECM-rich environment and a physiologically relevant oxygen tension. This hypothesis is supported by

previous works, which showed substantial changes in drug metabolism and gene expression when HepG2 cells were placed in tumor-relevant oxygen tensions.[23] Hypoxia is known to have global transcriptional changes in cells,[24] but few studies have evaluated the oxygen tensions found in healthy livers.

This work highlights the importance of evaluating microenvironmental influences in a culture platform that can evaluate individual factors, such as oxygen tension. To draw comparisons between monolayer and 3D culture environments, we used the paper-based culture platform first described by Whitesides and further developed in our laboratory.[25,26] This setup generates defined 3D culture regions by wax-printing sheets of paper, which are porous and able to support HepG2 cells suspended in a collagen I matrix. The paper scaffold based 3D cultures combine the benefits of the cell-cell contact of spheroid cultures and the cell-ECM interactions of slab based 3D cultures. Furthermore, the extracellular environment of paper based cultures can be tuned as the HepG2 cells in the paper don't form masses of cells limiting access to nutrients like spheroids. Our results support the need for continued toxicity studies with increasingly complex culture conditions. First, the muted CYP inducibility we observed in 3D formats is a consequence of the microenvironment and not due to limited accessibility of the AhR inducers 3-MC or TCDD. Second, HepG2 cells in the paper-scaffolds had hepatotoxic responses similar to PHHs when exposed to acetaminophen, cyclophosphamide, and aflatoxin B1 at physiological oxygen tensions. These responses are only plausible with altered metabolic profiles that are consequence of both oxygen and the collagen-rich microenvironment. Our findings demonstrate that while an important cellular regulator, oxygen is not the only factor needed to generate the most liver-like model. For example, transcript profiles under basal

conditions fail to correlate with phase I or II enzyme regulation in vivo. The induction of these genes was, however, similar to in vivo responses at physiological oxygen tensions.

2.2 Materials and methods

2.2.1 Reagents

All reagents were used as received unless otherwise noted. Cell culture medium and supplements were purchased from Gibco, except for fetal bovine serum (FBS, VWR) and collagen I (rat tail, Corning). Acetaminophen, aflatoxin B1, cyclophosphamide, 7-ethoxyresorufin (EROD), and 3-methoxycholanthrene (3-MC) were purchased from Sigma Aldrich. Calcein-AM, DMSO, Hoechst 33342, and propidium iodide (PI) were purchased from Fisher Scientific. TCDD (2,3,7,8-tetrachloro-p-dioxin) was purchased from Alfa Chemistry. CellTiter-Glo 2.0 (CTG) was purchased from Promega.

2.2.2 Cell Culture

HepG2 human hepatoma cells (American Type Culture Collection) were maintained as monolayers at 20% O_2, 37 ^oC, and 5% CO_2 in DMEM medium supplemented with 10% FBS, 1% penicillin-streptomycin, and 22.7 mM HEPES. This maintenance medium was exchanged every 2-3 days and the cells were passed at 75% confluency with TrypLE, using standard procedures. Fresh vials of HepG2 cells were removed from cryopreservation and sub cultured a total of 15 times, experiments were performed on cells between passage five and fifteen. HepG2 cells were STR-verified in 2016 and regularly evaluated for mycoplasma contamination. Experimental studies used standard 96-well plates containing 100 µL of maintenance medium and 40,000 cells/well. The cells were incubated overnight after plating to ensure attachment. Images of the

HepG2 cells seeded in the paper scaffold were imaged using a Zeiss LSM 710 spectral confocal laser scanning microscope. Images, Z-stack slice view and 3D renderings can be found in the **Appendix A.**

2.2.3 3D Culture Preparation

Cell containing regions in sheets of Whatman 105 lens paper were defined by a wax-printed border. The preparation and sterilization of these paper scaffolds was detailed previously by our lab; briefly, wax was printed on both sides of Whatmann 105 lens paper and baked at 99 ^{o}C for 15 minutes. [27,28] The individual paper scaffolds were cut out and sterilized with UV light for one hour. We used two scaffold designs in this work: small zone scaffolds (6.5 mm in diameter) fit directly into the well of a standard 96-well plate. Large zone scaffolds (18 mm in diameter) fit directly into the well of a standard 6-well plate. **Figure 2.1** contains photographs and detailed schematics of both scaffolds. Each scaffold was seeded with either cell-free or cell-laden collagen I (1.2 mg/mL) and incubated overnight before usage. The smaller scaffolds were seeded with 0.5 μL and the larger scaffolds with 12.5 μL of gel. Cell-laden scaffolds had a final density of 80,000 cells/μL ($1.81x10^8$ cell/cm^3). In both formats the wax patterned paper floats at the air-liquid interface of the well plate, minimizing the distance that oxygen needs to travel to the cell surface.

2.2.4 Hypoxia Chamber

Cells were incubated in a home-built hypoxia chamber (**Figure 2.2**). Gas composition was monitored with diffusion-based O_2 (model 2-BTA, Vernier) and CO_2 sensors (model K30, CO2Meter.com). PID controllers (model PXU21A20, Red Lion) monitoring the DC output from

each gas sensor used a low-current solid-state relay to actuate solenoid valves (Red Hat model 8262H020, ASCO) connected to supplies of either 100% N_2 or 100% CO_2. The oxygen controller was set to reverse output mode with the PID parameters P:97, I:150, and D:25. The carbon dioxide controller was set to direct output mode with the PID parameters P:7, I:120, and D:30. The hypoxia chamber was humidified and maintained at 37 ^oC and 5% CO_2 for all experiments. Prior to introducing the cells, the chamber was equilibrated to the appropriate oxygen tension for 18 h. The chambers regulated the gaseous oxygen at 8 and 3% O_2. Equations to describe the oxygen requirements at the cell surface, as described by Al-Ani et al, are described in **Appendix B**. [29]

2.2.5 Cellular Viability

Cellular viability was determined with a live-dead tri-color stain. Cell pellets were collected, resuspended in 100 µL of 1X PBS, and stained for 10 min in a 1X PBS solution containing 10 µg/µL of calcein-AM, 5 µg/µL PI, and 10 µg/µL Hoechst. The stained cells were imaged with a Nikon TE-2000i inverted microscope equipped with a QICAM Fast 1394 digital camera (QImaging). **Figure 2.3** contains representative brightfield and fluorescence images at each oxygen tension. Cell counts were determined with ImageJ using a previously published method, [30] as detailed in the SI.

2.2.6 Dose-Response Curves

Monolayers and small zone scaffolds were dosed for 48 hour in 200 µL of drug-containing medium. These solutions were prepared from stocks of acetaminophen (5 M), aflatoxin B1 (200 mM), and cyclophosphamide (5 M) in DMSO. The stock solutions were stored

at -20 °C until needed. All media contained 1% DMSO (v/v) to account for influence of the vehicle. Prior to analysis, the cells were washed with 1X PBS and lysed for 20 min in a 1:1 (v/v) solution of 1X PBS and CTG. Lysate aliquots (75 µL) were analyzed in an opaque 96-well plate on a Spectramax M5 Multi-Mode Microplate Reader (Molecular Devices) in luminescence mode with a 500 ms integration.

2.2.7 CYP1A Activity Assays

Monolayers and small zone scaffolds were incubated for 48 hour in 200 µL of induction medium: maintenance medium containing either 3-MC or TCDD. Stock solutions of 3-MC (20 mM) and TCDD (100 µM) were prepared in DMSO and stored at -20 °C until needed. All media contained 1% DMSO (v/v) to account for influence of the vehicle. Cells were washed once with 1X PBS and incubated for 1 hour in EROD assay solution: 100 µL of maintenance medium containing 10 µM EROD. Aliquots of EROD assay medium (80 µL) were analyzed in an opaque 96-well plate (560/590 ex/em) on a SpectraMax M5 Multi-Mode Microplate Reader. The remainder of the solution was removed from the cell-containing wells, the cells washed with 1X PBS, and viability measured with CTG.

2.2.8 RT-qPCR Analyses

Monolayers and large zone scaffolds were dosed for 48 hour with maintenance medium containing 3-MC (5 µM), TCDD (1 nM), aflatoxin B1 (10 nM), or acetaminophen (10 mM). Cells were lysed using a TRIzol Plus RNA Purification Kit (Fisher Scientific). The TRIzol reagent was added directly to the monolayer cultures; the cell-containing paper scaffolds were submersed in it. Both culture formats were agitated for 5 minutes at room temperature before

RNA isolation. Reverse transcription (RT) was performed immediately after RNA isolation with a High-Capacity cDNA Reverse Transcription Kit (Fisher Scientific) in an Eppendorf Master Cycler.

Table 2.1 lists the qPCR primer pair sequences, melting temperatures, optimized reaction concentrations, and reaction efficiencies (90-110%) for each primer set. Amplification reactions were performed with PowerUp SYBR Master Mix (Fisher Scientific), in a 384-well plate, on a QuantStudio 6 Flex Real-Time PCR system. Each sample was measured in triplicate, using the following program: 95 ºC for 60 sec, followed by 40 cycles of 95 ºC for 2 sec and 55 ºC for 30 sec. Each transcript was quantified using the $\Delta\Delta C_t$ method against *ACTB* (β-actin).[31] A fold-change of greater than 2.0 was considered significant.

2.2.9 Statistical Analyses

Experiments are reported as the average and standard error of the mean (SEM) of at least two separate cell passes (N); each cell pass contained at least three technical replicates (n). All data were analyzed with GraphPad Prism 7. Dose-response datasets were fit to a four-parameter logistics (4PL) fit, except for aflatoxin B1, which was fit to a three-parameter (3PL) logistics fit. The 4PL fit of the aflatoxin data had an ambiguous lower asymptote due to solubility constraints at the highest concentration. EC_{50} values were compared using an F-test. Statistically significant differences correspond to a *p*-value of ≤ 0.05.

2.3. Results

Figure 2.4 summarizes the experimental workflow used to evaluate hepatotoxicity and induction of phase I and II metabolizing enzymes at the gene and protein level in HepG2 cells.

By simultaneously evaluating monolayer and the paper-based 3D culture setups, we determined the effects of culture dimensionality and oxygen tension in the same passage of cells.
The cells are distributed throughout the paper scaffold in the XYZ axes of the paper. The collagen attaches to the paper fibers and bridges the void space giving the cells an area to grow. As seen in the SI document the HepG2 cells are in higher density in areas where the paper fibers converge, consequently, regions of low paper fiber density also gives rise to regions of lower cell density. Within the paper scaffold, the HepG2 cells can grow in higher density allowing for superior cell-cell and cell-ECM interaction as compared to 2D cultiures. The HepG2 cells can be visualized in SI, where the cellular actin and nuclei were are stained with phalloidin and DRAQ5, respectively.

2.3.1 Cell viability is not impacted by physiological oxygen tensions

Cell viability was assessed after a 48 hour incubation at each oxygen tension. Monolayer cultures were stained with calcein-AM, Hoechst 33342, and PI. **Figure 2.3** contains representative brightfield and fluorescence images of the HepG2 cells at each oxygen tension. Eqn. 1 summarizes the two ratios used to calculate the fraction of viable cells, where n_{live} is the number calcein-stained cells, n_{dead} is the number of PI-stained cells, and n_{total} is the number of Hoechst-stained cells.

$$\text{Fraction Viable Cells} = \left(1 - \frac{n_{\text{dead}}}{n_{\text{total}}}\right) \approx \left(\frac{n_{\text{live}}}{n_{\text{live}} + n_{\text{dead}}}\right) \qquad \text{Eqn. 1}$$

The fractions of viable cells at each oxygen tension were equivalent for the PI staining ratio, with an average of 0.94 +/- 0.01. The average calcein staining ratios at 20% and 8% O_2 were similar (0.90+/- 0.01) and confirmed with the PI staining data. The calcein stain at 3% O_2, however, indicated a significant drop in viability (0.42 +/- 0.01). Kang reported calcein viability was 40-

50% lower than PI at oxygen tensions less than 2% O_2. [32] They attributed this difference to decreased esterase availability or an impaired metabolic activity rather than truly reduced cell viability. **Table 2.2** summarizes the viability data for each oxygen tension. We relied on the PI staining data and assumed oxygen tension did not significantly affect viability.

2.3.2 Oxygen tension alters the potency and mechanism of action of hepatotoxic agents

Dose-response relationships of the hepatoxic drugs acetaminophen (1–200 mM), cyclophosphamide (1–100 mM), and aflatoxin B1 (0.001–200 nM) were determined at each oxygen tension. The concentration ranges were based on previously reported potency (EC_{50}) values.[33,34] Cell viability was compared to vehicle treatments, identical setups containing 1% (v/v) DMSO.

Acetaminophen was equally hepatoxic in the monolayer and 3D culture formats (**Figure 2.5**), with 200 mM killing 100% of the cells exposed at each oxygen tension. The potency of acetaminophen increased significantly in both culture formats when transitioning from standard culture conditions to physiologically relevant oxygen tensions. In 2D, the potency increased from 21.7 mM at 20% O_2, to 13.9 mM at 8% O_2, and 14.3 mM at 3% O_2. In the 3D cultures the potency changed from 27.0 mM at 20% O_2, to 8.4 mM at 8% O_2, and 18.4 mM at 3% O_2. While the potency values at between 8% and 3% were not statistically significant, the data does suggest an increased rate of accumulation for acetaminophen's cytotoxic byproduct, *N*-acetyl-p-benzoquinone imine (NAPQI) compared to 20%.

Figure 2.6 displays that oxygen tension had a significant effect on the metabolism of aflatoxin B1 and cyclophosphamide in the 3D culture format. For aflatoxin B1, the overall toxicity after a 200 nM exposure decreased from 100% at 20% O_2, to 89% at 8% O_2, and 56% at

3% O_2. The potency also significantly increased with decreasing oxygen concentration, with EC_{50} values of 21.1 nM at 20% O_2, 4.1 nM at 8% O_2, and 1.9 nM at 3% O_2. Cyclophosphamide had a clear trend of decreasing toxicity with decreasing oxygen tension, from 100% at 20% and 8% O_2, to 69% at 3% O_2. The potency values of cyclophosphamide did not match these trends, with statistically equivalent values at 20% (21.7 mM) and 3% (24.1 mM) O_2, but a significantly increased potency at 8% O_2 (10.0 mM). **Figures 2.7** and **Figure 2.8** display dose-response relationships for both the monolayer and 3D culture formats. **Tables 2.3** summarizes the statistical differences of EC_{50} values for each drug, culture condition, and culture format. This data suggests that at lower physiological oxygen the HepG2 cells are able to evade toxicity of both aflatoxin B1 and cyclophosphamide; however the mechanism of this is unclear.

2.3.3 Oxygen tension alters transcriptional regulation in response to toxins, supporting altered mechanisms of action

Transcript-level regulation of eight phase I and phase II enzymes was quantified with RT-qPCR. We chose *CYP1A1* and *CYP1A2* because they are readily inducible in HepG2 cells;[14,35] *CYP2E1* due to its low inducibility in monolayers at 20% O_2; [35–37] and SULT and UGT enzymes because of their known contributions to acetaminophen metabolism and their presence in HepG2 cells.[3] We also quantified the aryl hydrocarbon receptor (*AhR*), which is known to regulate the expression of CYP1A family.

The effect of culture conditions on the basal transcript profiles of HepG2 cells are summarized in **Figure 2.9**. These data highlight that culture format differentially regulates transcription when exposed to decreasing oxygen tensions. In the monolayer cultures (**Figure 2.9a**), each drug-metabolizing gene at 8% O_2, except for *SULT1A1* which remained unchanged, was upregulated compared to 20% O_2. In contrast, there was a significant decrease in transcript

levels when transitioning from 8% to 3% O_2, with a decrease in all genes except for *UGT1A1*, which remained unchanged. In the 3D cultures (**Figure 2.9b**), the transcript profiles at 8% and 3% O_2 were similar, with an overall upregulation of *CYP2E1*, *UGT1A1*, and *AhR* compared to 20% O_2. There also was a general downregulation in SULT1A1, *SULT1A2*, and *SULT1E1* compared to 20% O_2. The 3% O_2 environment also downregulated *UGT1A6* and *CYP1A2* which were unaffected at 8% O_2.

Figure 2.9c highlights the dramatic changes in regulation that occur between the 2D and 3D formats, with *CYP1A1*, *CYP1A2*, *UGT1A1*, and *UGT1A6* upregulated in 3D across all three oxygen tensions. At 20% O_2 *CYP2E1* and *AhR* were downregulated and *SULT2A1* and *SULT1E1* were upregulated in 3D. At 8% O_2 SULT1A1 and SULT1E1 were downregulated while *CYP2E1* was upregulated in 3D. At 3% O_2, *SULT2A1* and *AhR* were upregulated. Similar to Kim and colleagues, who compared PHH monolayers and collagen sandwich cultures [38], we observed transcriptional upregulation in the 3D culture format. Furthermore, our data suggests that transcriptional upregulation in 3D culture as compared to the monolayers, at atmospheric oxygen, is also observed at physiological oxygen. However, changing physiological oxygen tension prompts more nuanced transcriptional regulation of the CYP, UGT, and SULT enzymes.

Figure 2.10 maps transcriptional regulation in the 3D cultures at each oxygen tension, after a 48 hour exposure to acetaminophen (10 mM), aflatoxin B1 (10 nM), 3-MC (5 μM), or TCDD (1 nM). The AhR ligands 3-MC and TCDD are expected to upregulate the CYP1A and UGT1 family of enzymes as well as *SULT1A1*, and *SULT2A1.* In 3D, CYP1A2, *SULT1A1*, and *SULT1E1* were upregulated at 20, 8 and 3% O_2. In monolayer cultures, 3-MC and TCDD upregulated *CYP1A1* and *CYP1A2* at all three oxygen tensions (**Figure 2.11**) and are consistent with previous findings. [3,39,40]

Acetaminophen exposure shows that transcriptional regulation is dependent on the culture format (**Figure 2.12**). At 20% O_2, there was more CYP and UGT transcript in the 2D cultures. At 8% O_2, there was significantly more CYP, UGT and SULT transcript in the 3D cultures, suggesting an increased sensitivity at periportal oxygen tensions. Lastly, at 3% O_2, there was similar CYP transcripts between both culture dimensionalities, but more UGT and SULT transcript in the 2D cultures. The comparison of transcript amounts between 3D and 2D culture formats suggest that the responsiveness to the HepG2 cells to external stimuli is modulated by the extracellular environment.

Both 3-MC and TCDD differentially induced genes as oxygen tension decreases, suggesting that transcriptional regulation is fine-tuned by factors related to oxygen sensing and energy production. Specifically, 3-MC and TCDD induced more phase II enzymes at 8% O_2 while at 3% O_2 more CYPs are upregulated. The differential gene expression changes at different oxygen tensions are most pronounced in the presence of acetaminophen. In 3D at 20% O_2, acetaminophen upregulated *UGT1A1*, *UGT1A6*, *SULT1A1* and *AhR*. At physiological oxygen acetaminophen had a much different effect. At 8% O_2 nearly every gene measured was affected: *CYP1A1*, *SULT2A1* and *AhR* were downregulated; *CYP1A2*, *CYP2E1*, *UGT1A6*, *SULT1A1* and *SULT1E1* were upregulated. At 3% O_2 acetaminophen downregulated *CYP1A1*, *UGT1A1*, *UGT1A6*, *SULT2A1*, and *SULT1E1*. To our knowledge, no one has reported differentially induce genes at various physiological oxygen tensions as we have described; however, there is precedent of differential expression in vivo in a rabbit study. Audibert and colleagues observed reduced drug metabolism when exposing rabbits to hypoxemia (50 mmHg O_2).[41] Audibert explains that the reduced oxygen environment could be changing how drug is distributed and metabolized due to the reduction of CYP activity.

2.3.4 CYP1A activity was reduced at physiological oxygen and in 3D culture formats

Following a 48 hour exposure to increasing concentrations of either 3-MC or TCDD, CYP1A activity was quantified with a 1h EROD assay. CYP1A activity per live cell was calculated with Eqn. 2, where I_{EROD} is the average raw fluorescence intensity collected from replicate EROD assays and I_{CTG} is the vehicle-normalized luminescence values collected from the CTG assay; this normalization accounted for potential changes in viability caused by induction.

$$\text{CYP1A activity per live cell} = \frac{I_{\mathrm{EROD}}}{I_{\mathrm{CTG}}} \qquad \text{Eqn. 2}$$

Figure 2.13a plots the raw fluorescence values corresponding to the basal CYP1A activity for the monolayer and 3D cultures at each oxygen tension. We attribute the large variability to low basal activity levels. These results show that culture format and oxygen tension did not significantly alter CYP1A activity. **Figure 2.13b** is a heatmap of CYP1A activity per live cells at each oxygen tension. Both 3-MC and TCDD significantly induced activity in the 2D cultures at 20% O_2, matching the results reported previously.[42] TCDD also induced CYP1A activity at 3% O_2 at all concentrations, but only at 1 nM and 10 nM at 8% O_2. Similar trends were observed for 3-MC.

Induction in the 3D culture format was muted at each oxygen tension, when compared to the 2D cultures. At 20% O_2, 1 nM TCDD induced activity by 2.05-fold in 3D whereas the same concentration resulted in a 12.98-fold increase in 2D. 3-MC was able to induce CYP1A activity at 3D 20% O_2 only at 5 μM. Both 3-MC and TCDD were unable to induce activity at 8% and 3% O_2. **Table 2.4** lists the induction average for each culture condition and format.

2.4. Discussion

Despite the improved predictability of spheroids and liver-on-chip devices,[43,44] there is not a 3D culture platform that can easily assess microenvironmental impacts on liver zonation and the regulation of drug metabolizing enzymes. Such studies are needed to improve the predictability of current in vitro assays, identifying the minimal number of structural and chemical components to generate a functional sinusoid, lobule, or liver. In a recent review, Agarwal highlighted the potential of paper-based scaffolds for generating 3D liver models.[45] The current work highlights the paper-based culture platform and its ability to characterize extracellular gradients and microenvironmental factors on cellular regulation and zonation. Our results show that both the culture format and culture condition influence the expression and activity of phase I and II enzymes involved in drug metabolism. This work is the first of many such studies needed to systematically evaluate different aspects of the liver microenvironment by probing culture parameters individually or in combination.

2.4.1 Relation of physiological oxygen to CYP1A

CYP1A activity at 20% O_2 in the presence of 1 nM TCDD, highlights the significant effects of incorporating ECM with a 7.5-fold reduction in 3D (2-fold increase) compared to 2D (13-fold increase, **Figure 2.13b**). Muted CYP1A inducibility was also observed by Vrba and colleagues in HepG2 cultures,[42] with 5 nM TCDD inducing a 52-fold increase in 2D and a 3-fold increase in spheroids. This muted CYP1A activity is not inherent to 3D culture format alone, as basal activity is statistically equivalent between the two culture formats (**Figure 2.13a**). Similarly, CYP1A transcript induction with 3-MC and TCDD is less in 3D than in the 2D culture

format. This transcriptional inequality suggests that monolayers are more sensitive to induction possibly due to differences in cellular energy allocation between the two formats (**Figure 2.12**).

A comparison of cellular responses to 3-MC and TCDD also showed muted inducible activity for the physiological oxygen when compared to atmospheric oxygen at the same culture dimensionality (e.g., 2D 20% O_2 compared to 2D 8% O_2) (**Figure 2.13b**). These datasets suggest that incorporating extracellular matrix mimics small molecule delivery in tissues, by reducing exposure through non-specific adsorption and degradation in the extracellular environment. Both of these parameters are molecule dependent, but the similar potency and toxicity values of acetaminophen between the monolayer and 3D cultures suggest the cells are experiencing similar effective concentrations.

2.4.2 Responses of HepG2 cells at physiological oxygen concentrations are similar to PHHs

The dose-response curves in **Figure 2.5** and **Figure 2.6** highlight oxygen-dependent mechanisms of action. These data suggest that cellular responses at physiological oxygen tensions should be included in toxicological studies, as they could better predict risks of drug-drug interactions and drug-induced liver toxicity. Acetaminophen is a prototypical drug used to evaluate hepatoxicity.[14,46] Our results align well with these previous studies in both 2D and 3D culture formats, and support the continued use of paper-based scaffolds to evaluate drug-induced toxicity. This data also supports the further investigation of these oxygen-dependent mechanisms, which have clear consequences on predictions of acetaminophen potency.

Evaluating 3D cultures at physiologically relevant oxygen tensions is a logical next step to generate a liver model with improved metabolic competency. Direct comparisons of the HepG2 results to in vivo function is difficult, however PHHs are an attractive benchmark for the

potential of using HepG2 cells to preliminarily assess physiologically relevant conditions on hepatotoxicity as PHHs are the gold standard for in vitro studies of cellular induction, metabolism, and toxicity. When cultured as monolayers at 20% O_2, HepG2 cells have limited expression and induction of phase I and II enzymes when compared to PHHs. We found that HepG2 cells in a collagen-rich environment and physiologically relevant oxygen tension (8% or 3% O_2) have markedly different responses to inducers and hepatotoxic compounds. The acetaminophen potency values we obtained align with previous reports of PHHs in collagen sandwiches (10 mM) or spheroids (>10.0 mM).[47,48]

The altered dose-response relationship for acetaminophen for 3D cultures exposed to 3% O_2 suggests an oxygen-dependent access to a different mechanism of action than at 20% O_2. Acetaminophen toxicity is due to the accumulation of NAPQI, which forms protein adducts that lead to oxidative stress-induced cellular necrosis from glutathione (GSH) depletion.[49]. At 3% O_2, acetaminophen downregulation of UGT and SULT enzyme transcripts suggests metabolism is primarily accomplished by CYPs resulting in gradual NAPQI-protein adduction at low doses. Our observations are supported by Hinson, who showed NAPQI-protein adduct accumulation is localized around the perivenous region and spreads radially with continued exposure.[49,50]

2.4.3 HepG2 potency values for cyclophosphamide and aflatoxin B1 at physiological oxygen tensions are similar to PHHs

2.4.3.1 Cyclophosphamide

When placed in the 3D culture format, the cyclophosphamide potency values for the HepG2 cells at atmospheric (21.7 mM) and perivenous (24.1 mM) oxygen tensions were similar to those recorded for PHHs at 20% O_2 (25 mM).[51] The decrease in the overall toxicity and altered shape of the dose-response relationship between 20% and 3% O_2 suggest there is an alternative mechanism of action despite the similar potency values.

The changed shape of the dose response curve shapes can be explained by the ability for oxygen to dissolve into the culture. Al-Ani et al. explained oxygen diffusion into a culture as defined by Fick's first law. [29] In **Appendix B**, we calculated the oxygen consumption on the surface of the cells at each of the oxygen tension. At 20 and 8% O_2 the cell-surface oxygen at the bottom of the 96-well plate was above the required oxygen requirements of the cells. At 3% O_2 the cell-surface oxygen was insufficient likely resulting in an anoxic environment. The reduced oxygen availability for the HepG2 cell in the 3% O_2 environment could influence the method in which the cells metabolize cyclophosphamide and aflatoxin B1. Although the anoxic environment could explain the changed dose response curve shape between 20% and 3% O_2 in the traditional 2D set up, this doesn't explain the 3D culture method because the scaffold floated at the air-liquid interface. This means that distance the oxygen must diffuse to reach the cell-surface interface is much less resulting in cell-liquid oxygen tension similar to the gaseous oxygen tension.

One possible explanation for the difference between 20% and 3% O_2 is in the way the HepG2 cells metabolize the cyclophosphamide. Cyclophosphamide is metabolized to an active

4-hydroxycyclophosphamide which is further metabolized to toxic metabolites phosphoramide mustard, a DNA-alkylating agent,[52] and acrolein under anaerobic conditions.[53] At low oxygen, the change of dose response curve shape and the shifting metabolic enzyme expression/activity levels, may change the metabolism and detoxification of cyclophosphamide; one possibility is the metabolic ratio of phosphoramide mustard and acrolein change at the different physiological oxygen tensions which we observed as different EC_{50} values. The mechanical difference between 2D and 3D across different oxygen tensions should be further explored and compared to the mechanism of action of cyclophosphamide in PHHs.

2.4.3.2 Aflatoxin B1

The measured potency of aflatoxin B1 in the 3D culture format at both 8% and 3% O_2 was less than 4.5 μM, a value that agrees with previously reported EC_{50} values for PHHs on collagen-coated plates at atmospheric oxygen tensions:10.8 μM[54] and 4.7- 20 μM.[51] Aflatoxin B1 has several different mechanisms of action. The primary mechanism of action relies on CYP3A4 and CYP1A2 metabolizing aflatoxin B1 into aflatoxin B1-8,9-epoxide (AFBO). AFBO forms amine adducts with proteins and DNA.[55] AFBO also activates cellular death receptors culminating in apoptosis.[56]

The difference in cellular response between 8% and 3% O_2 suggests hepatocytes are metabolizing aflatoxin B1 differently. In 8% O_2, *CYP1A2* transcript is induced by aflatoxin B1 suggesting the mechanism of actions is via AFBO. At 3% O_2, aflatoxin B1 fails to significantly induce CYP transcription, resulting in a measured span of about 50%. The 50% span suggests that aflatoxin B1 is a less effective toxin in a 3% O_2 tension. Further transcript analysis suggests there is an oxygen-dependent shift in hepatocyte response. At 8% O_2, aflatoxin B1 induced

SULT enzyme transcripts; at 3% O_2, however, the SULT enzyme transcript remains unchanged (**Figure 2.10**). Although aflatoxin B1 isn't metabolized by SULT enzymes, aflatoxin B1 has been shown to activate the nuclear pregnane X receptor, resulting in the upregulation of SULTs.[57,58] The oxygen-dependent shift in cellular response to the drug indicates the possibility of drug-drug interactions not observed at atmospheric conditions.

2.5 Conclusion

The datasets collected here further support previous works that inclusion of an ECM reduces the inducibility of HepG2 cells while also sensitizing them to certain drugs. The data also highlights the importance of evaluating physiologically relevant oxygen tensions as an important step in generating a more predictive liver model, as evidenced by HepG2 potency measurements better matching observations in PHHs. While this study uses HepG2 cells, which are not an ideal surrogate for PHHs, the work highlights that small changes in culture conditions can improve some aspects of metabolic regulation and activity. Our results showed that responses to drugs are dependent on oxygen tension, offering insights to potential liver-induced injuries or drug-drug interactions that would be overlooked under standard culture conditions.

Our results also highlight that oxygen can improve some aspects of hepatic response, but it is not the only microenvironmental factor needed to obtain zonal expression of phase I and II enzymes. Zonation is marked by expression of SULT enzymes under periportal conditions and UGT enzymes under perivenous.[22] Our datasets lacked these basal level expression trends in both 2D and 3D culture formats (**Figure 2.9**). The paper-based culture platform is amenable to other studies into the microenvironment-cell function relationships. The ability to rapidly prototype and evaluate different paper-based structures, as demonstrated by our lab and others,

provides a means to not only test individual parameters as in this work but also can generate gradients of oxygen and nutrients similar to those found in vivo. The incorporation of gradients may provide representative responses to change in oxygen tension and perhaps more insight into in vivo happenings.

2.6 Figures and tables

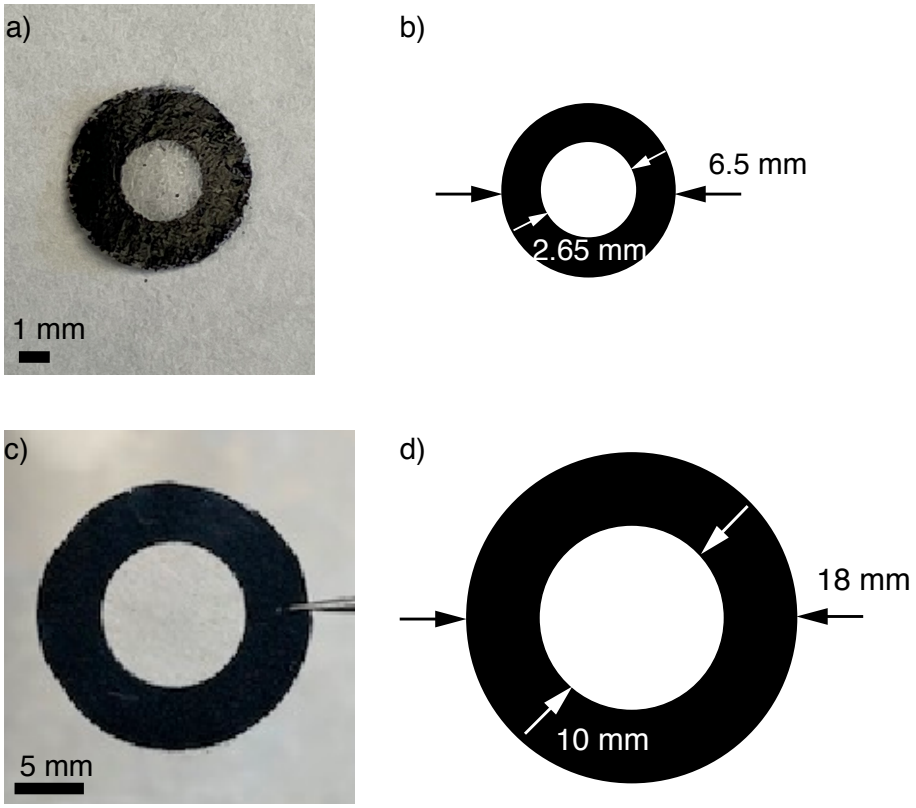

Figure 2.1. Photographs and schematics of the small and large zone paper scaffolds used in this work. Both scaffolds were drawn with Adobe Illustrator. The designs were patterned onto Whatman 105 lens paper with a Xerox ColorQube 8650 wax printer.(a,b) Photograph and schematic of a small zone scaffold, which contained a 2.65 mm seeding region surrounded by a 1.925 mm thick border. (c,d) Photograph and a schematic of a large zone scaffold, which contained a 10 mm seeding region surrounded by a 4 mm thick border.

a.

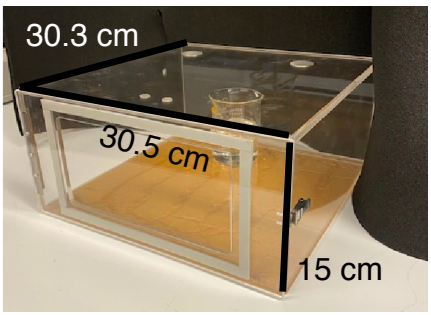

b.

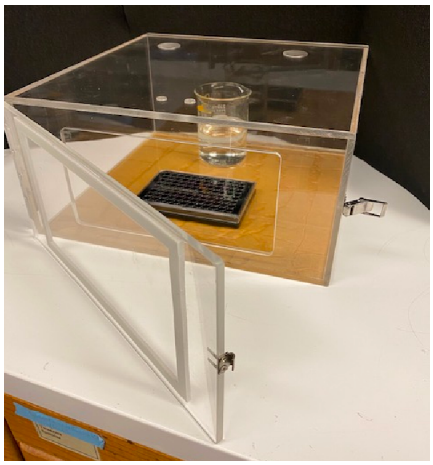

c.

Figure 2.2. Photographs of a hypoxia chamber assembled from 0.635 cm-thick cast acrylic sheets. The chamber dimensions are (a) 30.5 x 30.3 x 15 cm. (b) A latched door on the front face (20.3 x 10.3 cm) was used to load and unload samples. The door was fitted with a 0.32 x 0.95 cm (W x H)

thick foam gasket to form an airtight seal. (c) The top face contained two 2.9 cm-diameter holes, where CO_2 and O_2 gas sensor were mounted.

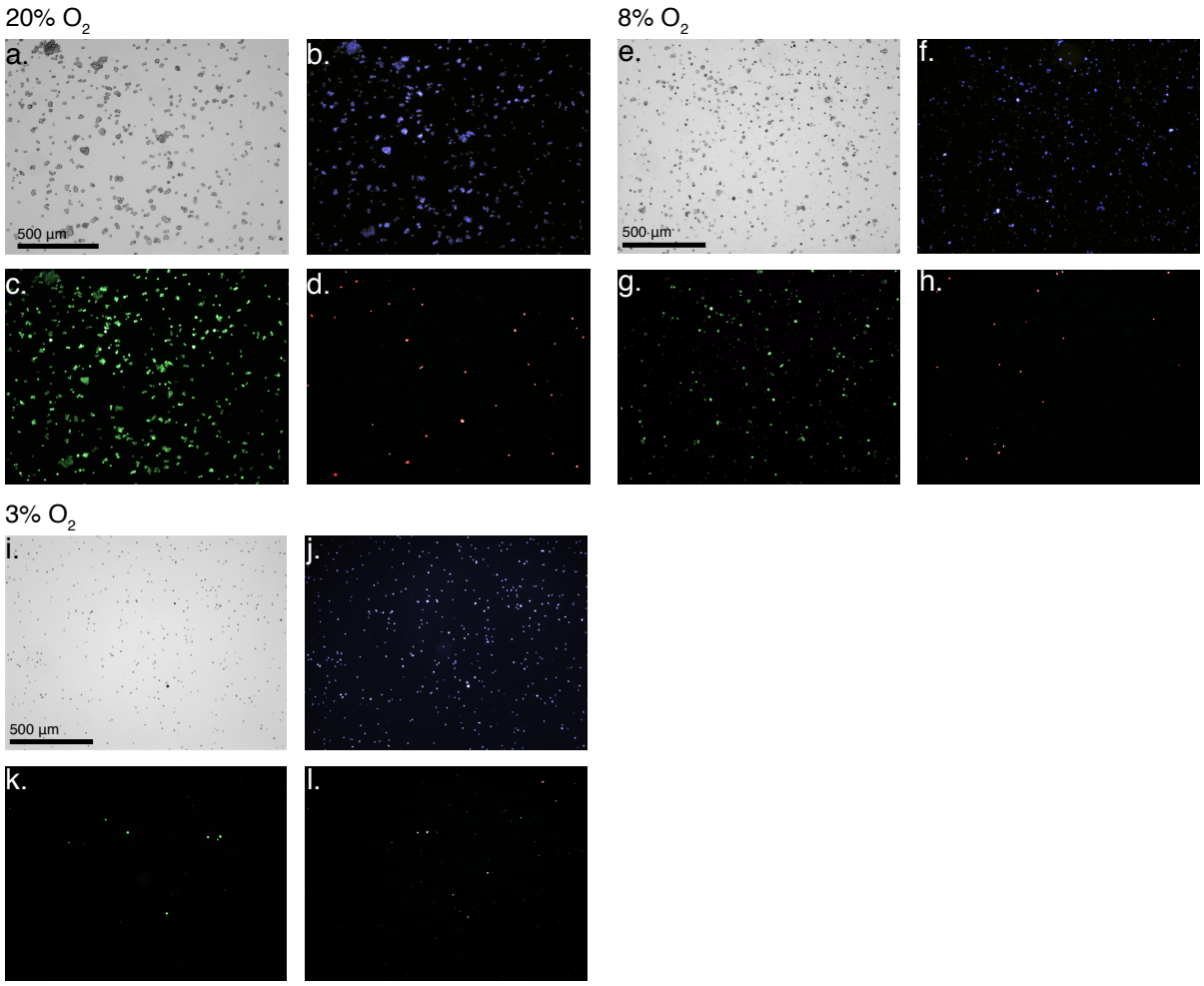

Figure 2.3 Representative images of HepG2 cells stained with calcein-AM, PI, and Hoechst 33342 after a 48 hour exposure to 20% (a-d), 8% (e-h) or 3% (i-l) O_2.

Image acquisition: Calcein-labeled cells were imaged with a filter cube containing a 470 ± 20 nm excitation filter, a 525 ± 25 nm emission filter, and a 495 nm dichroic mirror. PI-labeled cells were imaged with a filter cube containing a 560 ± 20 nm excitation filter, a 630 ± 35 nm emission filter, and a 585 nm dichroic mirror. Hoechst-labeled cells were imaged with a filter cube containing a 350 ± 22 nm excitation filter, a 460 ± 25 nm emission filter, and a 400 nm dichroic mirror. Images were collected with a 10x objective and 1x eyepiece. All fluorescence images collected with a 1000 ms integration time.

Image analysis: Each images was analyzed with ImageJ with a process previously described by Schneider. [30] First, images were thresholded using Otsu method. Next, particles in close proximity were separated using a watershed process. Lastly, the cells were analyzed using 'analyze particles' function with a size setting of 10-inifinte pixel range and 0-1.00 circularity range. Cell count values were used in equation 1 to determine cell viability.

Table 2.1. Table of primer sequences for qPCR

Gene	Forward Primer (5' – 3')	Tm (°C)	Reverse Primer (5' – 3')	Tm (°C)	Conc. (nM)	Efficiency (%)
β-Actin	CTGGCACCCAGCACAATG	57.1	GCCGATCCACACGGAGTACT	59.1	800	99.28
GAPDH	GAGTCCACTGGCGTCTTCAC	62.1	GGTGCTAAGCAGTTGGTGGT	65.5	800	115.36
CYP1A1	GCACAGAGGTAGTCTCACTGCTTG	59.3	AAGGGCAGAGGAATGTGATGTT	56.7	600	102.06
CYP1A2	CTTCGGACAGCACTTCCCTG	62.2	AGGGTTAGGCAGGTAGCGAA	65.7	400	119.44
CYP2E1	TTGAAGCCTCTCGTTGACCC	61.6	CGTGGTGGGATACAGCCAA	65.0	600	98.61
CYP3A4	CTTCATCCAATGGACTGCATAAAT	53.6	TCCCAAGTATAACACTCTACACAGACAA	57.1	100	97.37
UGT1A1	TGACGCCTCGTTGTACATCAG	61.0	CCTCCCTTTGGAATGGCAC	63.8	400	98.57
UGT1A6	AGCCCAGACCCTGTGTCCTA	64.4	CCACTCGTTGGGAAAAAGTCA	60.2	400	107.17
SULT1A1	GTCACCGAGCTCCCATCTTC	61.7	GTCTCCATCCCTGAGGGAATC	61.1	200	97.66
SULT1E1	TGGTGGCTGGTCATCCAAA	61.3	GAACCTGTCCTTGCATGAATTTC	59.7	200	105.26
SULT2A1	TCCAGTTATTCCCCAAGTCTTTCT	61.1	AAACATCTCTGGGATTTCTCATGAG	60.2	600	95.41
AhR	ACATCACCTACGCCAGTCGC	64.1	TCTATGCCGCTTGGAAGGAT	64.3	600	86.27

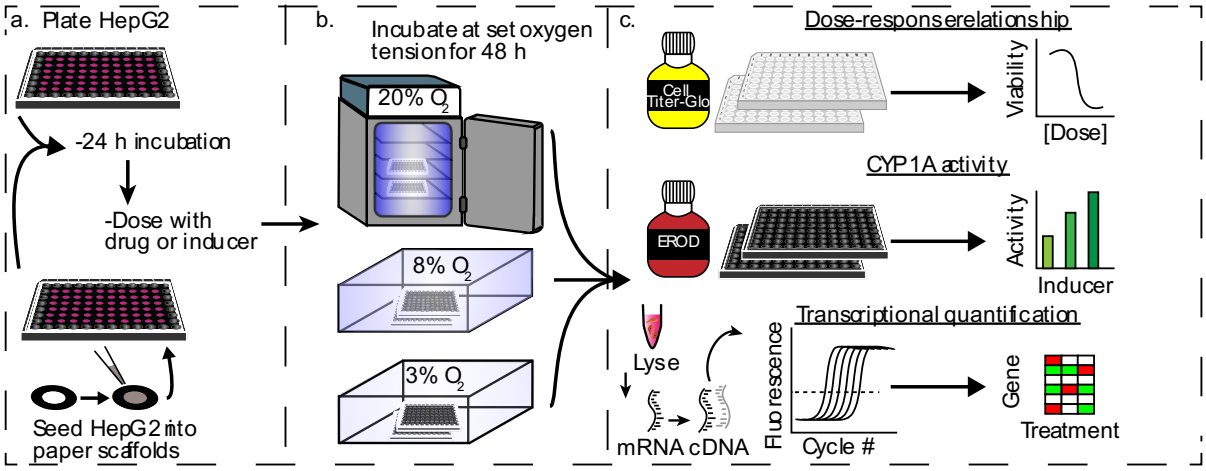

Figure 2.4 Experimental workflow comparing the responses of HepG2 cells exposed to different oxygen tensions where cells were maintained as monolayer on standard culture plasticware or were suspended in a collagen I matrix and seeded into a paper-based scaffold. (a) First, cells were placed in the appropriate culture format and incubated for 24 hour under standard culture conditions (20% O_2, 5% CO_2, and 37 ^oC). (b) Next, the cells were incubated in the presence of a drug or inducer for 48 hour at 37 ^oC, 5% CO_2 and either 20, 8 or 3% O_2. (c) Finally, hepatotoxicity was evaluated with the CellTiter-Glo viability assay, CYP1A activity quantified with the EROD assay, and transcriptional regulation was determined with RT-qPCR.

Table 2.2 Percentage of viable cells at each oxygen tension.[a]

	20% O_2	**8% O_2**	**3% O_2**[b]
Percentage live FDA/(FDA+PI)	89.9 +/- 3.5	90.9 +/- 2.0	42.4 +/- 13.9
Percentage not dead 1-(PI/Hoechst)	89.7 +/- 3.9	94.0 +/- 1.4	97.2 +/- 0.7

[a] Cells were stained with a combination of calcein-AM, PI, and Hoechst 33342.

[b] At 20 and 8% O_2 both viability calculations, percent live and percent not dead, were statistically equivalent. However, the percent live calculation for 3% O_2 isn't equivalent to the percentage not dead; this observation has been observed by Kang et al. who stained hepatocytes with Calcein-AM along an oxygen gradient (6.9% and 0.3% O_2). At low oxygen tensions the 40-50% of the cells did not stain with Calcein-AM.

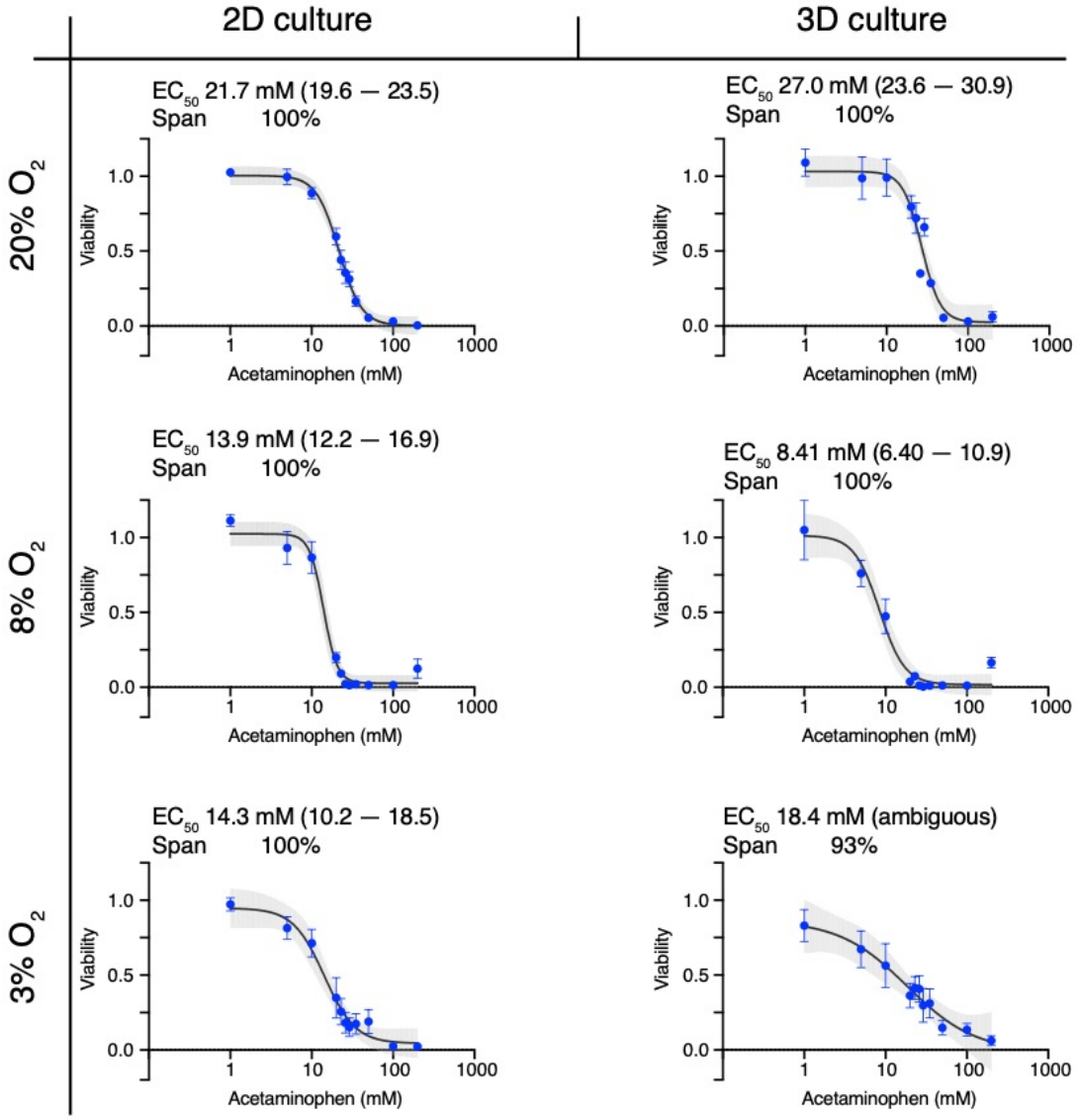

Figure 2.5. Dose-response relationships for a 48 hour exposure of 40,000 HepG2 cells in monolayer (left) or 3D (right) cultures to acetaminophen at atmospheric (20%), periportal (8%), or perivenous (3%) oxygen tensions. Each point is the average and SEM of at least six data points collected from different cell passages (N=2); each pass contained at least three technical replicates

(n=3). The black lines connecting the points represent the best-fit 4PL model; the gray shaded regions represent the 95% confidence intervals of those fits.

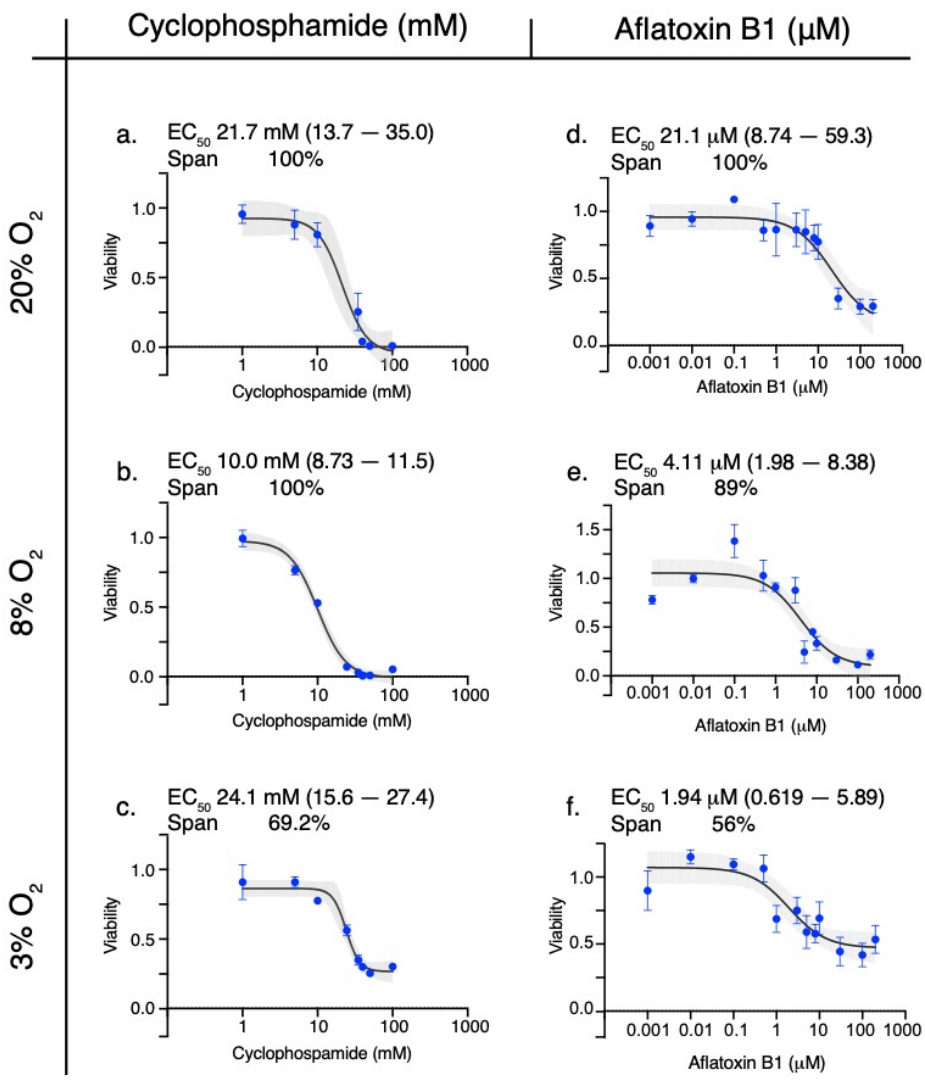

Figure 2.6. Dose-response relationships for a 48 hour exposure of 40,000 HepG2 cells in 3D culture format to either cyclophosphamide (a-c) or aflatoxin B1 (d-f) at atmospheric (20%), periportal (8%), or perivenous (3%) oxygen tensions. Each point is the average and SEM of at least six data points collected from different cell passages (N=2-3); each pass contained at least three technical replicates (n=3). The black lines connecting the points represent the best-fit 4PL model (cyclophosphamide) and 3-PL model (aflatoxin B1); the gray shaded regions represent the 95% confidence intervals of those fits.

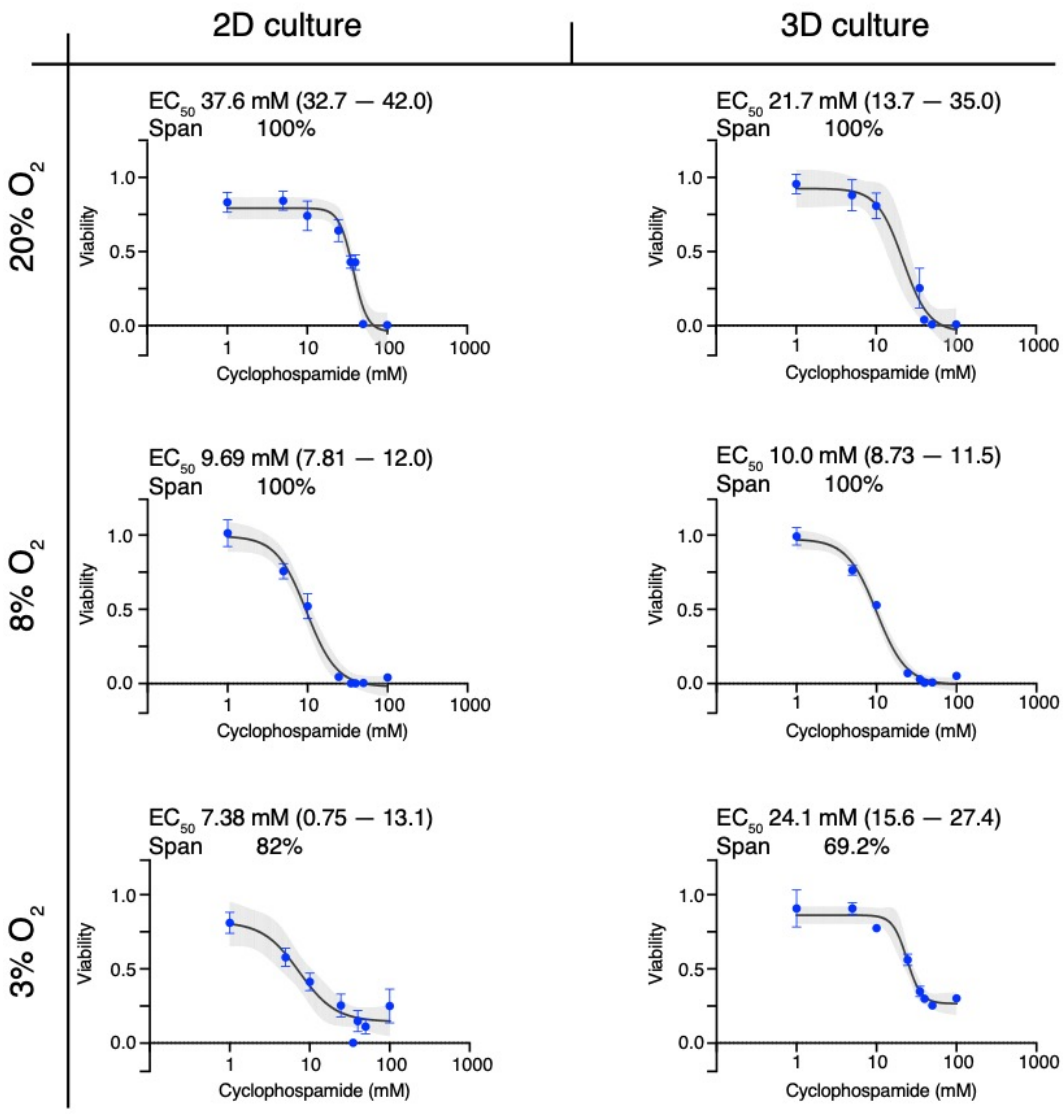

Figure 2.7. Dose-response relationship of a 48 hour exposure of 40,000 HepG2 cells in monolayer (left) or 3D (right) cultures to cyclophosphamide at atmospheric (20%), periportal (8%), or perivenous (3%) oxygen tensions. Plotted points are the average and SEM of at least six data points collected from different cell passages (N=2-3) with each pass containing at least three technical

replicates (n=3). The black lines connecting the points represent the best-fit 4PL model and the gray shaded areas represent the 95% confidence intervals of those fits.

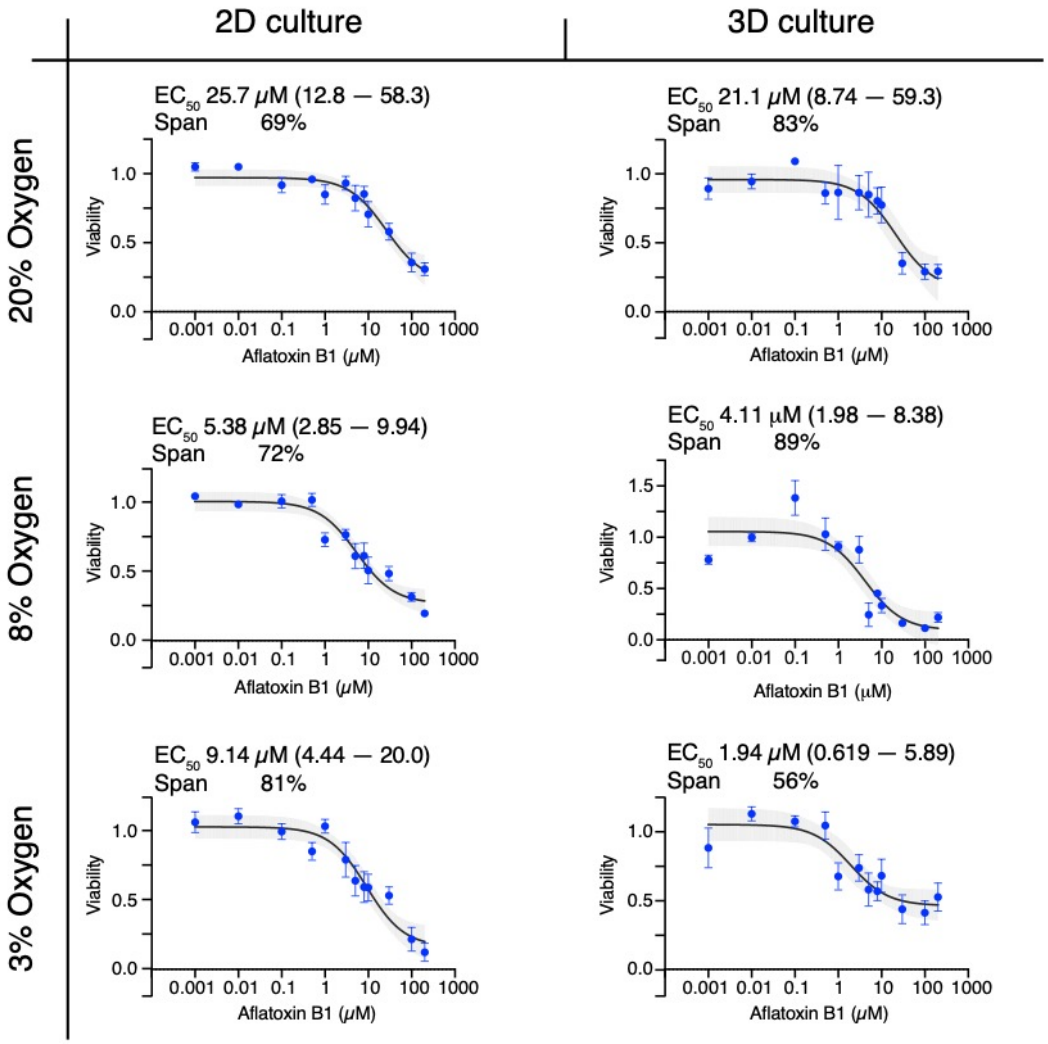

Figure 2.8. Dose-response relationship of a 48 hour exposure of 40,000 HepG2 cells in monolayer (left) or 3D (right) cultures to aflatoxin B1 at atmospheric (20%), periportal (8%), or perivenous (3%) oxygen tensions. Plotted points are the average and SEM of at least six data points collected from different cell passages (N=2-3) with each pass containing at least three technical replicates (n=3). The black lines connecting the points represent the best-fit 3 PL model and the gray shaded areas represent the 95% confidence intervals of those fits.

Table 2.3. Statistical comparison of EC_{50} between culture conditions and oxygen tensions.[a]

EC_{50} Acetaminophen F-Test

2D 20% O_2	**2D 8% O_2**	**2D 3% O_2**	**3D 20% O_2**	**3D 8% O_2**	**3D 3% O_2**	
	*	*	*			2D 20% O_2
		NS		*		2D 8% O_2
					NS	2D 3% O_2
				*	NS	3D 20% O_2
					NS	3D 8% O_2
						3D 3% O_2

EC_{50} Cyclophosphamide F-Test

2D 20% O_2	**2D 8% O_2**	**2D 3% O_2**	**3D 20% O_2**	**3D 8% O_2**	**3D 3% O_2**	
	*	*	*			2D 20% O_2
		NS		NS		2D 8% O_2
					*	2D 3% O_2
				*	NS	3D 20% O_2
					*	3D 8% O_2
						3D 3% O_2

EC_{50} Aflatoxin B1 F-Test

2D 20% O_2	**2D 8% O_2**	**2D 3% O_2**	**3D 20% O_2**	**3D 8% O_2**	**3D 3% O_2**	
	NS	NS	NS			2D 20% O_2
		*		NS		2D 8% O_2
					*	2D 3% O_2
				*	*	3D 20% O_2
					NS	3D 8% O_2
						3D 3% O_2

[a] One star indicates a P-value <0.05. NS indicates not significant.

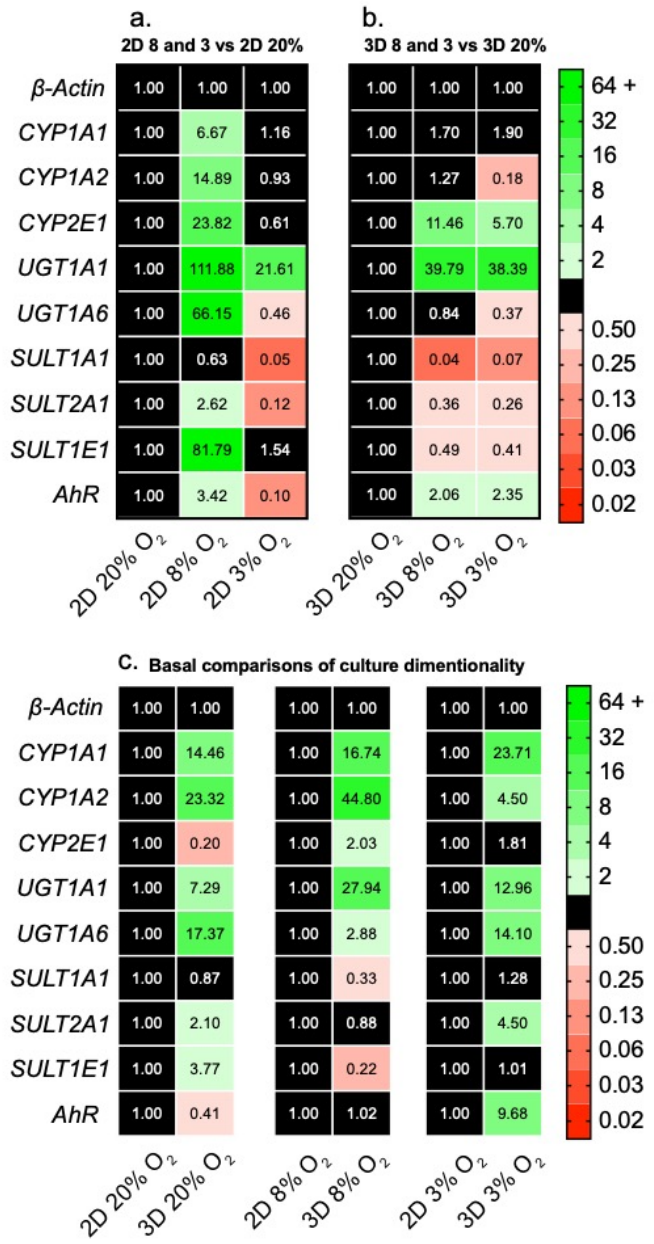

Figure 2.9. Transcript-level regulation of phase I and phase II genes in HepG2 (a) monolayer and (b) 3D cultures after a 48 hour exposure to 20%, 8%, or 3% O2. (c) Transcript-level regulation between monolayer and 3D culture formats at each oxygen tension. Each value is the average of

at least four datapoints, collected from N=2-3 cell passages. Each pass contained at least three technical replicates (n=3). A fold-change >2 indicates a significant increase in expression; <0.50 indicates a significant decrease. The numerical labels represent the average ΔΔCt value.

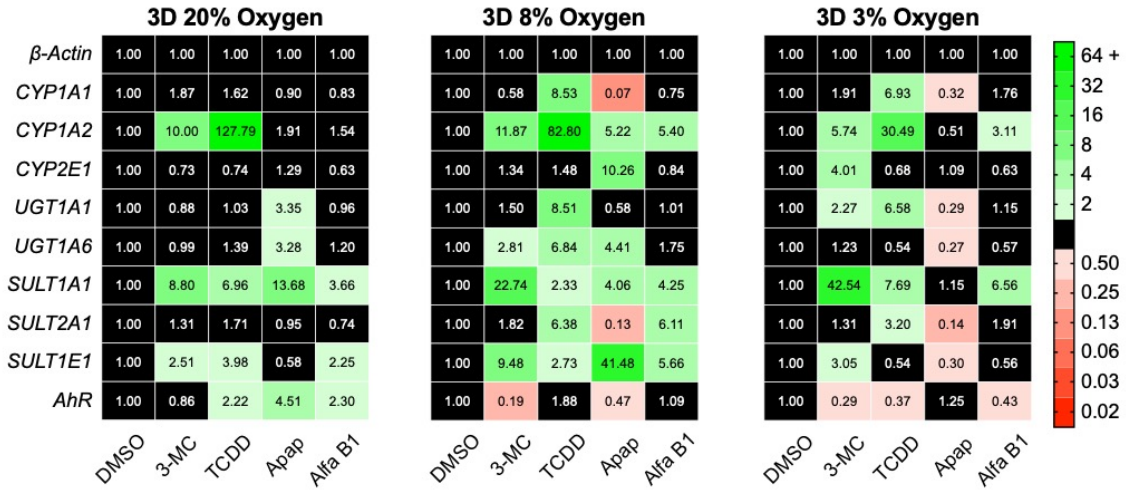

Figure 2.10 Transcript-level regulation of 3D cultures of HepG2 cells after a 48 hour incubation at atmospheric (20%), periportal (8%), or perivenous (3%) oxygen tension. The cells were treated with 5 µM 3-MC, 1 nM TCDD, 10 mM acetaminophen (apap), or 10 nM aflatoxin B1 (afla B1). Each value is the fold change of the average ΔΔCt value of at least 4 datapoints collected from N=2-3 cell passages. Each pass contained at least three technical replicates (n=3). A fold-change >2 indicates a significant increase in expression; <0.50 indicates a significant decrease. The numerical labels represent the average ΔΔCt value.

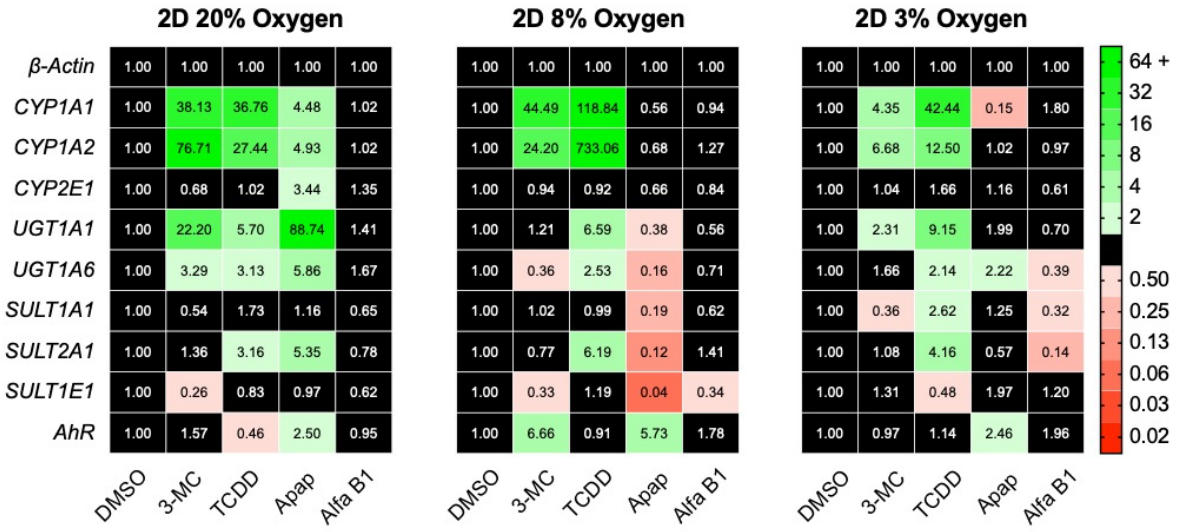

Figure 2.11. Transcript-level regulation of HepG2 cells cultured in a 2D culture format, plated on traditional plasticware after a 48 hour incubation at 20%, 8%, or 3% O2. The cells were treated with 5 μM 3-MC, 1 nM TCDD, 10 mM acetaminophen (apap), or 10 nM aflatoxin B1 (afla B1). Each value is the fold change of the average ΔΔCt value of at least 4 datapoints collected from different cell passages (N=2-3), each pass contained at least three technical replicates (n=3). A fold-change >2 indicates a significant increase in expression; <-2 indicates a significant decrease. The numerical value labels represent the average ΔΔCt value.

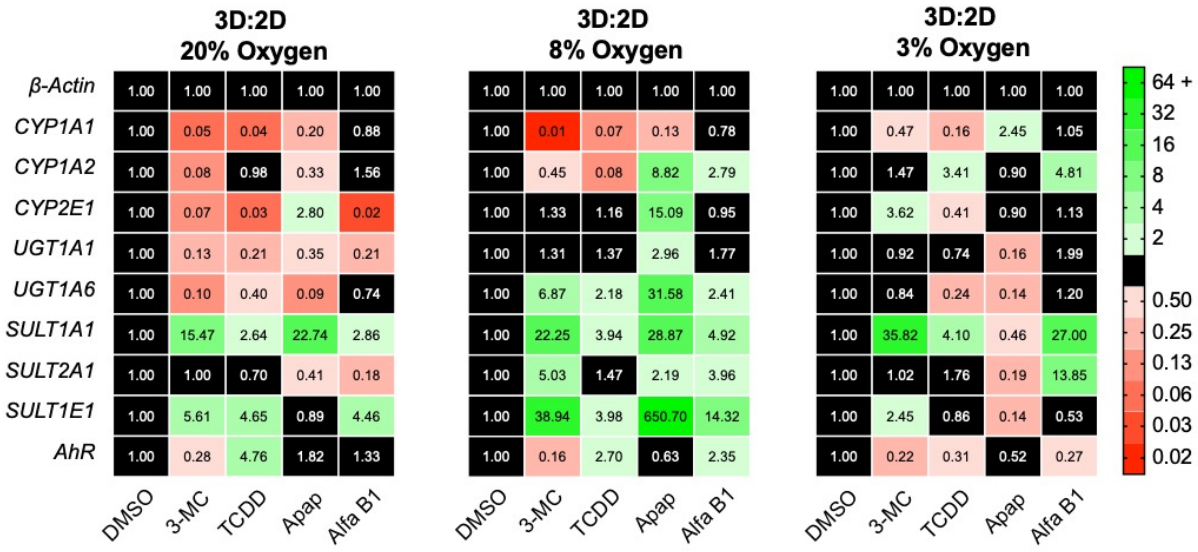

Figure 2.12. Transcript-level regulation ratio of 3D to 2D HepG2 cells cultured for a 48 hour incubation at atmospheric (20%), periportal (8%), or perivenous (3%) oxygen tension. The cells were treated with 5 µM 3-MC, 1 nM TCDD, 10 mM acetaminophen (apap), or 10 nM aflatoxin B1 (afla B1). Each value is the fold change of the average 3D ΔΔCt divided by the 2D ΔΔCt value of at least 4 datapoints collected from different cell passages (N=2 – 3), each pass contained at least three technical replicates (n=3). A fold-change >2 indicates a significant increase in expression; <-2 indicates a significant decrease. The numerical values labels represent the average ΔΔCt value.

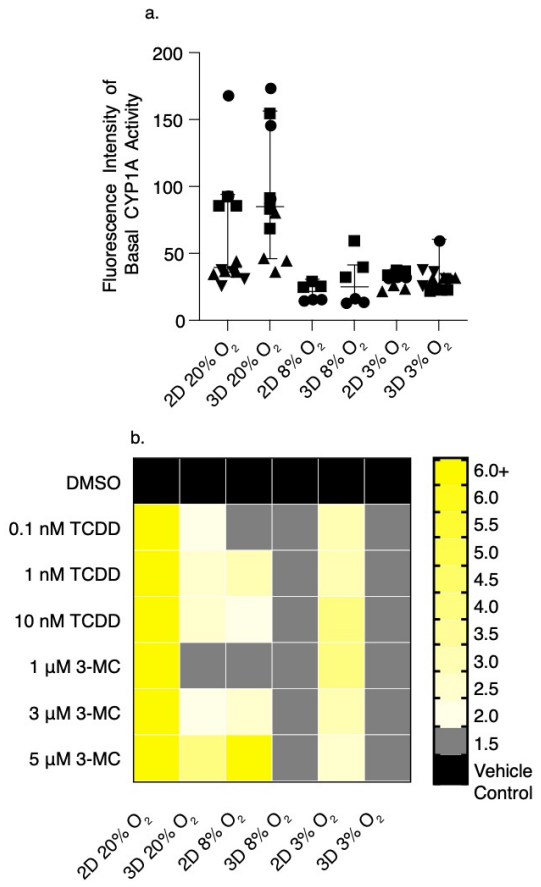

Figure 2.13. Average CYP1A activity of HepG2 cells as determined by the EROD assay. (a) Basal CYP1A activity, plotted as the raw fluorescent intensity, after a 48 hour incubation. (b) CYP1A activity after a 48 hour induction with increasing concentrations of 3-MC or TCDD. Values are the average of at least six data points collected from at least two cell passages (N=2). Each pass contained at least three technical replicates (n=3). A fold-change >2 indicates a significant increase in activity. The numerical values of the heatmap are found in Table 2.4.

Table 2.4. Numerical values of CYP1A fold induction corresponding Figure 2.13.

	2D 20% O_2	**3D 20% O_2**	**2D 8% O_2**	**3D 8% O_2**	**2D 3% O_2**	**3D 3% O_2**
Basal	0.96	1.18	0.79	0.95	1.03	0.74
0.1% DMSO	0.98	0.96	1.00	1.00	1.00	1.01
0.1 nM TCDD	12.64	1.74	1.08	0.94	2.58	0.74
1 nM TCDD	12.89	2.05	2.63	0.80	2.99	0.93
10 nM TCDD	17.57	2.22	1.95	0.81	3.55	0.58
1 μM 3-MC	16.16	1.32	1.43	1.02	3.72	0.78
3 μM 3-MC	13.55	1.84	2.19	0.80	2.52	0.78
5 μM 3-MC	11.08	3.56	11.33	1.22	2.19	0.88

REFERENCES

(1) Kenna, J. G.; Uetrecht, J. Do In Vitro Assays Predict Drug Candidate Idiosyncratic Drug-Induced Liver Injury Risk? *Drug Metab. Dispos.* **2018**, *46* (11), 1658–1669. https://doi.org/10.1124/dmd.118.082719.

(2) Parasrampuria, D. A.; Benet, L. Z.; Sharma, A. Why Drugs Fail in Late Stages of Development: Case Study Analyses from the Last Decade and Recommendations. *AAPS J.* **2018**, *20* (46). https://doi.org/10.1208/s12248-018-0204-y.

(3) Westerink, W. M. A.; Schoonen, W. G. E. J. Phase II Enzyme Levels in HepG2 Cells and Cryopreserved Primary Human Hepatocytes and Their Induction in HepG2 Cells. *Toxicol. Vitr.* **2007**, *21* (8), 1581–1591. https://doi.org/10.1016/j.tiv.2007.05.014.

(4) Gerets, H. H. J.; Hanon, E.; Cornet, M.; Dhalluin, S.; Depelchin, O.; Canning, M.; Atienzar, F. A. Selection of Cytotoxicity Markers for the Screening of New Chemical Entities in a Pharmaceutical Context: A Preliminary Study Using a Multiplexing Approach. *Toxicol. Vitr.* **2009**, *23* (2), 319–332. https://doi.org/10.1016/j.tiv.2008.11.012.

(5) Kitamoto, N.; Mattion, N. M.; Estes, M. K. Alterations in the Sequence of the Gene 4 from a Human Rotavirus after Multiple Passages in HepG2 Liver Cells. *Arch. Virol.* **1993**, *130* (1–2), 179–185. https://doi.org/10.1007/BF01319006.

(6) Zhao, Y.; Chen, Y.; Hu, Y.; Wang, J.; Xie, X.; He, G.; Chen, H.; Shao, Q.; Zeng, H.; Zhang, H. Genomic Alterations across Six Hepatocellular Carcinoma Cell Lines by Panel-Based Sequencing. *Transl. Cancer Res.* **2018**, *7* (2), 231–239. https://doi.org/10.21037/tcr.2018.02.14.

(7) Dunn, J. C. Y.; Tompkins, R. G.; Yarmush, M. L. Hepatocytes in Collagen Sandwich: Evidence for Transcriptional and Translational Regulation. *J. Cell Biol.* **1992**, *116* (4), 1043–1053. https://doi.org/10.1083/jcb.116.4.1043.

(8) Dunn, J. C. Y.; Yarmush, M. L.; Koebe, H. G.; Tompkins, R. G. Hepatocyte Function and Extracellular Matrix Geometry: Long-term Culture in a Sandwich Configuration. *FASEB J.* **1989**, *3* (2), 174–177. https://doi.org/10.1096/fasebj.3.2.2914628.

(9) Meyer, C.; Liebe, R.; Breitkopf-Heinlein, K.; Liu, Y.; Müller, A.; Rakoczy, P.; Thomas, M.; Weng, H.; Bachmann, A.; Ebert, M.; Dooley, S. Hepatocyte Fate Upon TGF-β Challenge Is Determined by the Matrix Environment. *Differentiation* **2015**, *89* (5), 105–116. https://doi.org/10.1016/j.diff.2015.04.001.

(10) Zeigerer, A.; Wuttke, A.; Marsico, G.; Seifert, S.; Kalaidzidis, Y.; Zerial, M. Functional Properties of Hepatocytes In Vitro Are Correlated With Cell Polarity Maintenance. *Exp. Cell Res.* **2017**, *350*, 242–252. https://doi.org/10.1016/j.yexcr.2016.11.027.

(11) Hewitt, N. J.; Lechón, M. J. G.; Houston, J. B.; Hallifax, D.; Brown, H. S.; Maurel, P.;

Kenna, J. G.; Gustavsson, L.; Lohmann, C.; Skonberg, C.; Guillouzo, A.; Tuschl, G.; Li, A. P.; Lecluyse, E.; Groothuis, G. M. M.; Hengstler, J. G. Primary Gepatocytes: Current Understanding of the Regulation of Metabolic Enzymes and Transporter Proteins, and Pharmaceutical Practice for the Use of Hepatocytes in Metabolism, Enzyme Induction, Transporter, Clearance, and Hepatotoxicity Studies. *Drug Metab. Rev.* **2007**, *39*, 159–234. https://doi.org/10.1080/03602530601093489.

(12) Guo, L.; Dial, S.; Shi, L.; Branham, W.; Liu, J.; Fang, J.-L.; Green, B.; Deng, H.; Kaput, J.; Ning, B. Similarities and Differences in the Expression of Drug-Metabolizing Enzymes Between Human Hepatic Cell Lines and Primary Human Hepatocytes. *Drug Metab. Dispos.* **2010**, *39* (3). https://doi.org/10.1124/dmd.110.035873.

(13) Chang, T. T.; Hughes-Fulford, M. Monolayer and Spheroid Culture of Human Liver Hepatocellular Carcinoma Cell Line Cells Demonstrate Distinct Global Gene Expression Patterns and Functional Phenotypes. *Tissue Eng. - Part A* **2009**, *15* (3), 559–567. https://doi.org/10.1089/ten.tea.2007.0434.

(14) Ramaiahgari, S. C.; Den Braver, M. W.; Herpers, B.; Terpstra, V.; Commandeur, J. N. M.; Van De Water, B.; Price, L. S. A 3D in Vitro Model of Differentiated HepG2 Cell Spheroids with Improved Liver-like Properties for Repeated Dose High-Throughput Toxicity Studies. *Arch. Toxicol.* **2014**, *88* (5), 1083–1095. https://doi.org/10.1007/s00204-014-1215-9.

(15) Gaskell, H.; Sharma, P.; Colley, H. E.; Murdoch, C.; Williams, D. P.; Webb, S. D. Characterization of a Functional C3A Liver Spheroid Model. *Toxicol. Res. (Camb).* **2016**, *5* (4), 1053–1065. https://doi.org/10.1039/c6tx00101g.

(16) Hirschhaeuser, F.; Menne, H.; Dittfeld, C.; West, J.; Mueller-Klieser, W.; Kunz-Schughart, L. A. Multicellular Tumor Spheroids: An Underestimated Tool Is Catching up Again. *J. Biotechnol.* **2010**, *148* (1), 3–15. https://doi.org/10.1016/j.jbiotec.2010.01.012.

(17) Prabhakar, N. R.; Semenza, G. L. Oxygen Sensing and Homeostasis. *Physiology* **2015**, *30* (5), 340–348. https://doi.org/10.1152/physiol.00022.2015.

(18) Jungermann, K.; Kietzmann, T. Oxygen: Modulator of Metabolic Zonation and Disease of the Liver. *Hepatology* **2000**, *31* (2), 255–260. https://doi.org/10.1002/hep.510310201.

(19) Kietzmann, T. Metabolic Zonation of the Liver: The Oxygen Gradient Revisited. *Redox Biol.* **2017**, *11* (January), 622–630. https://doi.org/10.1016/j.redox.2017.01.012.

(20) Oinonen, T.; Lindros, K. O. Zonation of Hepatic Cytochrome P-450 Expression and Regulation. *Biochem. J.* **1998**, *329*, 17–35. https://doi.org/10.1042/bj3290017.

(21) Braeuning, A.; Ittrich, C.; Köhle, C.; Hailfinger, S.; Bonin, M.; Buchmann, A.; Schwarz, M. Differential Gene Expression in Periportal and Perivenous Mouse Hepatocytes. *FEBS J.* **2006**, *273* (22), 5051–5061. https://doi.org/10.1111/j.1742-4658.2006.05503.x.

(22) Jancova, P.; Anzenbacher, P.; Anzenbacherova, E. Phase II Drug Metabolizing Enzymes. *Biomed. Pap.* **2010**, *154* (2), 103–116. https://doi.org/10.5507/bp.2010.017.

(23) Bowyer, C.; Lewis, A. L.; Lloyd, A. W.; Phillips, G. J.; MacFarlane, W. M. Hypoxia as a Target for Drug Combination Therapy of Liver Cancer. *Anticancer. Drugs* **2017**, *28* (7), 771–780. https://doi.org/10.1097/CAD.0000000000000516.

(24) Sonna, L. A.; Cullivan, M. L.; Sheldon, H. K.; Pratt, R. E.; Lilly, C. M. Effect of Hypoxia on Gene Expression by Human Hepatocytes (HepG2). *Physiol. Genomics* **2003**, *12* (9), 195–207. https://doi.org/10.1152/physiolgenomics.00104.2002.

(25) Derda, R.; Laromaine, A.; Mammoto, A.; Tang, S. K. Y.; Mammoto, T.; Ingber, D. E.; Whitesides, G. M. Paper-Supported 3D Cell Culture for Tissue-Based Bioassays. *Proc. Natl. Acad. Sci. U. S. A.* **2009**, *106* (44), 18457–18462. https://doi.org/10.1073/pnas.0910666106.

(26) Cramer, S. M.; Larson, T. S.; Lockett, M. R.; Hill, C.; States, U.; Hill, C.; Hill, C.; States, U. Next Generation of 3D Tissue Models. **2020**, *91* (17), 10916–10926. https://doi.org/10.1021/acs.analchem.9b02102.Tissue.

(27) Lloyd, C. C.; Boyce, M. W.; Lockett, M. R. Paper-Based Invasion Assays for Quantifying Cellular Movement in Three-Dimensional Tissue-like Structures. *Curr. Protoc. Chem. Biol.* **2017**, *9* (2), 75–95. https://doi.org/10.1002/cpch.22.

(28) Kenney, R. M.; Loeser, A.; Whitman, N. A.; Lockett, M. R. Paper-Based Transwell Assays: An Inexpensive Alternative to Study Cellular Invasion. *Analyst* **2019**, *144* (1), 206–211. https://doi.org/10.1039/c8an01157e.

(29) Al-Ani, A.; Toms, D.; Kondro, D.; Thundathil, J.; Yu, Y.; Ungrin, M. Oxygenation in Cell Culture: Critical Parameters for Reproducibility Are Routinely Not Reported. *PLoS One* **2018**, *13* (10), 1–13. https://doi.org/10.1371/journal.pone.0204269.

(30) Schneider, C. a; Rasband, W. S.; Eliceiri, K. W. NIH Image to ImageJ: 25 Years of Image Analysis. *Nat. Methods* **2012**, *9* (7), 671–675. https://doi.org/10.1038/nmeth.2089.

(31) Schmittgen, T. D.; Livak, K. J. Analyzing Real-Time PCR Data by the Comparative CT Method. *Nat. Protoc.* **2008**, *3* (6), 1101–1108. https://doi.org/10.1038/nprot.2008.73.

(32) Kang, Y. B.; Eo, J.; Bulutoglu, B.; Yarmush, M. L.; Usta, O. B. Progressive Hypoxia-on-a-Chip: An in Vitro Oxygen Gradient Model for Capturing the Effects of Hypoxia on Primary Hepatocytes in Health and Disease. *Biotechnol. Bioeng.* **2020**, *117* (3), 763–775. https://doi.org/10.1002/bit.27225.

(33) Wang, K.; Shindoh, H.; Inoue, T.; Horii, I. Advantages of in Vitro Cytotoxicity Testing by Using Primary Rat Hepatocytes in Comparison with Established Cell Lines. *J. Toxicol. Sci.* **2002**, *27* (3), 229–237. https://doi.org/10.2131/jts.27.229.

(34) Gerets, H. H. J.; Tilmant, K.; Gerin, B.; Chanteux, H.; Depelchin, B. O.; Dhalluin, S.; Atienzar, F. A. Characterization of Primary Human Hepatocytes, HepG2 Cells, and HepaRG Cells at the MRNA Level and CYP Activity in Response to Inducers and Their Predictivity for the Detection of Human Hepatotoxins. *Cell Biol. Toxicol.* **2012**, *28* (2), 69–87. https://doi.org/10.1007/s10565-011-9208-4.

(35) Drahushuk, A. T.; McGarrigle, B. P.; Larsen, K. E.; Stegeman, J. J.; Olson, J. R. Detection of CYP1A1 Protein in Human Liver and Induction by TCDD in Precision-Cut Liver Slices Incubated in Dynamic Organ Culture. *Carcinogenesis* **1998**, *19* (8), 1361–1368. https://doi.org/10.1093/carcin/19.8.1361.

(36) Gerbal-Chaloin, S.; Dumé, A. S.; Briolotti, P.; Klieber, S.; Raulet, E.; Duret, C.; Fabre, J. M.; Ramos, J.; Maurel, P.; Daujat-Chavanieu, M. The WNT/b-Catenin Pathway Is a Transcriptional Regulator of CYP2E1, CYP1A2, and Aryl Hydrocarbon Receptor Gene Expression in Primary Human Hepatocytes. *Mol. Pharmacol.* **2014**, *86* (6), 624–634. https://doi.org/10.1124/mol.114.094797.

(37) Sumida, A.; Fukuen, S.; Yamamoto, I.; Matsuda, H.; Naohara, M.; Azuma, J. Quantitative Analysis of Constitutive and Inducible CYPs MRNA Expression in the HepG2 Cell Line Using Reverse Transcription-Competitive PCR. *Biochem. Biophys. Res. Commun.* **2000**, *267* (3), 756–760. https://doi.org/10.1006/bbrc.1999.2029.

(38) Kim, Y.; Lasher, C. D.; Milford, L. M.; Murali, T. M.; Rajagopalan, P. A Comparative Study of Genome-Wide Transcriptional Profiles of Primary Hepatocytes in Collagen Sandwich and Monolayer Cultures. *Tissue Eng. - Part C Methods* **2010**, *16* (6), 1449–1460. https://doi.org/10.1089/ten.tec.2010.0012.

(39) Hewitt, N. J.; Hewitt, P. Phase I and II Enzyme Characterization of Two Sources of HepG2 Cell Lines. *Xenobiotica* **2004**, *34* (3), 243–256. https://doi.org/10.1080/00498250310001657568.

(40) Fradette, C.; Souich, P. Effect of Hypoxia on Cytochrome P450 Activity and Expression. *Curr. Drug Metab.* **2004**, *5* (3), 257–271. https://doi.org/10.2174/1389200043335577.

(41) Audibert, G.; Saunier, C. .; Souich, P. DU. In Vivo and In Vitro Effect of Cimetidine, Inflammation, and Hypoxia on Propofol Kinetics. *Drug Metab. Dispos.* **1993**, *21* (1), 7–12.

(42) Vrba, J.; Havlikova, M.; Gerhardova, D.; Ulrichova, J. Palmatine Activates AhR and Upregulates CYP1A Activity in HepG2 Cells but Not in Human Hepatocytes. *Toxicol. Vitr.* **2014**, *28* (4), 693–699. https://doi.org/10.1016/j.tiv.2014.02.008.

(43) Whitman, N. A.; McIntosh, J. C.; Penley, J. B.; Lockett, M. R. Microfabricated Devices for Studying the Metabolism and Cytotoxicity of Drug Candidates. *Curr. Pharm. Biotechnol.* **2016**, *17*, 755–771.

(44) Lauschke, V. M.; Hendriks, D. F. G.; Bell, C. C.; Andersson, T. B.; Ingelman-Sundberg, M. Novel 3D Culture Systems for Studies of Human Liver Function and Assessments of the Hepatotoxicity of Drugs and Drug Candidates. *Chem. Res. Toxicol.* **2016**, *29* (12), 1936–1955. https://doi.org/10.1021/acs.chemrestox.6b00150.

(45) Agarwal, T.; Borrelli, M. R.; Makvandi, P.; Ashrafizadeh, M.; Maiti, T. K. Paper-Based Cell Culture: Paving the Pathway for Liver Tissue Model Development on a Cellulose Paper Chip. *ACS Appl. Bio Mater.* **2020**, *3* (7), 3956–3974. https://doi.org/10.1021/acsabm.0c00558.

(46) Parikh, H.; Pandita, N.; Khanna, A. Phytoextract of Indian Mustard Seeds Acts by Suppressing the Generation of ROS against Acetaminophen-Induced Hepatotoxicity in HepG2 Cells. *Pharm. Biol.* **2015**, *53* (7), 975–984. https://doi.org/10.3109/13880209.2014.950675.

(47) Schyschka, L.; Sánchez, J. J. M.; Wang, Z.; Burkhardt, B.; Müller-Vieira, U.; Zeilinger, K.; Bachmann, A.; Nadalin, S.; Damm, G.; Nussler, A. K. Hepatic 3D Cultures but Not 2D Cultures Preserve Specific Transporter Activity for Acetaminophen-Induced Hepatotoxicity. *Arch. Toxicol.* **2013**, *87* (8), 1581–1593. https://doi.org/10.1007/s00204-013-1080-y.

(48) Bell, C. C.; Lauschke, V.; Vorrink, S.; Palmgren, H.; Duffin, R.; Andersson, T.; Ingelman-Sundberg, M. Transcriptional, Functional, and Mechanistic Comparisons of Stem Cell-Derived Hepatocytes, HepaRG Cells, and Three-Dimensional Human Hepatocyte Spheroids as Predictive In Vitro Systems for Drug-Induced Liver Injury. *Drug Metab. Dispos.* **2017**, *45* (4), 419–429. https://doi.org/10.1124/dmd.116.074369.

(49) Hinson, J.; Roberts, D.; James, L. Mechanisms of Acetaminophen-Induced Liver Necrosis. *Handb. Exp. Pharmacol.* **2010**, *196* (196), 369–405. https://doi.org/10.1007/978-3-642-00663-0.

(50) Roberts, D. W.; Bucci, T. J.; Benson, R. W.; Warbritton, A. R.; McRae, T. A.; Pumford, N. R.; Hinson, J. A. Immunohistochemical Localization and Quantification of the 3-(Cystein-S-Yl)-Acetaminophen Protein Adduct in Acetaminophen Hepatotoxicity. *Am. J. Pathol.* **1991**, *138* (2), 359–371.

(51) Yokoyama, Y.; Sasaki, Y.; Terasaki, N.; Kawataki, T.; Takekawa, K.; Iwase, Y.; Shimizu, T.; Sanoh, S.; Ohta, S. Comparison of Drug Metabolism and Its Related Hepatotoxic Effects in HepaRG, Cryopreserved Human Hepatocytes, and HepG2 Cell Cultures. *Biol. Pharm. Bull.* **2018**, *41* (5), 722–732. https://doi.org/10.1248/bpb.b17-00913.

(52) Rodriguez-Antona, C.; Ingelman-Sundberg, M. Cytochrome P450 Pharmacogenetics and Cancer. *Oncogene* **2006**, *25* (11), 1679–1691. https://doi.org/10.1038/sj.onc.1209377.

(53) Corina, I.; Caira, M. R. *Drug Metabolism Current Concepts*, 2005th ed.; Ionescu, C., Caira, M. R., Eds.; Springer, 2005. https://doi.org/10.1007/1-4020-4142-X.

(54) Li, A. P.; Uzgare, A.; Laforge, Y. S. Definition of Metabolism-Dependent Xenobiotic Toxicity with Co-Cultures of Human Hepatocytes and Mouse 3T3 Fibroblasts in the Novel Integrated Discrete Multiple Organ Co-Culture (IdMOC) Experimental System: Results with Model Toxicants Aflatoxin B1, Cyclo. *Chem. Biol. Interact.* **2012**, *199* (1), 1–8. https://doi.org/10.1016/j.cbi.2012.05.003.

(55) Deng, J.; Zhao, L.; Zhang, N. Y.; Karrow, N. A.; Krumm, C. S.; Qi, D. S.; Sun, L. H. Aflatoxin B1 Metabolism: Regulation by Phase I and II Metabolizing Enzymes and Chemoprotective Agents. *Rev. Mutat. Res.* **2018**, *778* (September), 79–89. https://doi.org/10.1016/j.mrrev.2018.10.002.

(56) Mughal, M. J.; Peng, X.; Zhou, Y.; Fang, J. Aflatoxin B1 Invokes Apoptosis via Death Receptor Pathway in Hepatocytes. *Oncotarget* **2017**, *8* (5), 8239–8249. https://doi.org/10.18632/oncotarget.14158.

(57) Ratajewski, M.; Walczak-Drzewiecka, A.; Sałkowska, A.; Dastych, J. Aflatoxins Upregulate CYP3A4 MRNA Expression in a Process That Involves the PXR Transcription Factor. *Toxicol. Lett.* **2011**, *205* (2), 146–153. https://doi.org/10.1016/j.toxlet.2011.05.1034.

(58) Sonoda, J.; Xie, W.; Rosenfeld, J. M.; Barwick, J. L.; Guzelian, P. S.; Evans, R. M. Regulation of a Xenobiotic Sulfonation Cascade by Nuclear Pregnane X Receptor (PXR). *Proc. Natl. Acad. Sci. U. S. A.* **2002**, *99* (21), 13801–13806. https://doi.org/10.1073/pnas.212494599.

CHAPTER 3: HEPARG CELL MONOLAYERS CULTURED AT PHYSIOLOGICAL MICROENVIRONMENTS MIMIC IN VIVO LIVER ZONATION

3.1 Introduction

In the preclinical drug-discovery pipeline, monolayers of primary human hepatocytes (PHHs) or immortalized hepatocyte-like cell lines are used to evaluate hepatoxicity, the induction of metabolic enzymes, and possible drug-drug interactions. These cell-based methods often fail to accurately predict drug-induced liver injury, which is a common reason for discontinuation of clinical trials.[1,2] One plausible reason for this failure is that monolayer culture formats lack many aspects of the tissue microenvironment, which has profound effects on cellular function. PHHs placed in an extracellular matrix (ECM)-rich environment, such as a collagen sandwich, maintain their polarization and metabolic function,[3,4] long after they would have dedifferentiated when cultured on plasticware as a monolayer.[5] Incorporating other aspects of the tissue microenvironment, such as the extracellular matrices and high numbers of cell-cell contacts found in spheroids, enhance the activity of phase I and II metabolic enzymes in PHHs when compared to those cultured in a monolayer.[6–8] These studies and others suggest that inclusion of physiological conditions in in vitro cultures will improve their predictiveness when screening potential drugs, but structure-function relationship studies are needed to determine which aspects of the liver lobule should be incorporated to improve current in vitro live models.

The liver lobule is the structural subunit of the liver. It is comprised of a portal triad where drug, nutrient, and oxygen-rich blood enter a sinusoid, which transverses the lobule and empties into a central vein where processed blood is redistributed into the body. The tissue

microenvironment surrounding the portal triad is starkly different from that of the central vein, the so-called periportal (PP) and perivenous (PV) regions of the lobule. The hepatocytes that reside in these two regions have distinct metabolic functions; this differential expression of various pathways is known as liver zonation[9,10]. The inclusion of microenvironmental factors of the PP and PV regions of the liver lobule in vitro can be beneficial for novel drug discovery. Oxygen is a global regulator of cellular function,[11] and an important aspect of the liver microenvironment. A steep oxygen gradient that forms along the sinusoids of the lobule, a consequence of the high rate of cellular respiration of hepatocytes: the blood oxygen partial pressure range from 65-60 mmHg O_2 (11-8% O_2) in the PP region, to 35-30 mmHg O_2 (5-3% O_2) in the PV region.[9,12,13]

In Chapter 2, we evaluated physiological oxygen tensions on HepG2 induction and hepatoxicity. This work showed that incorporating physiological oxygen tensions into monolayer and 3D culture formats can improve the drug metabolic activity of these cells, but oxygen alone isn't enough to mimic zonation. In this chapter, we introduce additional physiologically relevant factors to cultures of HepaRG cells. HepG2 cells are an immortalized hepatoma cell line that is often used to develop and benchmark new methods or screens for evaluating drug toxicity.[14,15] However, HepG2 cells have limited expression of phase I cytochrome P450 enzymes (CYPs) and thus are a poor predictor of in vivo outcomes when compared to PHHs.[16,17] The HepaRG immortalized line is derived from hepatocellular carcinoma cells, composed of hepatocyte-like and biliary-like cell phenotypes with a transcript and activity metabolic enzyme profile comparable to PHHs.[18] Furthermore, HepaRG cells have drug transporter transcript expression profiles similar to PHHs. The similarity of the transcript profile for phase I, II, and transporters

between PHHs and HepaRG cells makes HepaRG a good cell model to assess the effect of physiological culture conditions on in vitro hepatocyte cultures.

Specifically we evaluated the effects of the Wnt3a (Wnt) morphogen and Rspondin. The motivation for including Wnt and Rspondin along with different concentrations of oxygen to the culture aligns the theory of post-differentiation patterning. In this theory, one factor (oxygen) would have a broad effect on multiple hepatocytes while the second factor (Wnt + Rspondin) would finely tune cellular function. Oxygen regulates the activity of a particular set of transcription factors, of which hypoxia-inducible factor 1 (HIF1) alpha is a member. In hypoxic conditions, HIF1α is stabilized and transported to the nucleus where it dimerizes with the HIF1β subunit increase the transcription of hypoxia-regulated genes. In the presence of oxygen, HIF1α is hydroxylated by prolyl hydroxylase, marking HIF1α for ubiquitination; in the absence of oxygen, prolyl hydroxylase activity is reduced resulting in the stabilization and accumulation of HIF1α.[9,19] The stabilization of HIF1α in the liver has been associated with transcriptional zonation patterns, such as glycogen synthesis, phase I and II metabolism, and the production of urea, bile, and albumin.[20]

The Wnt pathway is a highly conserved pathway involved in determining cell fate and differentiation, polarity, proliferation, and homeostasis.[21] The canonical Wnt signaling pathway is inactive under basal conditions because of the degradation of the intracellular β-catenin transducer. In the absence of Wnt ligands, β-catenin is bound to a destruction complex which mediated facilitates the degradation of constitutively expressed β-catenin. Upon binding of extracellular Wnt to the membrane protein Frizzled, the Wnt/β-catenin pathway becomes active, preventing the degradation of β-catenin and allowing it to translocate to the nucleus.[21,22] R-spondin is an agonist of the Wnt pathway, recently shown to play a major role in the level of

Wnt/β-catenin activity. R-spondin protein binds to the transmembrane receptor leucine-rich repeat-containing g-protein coupled receptor (LGR) which prevents the clearance of Frizzled receptors on the membrane- promoting Wnt signaling.[9,23] Benhamouche and colleagues observed zonation-dependent expression of Wnt/β-catenin pathway gene transcripts, specifically those associated with carbohydrate metabolism and transport: with a low expression in the PP region and an increased expression in the PV region.[24]

Pathway regulation and preferential distribution of liver-specific activities in hepatocytes residing the PP and PV regions have been well studied.[25,26] The specific combinations of factors that lead to this zonation is still unclear, it is hypothesized that the gradients of oxygen, nutrients, morphogens, and hormones across the sinusoid modulate hepatocyte function in vivo. Despite the sophistication of 3D spheroids and organ-on-chip devices, in vitro mimicry of liver zonation remains experimentally challenging. Another limitation of these two approaches is the ability to isolate hepatocytes in a particular zone or identify the culture conditions resulting in a particular phenotype.[26] In this study, we exposed HepaRG cells to standard culture conditions and physiological conditions representative of the PP and PV region of the liver. In the PP conditions, cells were cultured at 11% O_2 tension; in the PV condition, cell were cultured in 5% O_2 tension and Wnt and Rspondin supplemented medium. Urea synthesis, CYP activity, and transcriptional regulation was measured and compared between the three culture formats. We found that the PV conditioned cells had enhanced CYP activity compared to the PP conditioned cells, however the transcriptional regulation do not match the activity trends.

3.2 Materials and methods

3.2.1 Chemicals

All chemicals and reagents were used as received unless otherwise specified. All cell culture medium and supplements were purchased from Gibco, except for those used in the maintenance of the HepaRG cell line (Lonza). Chlorzoxazone, dextromethorphan (hydrobromide hydrate), (S)-mephenytoin, midazolam, and testosterone were purchased from Cayman Chemical Company. Dimethyl sulfoxide and 7-hydroxycoumarin were purchased from Fisher Scientific. Collagen I (rat tail) was purchased from Enzo Life Sciences. Phenacetin and sodium hydroxide (NaOH) were purchased from Millipore Sigma. The CellTiter-Glo 2.0 (CTG) reagent was purchased from Promega.

3.2.2 Collagen scaffold preparation

Collagen slabs were prepared by neutralizing a solution of acidified collagen, with NaOH and phosphate-buffered saline (PBS). The neutralized collagen solution (2 mg/mL) was added to standard 12-well cell culture plates (263 μg of available collagen/cm^2) and incubated overnight at 37°C. Collagen slabs were washed once with 1x PBS prior to cell seeding.

3.2.3 LWRN cell culture and secretion

L-WRN cells, a transfected mouse mucosal cell lines to secrete Wnt3a, R-spondin 3, and noggin into, were purchased from the American Type Culture Collection and cultured as monolayers at 20% O_2, 37 ºC, and 5% CO_2 in Dulbecco's Modified Eagle's Medium (DMEM) medium supplemented with 10% FBS, 0.5 mg/mL G-418, and 0.5 mg/mL hygromycin B.

Maintenance medium was exchanged every 2-3 days and the cells were passed at 80% confluency with TrypLE, using standard procedures.

L-WRN conditioned medium was collected following ATCC's recommended protocol. Briefly, L-WRN cells were grown to confluency in a T150 flask without G-418 and hygromycin B. Cell were washed with 1X PBS followed by the addition of 25 mL of fresh medium to the flask and exchanged every 24 hours. The conditioned medium was collected, centrifuged at 1000 xg for 5 minutes, and the supernatant was decanted and stored at 4 ºC until processed further. Medium collected from days 1 – 4 were pooled, as was medium collected from days 5 – 8; the pooled conditioned medium was steri-filtered (0.22 μm) and stored at -80°C.

3.2.4 HepaRG cell culture

Differentiated NoSpin HepaRG Cryopreserved Cells were obtained from Lonza Bioscience. Cells were cultured at a density of 2.6 x 10^5 cells/cm^2 on each collagen scaffold. The cells were maintained for 24 hours in HepaRG medium containing basal medium supplement, a thawing and plating supplement, and 1% penicillin–streptomycin. After a medium exchange, the cells were maintained in HepaRG medium containing basal medium supplement, a maintenance and metabolism supplement, and 1% penicillin–streptomycin. The cells were incubated at 37°C and 5% CO_2. Medium was exchanged every two to three days.

After 6 days, the HepaRG cells were maintained in the same medium and exposed to one of three experimental physiological conditions: standard culture conditions, where cells were incubated at 37°C, atmospheric oxygen and 5% CO_2; PP conditions, where cells were incubated at 37°C, 11% O_2 and 5% CO_2; PV conditions, where the cells were incubated at 37°C, 11% O_2 and 5% CO_2 in a 1:1 ratio of medium and L-WRN conditioned medium. The oxygen tensions

were regulated with a custom-build hypoxia chamber with a PID gas control, as detailed previously.[27] Widefield images of the HepaRG cells were captured with a Nikon TE2000 microscope with a Photometrics Dyno CCD camera.

3.2.5 Evaluation of Cytochrome P450 (CYP) Activity

CYP activity was evaluated with a cocktail containing eight different substrates as described in **Table 3.1**; all substrates were dissolved in DMSO at 1000X working concentration.[28,29] The HepaRG cells were exposed to HepaRG basal containing the substrates and basal medium supplement for 2 hours. Medium supernatant was collected and stored at -20°C.

Each sample was mixed with cold acetonitrile at a 1:10 (v/v) ratio. The acetonitrile contained isotopically labeled standards of each product. The precipitated protein was pelleted at 12,000 xg for 15 min, the supernatant collected, and the solvent removed in vacuo. The residual solid was resuspended in 100 µL of HPLC-grade water (Optima) and separated on a Waters Acquity UPLC equipped with a BEH C18 column (2.1 x 50 mm, 1.7 µm) using a binary solvent system of (A) 0.5% formic acid (v/v) in water and (B) 0.5% formic acid (v/v) in acetonitrile (B). The total run time of each separation was nine min, using the following gradient profile at a 0.3 mL/min flow rate: 10% B for one min; a linear gradient to 70% B over 5 min; 95% B for one min; 10% B for two min to re-equilibrate the column. Representative chromatograms are displayed in **Figure 3.1**

Metabolites were detected and quantified with ion transition monitoring on a Thermo TSQ Vantage triple quadrupole instrument equipped with a heated electrospray ionization (HESI) source set to 300 °C. Two transitions of each product in the cocktail were monitored

to confirm its identity. The declustering voltage for each was optimized by direct infusion of neat solutions (10 μmM) in Optima water. Each analyte's transition was optimized for collision energy and reported in **Table 3.1**. Other parameters used for all analyses were: spray voltage (4800 V), vaporization temperature (300 °C), sheath gas pressure (50 psi), aux gas pressure (15 psi), capillary temperature (300 °C), and S-lens RF amplitude (120 V). Nitrogen gas was used for sheath, aux and collision gas. Data were collected and processed with Xcalibur.

A matrix blank which followed the same processing steps was prepared each time to account for any interferences in the chromatogram at the areas of analyte interest. The peak area for each metabolite was averaged across three technical replicates; we report the ratio of the averaged peak area of treatment to vehicle.

3.2.6 Urea production

After collecting the medium for the CYP activity assay, each well was washed once with 1X PBS and the cells incubated in fresh HepaRG medium containing basal supplement for 1 hour. Medium was collected to quantify urea concentration using quantitative colorimetric urea determination (QuantiChrom Urea Assay Kit-DIUR-100, BioAssay Systems). A seven-point calibration curve for urea concentration was prepared on each plate. Equal volume of reagent and medium was added to each well and the plate was mixed for 50 minutes at room temperature. The samples were measured on a SpectraMax i3x Microplate Reader at an optical density of 430 nm.

3.2.7 Transcript Expression Quantification with RT-qPCR

HepaRG cells were plated onto collagen scaffolds and incubated at experimental conditions for 48 hours. After CYP activity and urea collection, cells were washed and lysed using a TRIzol Plus RNA purification kit (ThermoFisher), according to the manufacturer's suggested protocol. The TRIzol reagent was added directly to the cells and agitated for 10 minutes prior to RNA isolation. Reverse Transcriptase PCR was performed immediately upon RNA isolation using the RNA isolation with a High-Capacity cDNA Reverse Transcription Kit (ThermoFisher) in an Eppendorf Master Cycler.

Table 3.2 lists the primer pair sequences, optimal concentrations, and reaction efficiency (90-110%) of each gene of interest. Amplification reactions were performed with PowerUp SYBR Master Mix (ThermoFisher), in a 384-well plate, on a QuantStudio 6 Flex Real-Time PCR system. Each sample was measured in triplicate, using the following program: 95 °C for 60 sec, followed by 40 cycles of 95 °C for 2 sec and 60 °C for 30 sec. Each transcript was quantified using the ΔΔCt method against 18sRNA. A fold-change of greater than 2.0 was considered significant.

3.2.8 Cell viability

HepaRG cells were seeded onto collagen coated 96-well plates following the same process as described above. Prior to analysis, the cells were washed with 1X PBS and lysed for 20 min in a 1:1 (v/v) solution of 1X PBS and CTG. Lysate aliquots (75 µL) were analyzed in an opaque 96-well plate on a SpectraMax i3x Microplate Reader in luminescence mode with a 140 ms integration.

3.2.9 Statistical Analysis

Datasets are reported as the average and standard error of the mean (SEM) of at least two separate cell vials, each cell vial contained at least two technical replicates. All data were analyzed with GraphPad Prism 7. Statistically significant differences correspond to a p-value of ≤ 0.05. To assess CYP activity, peak area or each metabolite product was normalized to a particular experiment condition, a normalized activity greater than 1.25 or less than 0.8 was considered significant since the LC-MS/MS peak area is highly reproducible, and 1.25/0.8 is statistically significantly outside of normal variability range (**Figure 3.2).**

3.3 Results and Discussion

Figure 3.3 summarizes the experimental workflow used to compare liver-specific function, metabolic enzyme activity and transcriptional regulation between HepaRG cells cultured at standard culture conditions to the periportal and perivenous.

3.3.1 HepaRG cell viability and liver specific activity follows in vivo zonation

HepaRG cells were plated and maintained for 6 days under standard culture conditions, and then followed by 2-day exposure to an experimental condition before urea secretion and viability were assessed (**Figure 3.4**). Cellular urea secretion was quantified with a colorimetric assay and viability assessed with the CTG 2.0 luminescence assay. The luminescence values obtained by the CTG assay were normalized to those obtained for the standard culture condition cells. Cells maintained under PV culture conditions had viability values similar to those under standard culture conditions, while the PP culture conditions decreased overall viability by approximately 70%. The HepaRG cells in the PP conditions could upregulate the transcription of

genes specific for gluconeogenesis enzymes such as phosphoenolpyruvate carboxykinase,[30] preferentially performing gluconeogenesis leading to inefficient ATP production as compared to the PV and Std conditioned cells. In vivo, glucose consumption is zonally distributed in which glycolysis is predominantly performed in the PV region and produces two ATP molecules. In the PP region, gluconeogenesis is predominant where lactate is turned into glucose by utilizing six ATPs.[26] Jungermann and Thurman experimentally observed the 'glucose paradox'[31] in which gluconeogenesis and glycolysis operate simultaneously and that lactate is circulated to the PP region for gluconeogenesis.[32]

In Chapter 2 HepG2 cell viability at each oxygen tension was measured with a tricolor cell stain and at 3% O_2 there was a decrease in the percentage of cells stained positive for calcein- attributed to reduced esterase/metabolism activity- but unchanged amount of PI stained cells. In the HepaRG cells, the PV conditions were at a low oxygen tension (5% O_2), however we did not observe a difference in cell viability. This discrepancy could be explained by the different oxygen tensions, indicating that the cell's metabolic response to 3% and 5% O_2 is different; as small changes in oxygen tension have measurable effects on cellular hypoxia and hypoxia related pathways. Also, the different cell lines- HepG2 to HepaRG- could respond differently to physiological conditions.

Urea synthesis and secretion is a marker for liver specific function and cell health. Under standard condition, 1 million HepaRG cells produced 0.015±0.002 milligrams of urea per 1 mL of medium per hour (mg/mL/hr/10^6 hepatocytes) (0.25 mM/hr/10^6 hepatocytes). The cells produced significantly more urea in the PP and PV conditions, 0.017±0.001 mg/mL/hr/10^6 hepatocytes (0.28 mM/hr/10^6 hepatocytes) and 0.023±0.002 mg/mL/hr/10^6 hepatocytes (0.38 mM/hr/10^6 hepatocytes) respectively. The amount of urea produced by the HepaRG cells in the

PP and PV conditions were not significantly different. Li and colleagues reported that HepaRG cells in spheroids secreted 3.0 mg/mLof urea per 1 million cells, and on culture plates they secreted 0.13mg/mL of urea per million HepaRG cells.[33] Hoekstra cultured HepaRG cells on traditional culture plates in the presence and absence of DMSO, they reported 1.2 nmol/hr/ 500,000 HepaRG in the absence of DMSO and 0.8 nmol/hr/ 500,000 HepaRG in the presence of DMSO.[34] The various range of urea secretion highlights that culture conditions significantly impact the urea secretion by HepaRG cells. The statistical increase in urea secretion observed by us and Li suggest increased cell health under tissue-like conditions. These findings contrast work of in perfusion systems on an intact rat liver, which observed increased urea secretion with increasing oxygen concentration from the PP to PV region.[35] The increase in urea production that we observed at physiological conditions compared to the standard culture condition indicate that physiological oxygen is enhances urea secretion. The standard conditions, at atmospheric oxygen, have increased oxidative stress and reactive oxygen species[36,37] which could be negatively impacting urea production and secretion.

3.3.2 HepaRG cell's drug metabolic activity increases until 11 days in culture

Metabolic activity is time-dependent in which the basal enzymatic activity changes depending on how long the HepaRG cells are in culture.[38] The enzyme activity and cell morphology of standard condition monolayers was measured every 4-5 days over an 24 day period. Metabolic enzyme activity was determined with an 8-in-1 cocktail in which the production of metabolites was quantified with LC-MS/MS using multiple reaction monitoring. Morphology was assessed widefield microscopy (**Figure 3.5**). The enzyme activity (**Figure 3.6)** of the cell were unchanged between day 1 and 4 and cell morphology was uniform across the

monolayer suggests the HepaRG cells are adapting to the collagen slab. The maximum enzyme activity increase, as compared to day 1, for each enzyme is summarized in **Table 3.3**; the enzymes with a notable increase were CYP1A2, 2C19, 2D6, and 3A4 (measured with midazolam) by 3.73, 4.01, 2.35, and 2.16-fold increase, respectively. From day 4 to day 11, activity increased. On day 7, cellular morphology indicates the HepaRG cells are displaying hepatocyte-like and biliary-like morphologies indicated by the cobblestone patterning and light and darker regions. On day 14, the cobblestone pattern between hepatocyte-like and biliary-like cells is more pronounced. Enzyme activity decreases day 11 until day 19, the decrease is to levels comparable to those measured on day 1. On day 24, all enzyme activity had significantly decreased.

Jackson and colleagues observed maximal drug metabolic activity 10 days after plating HepaRG cultured on a commercially available collagen-coated plates; this activity was maintained for 22 days, similar to what is observed with PHHs.[38] While the maximal activity values of the HepaRG cells on a 2mg/mL collagen slab was similar to the findings of Jackson, we observed a rapid decrease in CYP activity. Because of this rapid decrease in CYP activity we performed the remaining experiments on day 8, culturing the HepaRG cells for 6 days and exposing them to experimental conditions for 48 hours prior to analysis. Jackson suggests that the increase in enzyme activity with time is the HepaRG cells differentiating into a hepatocyte-like character. The drop in CYP activity after day 11 suggests the HepaRG cells are de-differentiating. Jackson hypothesized that time-dependent metabolic changes in the HepaRG cells is dynamic as a result of the HepaRG cells dedifferentiating throughout the culture period in response to standard culture practices such as media changes.[38]

3.3.3 HepaRG cells metabolic profile is amplified under standard conditions

To evaluate Phase I and II enzyme activity (**Figure 3.7**) and transcriptional regulation of Phase I, II, and transport proteins (**Figure 3.8**) of HepaRG under physiological conditions, we quantified metabolic enzyme activity then collected the mRNA from cells after 48-hour exposure to standard, PP, or PV conditions.

Compared to the standard conditioned HepaRG cells, CYP1A2, 2B6, 2C19, 2D6, and 3A4 (measured with midazolam) have significantly decreased activity in both the PP and PV conditions. For these CYPs, the activity was decreased more in the PP conditions than the PV condition- using CYP1A2 as an example, we measured a 0.02-fold decrease in the PP condition and a 0.09-fold decrease in the PV condition. The transcriptional regulation of *CYP1A2* closely followed activity trends, in which there was a 0.057-fold downregulation in the PP condition and a 0.153-fold downregulation in the PV condition. The closely followed trends between decreased activity and transcriptional downregulation was also observed for CYP3A4. The correlation between reduced transcript and reduced activity when comparing Std conditions to PP and PV conditions suggest that the observed CYP activity changes is driven by the transcriptional regulation. The transcriptional downregulation could be mediated via transcription factors Ahr, CaR and PxR (gene name: *AHR, NR113, NR112*). We measured a 0.279 and 0.337-fold downregulation of *NR112* in the PP and PV condition, respectively- PxR is a known transcription factor for CYP2C9 and 2C19. A downregulation in the *NR112* is accompanied by a downregulation of *CYP2C9* by 0.024 and 0.007-fold downregulation and a decreased activity of CYP2C19 by 0.38 and 0.67-fold.

The one exception to the measured transcript downregulation and decreased activity is CYP2E1. In PP conditions, *CYP2E1* is significantly upregulated by 869.334-fold; in PV

conditions the transcript is unchanged. However, upregulation of transcript in the PP condition does not manifest as an increase in CYP2E1 activity- rather no change in CYP2E1 activity was observed. This suggest there are other regulatory pathways acting on CYP2E1 to manifest the unchanged activity, such as post-translational modifications or regulated mRNA translation. The transcriptional downregulation being a knock-on effect of lower oxygen tension; one hypothesis is microRNA (miRNA), a class of 22-nuclotide non-coding RNA that has been shown to influence mRNA stability and translation. Furthermore, sets of miRNA have been induced by hypoxia, but the targets of these miRNAs is unknown.[39,40]

The activity of SULT and UGT is significantly downregulated in PP conditioned cells (0.113 and 0.034-fold decrease, respectively) but activity was unchanged in the PV condition. The transcriptional regulation does not match the activity trends, *UGT2B4* is upregulated in PP conditioned cells (95.93-fold) but downregulated in PV conditioned cells (0.071-fold). *SULT2A1* transcript is downregulated in both PP and PV conditioned cells.

van Wenum and colleagues compared HepaRG liver specific function at 5% 20% and 40% O_2; they found that the 40% O_2 environment improved liver specific function by 100-200% depending on the specific pathway being analyzed; for CYP3A4 activity, a hyperoxic (40% O_2) was increased by 174% as compared to atmospheric oxygen conditions. They concluded that the hyperoxic environment induced the upregulation of hepatic differentiation, metabolism and extracellular signaling genes.[41] The decreased enzymatic activity at low oxygen tensions was measured and described by Hernández-Gutiérrez et al. They measured the enzyme activity of CYP1A and 2B over time at decreasing oxygen tensions to determine Vmax (maximum rate of enzymatic reaction) and Km (the concentration of substrate at half the Vmax indicating enzyme affinity for the substrate); they concluded that Vmax decreased with decreasing oxygen tension

while Km remained constant indicating that oxygen tension plays a critical role in enzyme activity.[42] Std, PP and PV condition comparison is related to the conclusion by van Wenumm and Hernández-Gutiérrez in which cells cultured at lower oxygen tensions had downregulated metabolic enzyme transcripts and decreased enzymatic activity.

3.3.4 HepaRG cells cultured at physiological conditions display a metabolic profile similar to zonation

Comparisons of drug metabolic activity and transcript profiles of HepaRG cells exposed to PP and PV culture conditions allowed us to determine if metabolic patterns were representative of those regions in the liver. The initial hypothesis of this work was hepatocyte-like cells cultured under physiologically representative conditions would mimic zonation, where CYPs are most active in the PV region.

Figure 3.7b shows that the activity of CYP1A2, 2C19, 2D6, and 3A4 increase in the PV region, when normalized to the activity in the PP region. The activity of both the UGT and SULT families of enzymes also increased in the PV region, when normalized to the PP region. The increase in UGT activity matches zonation, as the glucuronide conjugation reactions are more common in the PV region of the liver. The increase in SULT family activity at lower oxygen tension is surprising, as these enzymes are more active in the PP region of the liver.[43] We note, however, that 7-hydroxycoumarin is not an enzyme-specific substrate so it can be conjugated by many members of both the SULT and UGT enzyme families.[44]

The cells we exposed to lower oxygen tension and Wnt are more metabolically active than the cells cultured at PP oxygen tension. The increased enzyme activity is likely a result of Wnt and Rspondin activating the Wnt/β-catenin signaling pathway and the 5% O_2 tension activating the HIF pathway. The activation of the Wnt/β-catenin signaling pathway at the

perivenous region of the liver has been deemed a master regulator of zonation.[9,26] Hailfinger *et al.* compared mouse hepatocytes under standard culture conditions using conditioned media containing or lacking Wnt. They observed a significant increase in transcript levels of various CYPs in the presence of Wnt.[45] Specifically, they saw a 2.5-fold increase in *CYP1A2*, which corresponds with the upregulation we observed in the HepaRG cells. To confirm the role of Wnt and Rspondin, we compared the drug metabolizing enzyme activity of HepaRG cells cultured at standard conditions with conditioned medium obtained from L-cell or L-WRN (**Figure 3.9**). We observed significant increase in CYP1A2, 2C19, 2D6, 3A4, SULT and UGT activity for cells exposed to the L-WRN conditioned media compared to the L-cell conditioned control. We hypothesize that the enzymatic activity and transcriptional regulation trends we observed in the PV conditioned cells compared to the PP conditioned cells is the combined effect of the Wnt/β-catenin pathway and HIF pathways. Kietzmann described these pathways stimulate the function of each other; one example is HIF1α binding to gene promoter regions that promote β-catenin.[9] Kaidi, Williams, and Paraskeva showed that HIF-1α and β-catenin interactions in immortalized human colon cancer cells (HCT116 and SW480) promote hypoxia-responsive genes, and enhance HIF-1-mediated transcription enabling cells to adapt to a hypoxic environment; furthermore they described interactions between HIF-1α and β-catenin mediated by T-cell factor-4 protein complex.[46]

Figure 3.7b displays the transcriptional differences between cells exposed to PP or PV conditions. The transcriptional regulation of the CYP enzymes was partially consistent with the data collected from the activity assays and the expectations of zonation; both *CYP1A2* and *CYP8B1* were upregulated in the PV region when compared to the PP region, however *CYP2E1* and *CYP2C9* were downregulated. One representative member of the SULT and UGT family

were quantified, *SULT2A1* and *UGT2B4* respectively. These two transcripts also corresponded to zonation expectation, with higher levels of *SULT2A1* in the PV conditions and higher levels of *UGT2B4* in the PP conditions.

The discrepancy between the CYP gene transcriptional regulation and the measured drug metabolic activity between the PP and PV conditions suggest that there are other regulatory pathways dictating enzyme activity. Traditionally, transcriptional factors such as hepatocyte nuclear factor 4α (HNF4),[47,48] β-catenin,[25,49] and HIF1α[9] have significant effects on the expression of metabolic enzyme transcripts in hepatocytes, in vivo and in vitro. However, this work suggests that at physiological culture conditions, some enzymes in vitro activity (CYP2E1, CYP3A4 and UGT) could be regulated with other pathways such as mRNA post-transcriptional regulation with miRNA- exploring these other regulatory pathways could help identify regulatory zonation patterns.

The expression of transport proteins, liver-specific proteins, adhesion markers and HIF1α-regulated genes were quantified for cells exposed to standard, PP, and PV conditions (**Figure 3.7d**). Expression of the drug uptake transporters *SLC22A1* and *SLCO2B1* , when compared to the PP region, were upregulated in PV conditions. Such an upregulation is expected due to the PV processing the majority of phase I drug metabolism. The efflux transporters *ABCB1, ABCC2, ABCC3, SLC10A1* and *ABCG2* were downregulated in the PV conditioned cells as compared to the PP conditioned cells. The distribution of drug transporters in vivo was measured by Tachikawa who concluded that OATP1B2 and OCT1 (gene name *SLCO1A2* and *SLC22A1*) were zonally distributed in the periportal region.[50] We hypothesize that the increased transporter expression in the PP region suggests that xenobiotics that enter hepatocytes in this region are expelled due to a low CYP activity.

Lastly, *KRT19* transcript (protein: CK-19) was downregulated in the PV conditioned cells; CK-19 is a common marker for biliary-like hepatocytes around the bile canaculi and CK-19 has been observed in proliferative cells.[51,52] The transcriptional regulation of *KRT19* between PP and PV cells suggesting that hepatocytes in the PP region are better primed for proliferation and growth. A recent study by He and colleagues concluded that midzonal hepatocytes were more proliferative with less proliferative cell in the PP while the liver is at homeostasis.[53] This makes sense from the in vivo liver because stem cell like cells are known to be found around the portal triad.[54,55]

3.4 Conclusions and future work

This study compared HepaRG cells cultured as monolayers on collagen slabs at standard culture conditions, and physiological conditions representative of the periportal and perivenous region of the liver lobule. The experimental design chose two physiological conditions of fixed composition rather than exposing cells to the entire gradient that spans the sinusoid. This design provided superior control over the extracellular environment, allowed for comparisons to zonal characteristics observed in vivo, and could incorporate large enough cell numbers in a single experiment to obtain viability, health, drug metabolic activity, and transcript profiles from the same set of cells.

In this work we cultured HepaRG cells at specific oxygen tensions and in the presence or absence of the Wnt morphogen and Rspondin, to model the physiological environment of the periportal and perivenous regions. At standard, PP and PV culture conditions, the HepaRG cells were viable and displaying liver specific function. We observed a decrease of metabolizing enzyme activity and downregulation of transcriptional regulation when comparing the standard

culture conditioned HepaRG cells to the PP and PV conditioned cells. The overall reduction of CYP and phase II enzyme activity at the PP and PV condoned cells is attributed to the reduction of oxygen tension by an order of magnitude; the lower oxygen culture, and reduced oxygen availability for the cells impacts the overall ability for the enzymes to function.[42] The reduction of transcript for nearly every gene measured at the PP and PV condition could be an effect of miRNA that has been shown to increase in hypoxic environments, the miRNA have been shown to influence mRNA stability. Despite the downregulated activity and transcript at physiological conditions, this may not be a negative for the physiological cultures because enhanced drug metabolic activity is not as important as modeling zonation patterns and trends *in vitro*.

The comparisons of drug metabolic activity and transcriptional regulation between PP and PV conditioned cells yielded exciting results. The CYP and Phase II enzyme activity is significantly upregulated in the PV conditioned cells, matching the expected zonal distribution of drug metabolizing enzymes; this suggests that the cells exposed to lower oxygen tension, Wnt and Rspondin, through HIF and β-catenin pathways, are responsible for the increased metabolically activity over the cells cultured at PP oxygen tension. However, transcriptional regulation does not follow the enzymatic activity which suggests other regulatory pathways could be explored, such as mRNA post-transcriptional regulation, differences in enzymatic post-translational modification between PP and PV cells and differences in enzyme-kinetics at different conditions. Analysis of various regulatory checkpoints of the metabolic enzymes could provide further insight into the rise of liver zonation.

Overall, the metabolic enzyme activity is highest under standard culture conditions, meaning the current culture method of HepaRG is appropriate to assess the metabolic pathway and metabolizing enzyme are acting upon a xenobiotic. However, maximal metabolic enzyme

activity in vitro may not represent physiological enzyme activity. It is difficult to assess physiological enzyme activity due person to person variability, but we do know that zonation patterning of the lobule is universal- specifically zonally distributed Phase I and II enzymes. Our integration physiological conditions representative of the PP and PV microenvironments were able to display zonal distribution of CYP and UGT enzymic activity, but not SULT enzymes. This is a promising step to develop an ideal in vitro liver model that can mimic zonal distribution and patterning. Incorporation of proteomic post translational modification analysis and further study into the activity of zonally distributed pathways, such as glycogen synthesis, could further support the use of physiological culture conditions.

3.5 Figures and tables

Table 3.1. MS/MS Transition monitoring for each drug metabolizing enzyme product using the 8-in-1 cocktail.

Enzyme	Substrate	Final Concentration (μM)	Product	Declustering Voltage (V)	Ion Mode	Parent m/z	Product m/z	Collision Energy (eV)
CYP1A2	Phenacetin	100	Acetaminophen	6	Positive	152.2	110	15
						152.2	65.03	30
CYP2B6	Bupropion	50	Hydroxy bupropion	6	Positive	256.02	238.1	8
						256.02	130.1	47
CYP2C19	(*S*)-mephenytoin	100	4'- Hydroxymephenytoin	6	Negative	232.9	190.1	19
						232.9	161.0	25
CYP2D6	Dextromethorphan	100	Dextrorphan	4	Positive	258.04	157.1	36
						258.04	199.1	25
CYP2E1	Chlorzoxazone	15	6-Hydroxychlorzoxazone	2	Negative	184.0	120.1	22
						184.0	64.0	33
CYP3A4	Midazolam	5	1-Hydroxymidazolam	6	Positive	342.04	324.1	19
						342.04	168.1	36
CYP3A4	Testosterone	50	6-beta-Testosterone	8	Positive	305.2	269.2	13
						305.2	105.1	36
SULT	7-hydroxycoumarin	100	7-Hydroxycoumarin sulfate	6	Negative	240.7	161.0	20
						240.7	133.0	34
UGT	7-hydroxycoumarin	100	7-Hydroxycoumarin glucuronide	6	Negative	337.0	161.0	29
						337.0	175.0	13

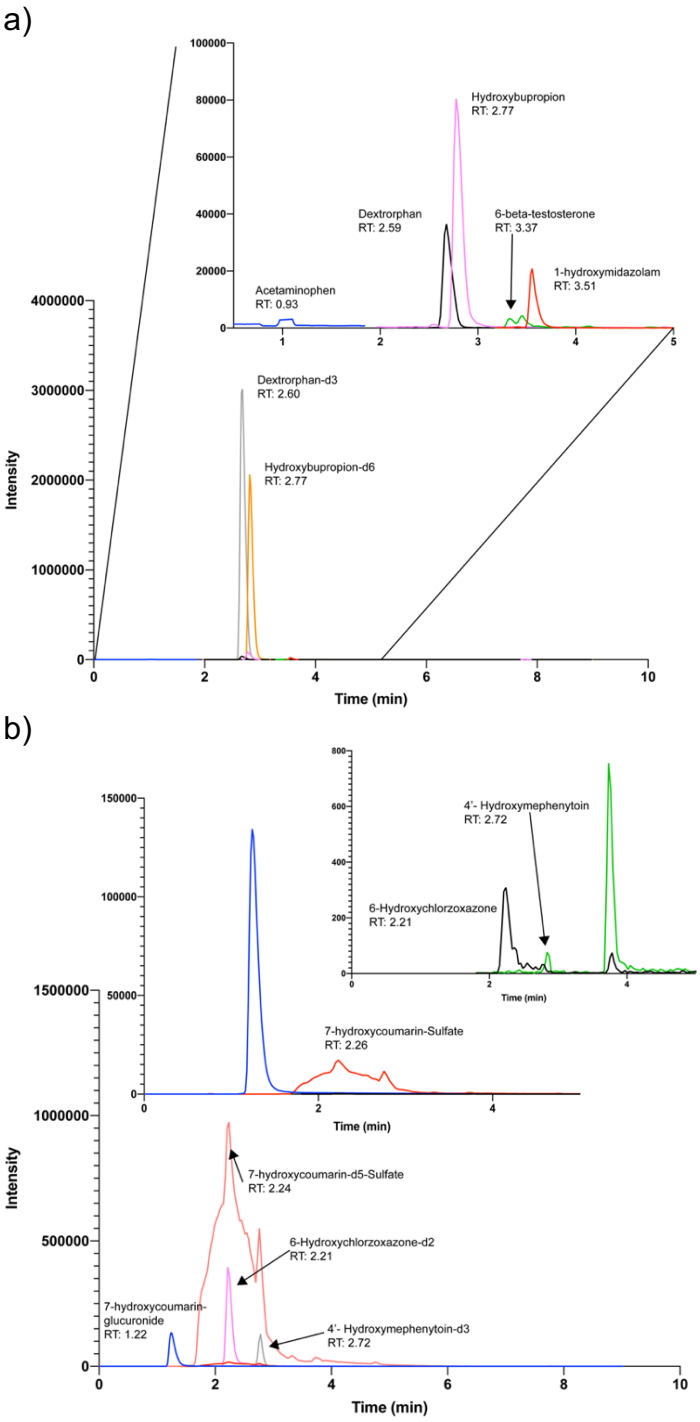

Figure 3.1. Representative chromatograms of 8-in-1 drug metabolizing enzyme activity cocktail after a 2-hour incubation with HepaRG cells. Samples were injected twice for products to be identified with MS/MS in in positive ion mode (a) and negative ion mode (b).

Table 3.2 List of 25 genes evaluated in this study.

Gene Symbol	Protein abbreviation	Main Function	Forward Primer (5' – 3')	Reverse Primer (5' – 3')	Efficiency (%)
18sRNA	18s rRNA	Ribosome	CGCCGCTAGAGGTGAAATTC	TTGGCAAATGCTTTCGCTC	107.5
CYP1A2	CYP1A2	Phase I Enzyme	CTTCGGACAGCACTTCCCTG	AGGGTTAGGCAGGTAGCGAA	103.9
CYP2E1	CYP2E1	Phase I Enzyme	TTGAAGCCTCTCGTTGACCC	CGTGGTGGGATACAGCCAA	109.9
CYP2C9	CYP2C9	Phase I Enzyme	TCCCTGACTTCTGTGCTACATG	ACTGGAGTGGTGTCAAGGTTC	113.9
CYP3A4	CYP3A4	Phase I Enzyme	TCACAAACCGGAGGCCTTTT	TGGTGAAGGTTGGAGACAGC	100.4
CYP8B1	CYP8B1	Phase I Enzyme	TGCACATGGACCCTGACATC	GTGTCAGGGTCCACCAACTC	91.9
UGT2B4	UGT2B4	Phase II Enzyme	ACACATGAAGGCCAAGGGAG	GAACCAGGTGAGGTCGTGG	94.3
SULT2A1	SULT2A1	Phase II Enzyme	TGAGGAGCTGAAACAGGACAC	AAGTCTTCAGCTTGGGCCAC	106.6
AHR	AhR	Transcription Factor	CTTCCAAGCGGCATAGAGAC	AGTTATCCTGGCCTCCGTTT	101.5
NR1I3	CaR	Transcription Factor	TGATCAGCTGCAAGAGGAGA	AGGCCTAGCAACTTCGCATA	102.6
NR1I2	PxR	Transcription Factor	CCAGGACATACACCCCTTTG	CTACCTGTGATGCCGAACAA	104.3
SLC10A1	NTCP	Transporter (Uptake)	GGGACATGAACCTCAGCATT	CGTTTGGATTTGAGGACGAT	101.4
SLC22A1	OCT1	Transporter (Uptake)	TAATGGACCACATCGCTCAA	AGCCCCTGATAGAGCACAGA	104.5
SLCO2B1	OATP2B1	Transporter (Uptake)	TGATTGGCTATGGGGCTATC	CATATCCTCAGGGCTGGTGT	106.5
SLOC1B1	OATP1B1	Transporter (Uptake)	GCCCAAGAGATGATGCTTGT	ATTGAGTGGAAACCCAGTGC	97.3
ABCB1	P-gp	Efflux Pump	GCCAAAGCCAAAATATCAGC	TTCCAATGTGTTCGGCATTA	93.6
ABCC2	MRP2	Transporter (Excretion)	TGAGCAAGTTTGAAACGCACAT	AGCTCTTCTCCTGCCGTCTCT	99.6
ABCC3	MRP3	Transporter (Excretion)	GTCCGCAGAATGGACTTGAT	TCACCACTTGGGGATCATTT	108.5
ABCG2	BCRP	Transporter (Excretion)	TGCAACATGTACTGGCGAAGA	TCTTCCACAAGCCCCAGG	101.5
ICAM1	ICAM-1	Cell-Cell Interaction	GGCCGGCCAGCTTATACAC	TAGACACTTGAGCTCGGGCA	101.9
KRT19	CK-19	Biliary-like/Progenitor Cell Marker	TTTGAGACGGAACAGGCTCT	AATCCACCTCCACACTGACC	100.8
ALB	Albumin	Globular Protein	TGAGCAGCTTGGAGAGTACA	GTTCAGGACCACGGATAGAT	124.1
TJP1	ZO-1	Tight-Junction	CGAGTTGCAATGGTTAACGGA	TCAGGATCAGGACGACTTACTGG	106.9
HIF1A	HIF1a	Transcription Factor	CATAAAGTCTGCAACATGGAAGGT	ATTTGATGGGTGAGGAATGGGTT	100.9
CAIX	CAIX	Hypoxia Responsive Element (Hydration catalyst)	GGGCCCGGAAGAAAACAGT	TCTTCCAAGCGAGACAGCAAC	104.8

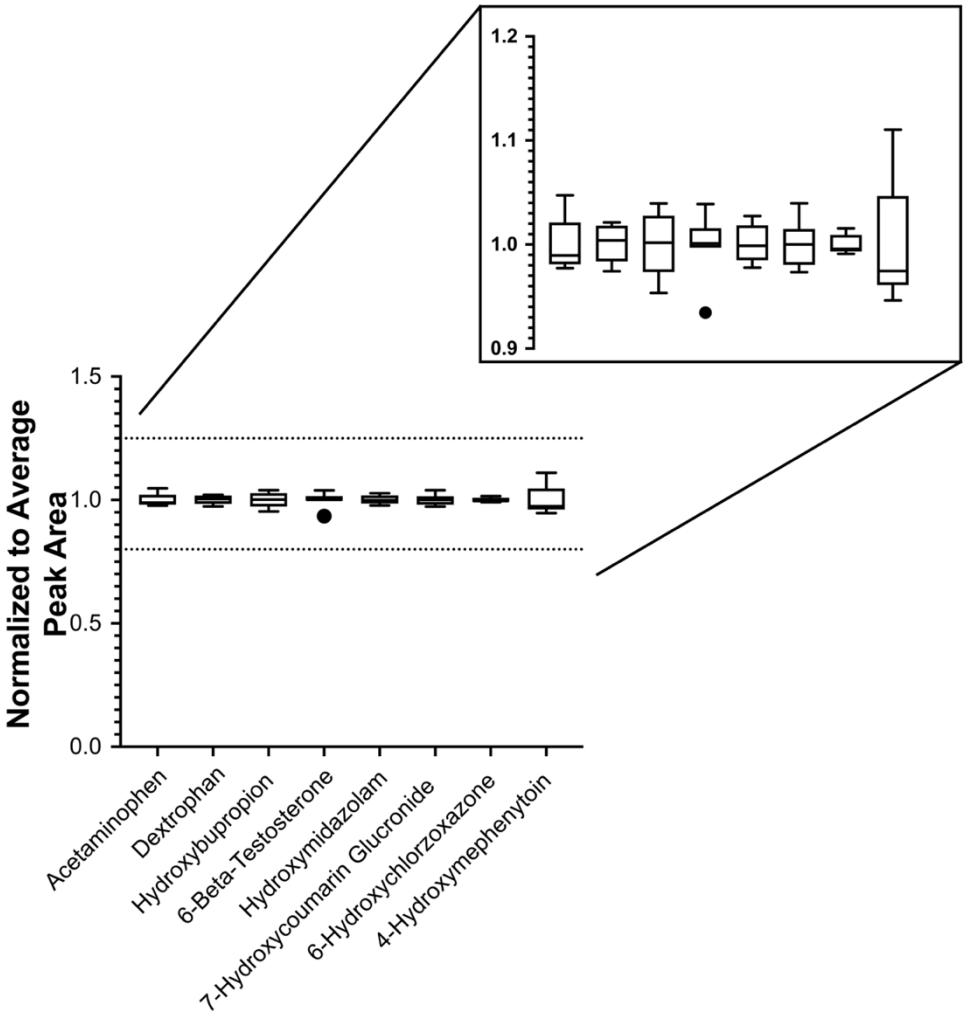

Figure 3.2. Variability of LC-MS/MS detection of the eight CYP cocktail products. A mixture of the nine products were injected ten times in sequence; 7-hydroxycoumarin Sulfate was undetectable and therefore not shown. Each injection was normalized to the average peak area of the substrate. Plotted is a Turkey box and whisker plot. Four standard deviations, accounting for 99.99% of deviation on a normal bell curve, was calculated to be a fold change of 1.25 and 0.8, represented by the black dotted lines.

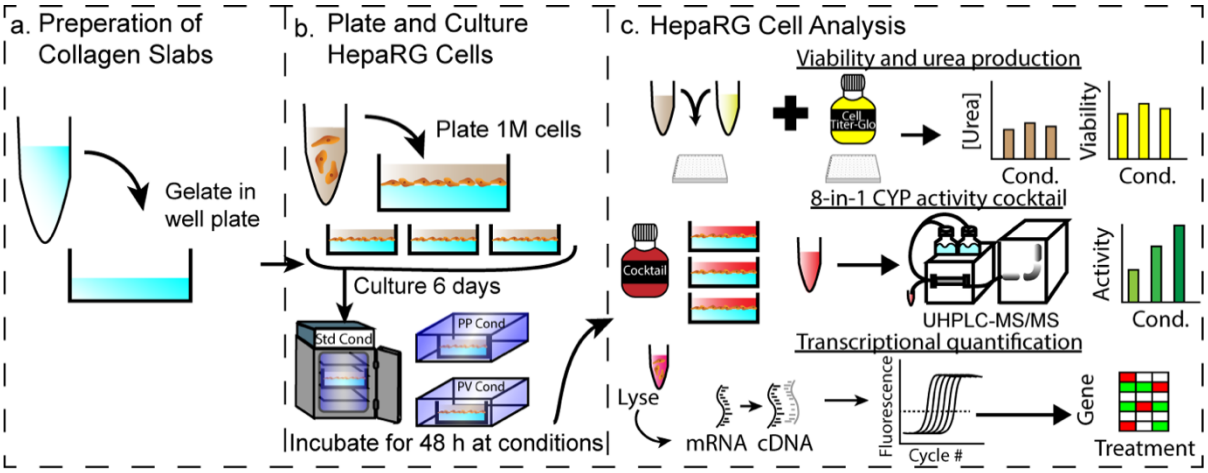

Figure 3.3. Experimental workflow comparing the responses of HepaRG cells exposed to different culture conditions where cells were maintained as monolayer on collagen I slabs. (a) Collagen slabs (2 mg/mL) coated the bottoms of a 12-well plate and allowed to gelate overnight (b) The HepaRG cells were seeded onto the collagen slabs and incubated for six days under standard culture conditions (20% O_2, 5% CO_2, and 37 ^oC) before being placed in at the experimental conditions for 48 h: standard (20% O_2, 5% CO_2), periportal (11% O_2, 5% CO_2) or perivenous (5% O_2, 5% CO_2, +Wnt). (c) Finally, cell health was evaluated with the CellTiter-Glo viability assay and urea secretion with a colorimetric urea assay, CYP activity was quantified with LC-MS/MS, and transcriptional regulation was determined with RT-qPCR.

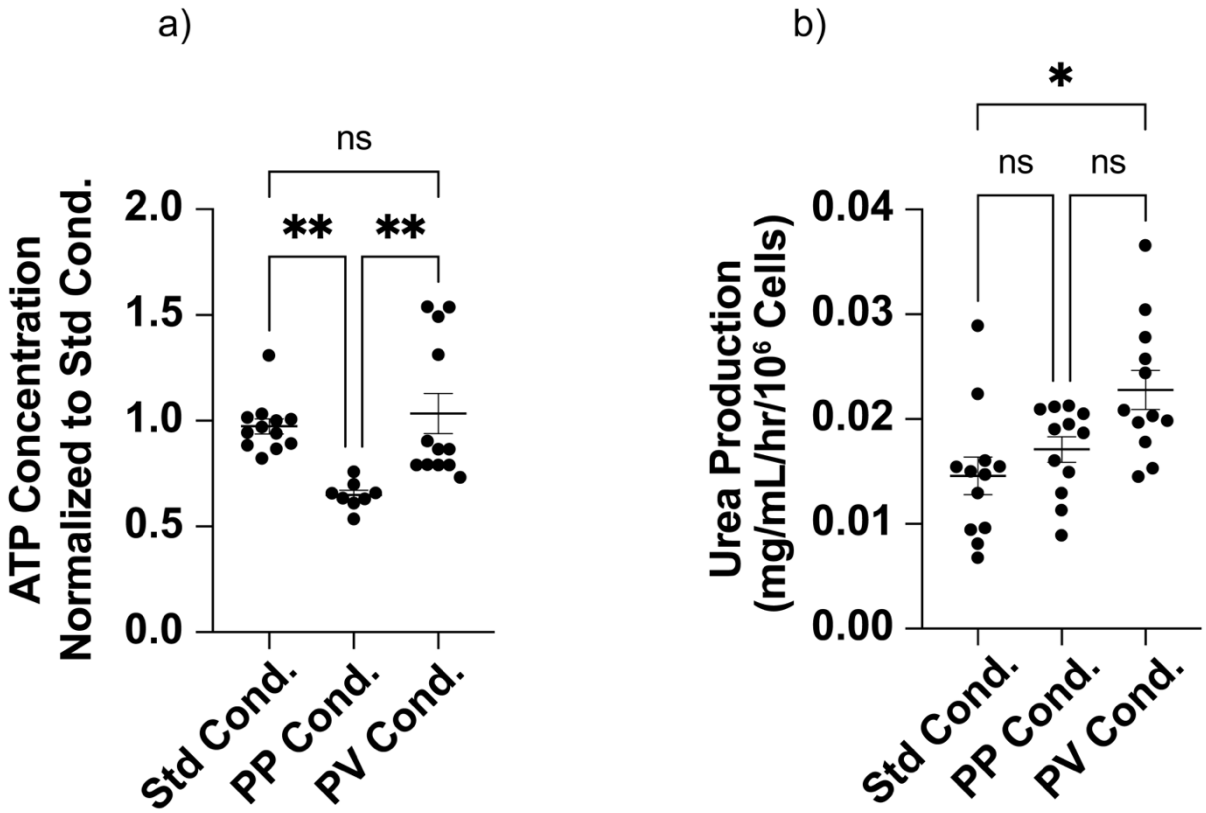

Figure 3.4. Assessment of HepaRG cell health and liver specific function after 48 hour in physiological conditions. (a) Quantification of ATP concentration using Cell-Titer Glo 2.0 from HepaRG cells normalized to the standard culture condition cells. (b) Urea secretion of the HepaRG cells quantified with a colorimetric assay (Bioassay Systems). Data points represent the individual technical replicates pooled from two biological replicates; the mean was plotted with error bars representing the SEM. Significant difference was measured with a one-way ANOVA analysis.

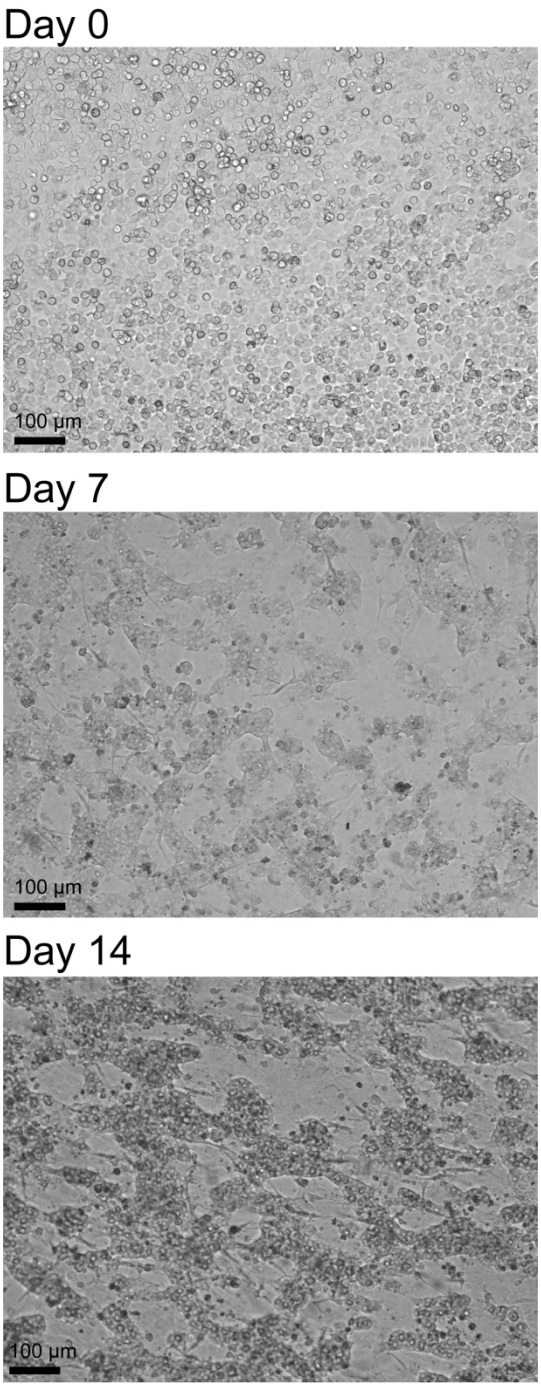

Figure 3.5. Widefield images of HepaRG cells grown over 24 days for metabolic competency. Over the 14 days displayed above, a clear morphological change can be observed. On day 0 the cells appear rounded are shape. On day 7 and 14 the cells are adopting a more cobblestone morphology and cord-like network representative of biliary-like and hepatocyte-like

morphologies. On day 7 and 14 the HepaRG morphology is similar to that of PHHs. Widefield images were collected using a Nikon TE2000 microscope, 10x objective and captured using a Photometrics Dyno CCD camera. Scale bars are 100 μm.

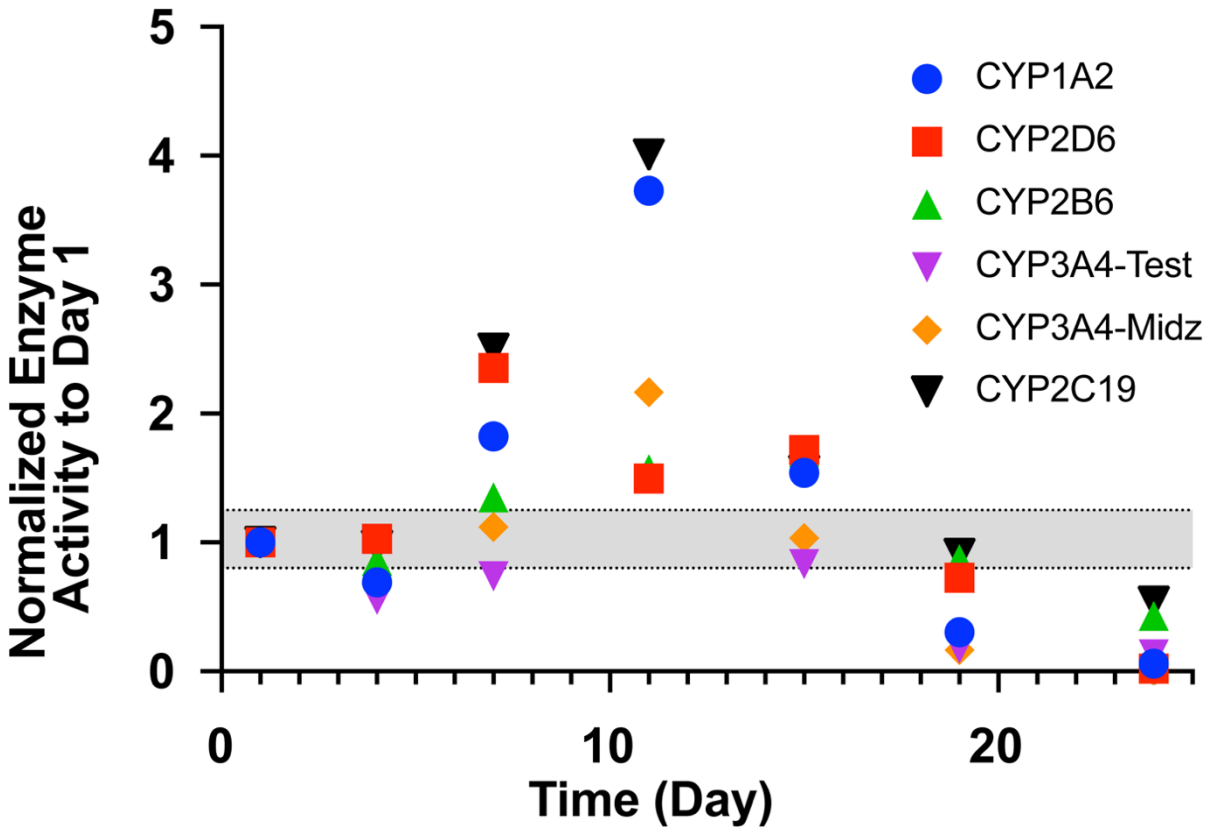

Figure 3.6. HepaRG cells were cultured on a collagen slab at standard culture conditions for 24 days. CYP activity was measured with the 8-in-1 CYP cocktail every 4 days and activity was normalized to day 1 measurements. Dotted black lines represent 1.25- and 0.8-fold change, those associated with a significant difference in activity. Data points represent the average of two biological replicates.

Table 3.3 Summary of maximal increase in drug metabolizing enzyme activity and day it was observed. [a]

	Day	Max Activity (Fold Change)
CYP1A2	11	3.73
CYP2B6	15	1.7
CYP2C19	11	4.01
CYP2D6	7	2.35
CYP2E1	--	N/A
CYP3A4- Midz	11	2.16
CYP3A4- Test	11	1.49
SULT	15	1.15
UGT	7	1.02

[a] --/ N/A indicates no increase in enzyme activity was observed over the 24 days.

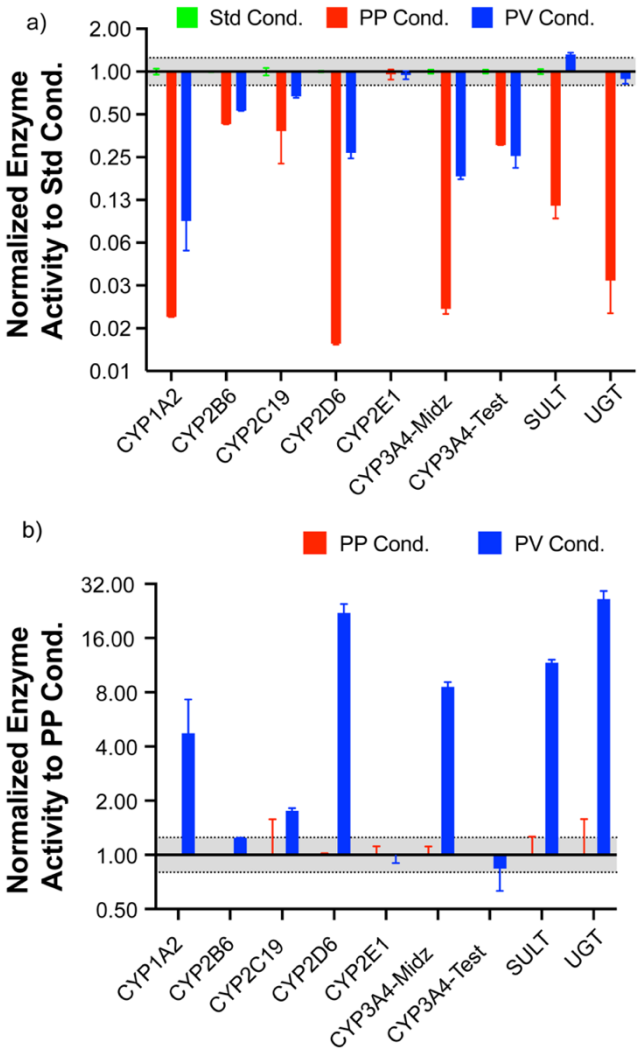

Figure 3.7. Metabolic enzyme activity of HepaRG cells cultured for 6 days followed by 48 hour at standard, PP or PV conditions. (a) Enzyme activity was normalized to the average standard condition activity for each CYP. (b) Enzyme activity was normalized to the average PP condition activity for each CYP; the standard condition was excluded to focus on changes between the PP and PV conditioned cells. Dotted black lines represent 1.25- and 0.8-fold change, those associated with a significant difference in activity. Bars represent the average ± SEM, from 2 biological replicates.

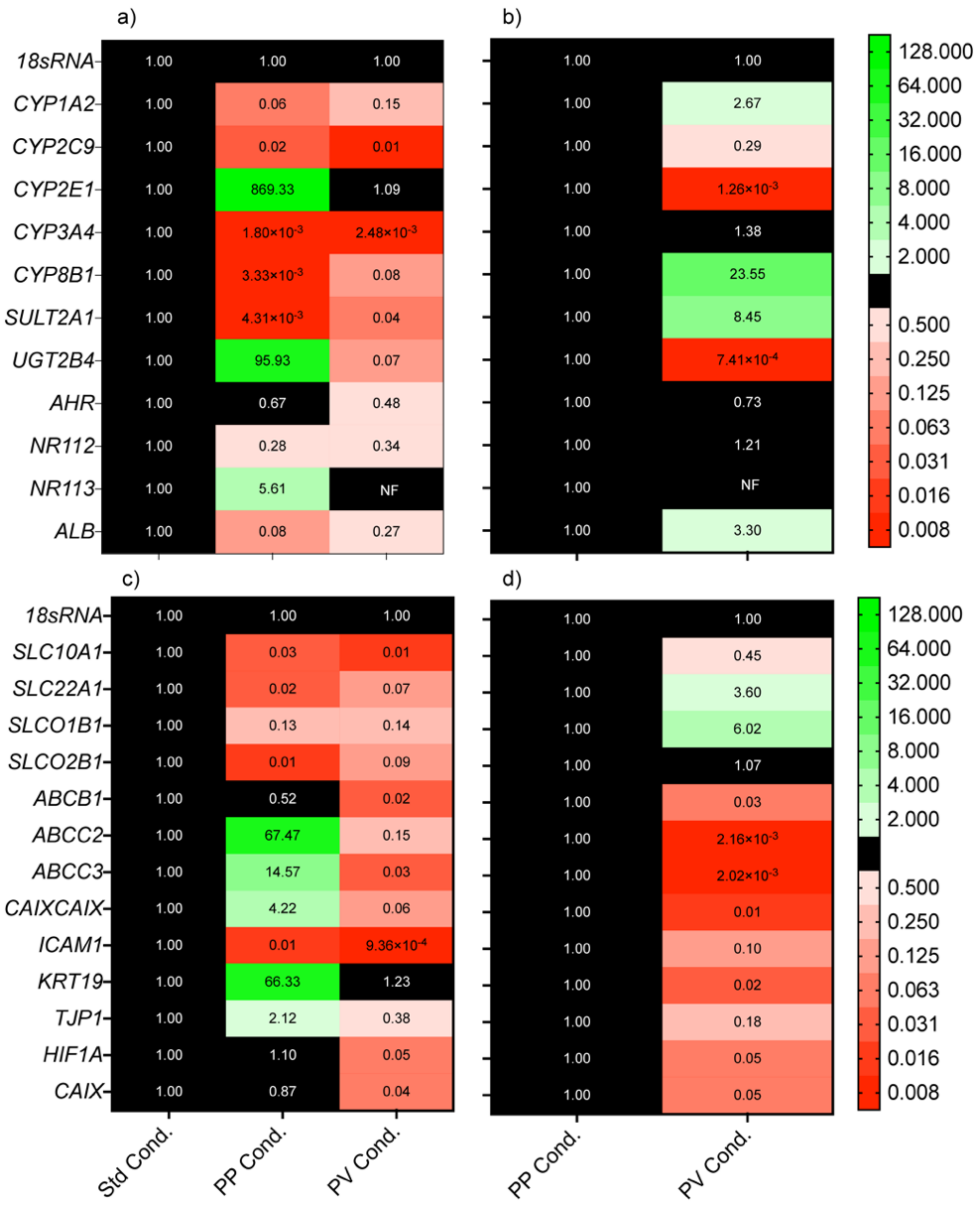

Figure 3.8. Transcript-level regulation of HepaRG cells cultured for 6 days followed by 48 hour at standard, PP or PV conditions was measured and compared. Transcript level analysis of phase I enzymes, phase II enzymes, and receptors compared to the standard conditioned HepaRG cells (a) and the PP conditioned HepaRG cells (b). Transcript level analysis of transporters, adhesion proteins and hypoxia response proteins were compared to the standard conditioned HepaRG cells (c) and the PP conditioned HepaRG cells (d); the standard condition was excluded to focus on changes between the PP and PV conditioned cells. Each value is the average of at least one

technical replicate, collected from two biological replicates. A fold-change >2 indicates a significant increase in expression; <0.50 indicates a significant decrease. The numerical labels represent the average fold change using the ΔΔCt method. NF indicates no transcript was quantified.

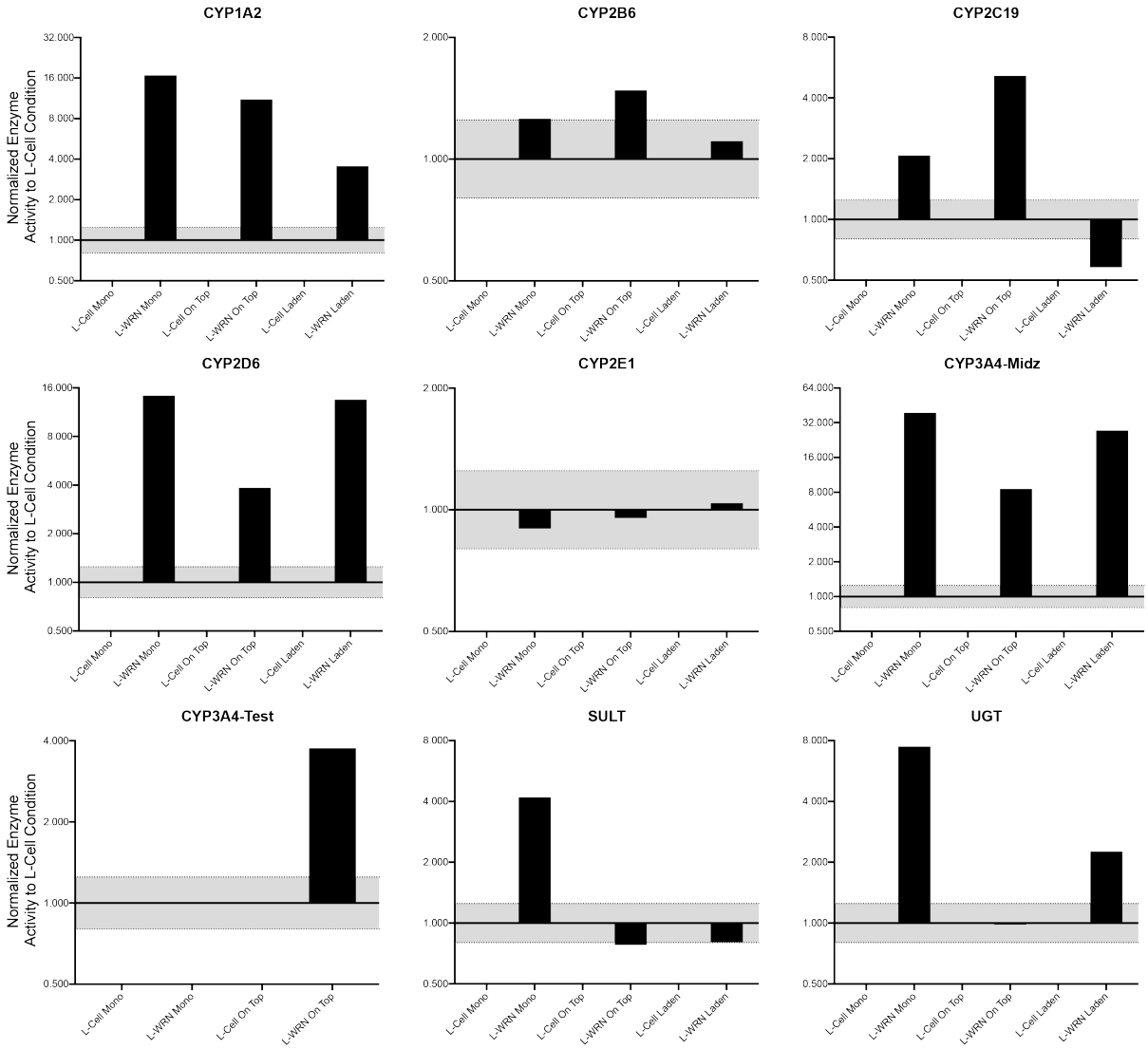

Figure 3.9. Basal drug metabolizing enzyme activity of HepaRG cells cultures with L-cell or L-WRN cell conditioned media. Activity was normalized to the enzyme activity of cells exposed to L-cell conditioned media after an 8-day culture period. The grey region of the curve represents 1.25- and 0.8-fold change, those bars outside of this region are considered a significant difference in activity.

REFERENCES

(1) Kenna, J. G.; Uetrecht, J. Do In Vitro Assays Predict Drug Candidate Idiosyncratic Drug-Induced Liver Injury Risk? *Drug Metab. Dispos.* **2018**, *46* (11), 1658–1669. https://doi.org/10.1124/dmd.118.082719.

(2) Parasrampuria, D. A.; Benet, L. Z.; Sharma, A. Why Drugs Fail in Late Stages of Development: Case Study Analyses from the Last Decade and Recommendations. *AAPS J.* **2018**, *20* (46). https://doi.org/10.1208/s12248-018-0204-y.

(3) Dunn, J. C. Y.; Tompkins, R. G.; Yarmush, M. L. Hepatocytes in Collagen Sandwich: Evidence for Transcriptional and Translational Regulation. *J. Cell Biol.* **1992**, *116* (4), 1043–1053. https://doi.org/10.1083/jcb.116.4.1043.

(4) Dunn, J. C. Y.; Yarmush, M. L.; Koebe, H. G.; Tompkins, R. G. Hepatocyte Function and Extracellular Matrix Geometry: Long-term Culture in a Sandwich Configuration. *FASEB J.* **1989**, *3* (2), 174–177. https://doi.org/10.1096/fasebj.3.2.2914628.

(5) Meyer, C.; Liebe, R.; Breitkopf-Heinlein, K.; Liu, Y.; Müller, A.; Rakoczy, P.; Thomas, M.; Weng, H.; Bachmann, A.; Ebert, M.; Dooley, S. Hepatocyte Fate Upon TGF-β Challenge Is Determined by the Matrix Environment. *Differentiation* **2015**, *89* (5), 105–116. https://doi.org/10.1016/j.diff.2015.04.001.

(6) Chang, T. T.; Hughes-Fulford, M. Monolayer and Spheroid Culture of Human Liver Hepatocellular Carcinoma Cell Line Cells Demonstrate Distinct Global Gene Expression Patterns and Functional Phenotypes. *Tissue Eng. - Part A* **2009**, *15* (3), 559–567. https://doi.org/10.1089/ten.tea.2007.0434.

(7) Ramaiahgari, S. C.; Den Braver, M. W.; Herpers, B.; Terpstra, V.; Commandeur, J. N. M.; Van De Water, B.; Price, L. S. A 3D in Vitro Model of Differentiated HepG2 Cell Spheroids with Improved Liver-like Properties for Repeated Dose High-Throughput Toxicity Studies. *Arch. Toxicol.* **2014**, *88* (5), 1083–1095. https://doi.org/10.1007/s00204-014-1215-9.

(8) Gaskell, H.; Sharma, P.; Colley, H. E.; Murdoch, C.; Williams, D. P.; Webb, S. D. Characterization of a Functional C3A Liver Spheroid Model. *Toxicol. Res. (Camb).* **2016**, *5* (4), 1053–1065. https://doi.org/10.1039/c6tx00101g.

(9) Kietzmann, T. Metabolic Zonation of the Liver: The Oxygen Gradient Revisited. *Redox Biol.* **2017**, *11* (January), 622–630. https://doi.org/10.1016/j.redox.2017.01.012.

(10) Oinonen, T.; Mode, A.; Lobie, P. E.; Lindros, K. O. Zonation of Cytochrome P450 Enzyme Expression in Rat Liver: Isozyme-Specific Regulation by Pituitary Dependent Hormones. *Biochem. Pharmacol.* **1996**, *51* (10), 1379–1387. https://doi.org/10.1016/0006-2952(96)00064-0.

(11) Prabhakar, N. R.; Semenza, G. L. Oxygen Sensing and Homeostasis. *Physiology* **2015**, *30* (5), 340–348. https://doi.org/10.1152/physiol.00022.2015.

(12) Oinonen, T.; Lindros, K. O. Zonation of Hepatic Cytochrome P-450 Expression and Regulation. *Biochem. J.* **1998**, *329*, 17–35. https://doi.org/10.1042/bj3290017.

(13) Braeuning, A.; Ittrich, C.; Köhle, C.; Hailfinger, S.; Bonin, M.; Buchmann, A.; Schwarz, M. Differential Gene Expression in Periportal and Perivenous Mouse Hepatocytes. *FEBS J.* **2006**, *273* (22), 5051–5061. https://doi.org/10.1111/j.1742-4658.2006.05503.x.

(14) Kitamoto, N.; Mattion, N. M.; Estes, M. K. Alterations in the Sequence of the Gene 4 from a Human Rotavirus after Multiple Passages in HepG2 Liver Cells. *Arch. Virol.* **1993**, *130* (1–2), 179–185. https://doi.org/10.1007/BF01319006.

(15) Zhao, Y.; Chen, Y.; Hu, Y.; Wang, J.; Xie, X.; He, G.; Chen, H.; Shao, Q.; Zeng, H.; Zhang, H. Genomic Alterations across Six Hepatocellular Carcinoma Cell Lines by Panel-Based Sequencing. *Transl. Cancer Res.* **2018**, *7* (2), 231–239. https://doi.org/10.21037/tcr.2018.02.14.

(16) Westerink, W. M. A.; Schoonen, W. G. E. J. Phase II Enzyme Levels in HepG2 Cells and Cryopreserved Primary Human Hepatocytes and Their Induction in HepG2 Cells. *Toxicol. Vitr.* **2007**, *21* (8), 1581–1591. https://doi.org/10.1016/j.tiv.2007.05.014.

(17) Gerets, H. H. J.; Hanon, E.; Cornet, M.; Dhalluin, S.; Depelchin, O.; Canning, M.; Atienzar, F. A. Selection of Cytotoxicity Markers for the Screening of New Chemical Entities in a Pharmaceutical Context: A Preliminary Study Using a Multiplexing Approach. *Toxicol. Vitr.* **2009**, *23* (2), 319–332. https://doi.org/10.1016/j.tiv.2008.11.012.

(18) Gerets, H. H. J.; Tilmant, K.; Gerin, B.; Chanteux, H.; Depelchin, B. O.; Dhalluin, S.; Atienzar, F. A. Characterization of Primary Human Hepatocytes, HepG2 Cells, and HepaRG Cells at the MRNA Level and CYP Activity in Response to Inducers and Their Predictivity for the Detection of Human Hepatotoxins. *Cell Biol. Toxicol.* **2012**, *28* (2), 69–87. https://doi.org/10.1007/s10565-011-9208-4.

(19) Kaelin, W. G. Proline Hydroxylation and Gene Expression. *Annu. Rev. Biochem.* **2005**, *74*, 115–128. https://doi.org/10.1146/annurev.biochem.74.082803.133142.

(20) Jungermann, K.; Kietzmann, T. Oxygen: Modulator of Metabolic Zonation and Disease of the Liver. *Hepatology* **2000**, *31* (2), 255–260. https://doi.org/10.1002/hep.510310201.

(21) Behari, J. The Wnt/β-Catenin Signaling Pathway in Liver Biology and Disease. *Expert Rev. Gastroenterol. Hepatol.* **2010**, *4* (6), 745–756. https://doi.org/10.1586/egh.10.74.

(22) Russel, J.; Monga, S. Wnt/β-Catenin Signaling in Liver Development, Homeostasis, and Pathobiology. *Annu. Rev. Pathol.* **2018**, *13*, 351–378. https://doi.org/10.1016/j.chemosphere.2012.12.037.Reactivity.

(23) Rocha, A. S.; Vidal, V.; Mertz, M.; Kendall, T. J.; Charlet, A.; Okamoto, H.; Schedl, A. The Angiocrine Factor Rspondin3 Is a Key Determinant of Liver Zonation. *Cell Rep.* **2015**, *13* (9), 1757–1764. https://doi.org/10.1016/j.celrep.2015.10.049.

(24) Benhamouche, S.; Decaens, T.; Godard, C.; Chambrey, R.; Rickman, D. S.; Moinard, C.; Vasseur-Cognet, M.; Kuo, C. J.; Kahn, A.; Perret, C.; Colnot, S. Apc Tumor Suppressor Gene Is the "Zonation-Keeper" of Mouse Liver. *Dev. Cell* **2006**, *10* (6), 759–770. https://doi.org/10.1016/j.devcel.2006.03.015.

(25) Kietzmann, T. Liver Zonation in Health and Disease: Hypoxia and Hypoxia-Inducible Transcription Factors as Concert Masters. *Int. J. Mol. Sci.* **2019**, *20* (9). https://doi.org/10.3390/ijms20092347.

(26) Godoy, P.; Hewitt, N. J.; Albrecht, U.; Andersen, M. E.; Ansari, N.; Bhattacharya, S.; Bode, J. G.; Bolleyn, J.; Borner, C.; Böttger, J.; Braeuning, A.; Budinsky, R. A.; Burkhardt, B.; Cameron, N. R.; Camussi, G.; Cho, C. S.; Choi, Y. J.; Craig Rowlands, J.; Dahmen, U.; Damm, G.; Dirsch, O.; Donato, M. T.; Dong, J.; Dooley, S.; Drasdo, D.; Eakins, R.; Ferreira, K. S.; Fonsato, V.; Fraczek, J.; Gebhardt, R.; Gibson, A.; Glanemann, M.; Goldring, C. E. P. P.; Gómez-Lechón, M. J.; Groothuis, G. M. M. M.; Gustavsson, L.; Guyot, C.; Hallifax, D.; Hammad, S.; Hayward, A.; Häussinger, D.; Hellerbrand, C.; Hewitt, P.; Hoehme, S.; Holzhütter, H. G.; Houston, J. B.; Hrach, J.; Ito, K.; Jaeschke, H.; Keitel, V.; Kelm, J. M.; Kevin Park, B.; Kordes, C.; Kullak-Ublick, G. A.; Lecluyse, E. L.; Lu, P.; Luebke-Wheeler, J.; Lutz, A.; Maltman, D. J.; Matz-Soja, M.; McMullen, P.; Merfort, I.; Messner, S.; Meyer, C.; Mwinyi, J.; Naisbitt, D. J.; Nussler, A. K.; Olinga, P.; Pampaloni, F.; Pi, J.; Pluta, L.; Przyborski, S. A.; Ramachandran, A.; Rogiers, V.; Rowe, C.; Schelcher, C.; Schmich, K.; Schwarz, M.; Singh, B.; Stelzer, E. H. K. K.; Stieger, B.; Stöber, R.; Sugiyama, Y.; Tetta, C.; Thasler, W. E.; Vanhaecke, T.; Vinken, M.; Weiss, T. S.; Widera, A.; Woods, C. G.; Xu, J. J.; Yarborough, K. M.; Hengstler, J. G. Recent Advances in 2D and 3D in Vitro Systems Using Primary Hepatocytes, Alternative Hepatocyte Sources and Non-Parenchymal Liver Cells and Their Use in Investigating Mechanisms of Hepatotoxicity, Cell Signaling and ADME. *Arch. Toxicol.* **2013**, *87* (8), 1315–1530. https://doi.org/10.1007/s00204-013-1078-5.

(27) DiProspero, T. J.; Dalrymple, E.; Lockett, M. R. Physiologically Relevant Oxygen Tensions Differentially Regulate Hepatotoxic Responses in HepG2 Cells. *Toxicol. Vitr.* **2021**, *74* (March), 105156. https://doi.org/10.1016/j.tiv.2021.105156.

(28) Dierks, E. A.; Stams, K. R.; Lim, H. K.; Cornelius, G.; Zhang, H.; Ball, S. E. A Method for the Simultaneous Evaluation of the Activities of Seven Major Human Drug-Metabolizing Cytochrome P450s Using an in Vitro Cocktail of Probe Substrates and Fast Gradient Liquid Chromatography Tandem Mass Spectrometry. *Drug Metab. Dispos.* **2001**, *29* (1), 23–29.

(29) Li, G.; Huang, K.; Nikolic, D.; Van Breemen, R. B. High-Throughput Cytochrome P450 Cocktail Inhibition Assay for Assessing Drug-Drug and Drug-Botanical Interactions. *Drug Metab. Dispos.* **2015**, *43* (11), 1670–1678. https://doi.org/10.1124/dmd.115.065987.

(30) Kietzmann, T.; Jungermann, K. Modulation by Oxygen of Zonal Gene Expression in Liver Studied in Primary Rat Hepatocyte Cultures. *Cell Biol. Toxicol.* **1997**, *13* (4–5), 243–255. https://doi.org/10.1023/A:1007427206391.

(31) Katz, J.; Kuwajima, M.; Foster, D. W.; McGarry, J. D. The Glucose Paradox: New Perspectives on Hepatic Carbohydrate Metabolism. *Trends Biochem. Sci.* **1986**, *3* (11), 136–140. https://doi.org/10.1101/cshperspect.a040568.

(32) Jungermann, K.; Thurman, R. G. Hepatocyte Heterogeneity in the Metabolism of Carbohydrates. *Enzyme* **1992**, *46* (1–3), 33–58. https://doi.org/10.1159/000468777.

(33) Li, J.; Settivari, R. S.; Lebaron, M. J.; Marty, M. S. Functional Comparison of HepaRG Cells and Primary Human Hepatocytes in Sandwich and Spheroid Culture as Repeated-Exposure Models for Hepatotoxicity. *Appl. Vitr. Toxicol.* **2019**, *5* (4), 187–195. https://doi.org/10.1089/aivt.2019.0008.

(34) Hoekstra, R.; Nibourg, G. A. A.; Van Der Hoeven, T. V.; Ackermans, M. T.; Hakvoort, T. B. M.; Van Gulik, T. M.; Lamers, W. H.; Elferink, R. P. O.; Chamuleau, R. A. F. M. The HepaRG Cell Line Is Suitable for Bioartificial Liver Application. *Int. J. Biochem. Cell Biol.* **2011**, *43* (10), 1483–1489. https://doi.org/10.1016/j.biocel.2011.06.011.

(35) Kari, F. W.; Yoshihara, H.; Thurman, R. G. Urea Synthesis from Ammonia in Periportal and Pericentral Regions of the Liver Lobule: Effect of Oxygen. *Eur. J. Biochem.* **1987**, *163* (1), 1–7. https://doi.org/10.1111/j.1432-1033.1987.tb10728.x.

(36) Stuart, J. A.; Fonseca, J.; Moradi, F.; Cunningham, C.; Seliman, B.; Worsfold, C. R.; Dolan, S.; Abando, J.; Maddalena, L. A. How Supraphysiological Oxygen Levels in Standard Cell Culture Affect Oxygen-Consuming Reactions. *Oxid. Med. Cell. Longev.* **2018**, *2018*. https://doi.org/10.1155/2018/8238459.

(37) Jagannathan, L.; Cuddapah, S.; Costa, M. Oxidative Stress Under Ambient and Physiological Oxygen Tension in Tissue Culture. *Curr. Pharmacol. Reports* **2016**, *2* (2), 64–72. https://doi.org/10.1007/s40495-016-0050-5.

(38) Jackson, J. P.; Li, L.; Chamberlain, E. D.; Wang, H.; Ferguson, S. S. Contextualizing Hepatocyte Functionality of Cryopreserved HepaRG Cell Cultures. *Drug Metab. Dispos.* **2016**, *44* (9), 1463–1479. https://doi.org/10.1124/dmd.116.069831.

(39) Rocha, S. Gene Regulation under Low Oxygen: Holding Your Breath for Transcription. *Trends Biochem. Sci.* **2007**, *32* (8), 389–397. https://doi.org/10.1016/j.tibs.2007.06.005.

(40) Chen, Y.; Verfaillie, C. M. MicroRNAs: The Fine Modulators of Liver Development and Function. *Liver Int.* **2014**, *34* (7), 976–990. https://doi.org/10.1111/liv.12496.

(41) van Wenum, M.; Adam, A. A. A.; van der Mark, V. A.; Chang, J. C.; Wildenberg, M. E.; Hendriks, E. J.; Jongejan, A.; Moerland, P. D.; van Gulik, T. M.; Oude Elferink, R. P.;

Chamuleau, R. A. F. M.; Hoekstra, R. Oxygen Drives Hepatocyte Differentiation and Phenotype Stability in Liver Cell Lines. *J. Cell Commun. Signal.* **2018**, *12* (3), 575–588. https://doi.org/10.1007/s12079-018-0456-4.

(42) Hernández-Gutiérrez, L.; Camacho-Carranza, R.; Hernández-Ojeda, S. L.; Govezensky, T.; Olguín-Reyes, S. R.; Espinosa-Aguirre, J. J. Reduction in CYP1A1 and 2B2 Activity at Low Oxygen Tension. *Toxicol. Lett.* **2020**, *330*, 90–95. https://doi.org/10.1016/j.toxlet.2020.05.006.

(43) Jungermann, K.; Katz, N. Functional Specialization of Different Hepatocyte Populations. *Physiol. Rev.* **1989**, *69* (3), 708–764. https://doi.org/10.1152/physrev.1989.69.3.708.

(44) Meech, R.; Hu, D. G.; McKinnon, R. A.; Mubarokah, S. N.; Haines, A. Z.; Nair, P. C.; Rowland, A.; Mackenzie, P. I. The UDP-Glycosyltransferase (UGT) Superfamily: New Members, New Functions, and Novel Paradigms. *Physiol. Rev.* **2019**, *99* (2), 1153–1222. https://doi.org/10.1152/physrev.00058.2017.

(45) Hailfinger, S.; Jaworski, M.; Braeuning, A.; Buchmann, A.; Schwarz, M. Zonal Gene Expression in Murine Liver: Lessons from Tumors. *Hepatology* **2006**, *43* (3), 407–414. https://doi.org/10.1002/hep.21082.

(46) Kaidi, A.; Williams, A. C.; Paraskeva, C. Interaction between β-Catenin and HIF-1 Promotes Cellular Adaptation to Hypoxia. *Nat. Cell Biol.* **2007**, *9* (2), 210–217. https://doi.org/10.1038/ncb1534.

(47) Jover, R.; Moya, M.; Gomez-Lechon, M. Transcriptional Regulation of Cytochrome P450 Genes by the Nuclear Receptor Hepatocyte Nuclear Factor 4-Alpha. *Curr. Drug Metab.* **2009**, *10* (5), 508–519. https://doi.org/10.2174/138920009788898000.

(48) Lu, H.; Gonzalez, F. J.; Klaassen, C. Alterations in Hepatic MRNA Expression of Phase II Enzymes and Xenobiotic Transporters after Targeted Disruption of Hepatocyte Nuclear Factor 4 Alpha. *Toxicol. Sci.* **2010**, *118* (2), 380–390. https://doi.org/10.1093/toxsci/kfq280.

(49) Gerbal-Chaloin, S.; Dumé, A. S.; Briolotti, P.; Klieber, S.; Raulet, E.; Duret, C.; Fabre, J. M.; Ramos, J.; Maurel, P.; Daujat-Chavanieu, M. The WNT/b-Catenin Pathway Is a Transcriptional Regulator of CYP2E1, CYP1A2, and Aryl Hydrocarbon Receptor Gene Expression in Primary Human Hepatocytes. *Mol. Pharmacol.* **2014**, *86* (6), 624–634. https://doi.org/10.1124/mol.114.094797.

(50) Tachikawa, M.; Sumiyoshiya, Y.; Saigusa, D.; Sasaki, K.; Watanabe, M.; Uchida, Y.; Terasaki, T. Liver Zonation Index of Drug Transporter and Metabolizing Enzyme Protein Expressions in Mouse Liver Acinuss. *Drug Metab. Dispos.* **2018**, *46* (5), 610–618. https://doi.org/10.1124/dmd.117.079244.

(51) Higuchi, Y.; Kawai, K.; Yamazaki, H.; Nakamura, M.; Bree, F.; Guguen-Guillouzo, C.;

Suemizu, H. The Human Hepatic Cell Line HepaRG as a Possible Cell Source for the Generation of Humanized Liver TK-NOG Mice. *Xenobiotica* **2014**, *44* (2), 146–153. https://doi.org/10.3109/00498254.2013.836257.

(52) Marion, M. J.; Hantz, O.; Durantel, D. The HepaRG Cell Line: Biological Properties and Relevance as a Tool for Cell Biology, Drug Metabolism, and Virology Studies. *Methods Mol. Biol.* **2010**, *640*, 261–272. https://doi.org/10.1007/978-1-60761-688-7_13.

(53) He, L.; Pu, W.; Liu, X.; Zhang, Z.; Han, M.; Li, Y.; Huang, X.; Han, X.; Li, Y.; Liu, K.; Shi, M.; Lai, L.; Sun, R.; Wang, Q. D.; Ji, Y.; Tchorz, J. S.; Zhou, B. Proliferation Tracing Reveals Regional Hepatocyte Generation in Liver Homeostasis and Repair. *Science (80-.).* **2021**, *371* (6532). https://doi.org/10.1126/science.abc4346.

(54) Bhatia, S. N.; Toner, M.; Foy, B. D.; Rotem, A.; Tompkins, N. R. G.; Yarmush, M. L. Zonal Liver Cell Heterogeneity: Effects of Oxygen on Metabolic Functions of Hepatocytes. *Cell. Eng* **1996**, *1* (2), 125–135.

(55) Matz-Soja, M.; Hovhannisyan, A.; Gebhardt, R. Hedgehog Signalling Pathway in Adult Liver: A Major New Player in Hepatocyte Metabolism and Zonation? *Med. Hypotheses* **2013**, *80* (5), 589–594. https://doi.org/10.1016/j.mehy.2013.01.032.

CHAPTER 4: ASSESSMENT OF LIVER-SPECIFIC FUNCTION WITH HEPARG CELL MONOLAYERS CULTURED ON COLLAGEN SCAFFOLDS SPANNING A RANGE OF PHYSIOLOGICAL STIFFNESS

4.1 Introduction

In the drug development pipeline, new chemical entities with therapeutic potential undergo a series of in vitro assays to determine their suitability for pre-clinical (animal) and clinical (human) trials. In addition to targeting a particular pathway or disease state, the adsorption, distribution, metabolism, excretion, and toxicity (ADMET) of each chemical entity is evaluated throughout the development pipeline.[1] The liver is the primary site of drug metabolism and a crucial component in early stage assessments of predominate metabolic pathway, potential drug-drug interactions, and hepatotoxicity of the parent molecule and its metabolites.[2] To be predictive of in vivo responses, cell-based assays require cell types with similar metabolic competencies as the primary human hepatocytes (PHHs), expressing equivalent basal phase I and phase II metabolizing enzyme activity and an inducible response to a similar magnitude. Metabolic competency is characterized by the activity of phase I and II metabolic enzymes.[3] Phase I metabolism is accomplished by the cytochrome P450 (CYP) enzyme family. Phase II metabolism involves a number of enzyme families capable of appending hydrophilic molecules to the drug molecules, these enzymes include both UDP-glucuronosyltransferases (UGTs) and sulfotransferases (SULTs). Standard assays have been developed to quantify the activity, induction, and inhibition of phase I and II enzymes.[4] These assays determine the metabolic

competency of cells, either as a quality control or when evaluating new cell lines or culture conditions.

Current cell-based drug toxicity assays rely on two-dimensional (2D) cell culture formats in which primary human hepatocytes (PHHs), immortalized cell lines derived from the liver, or induced pluripotent stem cells are maintained on plasticware.[5] PHHs are the current gold standard for drug metabolism and toxicity studies. Despite the easy use and throughput potential of the 2D cultures, the inability of this culture format to mimic structural components of the liver tissue often result in poor predictions of hepatotoxicity and drug-induced liver injury.[6] One structural limitation of 2D cultures is the reduced number cell-cell and cell-extracellular matrix (ECM) contacts that form on planar surfaces as compared to in vivo tissue organization. Furthermore, monolayer culture formats result in decreases liver-specific functions and gene expression, ultimately resulting in rapid de-differentiation of PHHs and reduced CYP activity, inducibility, and inhibition.[7–10]

In vitro hepatotoxicity models that employ three-dimensional (3D) culture platforms provide environments that sustain PHH differentiation and function for longer periods than 2D cultures;[11,12] these 3D environments also are better able to predict hepatotoxicity.[13] The inclusion of a 3D microenvironment has been shown to known to influence hepatocyte phenotype by alternating gene expression compared to 2D counterparts.[14–18] A common method for culturing hepatocytes is in a sandwich culture system, where hepatocytes are cultured between two layers of ECM. The sandwich culture method has been shown to improve PHH morphology and viability, maintain liver-specific function, and improved polarity when compared to those cultured with 2D monolayers.[19] The liver ECM is made up of fibronectin, laminin, peptidoglycans, and collagens; collagens account for about 60% of ECM molecules.[20] Because

collagen makes up the majority of the liver ECM, is easy to use, and improves stability of hepatocyte cultures, collagen is an ideal in vitro ECM mimic.[21]

The mechanical properties of the ECM impacts hepatocyte adhesion, motility, growth, and differentiation state.[22] Tissue stiffness is an important diagnostic for detecting disease states in the liver. Healthy liver tissue has stiffness values between 300 Pa to 6 kPa. Increased stiffness of the liver is associated with abnormalities such as tumor formation or fibrosis, with ranges between 8 – 12.5 kPa being indicative of stage 3 and 4 of fibrosis.[22,23] Liver models have incorporated synthetic hydrogels composed of polyvinyl alcohol (PVA) or polydimethylsiloxane (PDMS) since the stiffness of these materials can be tuned with crosslinking. These styles of cultures are a 2.5-dimentional method in which the hepatocytes are grown as monolayer on top of a hydrogel and still incorporate cell-ECM interactions similar to the sandwich culture method. Xia *et al*. prepared PVA hydrogels and tuned the stiffness by crosslinking the surface with glutaraldehyde; the PVA was then coated with fibronectin to promote cell attachment of the immortalized hepatocyte line L-02. They concluded that the stiffer PVA surfaces impaired migration and albumin production and promoted apoptosis.[24] Natarajan *et al*. cultured PHHs on various PDMS scaffold prepared with different ratios of Sylgard precursors to adjust the stiffness; PDMS scaffolds were coated with collagen to promote cell adhesion. The PHHs cultured on softer scaffolds maintained greater hepatocyte function (albumin and urea secretion, CYP activity, and cell morphology) than the stiffer scaffolds.[25]

In this work, we prepared collagen I scaffolds and tuned their stiffness with a combination of neutralization and chemical crosslinking techniques, followed by evaluating the metabolic profile of HepaRG cells cultured on the scaffolds at physiological stiffness. To ensure that the cells were exposed to similar chemical environments and attribute changes in cellular

drug metabolic activity to stiffness, each scaffold was coated with a thin layer of unmodified collagen before attaching the differentiated HepaRG cells. We chose the HepaRG cell line because their metabolic enzyme profile is similar to that of PHHs and HepaRG cells exhibit hepatocyte-like and other biliary-like cell characteristics.[26,27] HepaRG cells also express various drug metabolizing enzymes, transporters, and nuclear receptors at levels comparable to PHHs.[9,10] To characterize the metabolic activation of HepaRG cells on different stiffness scaffolds within the healthy liver range, we analyzed the basal metabolic activity of drug metabolizing enzymes, acute CYP induction, and transcriptional regulation.

4.2 Materials and methods

4.2.1 Chemicals

All chemicals and reagents were used as received unless otherwise specified. Cell culture medium and supplements were purchased from Gibco, except for those used in the maintenance of the Cryo Human Hepatocytes and HepaRG cell line (Lonza). Collagen I (rat tail) was purchased from Corning; 12-well CellAdhere Collagen I-coated flat bottom plates were purchased from Stem Cell Technologies. Chlorzoxazone, dextromethorphan (hydrobromide hydrate), (S)-mephenytoin, midazolam, testosterone, rifampicin, and O-[(3,4-dichlorophenyl)methyl]oxime 6-(4-chlorophenyl)-imidazo[2,1-b]thiazole-5-carboxaldehyde (CITCO) were purchased from Cayman Chemical Company. Dimethyl sulfoxide (DMSO), 2-(N-morpholino) ethanesulfonic acid (MES) monohydrate, and 7-hydroxycoumarin were purchased from Fisher Scientific. Phenacetin, 3-methylcholanthrene (3-MC), and sodium hydroxide (NaOH) were purchased from Millipore Sigma. 1-ethyl-3-(3-dimethylaminopropyl)carbodiimide hydrochloride (EDC) was purchased from Oakwood Chemical.

4.2.2 Collagen scaffold preparation

Collagen scaffolds were prepared in a standard 12-well cell culture plate with either 2 mg/mL (310 μg of collagen/culture area cm^2) or 4 mg/mL (625 μg of collagen/culture area cm^2) using one of three methods: neutralization (N), neutralization followed by chemical crosslinking of the gel's surface (Nx), or bulk crosslinking of the entire collagen scaffold (X). The neutralized collagen scaffolds were prepared by adding NaOH and phosphate-buffered saline (PBS) to a solution of acidified collagen. Once neutralized, the collagen solution was added to the 12-well plate and gelled overnight at 37°C. The neutralized-crosslinked scaffolds were prepared with the same neutralization procedure followed by a 1 hour, room temperature, incubation in crosslinking solution. The crosslinking solution contained a 60 mM:15mM ratio of EDC and NHS in MES buffer (0.1 M, pH = 5.0). The bulk crosslinked scaffolds were prepared by dissolving lyophilized acidic collagen in MES buffer (0.1 M, pH=5.0) to a final concentration of 5 mg/mL and then mixing with a 60 mM:15mM ratio of EDC and NHS to achieve desired collagen concentrations. The bulk crosslinked collagen mixture gelled for 60 min at room temperature. Both neutralized-crosslinked and bulk crosslinked scaffolds were placed in reverse osmosis water overnight to remove any residual EDC and NHS.

Each neutralized-crosslinked and bulk crosslinked scaffold after leeching was sterilized with a 70% ethanol (v/v) solution for 5 minutes; once the solution was removed the scaffolds were placed in the biosafety cabinet for 30 min. Prior to seeding cells, all scaffolds were incubated in a solution of collagen I (10 μg/mL) in 1x PBS overnight and then washed with 1x PBS.

4.2.3 Stiffness measurements

The Young's modulus of the collagen scaffolds, with the 10 μg collagen I surface coating, was determined with a Piuma Nanoindenter (Optics 11 Life) equipped with an indenter tip (0.033 N/m) fitted with a glass bead (8 μm radius). The indenter tips were calibrated on a glass surface before performing an 8x8 matrix scan in the center of a collagen scaffold. Each indentation in the matrix had a spacing of 100 μm to minimize interferences between the indentation points. The tips were cleaned between samples with collagenase and rinsed thoroughly with water, 70% ethanol, water, and 1X PBS buffer.

Force curves were acquired with an indentation rate of 500 nm/sec and fitted with the Hertz model and a Poisson ratio of 0.5. For the neutralized and neutralized-crosslinked collagen scaffolds, the fit was limited to an indentation of 1000 nm. For the bulk crosslinked scaffolds, the fit was limited to an indentation of 800 nm. The reported Young's modulus is the average and standard error of the mean of force curve fits for each indentation; any point in the indentation matrix whose force curve with a fit of $R^2 < 0.95$ was rejected and not included in these datasets.

4.2.4 Cell culture

Differentiated NoSpin HepaRG Cryopreserved Cells (Lonza Bioscience) were cultured at a density of 2.6 x 10^5 cells/cm^2 on each collagen scaffold and maintained at 37 ^oC and 5% CO_2. Upon thawing, the cells were maintained for 24 hours in HepaRG medium containing basal medium supplement, a thawing and plating supplement, and 1% penicillin–streptomycin. After a medium exchange, the cells were maintained in HepaRG medium containing basal medium supplement, a maintenance and metabolism supplement, and 1% penicillin–streptomycin. This medium was exchanged every 2 – 3 days. For induction experiments, the HepaRG cells were

cultured for 6 days, followed by exposure to inducers for 48 hours in the same medium. Stock solutions of 3-MC (10 mM), rifampicin (10 mM), and CITCO (1 mM) were prepared in DMSO and stored at -20 ^{o}C until needed. Each stock was diluted 1:1000 in culture medium and compared to a DMSO (0.1% v/v) vehicle control.

Cryopreserved Human Hepatocytes (Lonza Bioscience) were cultured at a density of 2.6 x 10^5 cells/cm^2 on each collagen scaffold and maintained at 37 ^{o}C and 5% CO_2. Upon thawing, the cells were maintained for one hour in Hepatocyte plating medium containing plating media supplement. After a medium exchange, the cells were maintained in Hepatocyte Culture Medium (HCM), supplemented with ascorbic acid, bovine serum albumin -fatty acid free, hydrocortisone, human epidermal growth factor (hEGF), transferrin, insulin, and aentamicin/amphotericin-B (HCM singleQuot Kit, Lonza). Medium was exchanged every day. Widefield images of the PHHs cells were captured with a Nikon TE2000 microscope, 10x objective using a Photometrics Dyno CCD camera.

4.2.5 Evaluation of metabolic enzyme activity

Metabolic enzyme activity was evaluated with eight different substrates (**Table 4.1**).[28,29] The substrates were dissolved in DMSO at 1000X working concentration. The HepaRG cells were exposed to culture medium containing the substrates and basal medium supplement for 2 hours, after which the medium was collected and stored at -20°C until analysis. The cell medium was mixed with cold acetonitrile containing known concentrations of isotopically labeled standards for each enzyme product at a 1:10 (v/v) ratio. A matrix blank containing fresh culture medium was run in parallel. After a 15 min incubation at -20°C, the precipitated protein was pelleted at 12,000 xg for 15 min at 4°C, the supernatant collected, and the solvent removed in

vacuo. The residual solid was resuspended in 100 µL of HPLC-grade water (Optima) and separated on a Waters Acquity UPLC equipped with a BEH C18 column (2.1 x 50 mm, 1.7 µm) using a binary solvent system of (A) 0.5% formic acid (v/v) in water and (B) 0.5% formic acid (v/v) in acetonitrile. The total run time of each separation was nine min, using the following gradient profile at a 0.3 mL/min flow rate: 10% B for one min; a linear gradient to 70% B over 5 min; 95% B for one min; 10% B for two min to wash and re-equilibrate the column. We did not observe carry over between sample injection and solvent blanks were injected every 10 samples

Metabolites were detected and quantified with multiple-reaction monitoring on a Thermo TSQ Vantage triple quadrupole instrument equipped with a heated electrospray ionization (HESI) source set to 300 °C. Two transitions of each product were monitored to confirm its identity. The declustering voltage for each was optimized by direct infusion of neat solutions (10 µM) in Optima water. Each product's transition was optimized for collision energy and reported in **Table 4.1**. Other parameters used for all analyses were: spray voltage (4800 V), vaporization temperature (300 °C), sheath gas pressure (50 psi), aux gas pressure (15 psi), capillary temperature (300 °C), and S-lens RF amplitude (120 V). Nitrogen gas was used for sheath, aux, and collision gas. Data were collected and processed with the Xcalibur software package. The peak area for each metabolite was averaged across three technical replicates; we report the ratio of the average peak area of treatment to the average peak area of vehicle.

4.2.6 Urea production

After collecting the medium for the CYP activity assay, the urea production of the cells was analyzed. Prior to collecting urea, each well was washed once with 1X PBS before

incubating in fresh HepaRG medium containing basal supplement for 1 hour. The medium was collected, and urea concentration quantified with the QuantiChrom Urea Assay (Kit-DIUR-100, BioAssay Systems) according to the manufacturer's protocol. Equal volume of reagent and medium was added to each well and the plate was mixed for 50 minutes at room temperature. The samples were measured on a SpectraMax i3x Microplate Reader at an optical density of 430 nm. Samples were compared to a seven-point calibration curve, which was prepared on each plate to account for plate-to-plate variation.

4.2.7 Transcript Expression Quantification with RT-qPCR

After collecting culture medium for CYP activity and urea measurements, the cells were washed and lysed using a TRIzol Plus RNA purification kit (ThermoFisher), according to the manufacturer's suggested protocol. The TRIzol reagent was added directly to the cells and agitated for 10 minutes prior to RNA isolation. Reverse Transcriptase PCR was performed immediately after RNA isolation using the RNA isolation with a High-Capacity cDNA Reverse Transcription Kit (ThermoFisher) in an Eppendorf Master Cycler.

Table 4.2 lists the primer pair sequences, optimal concentration, and reaction efficiency (90-110%) of each gene of interest. Amplification reactions were performed with PowerUp SYBR Master Mix (ThermoFisher), in a 384-well plate, on a QuantStudio 6 Flex Real-Time PCR system. Each sample was measured in triplicate, using the following program: 95 °C for 60 sec, 40 cycles of 95 °C for 2 sec, and 60 °C for 30 sec. Each transcript was quantified using the ΔΔCt method against 18sRNA.[30]

4.2.8 Cell viability

Viability was measured with the CellTiter96 AQueous One Solution Cell Proliferation (MTS) assay (Promega) after assessing enzyme activity and collecting culture medium for urea quantification. Prior to analysis, the cells were washed with 1X PBS. Working MTS assay solution was prepared by diluting the MTS reagent 1:5 (v/v) into HepaRG medium containing basal supplement. The cells were incubated at standard culture conditions for 2 hours, aliquots (100 µL) of medium transferred to a clear bottom 96-well plate, and absorbance values at 490 nm measured on a SpectraMax i3x Microplate Reader.

4.2.9 Statistical Analysis

Cell-related datasets are reported as the average and standard error of the mean (SEM) of at least two separate vials of differentiated cells, with at least two technical replicates per vial. All data were analyzed with GraphPad Prism 7. Statistically significant differences correspond to a p-value of ≤ 0.05. To assess CYP activity, peak area or each metabolite product was normalized to a particular experiment condition, a normalized activity greater than 1.25 or less than 0.8 was considered significant since the LC-MS/MS peak area is highly reproducible, and 1.25/0.8 is statistically significantly outside of normal variability range as measured in Chapter 3. For transcriptional regulation, a fold-change of greater than 2.0 was considered significant.

4.3 Results and Discussion

Figure 4.1 summarizes the experimental workflow used to compare liver-specific function, metabolic enzyme activity and transcriptional regulation between HepaRG cells cultured on different collagen scaffolds.

4.3.1 Changing collagen density and the amount of chemical crosslinking can be used to tune the stiffness of collagen scaffolds

Uniform collagen slabs were used as the ECM for HepaRG cell culture since collagen is the most abundant protein in both normal and cirrhotic livers.[31] Neutralizing the acid-solubilized collagen solution is a common method for generating collagen slabs.[32,33] Antoine et al. found the majority collagen hydrogels used in cell culture and tissue engineering applications have a final concentration of 2 mg/mL, therefore we decided to use this density as a baseline.[34] However, the stiffness of 2 mg/mL collagen slabs has been reported previously to be 9 – 20 Pa using rheometry measurements, which is significantly less stiff than healthy liver ECM (300 Pa – 6 kPa).[35,36]

To prepare stiffer collagen scaffolds within the physiological range we increased collagen concentration and degree of cross-linking. Increasing the concentration of collagen in the gelation process translates to an increase in the density of collagen fibers. Chemically crosslinking the collagen fibers increases the rigidity of the gel with bifunctional linkers, which promotes the formation of amide bonds between carboxylic acids and free amines on the surface of collagen fibers.[37] The baseline scaffold we prepared was 2 mg/mL of neutralized collagen (N2) as it is the most commonly used scaffold. We evaluated the effects of crosslinking the surface of the 2 mg/mL collagen scaffolds (Nx2) in combination with increasing collagen density

using a 4 mg/mL collagen slab (Nx4). We also evaluated the effect of crosslinking the entire scaffold by dissolving lyophilized collagen fibers in crosslinker resulting in a 2mg/mL scaffold prepared exclusively by crosslinking (X2). We evaluated how the degree of crosslinking effects stiffness by comparing N2, Nx2, and X2; we also can determine the effects of collagen density by comparing the Nx2 and Nx4 scaffolds. Lastly, all scaffolds received a thin layer of collagen (10 μg) on top.

The stiffness of the four scaffolds and a commercial collagen plate was measured with a nanoindentor by assessing 64 points in an 800 x 800 μm array (**Figure 4.2**). The individual force curves were fit to a Hertz model. Neutralization of collagen results in the most pliant surface with a stiffness of 28.8 Pa; this collagen scaffold was included in our studies despite its non-physiological relevance because it is a common method of preparation used in other works and an important point of comparison. Cross-linking the surface of the N2 collagen scaffold increased its stiffness approximately four-fold (116.1 Pa); this scaffold was included because it allows a direct comparison to the N2 scaffold based on their similar densities. Crosslinking the surface of the 4 mg/mL collagen scaffold (Nx4) resulted in a physiologically relevant stiffness of 882.3 Pa, as did the bulk crosslinked (X2) scaffold of 2 mg/mL (4190 Pa). Increasing collagen density increases the amount of fibers within the collagen scaffold; doubling the density of collagen fibers, from Nx2 to Nx4, the stiffness increases about 7.5-fold and modulates stiffness within one order of magnitude. The degree of crosslinking between the N2, Nx2 and X2 scaffolds indicate an order of magnitude change with increasing degrees of crosslinking. The surface crosslinking (Nx2) increased stiffness about 4.0-fold, while bulk crosslinking (X2) increased stiffness by 145.5-fold. These comparisons of density and crosslinking suggest that stiffness can be tuned by orders of magnitude with crosslinking and finely-tuned by increasing

the density of collagen. The commercial collagen coated plate has a surface stiffness of 18780 Pa, a stiffness that corresponds to late stage liver fibrosis (8-12.5 kPa)[22,38].

4.3.2 The viability and urea production of the HepaRG cell line and PHH is unaffected by culture surface stiffness

Before cells were seeded onto each scaffold a thin layer of collagen (10 μg) was added on top to allow for uniform integrin distribution on the surface of each scaffold enabling cell binding across all scaffolds, independent of mechanical or chemical modifications. Also, the thin-layer of collagen ensures the same density of binding motifs, circumventing effects cross-linking would have on cellular behavior.[39] HepaRG cells were cultured on each of the scaffolds for 8 days; PHHs were cultured on the scaffolds for 4 days. Hepatocyte viability was measured with an MTS assay and liver specific function was assessed by quantifying urea secretion.

Figure 4.3 compares the viability of the HepaRG and PHHs on each collagen scaffold; each value is normalized to N2 scaffold to compare viability as a function of increasing surface stiffness. This data shows that all three scaffold preparations are cell-compatible, and that substrate preparation, sterilization, and stiffness does not induce cellular death. Xia *et al.* reported similar findings for L-02, an immortalized human hepatocyte line, cultured on three different polyvinyl alcohol hydrogels with stiffness values of 4800, 21,270, and 45,210 Pa.[24] Collagen stiffness also did not affect urea production in either the HepaRG or PHH cells. The HepaRG cells on the collagen scaffolds secreted an average of 0.0066 ± 0.0002 mg/mL/hr/10^6 cells; the HepaRG cells secreted significantly less urea on the commercially coated collagen plates (0.0035 mg/mL/hr/10^6 cells). The PHHs secreted statistically equivalent amounts of urea on each substrate, including the commercially coated collagen plates, at a rate of 0.0035 ± 0.0006 mg/mL/hr/10^6 cells. These urea concentration values were collected from incubating 1

million cells in 1 mL of culture medium for 1 hour. Images were collected on day 1, 2 and 4 of the PHHs on each scaffold type (**Figure 4.4**); on day 2 and 4 the PHHs developed a cobblestone layout characteristic of healthy hepatocytes on each collagen scaffold.

The combination of both datasets suggests that the liver specific function of the HepaRG cells and PHHs is unaffected by underlying collagen scaffolds whose stiffness is less than or equal to physiological range associated with healthy liver tissue. Natarajan and colleagues measured urea secretion of PHHs cultured on collagen-coated PDMS slabs with stiffness values ranging between 2.36 – 3.00×10^6 kPa over a 7-day period. Initially urea secretion was equivalent across the PDMS slabs, however it decreased as a function of stiffness with increasing culture periods. On day 7, the difference between cells on the 2.36 kPa scaffold (155.4 μg/mL/million cells) was significantly greater than on the 3×10^6 kPa scaffold (74.5 μg/mL/million cells).[25] Therefore, there is precedent for impaired urea secretion of hepatocytes cultured on surfaces whose stiffness is orders of magnitude above a physiological range, however within a range of stiffness found in a healthy liver urea secretion is unchanged.

4.3.3 Trends in time-dependent basal metabolic enzyme activity of HepaRG cells is the same across all scaffolds

Jackson *et al*. found that basal level drug metabolic activity of cryo-preserved HepaRG cells cultured on commercial collagen coated plates varied over 22-day period;[3] they hypothesized these dynamic changes were due to de- and redifferentiation of the cells over the culture period stemming from high concentration of DMSO in metabolism and differentiation media. To determine if stiffness of the underlying ECM affects baseline drug metabolic activity, we evaluated HepaRG cells on each collagen scaffold, measuring the enzyme activity over a 24-day period. Enzyme activity was quantified with an 8-in-1 cocktail containing seven CYP-

specific substrates as well as a substrate for the phase II SULT and UGT families. The production of each metabolite was quantified with LC-MS/MS using multiple-reaction monitoring.

Figure 4.5 shows the basal drug metabolic activity over time of all four scaffolds; these values are normalized to day 1, allowing for overall changes in activity to be assessed as a function of time. The trends in enzyme activity are similar across all four collagen scaffolds. The drug metabolic activity is relatively unchanged during the first 4 days after plating, followed by an increase in activity until day 11. After day 11, the enzyme activity decreases until day 24. The maximum activity for each enzyme, as well as the maximum change in activity, for each collagen scaffold is summarized in **Table 4.3**. CYP1A2 activity highlights the activity trends over time for all scaffolds, on day 4 activity is relatively unchanged from the day 1 baseline. On day 7, activity increased by an average of 2.15-fold for all scaffolds and continued to increase to a peak on day 11 at 4.37, 3.08, 2.16, and 3.94-fold for N2, Nx2, Nx4 and X2, respectively. CYP1A2 activity decreased after day 11. This activity trend was observed in CYP2B6, 2C19, 2D6 and 3A4 (midazolam oxidation); measure activity did not changes with time for CYP2E1, SULT and UGT.

These data agree with the results obtained in Chapter 3, that HepaRG cultures prepared as monolayers on ECM-coated plates or scaffolds can maintain drug metabolic activity until day 11, after which is a rapid decline in activity. The trends in basal metabolic enzyme activity over the 24-day culture period appears to be stiffness-independent. This could mean that drug metabolizing enzyme expression and activity is decoupled from surface stiffness. These results could also suggest that the interaction with the underlying ECM is a determining factor in metabolism, as the cells were in direct contact with the thin layer of collagen at the same density

and composition. The thin layer of collagen enables the cells to "feel" the stiffer scaffolds while keeping the cell-ECM contact consistent across each slab. Wang observed that *CYP3A4* and *Alb* expression in the Huh-7.5 hepatocarcinoma cell line were markedly different when cultured on collagen or fibronectin; these genes are indicative of metabolic function and cellular health.[40] This study also found the cells produced significantly more albumin when cultured on fibronectin indicating that the ECM composition ins an important factor of in vitro hepatocyte cultures.

4.3.4 Basal drug metabolic activity of HepaRG and PHHs is differentially expressed depending on scaffold stiffness

4.3.4.1 HepaRG cells

The metabolic enzyme activity (**Figure 4.6**) and transcriptional regulation of metabolic enzymes (**Figure 4.7a**) were quantified in HepaRG cells after an 8-day incubation. When compared to cells maintained on the N2 scaffolds, CYP1A2, 2C19, 2E1, and SULT activity were unchanged on the other collagen scaffolds and in the commercially coated collagen plates. The transcript number for *CYP1A2*, *2C19*, and *2E1* were also unchanged; *CYP2E1* was significantly downregulated at the stiffer surfaces (Nx4, X2 and the CCP) and indicates that activity is likely a consequence of translational regulation. We probed a single SULT transcript (SULT2A1) as a representative of the family. The significant upregulation of *SULT2A1* could indicate alternative regulatory pathways influence SULT translation, although it could also indicate that *SULT2A1* is not representative of the other family members. CYP2B6 activity was unchanged on the collagen scaffolds, however, it was significantly downregulated (0.65-fold change) on the commercial collagen plate. Gao *et al* measured clearance of CYP-specific substrates from microsomes

prepared using patient liver samples identified to be fibrotic or cirrhotic and compared to healthy controls. They use the clearance data to calculate difference in CYP activity between healthy and diseased state livers in vivo and they concluded that CYP1A2, 2B6, 2C19, and 3A4 were significantly lower in fibrotic/cirrhotic tissue.[41]

A second grouping of enzymes is CYP2D6 and 3A4, whose activity was unchanged on Nx2 and Nx4 scaffolds; downregulated on the X2; and upregulated on the commercial plate. The X2 scaffold downregulation was 0.70-, 0.74- and 0.73-fold change for CYP2D6, 3A4 probed with midazolam (3A4-Midz), and 3A4 probed with testosterone (3A4-Test), respectively. On the commercial collagen plate there is a 1.22-, 1.40- and 1.37-fold increase for CYP2D6, 3A4-Midz, and 3A4-Test, respectively. These trends for CYP3A4 are also observed in the transcriptional regulation in which there is an observed downregulation on the X2 scaffold. The shared transcriptional and activity decreases of CYP2D6 and 3A4 was previously observed by Fisher et al, who quantified the amount of CYP2D6 and 3A4 enzymes with western blot from healthy or diseased (inflamed and fibrotic) liver explants.[42] This could be explained by increased interleukin-6 (IL-6) or activation of a similar signaling pathway as increased concentrations of IL-6 has been associated with downregulation of *CYP2D6* and *CYP3A4* transcript.[43] IL-6 is a proinflammatory cytokine that has been associated with liver fibrosis.[44]

The UGT enzyme family activity increase was about the same for the stiffer collagen scaffolds with an average increase of 1.77± 0.21-fold. This aligns with *UGT2B4* transcriptional upregulation; Nx2 and X2 were upregulated about the same at 5.35 and 6.44-fold while Nx4 was upregulated significantly more by 11.63-fold. The UGT activity and transcript on the commercial collagen plate is unchanged from the N2 scaffold. There has been limited literature into stiffness

effects, and fibrosis/cirrhosis effect on UGT activity; however, one report concluded no changes in UGT2B7 activity in fibrotic liver.[45]

4.3.4.2 PHHs

The metabolic enzyme activity (**Figure 4.8**) and transcriptional regulation of metabolic enzymes (**Figure 4.7b**) were quantified in PHHs after an 8-day incubation. When compared to cells cultured on the N2 scaffolds, stiffness of the underlying Nx2, Nx4, and X2 ECM had no significant effect on the activity of CYP2B6, 2C19 and 2E1. This trend corresponds with our observations in the HepaRG cells and suggests the translation of these CYPs is not affected by ECM stiffness. The transcriptional regulation of these enzymes also mirrors the HepaRG cells, with a significant downregulation in *CY2E1* expression with increasing substrate stiffness. On the commercial collagen plates, the activity of CYP2B6 and CYP2E1 were unchanged.

Increased ECM stiffness of the Nx2, Nx4, and X2 resulted in decreased CYP1A2, 2D6, 3A4-Midz, SULT and UGT activity. The decrease in activity of these enzymes does not appear to be dependent on the magnitude of stiffness surface, but rather a universal decrease in activity at Nx2, Nx4 and X2 scaffolds. Decreases in activity correlate consistently across each stiffness scaffolds in the down regulation of transcripts for all enzymes except for *UGT2B4*, which was only downregulated on the Nx2 scaffolds; the expression level of *UGT2B4* on the Nx4 and X2 scaffolds was indistinguishable from cells on the N2 scaffolds. On the commercial collagen plate, CYP2C19, 2D6, and 3A4-Test activity was increased. Interestingly, the transcript regulation trends observed with PHHs cultured on prepared scaffolds and the commercial collagen plates is similar, which could indicate that the PHHs respond similarly to stiff scaffolds

until a particular point- potentially under 30 Pa like the N2 scaffold- in which the cell's behavior changes.

A potential explanation for these changes, in both HepaRG and PHHs, is the cells recognize the stiffer surfaces as inflamed or "unhealthy" causing the hepatocytes to illicit an immune response to signal help from non-parenchymal and immune cells. Furthermore, the sensitivity of PHHs in comparison to HepaRG cells to surface stiffness is displayed in the overall trends of the enzyme activity and transcriptional data, in which the PHHs enzyme activity and transcript was downregulated on the Nx2 scaffold. The HepaRG cells didn't have significant transcriptional downregulation or decreased enzyme activity until higher surface stiffness on the X2 scaffold.

4.3.4.3 Hepatocytes could recognize the increased ECM stiffness as inflammation of an immune response

The observed transcript and activity changes for the various metabolizing enzymes could indicate that cellular ECM stiffness modulates some of the metabolizing enzyme's transcriptional regulation and activity; this has been previously measured in fibrotic/cirrhotic livers and summarized in a review by Cobbina.[45] Looking into liver physiology, increased liver stiffness is associated with fibrosis and cirrhosis; a leading cause of fibrosis and cirrhosis is chronic liver inflammation.[46] This results in the liver actively sending signals to the body to mount an immune system response, which is usually mediated by nonparenchymal cells. The signaling molecules of an immune response are known as cytokines such as interleukins-1β (IL-1β), interleukin-6 (IL-6), and tumor necrosis factor-α (TNF-α). It has been observed that in response to liver injury and inflammation, stellate cells and hepatocytes secrete mediators and cytokines to modulate the immune response. [47,48] Rowell and colleagues concluded that

hepatocytes cultured in vitro can secrete various cytokines and modulate the quantity of these cytokines in response to the environment. Rowell induced cytokine production with bacterial infections and proinflammatory signaling.[49] One example of the effect these cytokines have on hepatocytes was displayed by Hakkola *et al.*, who showed that CYP2E1 expression was downregulated in the presence of interleukin- 1β, TNF-α, and IL- 6.[50] Another example is by Kim et al., who observed that increased concentrations of IL-6 was associated with downregulation of *CYP2D6* and *CYP3A4* transcript.[43] These literatures suggest that HepaRG cells cultured on the stiffer surfaces could recognize the stiff surface as "liver injury" and therefore send inflammatory signals to illicit an immune response, which ,in turn, inhibits or induces metabolic enzyme transcripts.

4.3.5 HepaRG cells inducibility is unaffected by the culture stiffness

The inducibility of the HepaRG cells on the various scaffolds was determined by exposing the cells to: 3-methylcholanthrene (3-MC), a known inducer of aryl hydrocarbon receptor (AhR) which upregulates the expression of *CYP1A2* transcript; rifampicin (Rif), a known inducer of the pregnane X receptor (PxR), which upregulates the expression of *CYP3A4*, *2C19*, and *UGT1A* family*;* CITCO, a known inducer of receptor constitutive androstane receptor (CaR), which upregulates the expression of *CYP2B6.* After a 48-hour exposure each inducer, metabolic enzyme activity (**Figure 4.9**) and transcriptional regulation (**Figure 4.10**) were measured.

Exposure to 3-MC did not increase CYP1A2 activity as expected, with only cells on the N2 scaffold experiencing a discernible change (1.47-fold change) from the vehicle control. CYP1A2 activity between the induced and vehicle controls were indistinguishable on the Nx2,

Nx4 and X2 scaffolds; cells on the commercial collagen plate had reduced CYP1A2 activity (0.40-fold) compared to the vehicle. Transcript analysis confirmed the activity of 3-MC by upregulating *CYP1A2* as expected. The extent of upregulation is stiffness-dependent with a 25.6-fold increase on the N2 scaffold, a 17.58-fold increase on the Nx2 scaffold, a 33.13-fold increase on the Nx4 scaffold, a 10.06-fold increase on the X2 scaffold, and a 3.07-fold increase on the commercial plates.

Rifampicin induced CYP3A4 activity on all scaffolds when measuring the testosterone oxidation, however activity probed with midazolam oxidation only indicates increased CYP3A4 activity on the X2 scaffolds and the commercial collagen plate. CYP3A4 activity increased on the N2 scaffold, by 1.23 and 1.00-fold when probed with testosterone and midazolam, respectively. On Nx2, 1.28 and 1.03-fold; on Nx4, 1.25 and 1.05-fold; on X2, 1.39 and 1.26-fold; and on the commercial collagen plate, 1.71 and 1.31-fold, probed with testosterone and midazolam, respectively. CYP2C19 activity was induced on only the X2 scaffold; UGT activity was unchanged on all scaffolds in the presence of rifampicin. These results suggest that the inductive potential of rifampicin on enzyme activity is somewhat effective for CYP3A4-Test, albeit slightly higher than when probed with midazolam. The HepaRG cells inductive potential with rifampicin might be preferential to stiffer scaffolds since CYP3A4 and 2C19 activity was increased more on the X2 and commercial plate. There also was not clear trend in transcriptional regulation of *CYP3A4*, *CYP2C9* and *UGT2B4* when comparing the results for each scaffold. For the N2 and Nx4 scaffolds, rifampicin downregulates *CYP2C9* and *UGT* transcript, but has no effect on *CYP3A4* genes (N2: 0.87-, 0.27- and 0.38-fold change; Nx4: 1.47-, 0.29-, 0.27-fold change for *CYP3A4*, *CYP2C9*, and *UGT*, respectively). HepaRG cells on Nx2 and commercial collagen plates were unaffected on the transcript level regulation. The cells from the X2 scaffold

had upregulated transcript for *CYP3A4* and *CYP2C9* (5.14-, 2.25- fold change), but downregulated *UGT2B4* (0.36-fold change), which is contestant with the activity observations. Comparing the effect of rifampicin across the scaffolds, we compared the inducibility of *CYP2C9*. In the presence of rifampicin, on the N2 scaffolds, *CYP2C9* was downregulated 0.27-fold; on Nx2 a 1.20-fold upregulation; on Nx4 a 0.29-fold downregulation; on the X2 a 2.25-fold upregulation; and on the commercial collagen plate a 1.46-fold upregulation. The effect of rifampicin on the HepaRG cells is dependent on scaffold stiffness in which stiffer scaffolds (X2) exhibit an inductive effect while softer scaffolds (N2 and Nx4) exhibit an inhibitory effect. These transcriptional trends are also correlated with enzyme activity where the stiffer scaffolds have increased activity. This could suggest that the surface stiffness is modulating the effect or sensitivity of the cells to extracellular inducers.

Exposure to CITCO did significantly increase the activity of CYP2B6 in cells on all scaffolds on average 1.56±0.06 -fold, as expected. However, we did not measure increased CYP2B6 activity on the commercial collagen plate. We measured the transcriptional regulation of CaR protein (gene name *NR112)* to confirm activity of CITCO, but there was no consistency with increase on the transcript level. *NR112* was unaffected in cells cultured on the N2, Nx2 and X2 scaffolds, and upregulated on the Nx4 (3.36-fold increase) and commercial collagen plate cultured cells (2.25-fold increase). The inconsistency of upregulation could be a result of measuring the receptor transcript rather than *CYP2B6* directly.

The discrepancy between activity and transcript is interesting because on the transcript level, the HepaRG cells responded as expected in the presence of the respective inducer. 3-MC had expected inductive effects at the transcript level but failed to increase CYP1A2 activity on stiffer scaffolds. Rifampicin had inconsistent inductive effect at the transcript level and increased

activity only in the cells cultured on the stiffer surfaces (X2 and commercial collagen plate). The inducible effect of CITCO on CYP2B6 activity is unmodulated by culture stiffness as the increase in CYP2B6 activity was uniform all collagen scaffolds. The magnitude of inductive effect the three inducers have on the cells could be modulated by the effect the surfaces have on the cells. The different ECM stiffness scaffolds could be influencing how the cells are regulating pathways such as post-translational modifications on the enzyme level or post-transcriptional regulation of mRNA.

4.4 Conclusions and future work

This study compared HepaRG cells cultured on different collagen scaffolds ranging in stiffness from below to above healthy liver stiffness. HepaRG cells were plated onto collagen scaffolds and cultured for eight days. We measured cell health and viability, metabolic changes over 24 days, basal and induced metabolic enzyme activity, and transcriptional regulation. We also evaluated PHHs basal metabolic enzyme activity and transcriptional regulation on the different collagen scaffolds.

ECM stiffness has little influence on the transcriptional regulation and activity of drug metabolizing enzymes in HepaRG cells. On the transcriptional level, metabolic enzyme transcripts were relatively unchanged, except in the Nx4 (4190 Pa) scaffold in which there was significant downregulation. The drug metabolic enzyme activity trends for each enzyme were unique; however, the overall trend in HepaRG cells was that activity remain unchanged with increasing stiffness of the physiological stiffness scaffolds (N2, Nx2, Nx4 and X2). We observed conflicting activity trends between the collagen scaffolds and commercial collagen plates for CYP2B6, CYP3A4, and UGT. Across all measurements of liver specific function (urea

production, basal and time dependent metabolic enzyme activity, and transcript analysis), the HepaRG cells behave similarly across all scaffolds we evaluated. This suggests that the HepaRG cells are relatively insensitive to a wide range of ECM stiffness.

On the other hand, the PHHs were more sensitive to changes in ECM stiffness. This is clear from the transcript analysis, in which most of the measured drug metabolism enzyme genes were significantly downregulated in all stiffnesses above N2. Furthermore, the basal metabolic enzyme activity for CYP1A2, 2C19, 2D6, 3A4, SULT and UGT were significantly downregulated on the stiffer collagen scaffolds. The PHHs did behave differently on the commercial collagen plates in which we observed increased activity for CYP2C19, 2D6, and 3A4. All in all, the significant transcriptional downregulation and drug metabolizing enzyme activity decreases between N2 and Nx2 (a difference of 86.3 Pa) indicates that small stiffness changes can have dramatic effect on PHHs drug metabolizing enzyme profile.

Overall, the ECM stiffness has little effect on HepaRG cells for ECM within the large range of healthy liver stiffness (300-8000 Pa), but ECM stiffness should be taken into account for PHHs. The HepaRG cells are more resilient to ECM stiffness changes indicating that any physiological ECM stiffness will result in constant liver-specific function. In future studies, changing ECM stiffness is not necessary to assess an ideal liver model. An important insight we have highlighted, though, is that quantification of both enzyme activity and transcriptional regulation is necessary to assess changes in hepatocyte metabolic profile. While zonation has been observed at the transcriptional level, this work emphasizes transcriptional and enzyme activity changes do not always align, suggesting there are alternative regulatory pathways that must be considered in vitro. Some pathways to consider are post-transcriptional regulation, post-translational modification, and enzyme kinetics.

Analysis of this work led to the hypothesis that hepatocytes could recognize increasing surface stiffness as an inflammatory immune response, as evident by downregulation of nuclear receptor transcripts. Physiologically, Wang *et al*. measured the difference between healthy and fibrotic rat livers. They measured fibrotic liver at 1.8 kPa and healthy liver at 1.5 kPa- a 20% increase in overall liver stiffness.[51] The decrease in metabolic enzyme transcripts as ECM surface stiffness increases could be explained by the hepatocytes recognizing the stiff surface as a chronic inflammatory response causing the release of cytokines. If this is the case, then modulating ECM stiffness and composition would be beneficial to understand the effect chronic inflammation has on hepatocyte function.

4.5 Figures and tables

Table 4.1. MS/MS Transition monitoring for each drug metabolizing enzyme product using the 8-in-1 cocktail.

Enzyme	Substrate	Final Concentration (µM)	Product	Declustering Voltage (V)	Ion Mode	Parent m/z	Product m/z	Collision Energy (eV)
CYP1A2	Phenacetin	100	Acetaminophen	6	Positive	152.2	110	15
						152.2	65.03	30
CYP2B6	Bupropion	50	Hydroxy bupropion	6	Positive	256.02	238.1	8
						256.02	130.1	47
CYP2C19	(*S*)-mephenytoin	100	4'- Hydroxymephenytoin	6	Negative	232.9	190.1	19
						232.9	161.0	25
CYP2D6	Dextromethorphan	100	Dextrorphan	4	Positive	258.04	157.1	36
						258.04	199.1	25
CYP2E1	Chlorzoxazone	15	6-Hydroxychlorzoxazone	2	Negative	184.0	120.1	22
						184.0	64.0	33
CYP3A4	Midazolam	5	1-Hydroxymidazolam	6	Positive	342.04	324.1	19
						342.04	168.1	36
CYP3A4	Testosterone	50	6-beta-Testosterone	8	Positive	305.2	269.2	13
						305.2	105.1	36
SULT	7-hydroxycoumarin	100	7-Hydroxycoumarin sulfate	6	Negative	240.7	161.0	20
						240.7	133.0	34
UGT	7-hydroxycoumarin	100	7-Hydroxycoumarin glucuronide	6	Negative	337.0	161.0	29
						337.0	175.0	13

Table 4.2 List of 22 genes evaluated in this study.

Gene Symbol	Protein Abbreviation	Main Function	Forward Primer (5' – 3')	Reverse Primer (5' – 3')	Efficiency (%)
18sRNA	18s rRNA	Ribosome	CGCCGCTAGAGGTGAAATTC	TTGGCAAATGCTTTCGCTC	107.5
CYP1A2	CYP1A2	Phase I Enzyme	CTTCGGACAGCACTTCCCTG	AGGGTTAGGCAGGTAGCGAA	103.9
CYP2C9	CYP2C9	Phase I Enzyme	TCCCTGACTTCTGTGCTACATG	ACTGGAGTGGTGTCAAGGTTC	113.9
CYP2E1	CYP2E1	Phase I Enzyme	TTGAAGCCTCTCGTTGACCC	CGTGGTGGGATACAGCCAA	109.9
CYP3A4	CYP3A4	Phase I Enzyme	TCACAAACCGGAGGCCTTTT	TGGTGAAGGTTGGAGACAGC	100.4
CYP8B1	CYP8B1	Phase I Enzyme	TGCACATGGACCCTGACATC	GTGTCAGGGTCCACCAACTC	91.9
SULT2A1	SULT2A1	Phase II Enzyme	TGAGGAGCTGAAACAGGACAC	AAGTCTTCAGCTTGGGCCAC	106.6
UGT2B4	UGT2B4	Phase II Enzyme	ACACATGAAGGCCAAGGGAG	GAACCAGGTGAGGTCGTGG	94.3
AHR	AhR	Transcription Factor	CTTCCAAGCGGCATAGAGAC	AGTTATCCTGGCCTCCGTTT	101.5
NR1I3	CaR	Transcription Factor	TGATCAGCTGCAAGAGGAGA	AGGCCTAGCAACTTCGCATA	102.6
NR1I2	PxR	Transcription Factor	CCAGGACATACACCCCTTTG	CTACCTGTGATGCCGAACAA	104.3
ABCB1	P-gp	Efflux Pump	GCCAAAGCCAAAATATCAGC	TTCCAATGTGTTCGGCATTA	93.6
ABCC2	MRP2	Transporter (Excretion)	TGAGCAAGTTTGAAACGCACAT	AGCTCTTCTCCTGCCGTCTCT	99.6
ABCC3	MRP3	Transporter (Excretion)	GTCCGCAGAATGGACTTGAT	TCACCACTTGGGGATCATTT	108.5
ABCG2	BCRP	Transporter (Excretion)	TGCAACATGTACTGGCGAAGA	TCTTCCACAAGCCCCAGG	101.5
SLOC1B1	OATP1B1	Transporter (Uptake)	GCCCAAGAGATGATGCTTGT	ATTGAGTGGAAACCCAGTGC	97.3
SLCO2B1	OATP2B1	Transporter (Uptake)	TGATTGGCTATGGGGCTATC	CATATCCTCAGGGCTGGTGT	106.5
SLC10A1	NTCP	Transporter (Uptake)	GGGACATGAACCTCAGCATT	CGTTTGGATTTGAGGACGAT	101.4
SLC22A1	OCT1	Transporter (Uptake)	TAATGGACCACATCGCTCAA	AGCCCCTGATAGAGCACAGA	104.5
ALB	Albumin	Globular Protein	TGAGCAGCTTGGAGAGTACA	GTTCAGGACCACGGATAGAT	124.1
KRT19	CK-19	Biliary-like/Progenitor Cell Marker	TTTGAGACGGAACAGGCTCT	AATCCACCTCCACACTGACC	100.8
TJP1	ZO-1	Tight-Junction	CGAGTTGCAATGGTTAACGGA	TCAGGATCAGGACGACTTACTGG	106.9

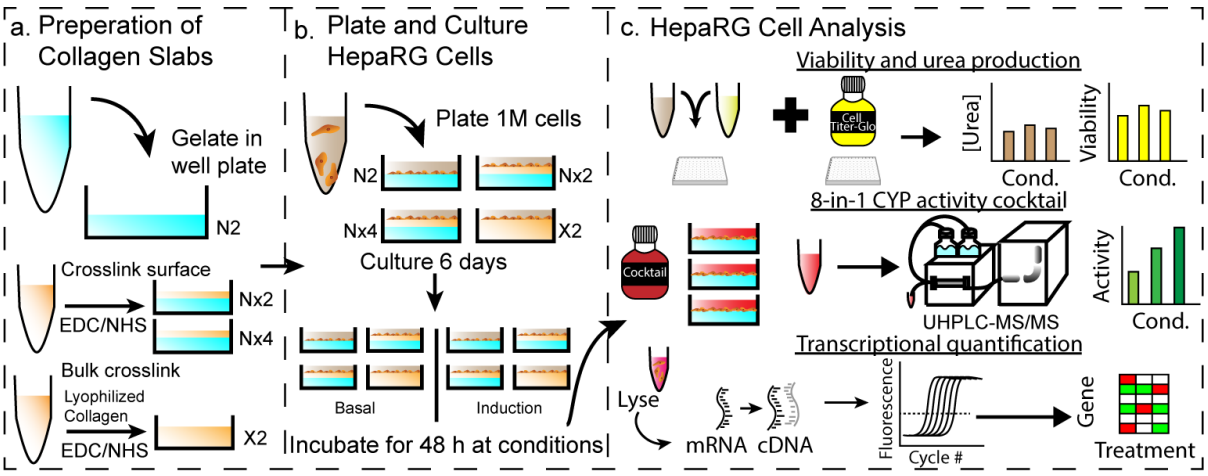

Figure 4.1. Experimental workflow comparing the responses of HepaRG cells cultured collagen scaffolds of increasing stiffness. (a) Collagen I scaffolds with densities of either 2 or 4 mg/mL were prepared in a 12-well plate. The collagen was pipetted into the wells and gelated with neutralization (N2), neutralization and cross-linking of surface proteins with EDC/NHS (Nx2 and Nx4), or bulk crosslinked by resuspending lyophilized in a EDC/NHS-containing solution (X2). (b) Each scaffold was coated with a thin layer of collagen I, the HepaRG cells were seeded onto the scaffolds, and maintained for six days under standard culture conditions. For the next 48 hours HepaRG and PHH cells were left in standard conditions to assess basal activity levels or induced with one of three different CYP inducers (3-MC, rifampicin or CITCO). (c) Finally, hepatocyte viability was evaluated with the MTS assay, urea secretion with a colorimetric assay, metabolic enzyme activity was evaluated with a quantitative LC-MS/MS method, and transcriptional regulation was evaluated with RT-qPCR.

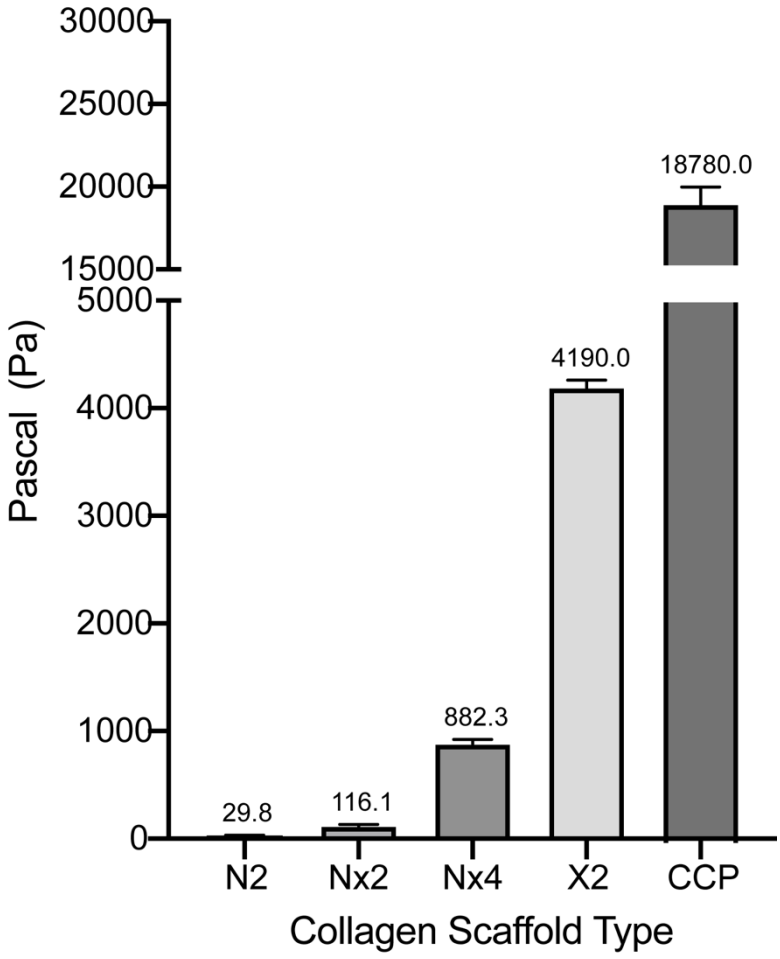

Figure 4.2 The stiffness of the four scaffolds and a commercial collagen plate (CCP) were measured with a nanoindentor by assessing 64 points in an 800 x 800 μm array. The individual force curves were fit to a Hertz model. The average Young's modulus was plotted with SEM of force curve fits for each indentation

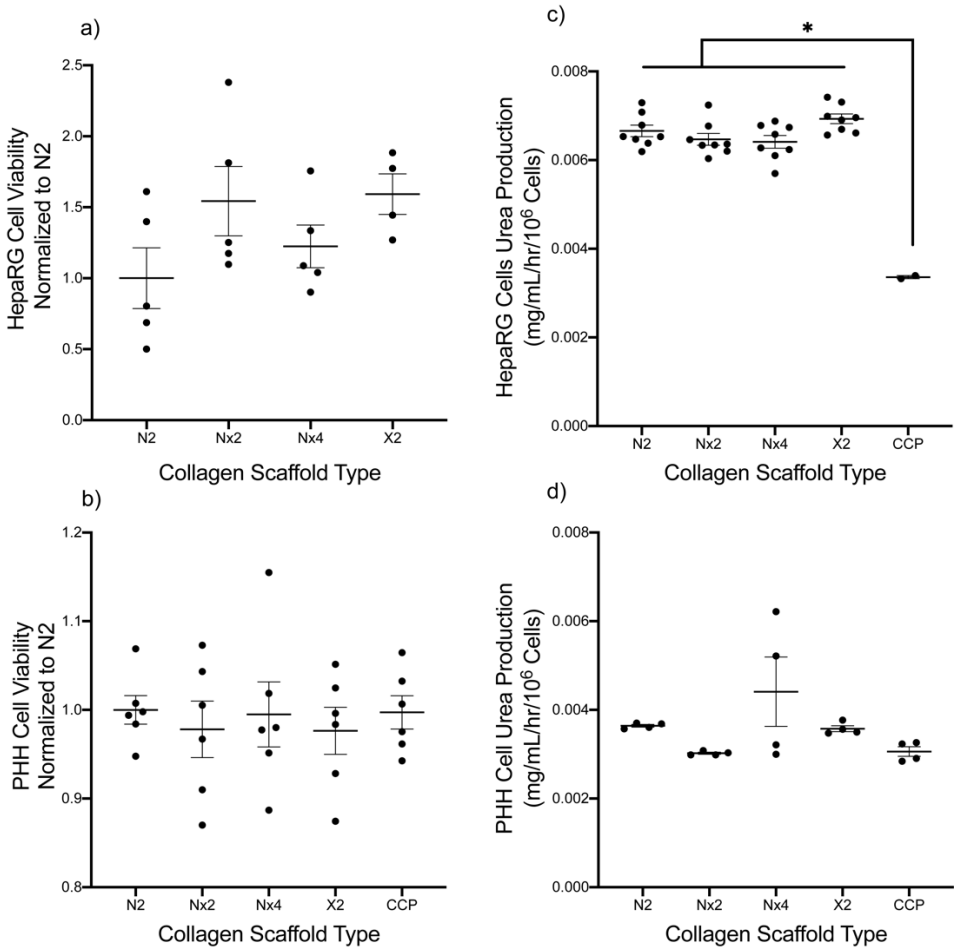

Figure 4.3. (a, b) Cell viability and (c,d) urea secretion of HepaRG cells after an 8 days culture on collagen scaffolds with different underlying stiffnesses. Data points represent the separate cultures setup from two vials of cells; the mean was plotted with error bars representing the SEM. Significance was determined with a one-way ANOVA analysis.

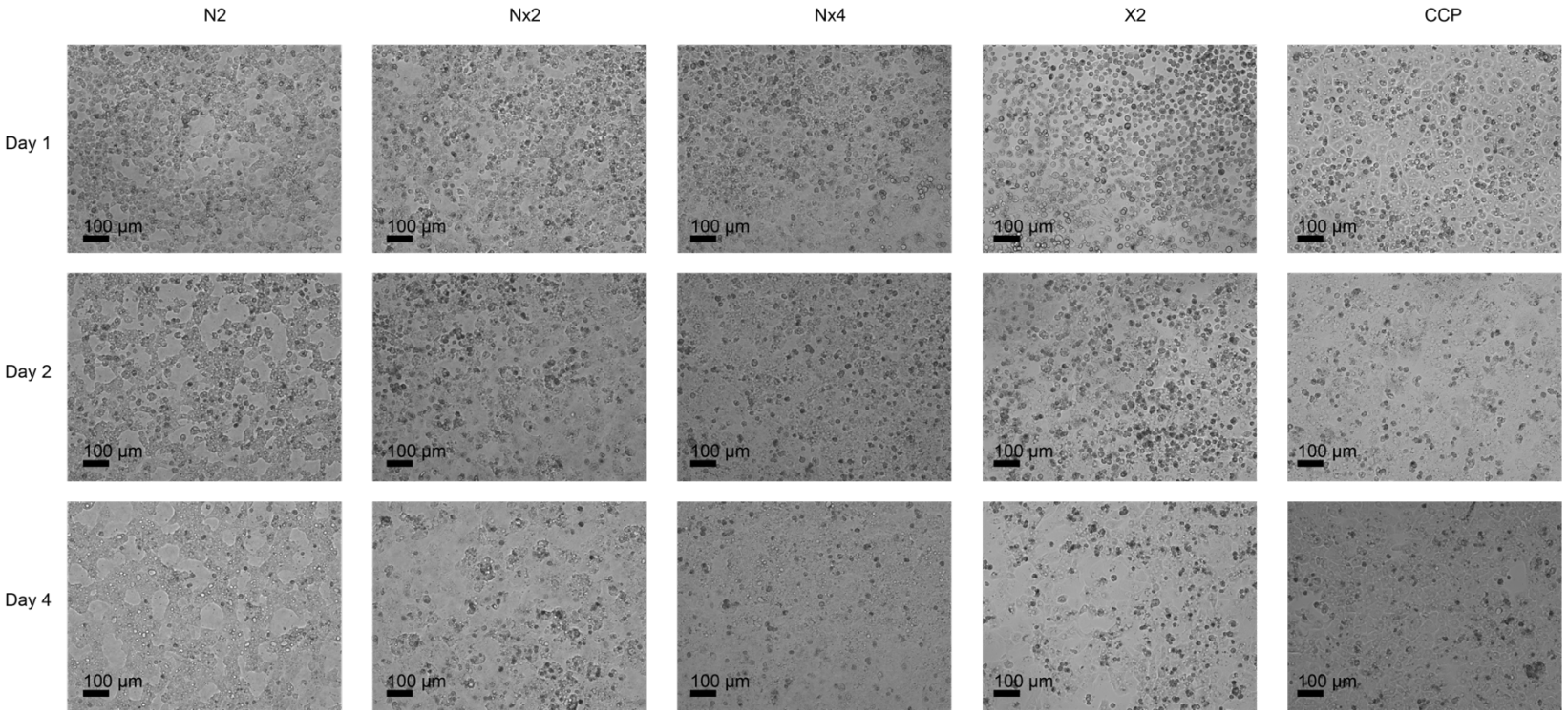

Figure 4.4. Widefield images of PHHs cells grown over 4 days for basal metabolic enzyme activity on different collagen stiffnesses. Over the 4 days displayed above, a clear morphological change can be observed. On day 0 the cells appear rounded are shape. On day 2 and 4 the cells are adopting a more cobblestone morphology. The PHHs on the Nx2, Nx4 and X2 scaffolds on day 4 appear to have more dark regions of cells which could be indicative of cells spreading on top of their neighbors (like spheroids). Images were collected using a Nikon TE2000 microscope, 10x objective and captured with a Photometrics Dyno CCD camera. Scale bars are 100 µm.

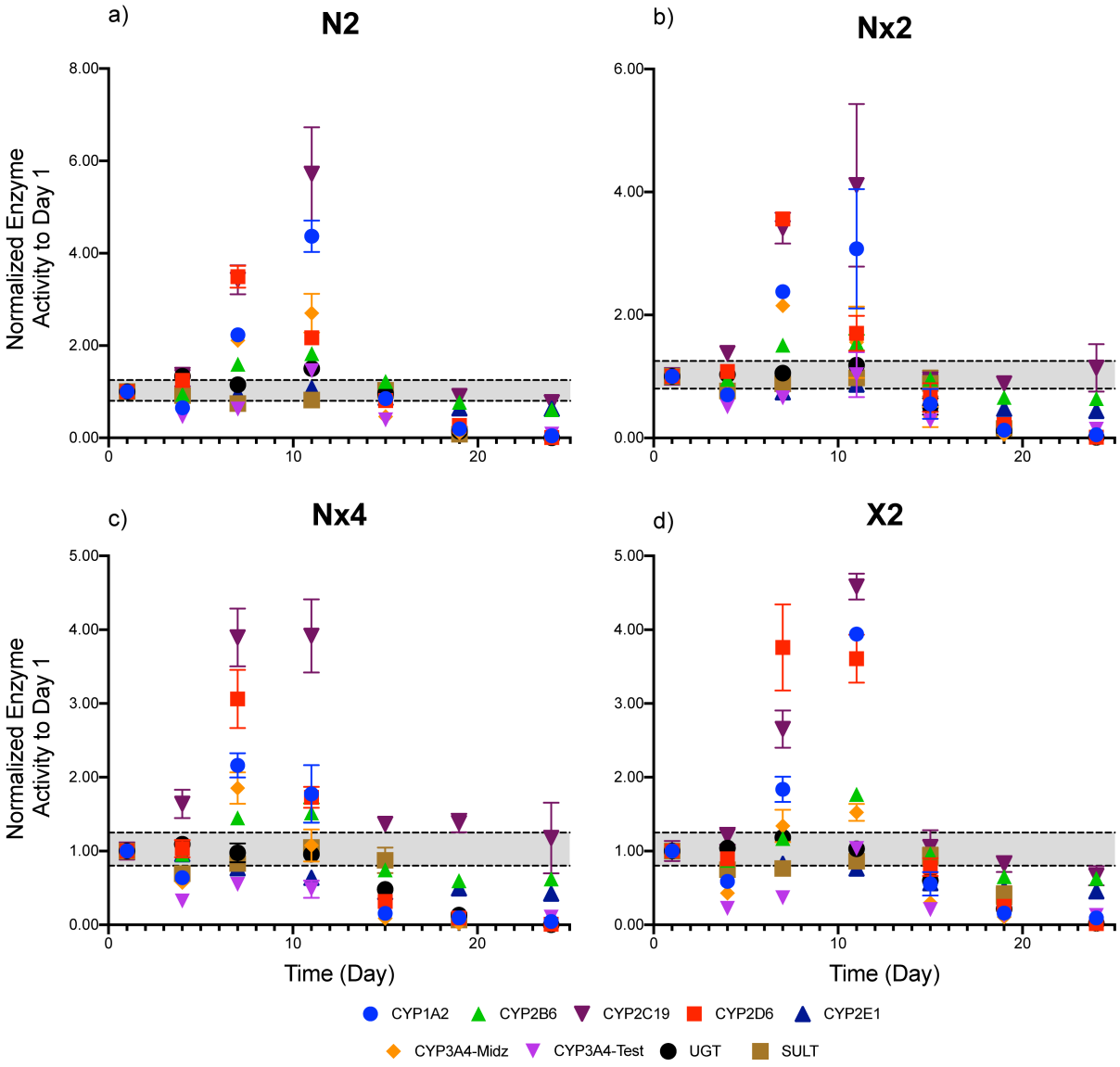

Figure 4.5 Metabolic enzyme activity of HepaRG cells on the different collagen scaffolds over a 24 day period. Metabolic activity was determined with an LC-MS/MS method in which the products of an 8-in-1 cocktail were identified and quantified against standards using multiple reaction monitoring. Each time point is normalized to Day 1. The dotted black lines and grey box represent 1.25- and 0.8-fold change from the average value collated on Day 1 and represent a significant difference in activity. Data points represent the average of two biological replicates ± SEM.

Table 4.3. Summary of maximal increase in drug metabolizing enzyme activity and day it was observed. [a]

	N2		Nx2		Nx4		X2	
	Day	**Max Activity (Fold Change)**	**Day**	**Max Activity (Fold Change)**	**Day**	**Max Activity (Fold Change)**	**Day**	**Max Activity (Fold Change)**
CYP1A2	11	4.37	11	3.08	7	2.16	11	3.94
CYP2B6	11	1.82	11	1.55	11	1.52	11	1.77
CYP2C19	11	5.72	11	4.11	11	3.92	11	4.59
CYP2D6	7	3.49	7	3.56	7	3.06	7	3.76
CYP2E1	11	1.07	--	N/A	--	N/A	--	N/A
CYP3A4- Midz	11	2.70	7	2.15	7	1.85	11	1.53
CYP3A4- Test	11	1.46	11	1.03	--	N/A	11	1.03
SULT	15	1.03	N/A	N/A	11	1.05	N/A	N/A
UGT	11	1.50	11	1.18	4	1.09	7	1.18

[a] --/ N/A indicates no increase in enzyme activity was observed over the 24 days.

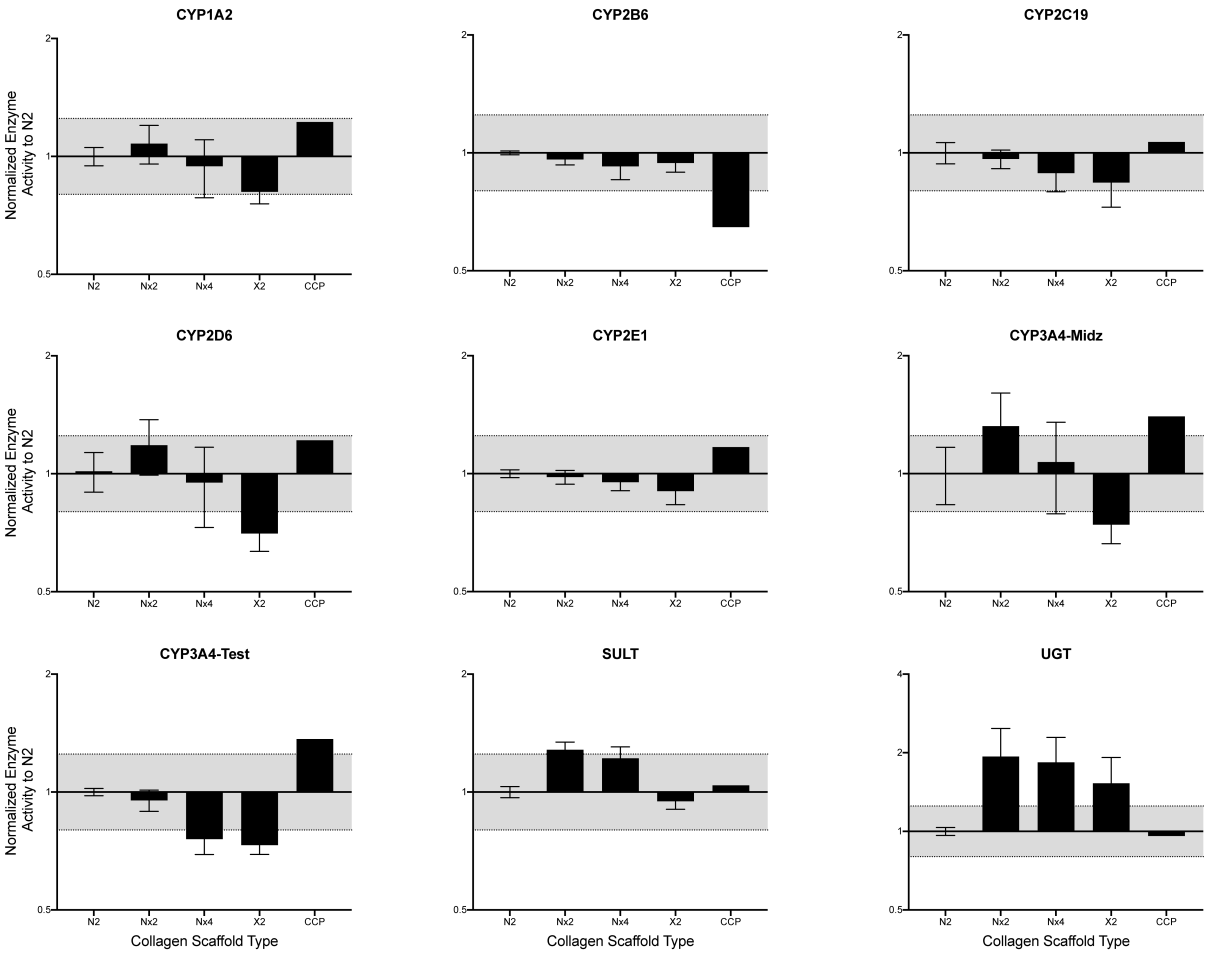

Figure 4.6 Basal metabolic enzyme activity of HepaRG, normalized to the average enzyme activity for cells on the N2 scaffolds for each enzyme, after an 8 day culture period. The grey region of the curve represents 1.25- and 0.8-fold change, those bars outside of this region are considered a significant difference in activity. Bars represent the average ± SEM, from 2 biological replicates.

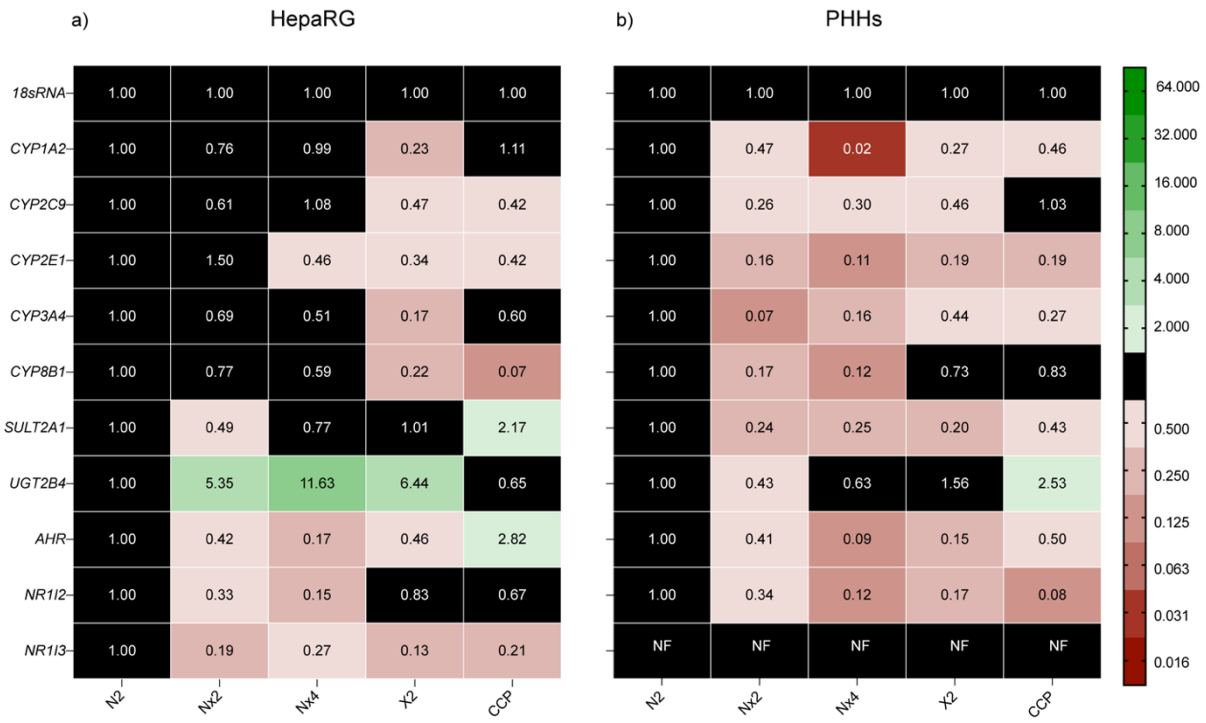

Figure 4.7 Transcript-level regulation of (a) HepaRG and (b) PHH cells cultured for 8 days. Transcript level analysis of phase I and phase II enzymes, nuclear receptors, genes compared to the N2 cultured cells. Each value is the average of at least one technical replicate, collected from two biological replicates. A fold-change >2 indicates a significant increase in expression; <0.50 indicates a significant decrease. The numerical labels represent the average fold change using the ΔΔCt method. NF indicates no transcript was quantified.

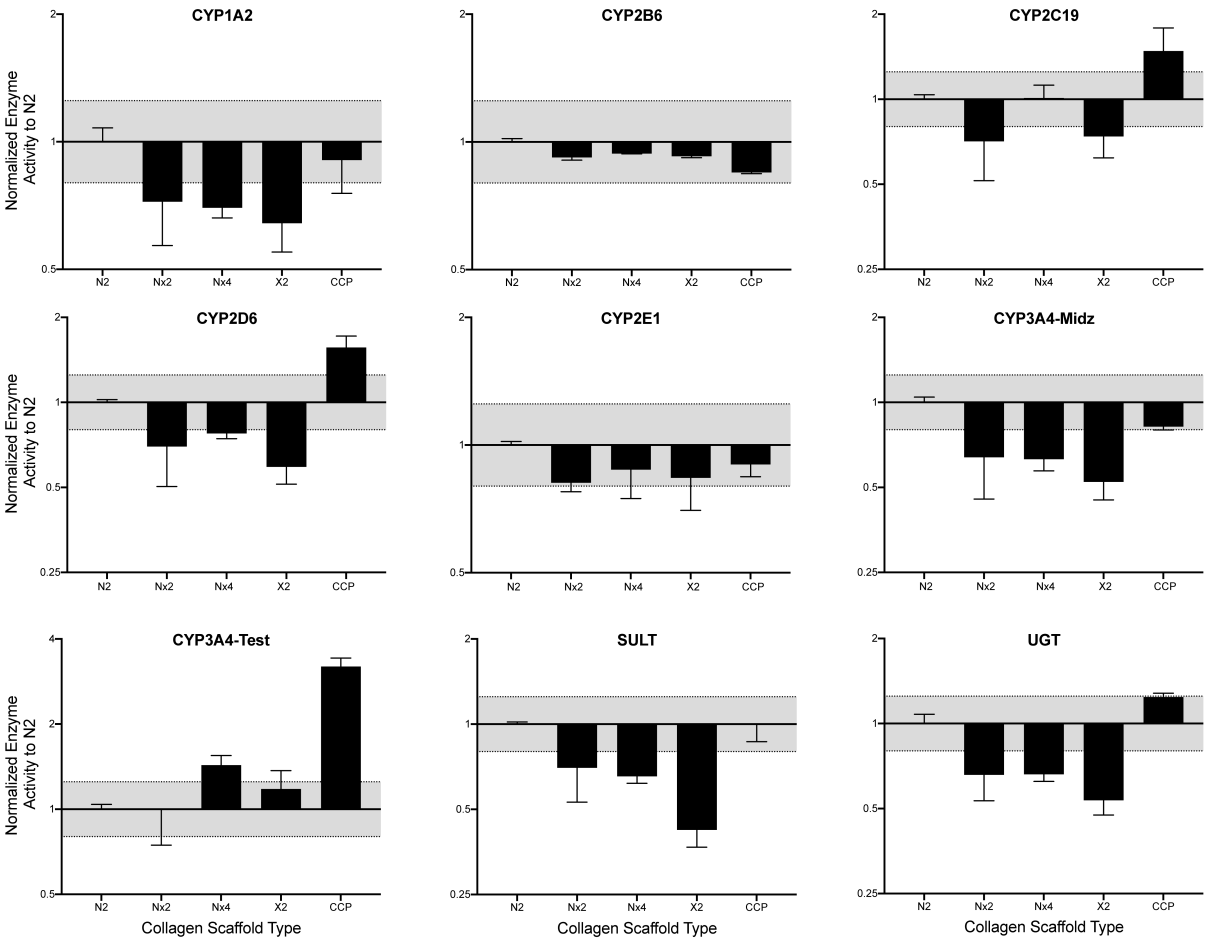

Figure 4.8. Basal metabolic enzyme activity of PHHs cultured for 4 days. Enzyme activity was normalized to the average enzyme activity for cells on the N2 scaffolds for each enzyme. The grey region of the curve represents 1.25- and 0.8-fold change, those bars outside of this region are considered a significant difference in activity. Bars represent the average ± SEM, from 2 biological replicates.

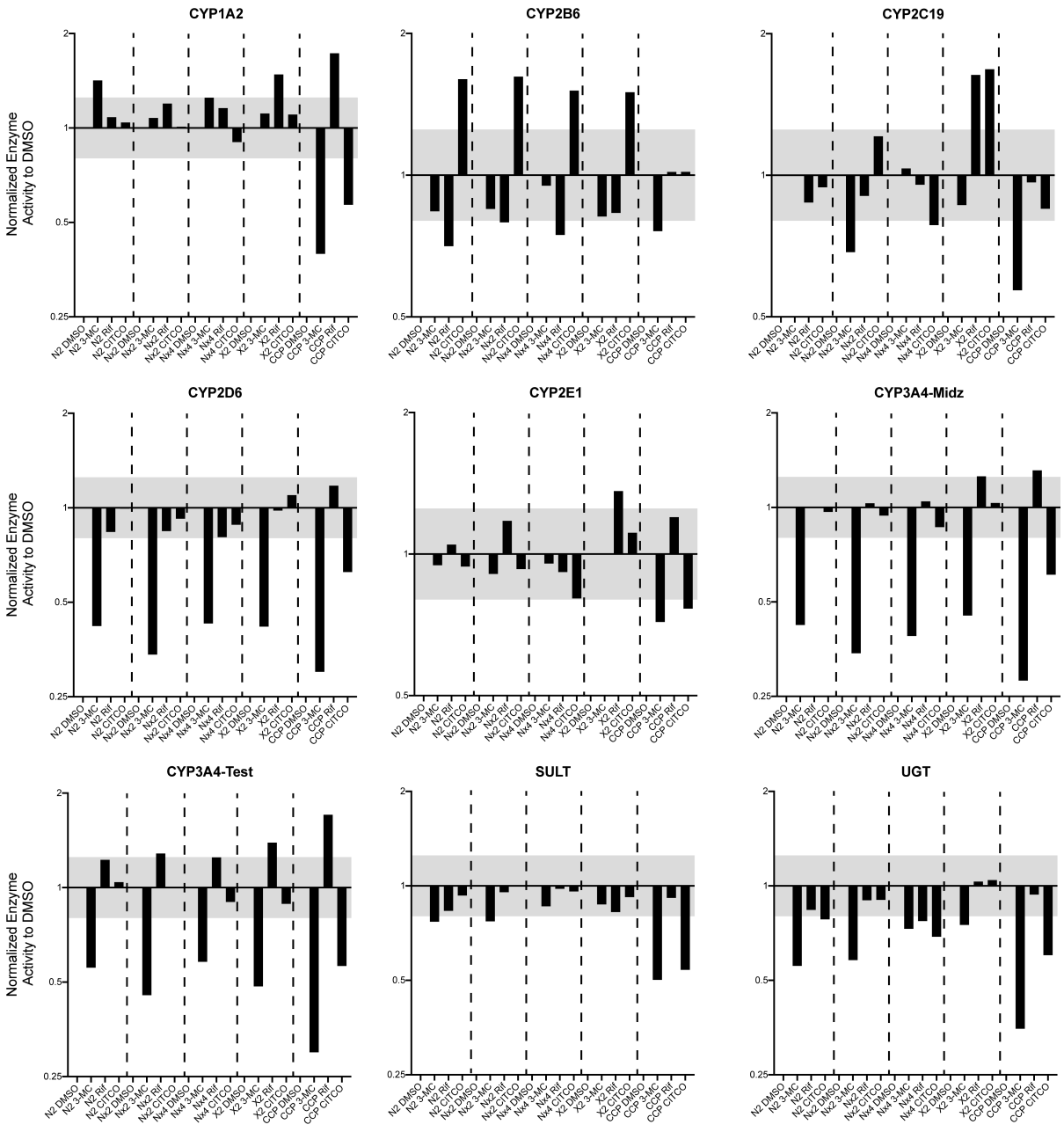

Figure 4.9. Induced metabolic enzyme activity of HepaRG cells cultured for 6 days followed by 48 hours exposed to one of three inducers (3-MC, rifampicin, or CITCO). Enzyme activity was normalized to the DMSO vehicle control for each metabolic enzyme. The grey region of the curve represents 1.25- and 0.8-fold change, those bars outside of this region are considered a significant difference in activity.

Figure 4.10 Transcript-level regulation of HepaRG cells after a 48 hour induction with either 3-MC, rifampicin, or CITCO. The numerical labels represent the average fold change using the ΔΔCt method, using 18sRNA as the housekeeping gene and a DMSO vehicle control. Each value is the average of at least one technical replicate collected from two separate experimental setups. A fold-change >2 indicates a significant increase in expression; <0.50 indicates a significant decrease.

REFERENCES

(1) Hodgson, J. ADMET—Turning Chemicals into Drugs. *Nat. Biotechnol.* **2001**, *19*, 722–726. https://doi.org/https://doi.org/10.1038/90761.

(2) Bowes, J.; Brown, A. J.; Hamon, J.; Jarolimek, W.; Sridhar, A.; Waldron, G.; Whitebread, S. Reducing Safety-Related Drug Attrition: The Use of in Vitro Pharmacological Profiling. *Nature Reviews Drug Discovery*. 2012, pp 909–922. https://doi.org/10.1038/nrd3845.

(3) Jackson, J. P.; Li, L.; Chamberlain, E. D.; Wang, H.; Ferguson, S. S. Contextualizing Hepatocyte Functionality of Cryopreserved HepaRG Cell Cultures. *Drug Metab. Dispos.* **2016**, *44* (9), 1463–1479. https://doi.org/10.1124/dmd.116.069831.

(4) Zhang, D.; Luo, G.; Ding, X.; Lu, C. Preclinical Experimental Models of Drug Metabolism and Disposition in Drug Discovery and Development. *Acta Pharm. Sin. B* **2012**, *2* (6), 549–561. https://doi.org/10.1016/j.apsb.2012.10.004.

(5) Collins, S. D.; Yuen, G.; Tu, T.; Budzinska, M. A.; Spring, K.; Bryant, K.; Shackel, N. A. *Hepatocellular Carcinoma: Chapter 3 In Vitro Models of the Liver: Disease Modeling, Drug Discovery and Clinical Applications*; 2019.

(6) Borlak, J.; Chougule, A.; Singh, P. K. How Useful Are Clinical Liver Function Tests in in Vitro Human Hepatotoxicity Assays? *Toxicol. Vitr.* **2014**, *28* (5), 784–795. https://doi.org/10.1016/j.tiv.2014.03.006.

(7) Soldatow, V. Y.; Lecluyse, E. L.; Griffith, L. G.; Rusyn, I. In Vitro Models for Liver Toxicity Testing. *Toxicology Research*. Royal Society of Chemistry 2013, pp 23–39. https://doi.org/10.1039/c2tx20051a.

(8) Chang, T. T.; Hughes-Fulford, M. Monolayer and Spheroid Culture of Human Liver Hepatocellular Carcinoma Cell Line Cells Demonstrate Distinct Global Gene Expression Patterns and Functional Phenotypes. *Tissue Eng. Part A* **2009**, *15* (3), 559–567. https://doi.org/10.1089/ten.tea.2007.0434.

(9) Gerets, H. H. J.; Tilmant, K.; Gerin, B.; Chanteux, H.; Depelchin, B. O.; Dhalluin, S.; Atienzar, F. A. Characterization of Primary Human Hepatocytes, HepG2 Cells, and HepaRG Cells at the MRNA Level and CYP Activity in Response to Inducers and Their Predictivity for the Detection of Human Hepatotoxins. *Cell Biol. Toxicol.* **2012**, *28* (2), 69–87. https://doi.org/10.1007/s10565-011-9208-4.

(10) Guillouzo, A.; Corlu, A.; Aninat, C.; Glaise, D.; Morel, F.; Guguen-Guillouzo, C. The Human Hepatoma HepaRG Cells: A Highly Differentiated Model for Studies of Liver Metabolism and Toxicity of Xenobiotics. *Chem. Biol. Interact.* **2007**, *168* (1), 66–73. https://doi.org/10.1016/J.CBI.2006.12.003.

(11) Zhou, Y.; Shen, J. X.; Lauschke, V. M. Comprehensive Evaluation of Organotypic and Microphysiological Liver Models for Prediction of Drug-Induced Liver Injury. *Frontiers in Pharmacology*. Frontiers Media S.A. 2019. https://doi.org/10.3389/fphar.2019.01093.

(12) Gaskell, H.; Sharma, P.; Colley, H. E.; Murdoch, C.; Williams, D. P.; Webb, S. D. Characterization of a Functional C3A Liver Spheroid Model. *Toxicol. Res. (Camb).* **2016**, *5* (4), 1053–1065. https://doi.org/10.1039/c6tx00101g.

(13) Skardal, A.; Smith, L.; Bharadwaj, S.; Atala, A.; Soker, S.; Zhang, Y. Tissue Specific Synthetic ECM Hydrogels for 3-D in Vitro Maintenance of Hepatocyte Function. *Biomaterials* **2012**, *33* (18), 4565–4575. https://doi.org/10.1016/j.biomaterials.2012.03.034.

(14) Wang, B.; Li, W.; Dean, D.; Mishra, M. K.; Wekesa, K. S. Enhanced Hepatogenic Differentiation of Bone Marrow Derived Mesenchymal Stem Cells on Liver ECM Hydrogel. *J. Biomed. Mater. Res. - Part A* **2018**, *106* (3), 829–838. https://doi.org/10.1002/jbm.a.36278.

(15) Dipersio, C. M.; Jackson, D. A.; Zaret, K. S. *The Extracellular Matrix Coordinately Modulates Liver Transcription Factors and Hepatocyte Morphology*; 1991; Vol. 11.

(16) Tibbitt, M. W.; Anseth, K. S. Hydrogels as Extracellular Matrix Mimics for 3D Cell Culture. *Biotechnology and Bioengineering*. 2009, pp 655–663. https://doi.org/10.1002/bit.22361.

(17) Zhang, Y.; He, Y.; Bharadwaj, S.; Hammam, N.; Carnagey, K.; Myers, R.; Atala, A.; Van Dyke, M. Tissue-Specific Extracellular Matrix Coatings for the Promotion of Cell Proliferation and Maintenance of Cell Phenotype. *Biomaterials* **2009**, *30* (23–24), 4021–4028. https://doi.org/10.1016/j.biomaterials.2009.04.005.

(18) Yang, K.; Guo, C.; Woodhead, J. L.; Claire Iii, R. L.; Watkins, P. B.; Siler, S. Q.; Howell, B. A.; Brouwer, K. L. Sandwich-Cultured Hepatocytes as a Tool to Study Drug Disposition and Drug-Induced Liver Injury. *J Pharm Sci* **2016**, *105* (2), 443–459. https://doi.org/10.1016/j.xphs.2015.11.008.

(19) Baiocchini, A.; Montaldo, C.; Conigliaro, A.; Grimaldi, A.; Correani, V.; Mura, F.; Ciccosanti, F.; Rotiroti, N.; Brenna, A.; Montalbano, M.; D'Offizi, G.; Capobianchi, M. R.; Alessandro, R.; Piacentini, M.; Schininà, M. E.; Maras, B.; Del Nonno, F.; Tripodi, M.; Mancone, C. Extracellular Matrix Molecular Remodeling in Human Liver Fibrosis Evolution. *PLoS One* **2016**, *11* (3), 1–14. https://doi.org/10.1371/journal.pone.0151736.

(20) Kleinman, H. K.; Klebe, R. J.; Martin, G. R. Role of Collagenous Matrices in the Adhesion and Growth of Cells. *J. Cell Biol.* **1981**, *88* (3), 473–485. https://doi.org/10.1083/jcb.88.3.473.

(21) Wells, R. G. The Role of Matrix Stiffness in Regulating Cell Behavior. *Hepatology*. 2008,

pp 1394–1400. https://doi.org/10.1002/hep.22193.

(22) Mueller, S.; Sandrin, L. *HMER-7394-Liver-Stiffness-as-Novel-Parameter-for-the-Diagnosis-of-Live*; 2010; Vol. 2.

(23) Xia, T.; Zhao, R.; Feng, F.; Yang, L. The Effect of Matrix Stiffness on Human Hepatocyte Migration and Function-An in Vitro Research. *Polymers (Basel).* **2020**, *12* (9). https://doi.org/10.3390/POLYM12091903.

(24) Natarajan, V.; Berglund, E. J.; Chen, D. X.; Kidambi, S. Substrate Stiffness Regulates Primary Hepatocyte Functions. *RSC Adv.* **2015**, *5* (99), 80956–80966. https://doi.org/10.1039/c5ra15208a.

(25) Marion, M. J.; Hantz, O.; Durantel, D. The HepaRG Cell Line: Biological Properties and Relevance as a Tool for Cell Biology, Drug Metabolism, and Virology Studies. *Methods Mol. Biol.* **2010**, *640*, 261–272. https://doi.org/10.1007/978-1-60761-688-7_13.

(26) Cerec, V.; Glaise, D.; Garnier, D.; Morosan, S.; Turlin, B.; Drenou, B.; Gripon, P.; Kremsdorf, D.; Guguen-Guillouzo, C.; Corlu, A. Transdifferentiation of Hepatocyte-like Cells from the Human Hepatoma HepaRG Cell Line through Bipotent Progenitor. *Hepatology* **2007**, *45* (4), 957–967. https://doi.org/10.1002/hep.21536.

(27) Dierks, E. A.; Stams, K. R.; Lim, H. K.; Cornelius, G.; Zhang, H.; Ball, S. E. A Method for the Simultaneous Evaluation of the Activities of Seven Major Human Drug-Metabolizing Cytochrome P450s Using an in Vitro Cocktail of Probe Substrates and Fast Gradient Liquid Chromatography Tandem Mass Spectrometry. *Drug Metab. Dispos.* **2001**, *29* (1), 23–29.

(28) Li, G.; Huang, K.; Nikolic, D.; Van Breemen, R. B. High-Throughput Cytochrome P450 Cocktail Inhibition Assay for Assessing Drug-Drug and Drug-Botanical Interactions. *Drug Metab. Dispos.* **2015**, *43* (11), 1670–1678. https://doi.org/10.1124/dmd.115.065987.

(29) Schmittgen, T. D.; Livak, K. J. Analyzing Real-Time PCR Data by the Comparative CT Method. *Nat. Protoc.* **2008**, *3* (6), 1101–1108. https://doi.org/10.1038/nprot.2008.73.

(30) Rojkind, M.; Giambrone, M. A.; Biempica, L. Collagen Types in Normal and Cirrhotic Liver. *Gastroenterology* **1979**, *76* (4), 710–719. https://doi.org/10.1016/S0016-5085(79)80170-5.

(31) Sackett, S. D.; Tremmel, D. M.; Ma, F.; Feeney, A. K.; Maguire, R. M.; Brown, M. E.; Zhou, Y.; Li, X.; O'Brien, C.; Li, L.; Burlingham, W. J.; Odorico, J. S. Extracellular Matrix Scaffold and Hydrogel Derived from Decellularized and Delipidized Human Pancreas. *Sci. Rep.* **2018**, *8* (1). https://doi.org/10.1038/s41598-018-28857-1.

(32) Burkel, B.; Morris, B. A.; Ponik, S. M.; Riching, K. M.; Eliceiri, K. W.; Keely, P. J. Preparation of 3D Collagen Gels and Microchannels for the Study of 3D Interactions In

Vivo. *J. Vis. Exp.* **2016**, *2016* (111). https://doi.org/10.3791/53989.

(33) Antoine, E. E.; Vlachos, P. P.; Rylander, M. N. Review of Collagen I Hydrogels for Bioengineered Tissue Microenvironments: Characterization of Mechanics, Structure, and Transport. *Tissue Eng. Part B Rev.* **2014**, *20* (6), 683–696. https://doi.org/10.1089/ten.teb.2014.0086.

(34) Anguiano, M.; Castilla, C.; Maška, M.; Ederra, C.; Peláez, R.; Morales, X.; Muñoz-Arrieta, G.; Mujika, M.; Kozubek, M.; Muñoz-Barrutia, A.; Rouzaut, A.; Arana, S.; Garcia-Aznar, J. M.; Ortiz-de-Solorzano, C. Characterization of Three-Dimensional Cancer Cell Migration in Mixed Collagen-Matrigel Scaffolds Using Microfluidics and Image Analysis. *PLoS One* **2017**, *12* (2). https://doi.org/10.1371/journal.pone.0171417.

(35) Miron-Mendoza, M.; Seemann, J.; Grinnell, F. The Differential Regulation of Cell Motile Activity through Matrix Stiffness and Porosity in Three Dimensional Collagen Matrices. *Biomaterials* **2010**, *31* (25), 6425–6435. https://doi.org/10.1016/j.biomaterials.2010.04.064.

(36) Yang, C. *Enhanced Physicochemical Properties of Collagen by Using EDC/NHS-Crosslinking*; 2012; Vol. 35.

(37) Mueller, S. Introduction to Liver Stiffness: A Novel Parameter for the Diagnosis of Liver Disease. *Liver Elastography Clin. Use Interpret.* **2020**, 3–9. https://doi.org/10.1007/978-3-030-40542-7_1.

(38) Gu, L.; Shan, T.; Ma, Y. xuan; Tay, F. R.; Niu, L. Novel Biomedical Applications of Crosslinked Collagen. *Trends in Biotechnology*. Elsevier Ltd 2019, pp 464–491. https://doi.org/10.1016/j.tibtech.2018.10.007.

(39) Wang, Y.; Kim, M. H.; Shirahama, H.; Lee, J. H.; Ng, S. S.; Glenn, J. S.; Cho, N. J. ECM Proteins in a Microporous Scaffold Influence Hepatocyte Morphology, Function, and Gene Expression. *Sci. Rep.* **2016**, *6*. https://doi.org/10.1038/srep37427.

(40) Gao, J.; Zhou, J.; He, X. P.; Zhang, Y. F.; Gao, N.; Tian, X.; Fang, Y.; Wen, Q.; Jia, L. J.; Jin, H.; Qiao, H. L. Changes in Cytochrome P450s-Mediated Drug Clearance in Patients with Hepatocellular Carcinoma in Vitro and in Vivo: A Bottom-up Approach. *Oncotarget* **2016**, *7* (19), 28612–28623. https://doi.org/10.18632/oncotarget.8704.

(41) Fisher, C. D.; Lickteig, A. J.; Augustine, L. M.; Ranger-Moore, J.; Jackson, J. P.; Ferguson, S. S.; Cherrington, N. J. Hepatic Cytochrome P450 Enzyme Alterations in Humans with Progressive Stages of Nonalcoholic Fatty Liver Disease. *Drug Metab. Dispos.* **2009**, *37* (10), 2087–2094. https://doi.org/10.1124/dmd.109.027466.

(42) Kim, S.; Östör, A. J. K.; Nisar, M. K. Interleukin-6 and Cytochrome-P450, Reason for Concern? *Rheumatol. Int.* **2012**, *32* (9), 2601–2604. https://doi.org/10.1007/s00296-012-2423-3.

(43) Fuster, D.; Tsui, J. I.; Cheng, D. M.; Quinn, E. K.; Armah, K. A.; Nunes, D.; Freiberg, M. S.; Samet, J. H. Interleukin-6 Is Associated with Noninvasive Markers of Liver Fibrosis in HIV-Infected Patients with Alcohol Problems. *AIDS Res. Hum. Retroviruses* **2013**, *29* (8), 1110–1116. https://doi.org/10.1089/aid.2012.0348.

(44) Cobbina, E.; Akhlaghi, F. Non-Alcoholic Fatty Liver Disease (NAFLD) - Pathogenesis, Classification, and Effect on Drug Metabolizing Enzymes and Transporters Enoch. *Drug Metab. Rev.* **2017**, *42* (2), 197–221. https://doi.org/10.1080/03602532.2017.1293683.Non-Alcoholic.

(45) Koyama, Y.; Brenner, D. A. Liver Inflammation and Fibrosis. *J. Clin. Invest.* **2017**, *127* (1), 55–64. https://doi.org/10.1172/JCI88881.

(46) Lee, U. E.; Friedman, S. L. Mechanisms of Hepatic Fibrogenesis Ursula. *Best Pr. Res Clin Gastroenterol* **2011**, *25* (2), 195–206. https://doi.org/10.1016/j.bpg.2011.02.005.Mechanisms.

(47) Beringer, A.; Molle, J.; Bartosch, B.; Miossec, P. Two Phase Kinetics of the Inflammatory Response from Hepatocyte-Peripheral Blood Mononuclear Cell Interactions. *Sci. Rep.* **2019**, *9* (1), 1–10. https://doi.org/10.1038/s41598-019-44840-w.

(48) Rowell, D. L.; Eckmann, L.; Dwinell, M. B.; Carpenter, S. P.; Raucy, J. L.; Yang, S. K.; Kagnoff, M. F. Human Hepatocytes Express an Array of Proinflammatory Cytokines after Agonist Stimulation or Bacterial Invasion. *Am. J. Physiol. - Gastrointest. Liver Physiol.* **1997**, *273* (2 36-2). https://doi.org/10.1152/ajpgi.1997.273.2.g322.

(49) Hakkola, J.; Hu, Y.; Ingelman-Sundberg, M. Mechanisms of Down-Regulation of CYP2E1 Expression by Inflammatory Cytokines in Rat Hepatoma Cells. *J. Pharmacol. Exp. Ther.* **2003**, *304* (3), 1048–1054. https://doi.org/10.1124/jpet.102.041582.

(50) Lin, L.; Yee, S. W.; Kim, R. B.; Giacomini, K. M. SLC Transporters as Therapeutic Targets: Emerging Opportunities. *Nat. Rev. Drug Discov.* **2015**, *14* (8), 543–560. https://doi.org/10.1038/nrd4626.

(51) Ware, B. R.; Liu, J. S.; Monckton, C. P.; Ballinger, K. R.; Khetani, S. R. Micropatterned Coculture With 3T3-J2 Fibroblasts Enhances Hepatic Functions and Drug Screening Utility of HepaRG Cells. *Toxicol. Sci.* **2021**, *181* (1), 90–104. https://doi.org/10.1093/toxsci/kfab018.

(52) Kvale, D.; Brandtzaeg, P. Immune Modulation of Adhesion Molecules ICAM-1 (CD54) and LFA-3 (CD58) in Human Hepatocytic Cell Lines. *J. Hepatol.* **1993**, *17* (3), 347–352. https://doi.org/10.1016/S0168-8278(05)80216-8.

(53) Gulubova, M. V. Intercellular Adhesion Molecule-1 (ICAM-1) Expression in the Liver of Patients with Extrahepatic Cholestasis. *Acta Histochem.* **1998**, *100* (1), 59–74. https://doi.org/10.1016/s0065-1281(98)80006-8.

(54) Orbán, E.; Szabó, E.; Lotz, G.; Kupcsulik, P.; Páska, C.; Schaff, Z.; Kiss, A. Different Expression of Occludin and ZO-1 in Primary and Metastatic Liver Tumors. *Pathol. Oncol. Res.* **2008**, *14* (3), 299–306. https://doi.org/10.1007/s12253-008-9031-2.

(55) Wang, M. H.; Palmeri, M. L.; Guy, C. D.; Yang, L.; Hedlund, L. W.; Diehl, A. M.; Nightingale, K. R. In Vivo Quantification of Liver Stiffness in a Rat Model of Hepatic Fibrosis with Acoustic Radiation Force. *Ultrasound Med. Biol.* **2009**, *35* (10), 1709–1721. https://doi.org/10.1016/j.ultrasmedbio.2009.04.019.

CHAPTER 5: HEPARG CELLS CULTURED IN 3D PAPER-SCAFFOLDS ENHANCES DRUG METABOLIC ENZYME ACTIVITY IN RESPONSE TO PHYSIOLOGICALLY RELEVANT MICROENVIRONMENTS

5.1 Introduction

Current cell-based assays cannot accurately predict drug-induced liver injury or hepatotoxicity in patients—two factors which account for a significant number of late-stage drug failures.[1,2] Preclinical assays often employ primary human hepatocytes (PHHs) and cell lines presenting hepatocyte-like characteristics, however, these cells do not maintain the characteristics and metabolic activity of hepatocytes in vivo. One plausible reason for this failure is the monolayer culture format, which are commonly relied on due to their ease of setup, maintenance, and analysis, but lack many aspects of the tissue microenvironment. Microenvironmental aspects include tissue structure defined by the arrangement of multiple cell types, extracellular matrix organization, and extracellular components. The extracellular components include soluble factors that influence cellular health and behavior, including signaling molecules, oxygen and nutrients, and excreted waste products. The tissue microenvironment has profound effects on cellular function, although it is not clear which of these components are most important for generating liver-like conditions and responses in vitro.

In Chapter 3 we evaluated the effects of both oxygen concentration and the presence of signaling molecules in the Wnt pathway on enzyme activity and transcriptional regulation of HepaRG cells in a monolayer format. Specifically, we compared cells cultured under standard conditions (21% O_2) to oxygen concentrations representative of the periportal (PP) and

perivenous (PV) regions of the liver. These studies were guided by extensive studies of in vivo pathway regulation and preferential distribution of liver-specific activities in hepatocytes.[3,4] While the phenomena of zonation is known to occur, the underlying microenvironmental cues that generate this patterning is unknown. This initial work focused on oxygen, as there is a substantial difference of oxygen supplies in the PV and PP regions. Furthermore, oxygen is a key regulator of many cellular processes, not only through hypoxia regulated genes but also through its influence on ATP-generating processes and mitochondrial stress.

The datasets from our initial studies confirm that phycological factors, including oxygen and morphogens, play an important role in modulating the basal hepatic function of hepatoma HepG2 line and differentiated HepaRG cells. These results also highlight the importance of considering oxygen concentrations when preparing in vitro liver model assays, as cytochrome P450 (CYP) enzyme activity and differences in transcriptional regulation of these enzymes in the PV and PP culture conditions aligned with zonation. Discrepancies in activity of conjugating enzymes in the sulfotransferase (SULT) and uridine 5'-diphospho-glucuronosyltransferase (UGT) family suggest further culture parameters must be considered.

In this chapter, we expand on this preliminary study to assess the effect of PV and PP oxygen tensions as well as Wnt and Rspondin in culture methods that include a 3D collagen matrix. Specifically, we compared liver-specific function, enzymatic activity, and transcriptional regulation across HepaRG cells cultured as monolayers on collagen slabs and with two different paper-based cell culture formats: the cell-laden method and the on top method. The cell-laden method consisted of a cell and collagen ECM mixture distributed throughout the entire thickness of the paper. The on top method is a combination of the collagen monolayer and paper-based cell-laden formats, where the volume of the paper is filled with a collagen ECM to form a paper

fiber and collagen-based scaffold and the cell are cultured as a monolayer on top of the paper-collagen scaffold.

The paper-based culture platform uses the stacked cellulose fibers of a sheet of paper to provide a three-dimensional (3D) space to support cells suspended in a hydrogel.[5] The paper fibers provide a pre-organized scaffold framework to support the cell-laden hydrogels, which provide the necessary ECM to mimic that aspect of the tissue microenvironment. This 3D environment offers increased cell-cell and cell-ECM interactions compared to monolayer cultures.[6] An additional benefit of the hydrogel is a nutrient distribution that matches the diffusion-limited regime observed in epithelial and stromal tissues. Such an environment is not capable of forming in monolayer cultures, where all cells are exposed to a uniform concentration of nutrients and oxygen[7,8].

Previous studies found that placing PHHs in an extracellular rich environment, such as a collagen sandwich, allows the cells to maintain a differentiated and active state that is maintained much longer than those in 2D cultures.[9,10] The inclusion of a 3D environment results in the ability to better predict hepatotoxicity. Common 3D liver model methods include spheroid and organoid cultures.[11] Higuchi *et al*. showed that HepaRG spheroids have a 2-fold higher secretion of albumin and a 1.5-fold increase in CYP3A4 activity than with monolayer formats.[12] The improved predictive nature of spheroids is attributed to the biocomplexity and pericellular interactions formed in these multicellular aggregates.[6,13–16] However, the interpretation of the effect of the cellular microenvironment can become more challenging because microenvironmental influences on cellular behavior require histological slicing. The overlapping gradients of oxygen, nutrients, and soluble factors that extend across these structures also make it difficult to probe microenvironment-cellular function relationships—individually or in concert.[17]

The paper-based culture platform overcomes many of the limitations of spheroids: By simply stacking cell-containing sheets, paper-based cultures enable for a rapid, modular assembly of thick, tissue-like structures. The modularity of this platform also grants the ability to generate defined extracellular environments through controlled composition of the stacked structures, which can also include the combination with luminescent sensors. Furthermore, the ability to separate the cell populations by simply peeling apart the layers provides a means to evaluate live cells as a function of extracellular environment without the need for fixation.

This platform was first described by Whitesides and further developed in our laboratory.[5,18] We show in Chapter 2 that using paper scaffold to culture HepG2 cells prevented masses of cells from forming, allowing us to better assess the access of the cells accessibility to nutrients. We also showed that the cellular distribution around the paper fibers and the distribution of nutrients throughout the scaffold via capillary action through the paper fibers,[14–16] are promising features that support hepatocyte-specific function.

In the current study we exposed HepaRG cells in either monolayers, atop collagen slabs in paper scaffolds, or suspended in collagen within paper scaffolds to different culture conditions. A standard culture condition of standard media and atmospheric oxygen (std); a PP conditions of standard culture medium and PP oxygen concentrations (11% O_2 tension); or a PV condition with culture medium containing Wnt and Rspondin and PV oxygen concentrations (5% O_2 tension). Urea synthesis, CYP activity, and transcriptional regulation were compared between the three culture methods and across the three microenvironmental conditions. We noted that the urea synthesis across the microenvironmental culture conditions was equivalent, meaning the cultured conditions did not affect cell health. The standard condition microenvironment resulted in the highest metabolic enzyme activity. Maximum enzyme activity was culture format-

dependent, with the highest activity measured in the monolayer or laden format. In vivo-like zonation trends for CYP activity and transcript were measured between the PP and PV conditions paper-based culture methods and showed further enhanced activity and transcriptional distribution between the PP and PV microenvironment.

5.2 Materials and methods

5.2.1 Chemicals

All chemicals and reagents were used as received unless otherwise specified. All cell culture medium and supplements were purchased from Gibco, except for those used in the maintenance of the HepaRG cell line (Lonza). Chlorzoxazone, dextromethorphan (hydrobromide hydrate), (S)-mephenytoin, midazolam, and testosterone were purchased from Cayman Chemical Company. Dimethyl sulfoxide and 7-hydroxycoumarin were purchased from Fisher Scientific. Collagen I (rat tail) was purchased from Enzo Life Sciences. Phenacetin and sodium hydroxide (NaOH) were purchased from Millipore Sigma. The CellTiter-Glo 2.0 (CTG) reagent was purchased from Promega.

5.2.2 Preparation of paper scaffold

Cells were cultured in paper scaffolds, whose preparation and sterilization was detailed previously by our lab.[22,23] Briefly, sheets of Whatman 105 lens paper were patterned with wax borders using a Xerox ColorQube 8570 printer. Each scaffold was 18 mm in diameter and contained a 4 mm wax border, which defined the cell culture region (10 mm in diameter). The wax border also ensured the scaffolds remained at the air-medium interfaces throughout the duration of the culture. Once both sides of the paper were wax patterned, it was baked at 99 ^{o}C

for 15 min. Prior to use, the individual paper scaffolds were cut out and sterilized under UV light for one hour. Each scaffold fit into the well of a standard 6-well plate.

5.2.3 LWRN cell culture and secretion

Both the L and L-WRN cell lines were purchased from the American Type Culture Collection (ATCC). The cell lines were maintained as monolayers at 20% O_2, 37 ºC, and 5% CO_2 in Dulbecco's Modified Eagle's Medium (DMEM) medium supplemented with 10% FBS, 0.5 mg/mL G-418, and 0.5 mg/mL hygromycin B. This maintenance medium was exchanged every 2-3 days and the cells were passed at 80% confluency with TrypLE, using standard procedures.

Conditioned medium was collected following the protocol recommended by ATCC. Each cell type was maintained in a T150 flask with DMEM medium supplemented with 10% FBS. The cells were washed with 1X PBS, 25 mL of fresh medium added to flask to the flask, and the medium exchanged every 24 hours. The conditioned medium was collected, centrifuged at 1000 xg for 5 min, the supernatant decanted, and stored at 4 ºC until processed further. Medium collected from days 1 – 4 and 5 – 8 were pooled, steri-filtered (0.22 μm), and stored at -80°C.

5.2.4 HepaRG cell culture

Differentiated NoSpin HepaRG Cryopreserved Cells were obtained from Lonza Bioscience and cultured as monolayers on collagen slabs, monolayers on sheets of collagen-laden paper, or as suspensions in collagen that were seeded into the paper sheets. The collagen slabs were prepared by neutralizing a solution of acidified collagen I, with NaOH and phosphate-buffered saline (PBS). The neutralized collagen solution (2 mg/mL) was added to standard 12-

well cell culture plates and incubated overnight at 37°C (263 μg of accessible collagen/cm^2). Collagen slabs were washed once with 1x PBS prior to cell seeding. The paper scaffolds were prepared by filling the cell containing region with a uniform layer of collagen (25 μL collagen at 2 mg/mL). Preformed collagen slabs in the paper were incubated overnight at 37°C in 1x PBS, prior to cell seeding. Cell-laden scaffolds seeded by adding cell-laden collagen into an empty paper scaffold; the HepaRG cells were suspended in 2 mg/mL collagen for a final density of 80,000 cells/μL ($1.81x10^8$ cell/cm^3) and each scaffold was seeded with 12.5 μL of gel. A total of 1 million HepaRG cells were seeded to all three culture methods.

Once seeded, the cells were maintained for 24 hours in HepaRG medium containing basal medium supplement, a thawing and plating supplement, and 1% penicillin–streptomycin. After a medium exchange, the cells were maintained in HepaRG medium containing basal medium supplement, a maintenance and metabolism supplement, and 1% penicillin–streptomycin. Medium was exchanged every two to three days. On day 6, the cells were exposed to one of three experimental conditions for 48 hours: standard culture conditions (std), PP conditions, or PV conditions. At std conditions cells were incubated at 37°C, atmospheric oxygen and 5% CO_2. At PP conditions cells were incubated at 37°C, 11% O_2 and 5% CO_2. At PV conditions cells were incubated at 37°C, 11% O_2 and 5% CO_2 in a 1:1 ratio of medium and L-WRN conditioned medium. The oxygen tensions were regulated in a custom-build hypoxia chamber, as detailed previously.[24]

5.2.5 Evaluation of metabolic enzyme activity

Drug metabolizing enzyme activity was evaluated with eight different substrates (**Table 5.1**).[25,26] The substrates were dissolved in DMSO at 1000X working concentration. The HepaRG

cells were exposed to culture medium containing the substrates and basal medium supplement for 2 hours, after which the medium was collected and stored at -20°C until analysis. The cell medium, and a matrix blank of just culture medium, was mixed with cold acetonitrile containing known concentrations of isotopically labeled standards (**Table 5.2**) for each enzyme product at a 1:10 (v/v) ratio. After a 15 min incubation at -20°C, the precipitated protein was pelleted at 12,000 xg for 15 min at 4°C, the supernatant collected, and the solvent removed in vacuo. The residual solid was resuspended in 100 μL of HPLC-grade water (Optima) and separated on a Waters Acquity UPLC equipped with a BEH C18 column (2.1 x 50 mm, 1.7 μm) using a binary solvent system of (A) 0.5% formic acid (v/v) in water and (B) 0.5% formic acid (v/v) in acetonitrile. The total run time of each separation was nine min, using the following gradient profile at a 0.3 mL/min flow rate: 10% B for one min; a linear gradient to 70% B over 5 min; 95% B for one min; 10% B for two min to wash and re-equilibrate the column. We did not observe carry over between sample injection and solvent blanks were injected every 10 samples.

Metabolites were detected and quantified with multiple-reaction monitoring on a Thermo TSQ Vantage triple quadrupole instrument equipped with a heated electrospray ionization (HESI) source set to 300 °C. Two transitions of each product were monitored to confirm its identity. The declustering voltage for each product was optimized by direct infusion of neat solutions (10 μM) in Optima water. Each product's transition was optimized for collision energy and reported in **Table 5.1**. Other parameters used for all analyses were: spray voltage (4800 V), vaporization temperature (300 °C), sheath gas pressure (50 psi), aux gas pressure (15 psi), capillary temperature (300 °C), and S-lens RF amplitude (120 V). Nitrogen gas was used for sheath, aux, and collision gas. Data were collected and processed with the Xcalibur

software package (Thermo Scientific). The peak area for each metabolite was averaged across three technical replicates; we report the ratio of the average peak area of treatment to the average peak area of vehicle.

5.2.6 Urea production

After collecting the medium for the CYP activity assay, the urea production of the cells was analyzed. Prior to collecting urea, each well was washed once with 1X PBS before incubating in fresh HepaRG medium containing basal supplement for 1 hour. The medium was collected, and urea concentration quantified with the QuantiChrom Urea Assay (Kit-DIUR-100, BioAssay Systems) according to the manufacturer's protocol. Equal volume of reagent and medium was added to each well and the plate was mixed for 50 minutes at room temperature. The samples were measured on a SpectraMax i3x Microplate Reader at an optical density of 430 nm. Samples were compared to a seven-point calibration curve, which was prepared on each plate to account for plate-to-plate variation.

5.2.7 Transcript Expression Quantification with RT-qPCR

After collecting culture medium for CYP activity and urea measurements, the cells were washed and lysed using a TRIzol Plus RNA purification kit (ThermoFisher), according to the manufacturer's suggested protocol. The TRIzol reagent was added directly to the cells and agitated for 10 minutes prior to RNA isolation. Reverse Transcriptase PCR was performed immediately after RNA isolation using the RNA isolation with a High-Capacity cDNA Reverse Transcription Kit (ThermoFisher) in an Eppendorf Master Cycler.

Table 5.3 lists the primer pair sequences, optimal concentration, and reaction efficiency (90-110%) of each gene of interest. Amplification reactions were performed with PowerUp SYBR Master Mix (ThermoFisher), in a 384-well plate, on a QuantStudio 6 Flex Real-Time PCR system. Each sample was measured in triplicate, using the following program: 95 °C for 60 sec, 40 cycles of 95 °C for 2 sec, and 60 °C for 30 sec. Each transcript was quantified using the ΔΔCt method against 18sRNA.[27] A fold-change of greater than 2.0 was considered significant.

5.2.8 Statistical Analysis

Cell-related datasets are reported as the average and standard error of the mean (SEM) of at least two separate vials of differentiated cells, with at least two technical replicates per vial. All data were analyzed with GraphPad Prism 7. Statistically significant differences correspond to a p-value of ≤ 0.05. To assess CYP activity, peak area of each metabolite product was normalized to a particular experiment condition. A normalized activity greater than 1.25 or less than 0.8 was considered significant since the LC-MS/MS peak area is highly reproducible and 1.25/0.8 is statistically significantly outside of normal variability range based on previous data (see Chapter 3). For transcriptional regulation, a fold-change of greater than 2.0 was considered significant.

5.3 Results and Discussion

Figure 5.1 summarizes the experimental workflow followed to compare liver-specific function, metabolic enzyme activity, and transcriptional regulation between HepaRG cells cultured on different collagen scaffolds.

5.3.1 HepaRG urea secretion is unaffected by culture microenvironment but influenced by culture method

HepaRG cells were seeded and maintained under standard culture conditions for 6 days then exposed to experimental conditions for 2 days before urea secretion was assessed (**Figure 5.2**). Urea synthesis and secretion is a marker for liver specific function and cell health. Under standard culture conditions, HepaRG cells cultured as a monolayer on a collagen slab produced 0.020 milligrams of urea per 1 mL of culture medium per hour (mg/mL/h/10^6 cells, or 0.71 mM/h/10^6 cells). Monolayers of HepaRG cells placed on top a collagen-laden paper scaffolds, termed the *on top* format, produced 0.013 mg/mL/h/10^6 cells (or 0.46 mM/h/10^6 cells. Cells suspended in collagen and seeded directly into the paper scaffolds, termed *laden* format, produced 0.011 mg/mL/h/10^6 cells (or 0.39 mM/h/10^6 cells). The amounts of urea secreted by the HepaRG cells in the monolayer, on top, and laden formats were equivalent (**Figure 5.2a**). When exposed to PP conditions, the HepaRG cells in each format secreted statistically equivalent amounts of urea. The PP conditioned HepaRG cells also secreted statistically equivalent amounts of urea as the standard conditioned HepaRG cells. Urea secretion was culture format-dependent when cultured in the PV condition, with both the on top and laden secreting significantly lower amounts of urea than the monolayer cultures: a 0.51- and 0.56-fold decrease, respectively (**Figure 5.2b**). Compared to standard conditions, the PV conditioned HepaRGs secreted statistically equivalent amounts of urea.

A comparison of urea secretion as a function of culture conditions and format highlight that there is no single setup that significantly improves HepaRG cell health. These results also highlight that the paper scaffolds do not reproducibly hinder cellular health and thus these 3D cultures could be used for drug metabolism and hepatotoxicity studies. We are not aware of other studies that compared hepatocyte-like cell health as a function of culture conditions and format,

although, the work by Janani and Mandal highlight that the way cells interact with the ECM in a 3D culture can have profound effects on urea secretion.[28] Primary rat neonatal hepatocytes cultured on liver ECM-coated silk scaffolds for 10 days showed that urea synthesis increased when scaffolds contained large pore sizes (70-80 μm); a high porosity (90% void volume), resulting in a significantly higher swelling ratio. Their hypothesis was that scaffolds with large pore sizes promoted cellular aggregates to form from a rough surface architecture, thus demonstrating an increased amount of urea synthesis. Li *et al*. found similar results in which HepaRG cells secreted more urea in a highly packed spheroid. They compared urea secretion of HepaRG cells cultured as sandwich cultures and spheroids and found that spheroids secreted on average 23.5-fold more urea (2 mg/mL/10^6 HepaRG cells of urea secreted by spheroids).[29]

5.3.2 The trends in drug metabolizing enzyme activity of HepaRG cells is culture method dependent

Previous characterization of cryo-preserved HepaRG cells cultured on commercial collagen coated plates found that the basal-level activity of drug metabolizing enzymes varied over a 22-day period.[30] The authors hypothesized these dynamic changes were due to de- and redifferentiation of the cells—a consequence of a high concentration of DMSO in the culture medium. To determine if placing the HepaRG in the 3D environment afforded by the laden culture stabilized their drug metabolizing activity, we quantified the activity of 6 CYPs and the SULT and UGT families over a 24-day period. In this experimental setup, enzyme activity was measured every 4-5 days using an 8-in-1 cocktail of substrates, whose metabolites were quantified against isotopically labeled internal standards with LC-MS/MS using multiple-reaction monitoring. We compared HepaRG cell stability and activity as a function of time between traditional monolayer cultures and the 3D paper scaffold culture methods; ensuring that

the enzyme activity of the cells were reproducible and consistent between setups. The on top format served to bridge the gap between monolayers and laden culture method, assessing if the paper-fibers altered liver-specific function.

In **Figure 5.3**, we measured the enzyme activity of the HepaRG cells cultured as monolayers on collagen; maximal enzyme activity is summarized in **Table 5.4**. The metabolic activity is relatively unchanged during the first 4 days after plating. From days 4 to 11, the enzyme activity of cells increased, with significant increases of CYP1A2, 2C19, 2D6 and 3A4 activity measured. After day 11, activity decreased until day 24. The measured increase in CYP activity is similar to the trends found by Jackson *et al*, who observed increased CYP and Phase II enzyme activity until about day 10, after which enzyme activity leveled off or slightly decreased until day 22. They measured the largest changes in CYP2A6, 2B6, and 2C9 activity and smaller changes in CYP1A2, 2C19 and 3A4,[30] which is similar to our measurements in which some CYPs showed large changes in activity while other did not vary over time. One notable difference between our measurements and Jackson's is that we observed a decrease in CYP activity after day 10 back down to activity levels observed on day 1. These data are similar to the results obtained in Chapter 3 and 4, which show that HepaRG cultures prepared as monolayers on ECM-coated plates or slabs can maintain metabolic activity until day 11, after which they show a rapid decline in activity.

The trends in enzyme activity for the laden format indicates most CYPs activity was unchanged over the first four days, except for CYP1A2 which increased in activity. From day 4 to 11 the enzyme activity of CYP1A2, 2B6, 2C19, 2D6, and 3A4 all significantly increased and maintained increased activity until day 15—a notable difference from the monolayer culture format. From days 15 to 24, enzyme activity decreased significantly below the activity measured

on day 1. The increased enzymatic activity from day 7 until day 15, which is different from the monolayer format, suggests that the HepaRG cell laden throughout the paper-scaffolds are maintaining elevated enzymatic activity longer, enabling longer culture times with consistent enzyme activity.

The on top format followed similar trends to the laden and monolayer format; during the first 4 days, CYP1A2 and CYP2C19 demonstrated increased activity similar to the laden culture. Also, on day 4 the UGT and SULT enzyme activity was significantly decreased—the Phase II activity maintained this trend over all 24 days. From days 4 to 7 the enzyme activity of CYP1A2, 2B6, 2C19, and 3A4 increased and was followed by a declining activity after day 7 until day 24, during which the enzyme activity was significantly decreased as compared to the day 1 activity.

The on top culture method's activity trends are unique from both the monolayer and laden format. In the on top format significant increases and decreases in enzyme activity on day 4 is similar to the laden culture method suggesting that the paper-scaffold cultures are enabling changes in enzymatic regulation earlier than the monolayer. Also, the peak in metabolic activity on day 7 in the on top method, rather than day 11 in the monolayer, indicates the HepaRGs can adapt to the environment quicker on the paper scaffolds. This could be a result of the paper-scaffolds cultures to float at the air-medium interface, minimizing the distance oxygen needs to travel. Also, the hydrophilic cellulose paper fibers act as highways for nutrients to be delivered throughout the entire culture providing more in vivo like nutrient delivery. The enzyme activity in the on top culture method, however, does quickly decease after day 7 which is constant with the monolayer format.

These data are similar with the results obtained in Chapter 3 and 4, that HepaRG cultures prepared as monolayers on ECM-coated plates or slabs can maintain metabolic activity until day

11, after which is a rapid decline in activity. However, with the cell-laden paper-based culture methods, the trends in metabolic enzyme activity over the 24-day culture period appears to be culture-method dependent because of the prolonged increase in activity.

5.3.3 HepaRG cells basal metabolic activity is influenced by the culture method

Based on the data obtained from the 24-day culture experiment, we quantified the enzyme activity and transcriptional regulation after 6 days in standard culture conditions followed by 48 hours at liver specific culture condition because all culture formats around day 8 exhibited increasing trends in enzyme activity. We were confident that the HepaRG cells, regardless of culture method, needed time to increase activity of the CYPs and Phase II enzymes- allowing the cells to adjust to the culture format prior to introduction to a physiological microenvironment. The 48 hours in the physiological conditions enabled further enzyme activity and transcript modulation as a result of the microenvironment.

Metabolic enzyme activity (**Figure 5.4**) and transcript (**Figure 5.5b**) was normalized to the cell monolayers to assess the effect of culture method independent of the cultures microenvironment. Comparing cell culture methods between the standard condition and physiological microenvironments, we measured a decrease in activity of: CYP1A2, 2D6, 3A4, SULT, and UGT for the on top culture method and a decreased activity of CYP1A2, 2B6, 2C19, 2D6, 3A4, SULT, and UGT in the laden culture method. However, transcriptional regulation suggests the opposite trends in which *CYP1A2* is upregulated 29.86- and 13.61-fold in the on top and laden culture, respectively. The *CYP3A4* transcript was unaffected by culture format. Furthermore, *CYP2E1* is significantly upregulated in the on top and laden culture, but on the activity level CYP2E1 is unchanged in the different culture format. The only matching trends

between activity and transcript was UGT activity and *UGT2B4* transcript in which there is decreased activity and transcriptional downregulation in the on top format; in the laden format there was no effect on activity and a significant transcriptional upregulation.

Transcriptional regulation of transporters and cell polarization markers are significantly different based on culture format. Two markers for hepatocyte differentiation are cytokeratin-19 (CK-19, *KRT19*) and albumin. CK-19 is a common marker for biliary-like HepaRG cells and CK-19 has been observed in hepatocytes around the bile canaculi.[32] Albumin is a protein secreted by normal functioning hepatocytes—an elevated albumin transcript and albumin production is a traditional marker for hepatic-like function.[33] On the transcript level, the paper-based culture methods have upregulated *KRT19* in all culture conditions and an upregulation of *Alb* transcript in the PP and PV conditioned cultures as compared to the monolayer cultures. The upregulation of biliary-like and hepatocyte-like differentiation markers in the paper-based culture methods suggest the paper scaffolds help maintain HepaRG differentiation. Leite and colleagues observed increased differentiation of HepaRG cells cultured as small spheroids in a spinner-bioreactor.[34] While Janani and Mandal cultured rat hepatocytes on custom silk fiber hydrogels, one surface was significantly more porous than the others resulting in a softer, rougher surface for cells, when the fibers were hydrated. They observed increased CK-19 positive rat hepatocytes on the rougher surface and concluded that the cellular aggregation in on the rough surface contributed to hepatocyte differentiation.[28]

Transporters and tight-junction proteins are good markers cell polarization. At the transcript level, we measured an upregulation of multiple transporters, *ABCB1, ABCC2, ABCC3, SLCO1B1,* and *SLCO10A1* from monolayer to the paper-based culture methods. MRP2 (gene *ABCC2)* is a well-studied transporter and has been shown to have increased activity as HepaRG

cells differentiate and polarize.[35] *ABCC2*, was upregulated by 7.26- and 37.59-fold under standard conditions in the on top and laden format, respectively. Under PP conditions, there was an 8.65-fold increase in the on top method and no effect in the laden method; for the PV conditions, *ABCC2* was upregulated 3.92- and 428.7-fold when cultured on top of the paper scaffold and laden, respectively. Török and colleagues compared transcriptional regulation of *ABCC2* in HepaRG cells, cultured between two layers of Matrigel, to mature hepatocytes differentiated from human embryonic stem cells (HUES9); the differentiated HUES9 are a baseline for differentiated and polarized hepatocytes. The HepaRG had 43-fold increase in *ABCC2* and various other upregulated transporter genes,[36] and concluded that the higher expression of *ABCC2* in HepaRG is indicative hepatocyte polarization. We can conclude that the HepaRG cells in the paper-based cultures have better polarization than the monolayers potentially as a result of the paper-fibers acting as a sinusoid for nutrients.

The paper-based culture methods provide a benefit to the overall function of HepaRG cells as indicated by modulating the influence of microenvironmental factors on metabolic enzyme activity and increasing the transcript of various transporters potentially indicating enhanced cell polarizability and differentiation. The paper fibers themselves and the distribution of HepaRG cells around the fibers may facilitate radial nutrient delivery to the hepatocytes similar to the in vivo liver sinusoid. Integration of in vivo like characteristics such as nutrient distribution via culture method, and inclusion of physiologically relevant microenvironments may benefit the overall responsiveness of HepaRG cells to their microenvironment.

5.3.4 The maximum metabolic activity of HepaRG cells is observed under standard culture conditions

We quantified the enzyme activity and transcriptional regulation after 6 days in culture followed by 48 hours at specific culture condition. Metabolic enzyme activity (**Figure 5.6**) and transcriptional regulation (**Figure 5.5a**) of HepaRG was normalized to the standard condition microenvironment to assess the effect of cultured microenvironment independent of the culture method. As monolayers HepaRG cells cultured at both PP and PV conditions has decreased CYP1A2, 2B6, 2C19, 2D6, and 3A4 enzyme activity as compared to the standard conditions. The activity of UGT and SULT were decreased at PP conditions but unchanged at the PV conditions. The activity decrease from the standard condition to the physiological condition is similar to the results obtained in Chapter 3 in which the PP and PV monolayer conditions had decreased metabolic enzyme activity. At the transcript level, these activity decreases are reflected as a downregulation of the CYP genes in the monolayer cultures; at both PP and PV microenvironmental conditions there is significant downregulation of the *CYP1A2*, *CYP2C9*, *CYP3A4,* and *UGT2B4* transcript much like activity decrease; the one exception is that *SULT1A2* was significantly upregulated under the PP condition, but SULT activity was decreased.

In the on top culture format, we measured decreased CYP1A2, 2B6, 2C19, 2D6, 3A4, UGT and SULT enzyme activity in the PP conditions as compared to the standard conditions. For the PV conditions we measured decreased CYP2B6, 2C19, 2D6, and 3A4 enzyme activity, and increased CYP2E1 activity. At the transcript level, these activity decreases are reflected as a downregulation of the CYP genes in the PP cultures as *CYP1A2, CYP2C9*, and *CYP3A4* are significant downregulated. However, the transcriptional regulation of the PV conditions do not match the activity trends; *CYP2C9* and *CYP2E1* are both downregulated, *CYP1A2* and *CYP3A4* are unchanged.

In the laden culture format, we measured decreased CYP1A2, 2B6, 2D6, 3A4, UGT and SULT enzyme activity in the PP conditions as compared to the standard conditions. For the PV conditions we no enzyme decreased in activity while CYP1A2, UGT and SULT measured increased activity as compared to the standard condition. At the transcript level, the decreased activity trend is reflected as a downregulation of the CYP genes in the PP cultures as *CYP1A2, CYP2C9*, *CYP2E1* and *CYP3A4*. However, the transcriptional regulation for CYPs and SULT in the PV conditions unchanged.

Overall, the decreased enzyme activity trends in the paper-based cultures is predominantly due to the PP and PV microenvironments. Yet, the magnitude of decrease observed between the monolayer to the laden culture formats are different, specifically highlighted by CYP1A2, and CYP2C19. The culture methods (monolayer vs laden) modulate the effect the PP and PV microenvironments have on the HepaRG cells. CYP1A2 activity decreased by 0.02- and 0.09-fold under the PP and PV conditions, respectively, when cultured as a monolayer; However, in the laden format, CYP1A2 activity decrease was 0.11- and 1.53-fold change in the PP and PV conditions, respectively. For CYP2C19, in the monolayer format, activity decreased by 0.38- and 0.67-fold at the PP and PV conditions, respectively; in the laden format, activity decreased by 0.92- and 1.20-fold change under the PP and PV conditions, respectively.

The reduced effect of the cultured microenvironment between the monolayer, on top and laden culture method holds true for both transcriptional regulation and enzyme activity. The nonuniform downregulation of enzyme activity between the collagen monolayer and paper-based culture methods could be due to the path by which oxygen and other nutrients travel from bulk medium to the cell. In the monolayers, all the cells are at the bottom of the well-plate, so cells

take oxygen and nutrients directly from the media around themselves— nutrients are refreshed via diffusion from bulk medium. In the paper-based cultures, the cells take nutrients and oxygen from the various parts of the scaffold (paper fibers, collagen ECM, or medium) which is then replenished via diffusion and distributed via capillary action of the paper fibers. The microenvironmental impact on the HepaRG cells is felt in both the monolayer and paper-based cultured, but the magnitude of these effects is influenced by the culture method.

The enzyme activity data overall points to the standard culture condition and monolayer method yielding the highest overall enzymatic activity. But highest enzyme activity in a non-physiologically relevant environment but may not be the same as in vivo activity. Rather, making comparisons between physiologically relevant culture conditions in a head-to head comparison to observe trends in environmental changes is more important.

5.3.5 Basal metabolic activity of the HepaRG cells follows liver zonation trends when comparing physiological conditions

We quantified the enzyme activity and transcriptional regulation after 6 days in culture followed by 48 hours at specific culture condition. Metabolic enzyme activity (**Figure 5.7**) and transcript (**Figure 5.8**) of all three culture methods in the PP and PV conditions was measured. Measurements were normalized to the monolayer cultured at the PP microenvironmental conditions to assess the effect of integrating physiologically relevant culture formats.

The zonal distribution of CYPs and Phase II enzyme activity in the liver is the CYPs and UGT activity is higher in the perivenous region while SULT activity is higher in the periportal region. We observed these zonally distributed trends of the measured enzymatic activity for CYPs and UGT between the PP and PV microenvironment; however, we did not observe zonal trends in SULT activity. Comparison of the PV monolayer to the PP monolayer, we measured

significant increased activity of the CYP1A2, 2B6, 2C19, 2D6, and 3A4 with midazolam, SULT and UGT; the largest increase in activity in the PV monolayer was CYP1A2 at 4.74-fold, CYP2D6 at 22.07-fold, and CYP3A4 at 8.56-fold. The increased activity in the PV microenvironment follows the same trends observed in Chapter 3.

The paper-based cultures enhance metabolic activity and responsiveness to the microenvironment. CYP1A2 and 2D6 activity is modulated in the paper-scaffold cultures indicated by the magnitude of the enzymatic activity increase between the monolayer and laden culture method all within the PP microenvironment: CYP1A2 activity increases by 2.45-fold when comparing the PP monolayer to the PP laden format. The modulated activity effect by the culture method also holds true when comparing the PV culture conditions to the PP monolayer: CYP1A2 activity increases 4.74-fold in PV monolayer, 15.84-fold in PV on top, and 35.40-fold in PV laded. The increased activity of CYP2C19, 2D6, 3A4 with midazolam, and UGT between the PP and PV microenvironment is independent of the culture method indicated by a similar activity increase across the monolayer, on top, and laden culture formats.

At the transcript level, comparisons of the PP and PV monolayer formats show *CYP1A2* and *SULT2A1* transcripts were upregulated by 2.67, and 8.45-fold, respectively while *CYP2C9, CYP2E1,* and *UGT2B4* were downregulated by 0.29, 0.001, and 0.001-fold, respectively. The discrepancy between the PP and PV monolayer transcriptional regulation and enzymatic activity suggests there are alternative regulatory pathways promoting increased enzymatic activity in the absence of increased transcript. Within the paper-based culture methods, *CYP1A2, CYP2C9, CYP3A4,* and *SULT2A1* were significantly upregulated at both PP and PV conditions suggesting that the paper scaffold is contributing to transcriptional regulation. Furthermore, the PV conditioned paper-based culture methods have significantly more transcriptional upregulation

than the PP conditioned cells; cells in the on top method for the PP microenvironment has 10.79, 1.70, 2.75, and 4.02-fold increases for *CYP1A2, CYP2C9, CYP3A4,* and *SULT2A1*, respectively. Cell in the on top format within the PV microenvironment we measured a 939.59, 38.00, 579.93, and 582.4- fold increase for *CYP1A2, CYP2C9, CYP3A4,* and *SULT2A1*, respectively. The laden formats followed the same trends in upregulation between the PP and PV cultured microenvironments.

The enzymatic activity and transcriptional regulation between the PP and PV culture conditions as well as the enhancement effect by the paper-based culture format suggests that the inclusion of physiological conditions- both microenvironmental and culture method— into HepaRG cell culture promotes zonation-like patterning of metabolic enzymes. The zonation-like patterning observed between the PP and PV microenvironmental culture conditions is more important than the magnitude of enzymatic activity because the inclusion of zonation trends means that the HepaRG cells are behaving more like their in vivo counterparts.

5.4 Conclusions and future work

This study compared the effect of two physiological conditions— 3D culture method and culture microenvironment— on the metabolic enzyme activity and transcriptional regulation of HepaRG cells. We cultured the HepaRG cells as monolayers on collagen slabs, on top of collagen coated paper scaffolds and within the paper-scaffold with cell-laden collagen; HepaRG cells in these three methods were cultured under standard culture conditions, and physiological conditions representative of the periportal and perivenous region of the liver lobule. This design provided for superior control over the extracellular environment, allowed for comparisons to zonal characteristics observed in vivo. Single-region modeling, rather than an entire gradient

allowed us to culture large numbers of cells in a single experiment enabling viability, health, metabolic activity, and transcript profile measurements from the same set of cells; for comparison spheroid cultures accommodate 1000- 20,000 cells per spheroid.[37]

The enzyme activity and transcriptional regulation of drug metabolizing enzymes was significantly decreased and downregulated, respectively, when comparing standard culture condition HepaRG cells to those cultured in the PP and PV microenvironments. The decrease in metabolic enzyme activity is likely a result of physiological oxygen tension as it is less than the standard 21% oxygen tension- the enzymatic activity of CYP1A and 2B families decrease by about 0.5-fold at when oxygen tension is reduced from 6.5 ppm O_2 at atmospheric levels to 3.3 ppm O_2.[38]

The inclusion of paper-based culture methods significantly influenced time-dependent and basal drug metabolizing enzyme activity. The laden paper-based scaffold culture extended the HepaRG cells stable enzyme activity by four days as compared to the monolayer and on top culture formats; this enabling HepaRGs in the laden format to be cultured for extended periods of time with stable enzymatic activity. The maximal basal enzyme activity was measured in the standard condition monolayers compared to the paper-based culture formats, but the inclusion of the paper-based culture method did appear to modulate the responsiveness of HepaRG cells to the culture microenvironment. This indicates that the culture method is an important factor when modeling in vivo liver physiology. Furthermore, the paper-based culture methods have upregulated transporter transcripts, *KRT19,* and *Alb* all three of which indicate the HepaRG are maintaining differentiation and cellular polarization better than the monolayer culture format. Others have observed enhanced differentiation of HepaRG cells when cultured as spheroids.[12] We hypothesize that the culture method dictates nutrient delivery to the cells— monolayers are a

relatively static culture environment where cells take in nutrients from their surroundings and diffusion replenishes the nutrients. The paper-based culture is more dynamic in which the paper fibers help distribute nutrients throughout the culture which then diffuses into the collagen ECM and then the cells. The dynamic nutrient distribution the of the paper-based cultures allows the hepatocytes to better respond to microenvironmental changes suggesting that paper-based culture methods are an improvement to in vitro liver modeling.

Although the standard condition monolayer has the highest activity of metabolic enzymes as compared to the PP and PV conditions, enhanced metabolic activity is not as important as modeling zonation patterns and trends in vitro. When making direct comparisons between the HepaRG cells cultured at the PP and PV microenvironments, we observed increased metabolic activity in the PV conditioned cells for all the enzymes measured as well as upregulated metabolic enzyme transcripts in the PV conditioned cells. Furthermore, the laden culture format further enhanced increased in drug metabolizing enzyme activity and upregulation in transcript due to increased polarization and differentiation as compared to the monolayers. As a result, comparison between HepaRG cells cultured in paper scaffolds at PP and PV relevant conditions would provide relevant insights to in vivo zonation patterns.

Future works into physiological microenvironments should include other mutagens present in the liver, as well as nutrient gradients such as glucose. Furthermore, since the transcriptional regulation between the standard, PP and PV cultured microenvironment fails to match trends in enzymatic activity, other regulatory pathways such as post translational modifications and enzyme kinetics should be explored. Comparing these regulatory pathways to primary human hepatocytes or freshly isolated hepatocytes could help us better understand the

differentially regulated metabolic enzyme activity in the liver and connections to in vitro culture methods.

5.5 Figures and tables

Table 5.1. MS/MS Transition monitoring for each drug metabolizing enzyme product using the 8-in-1 cocktail.

Enzyme	Substrate	Final Concentration (µM)	Product	Declustering Voltage (V)	Ion Mode	Parent m/z	Product m/z	Collision Energy (eV)
CYP1A2	Phenacetin	100	Acetaminophen	6	Positive	152.2	110	15
						152.2	65.03	30
CYP2B6	Bupropion	50	Hydroxy bupropion	6	Positive	256.02	238.1	8
						256.02	130.1	47
CYP2C19	(*S*)-mephenytoin	100	4'-Hydroxymephenytoin	6	Negative	232.9	190.1	19
						232.9	161.0	25
CYP2D6	Dextromethorphan	100	Dextrorphan	4	Positive	258.04	157.1	36
						258.04	199.1	25
CYP2E1	Chlorzoxazone	15	6-Hydroxychlorzoxazone	2	Negative	184.0	120.1	22
						184.0	64.0	33
CYP3A4	Midazolam	5	1-Hydroxymidazolam	6	Positive	342.04	324.1	19
						342.04	168.1	36
CYP3A4	Testosterone	50	6-beta-Testosterone	8	Positive	305.2	269.2	13
						305.2	105.1	36
SULT	7-hydroxycoumarin	100	7-Hydroxycoumarin sulfate	6	Negative	240.7	161.0	20
						240.7	133.0	34
UGT	7-hydroxycoumarin	100	7-Hydroxycoumarin glucuronide	6	Negative	337.0	161.0	29
						337.0	175.0	13

Table 5.2 Concentration of isotopically labeled standards.

Isotopically labeled standard	Stock concentration	Concentration in ACN	Final concentration in sample
6-hydroxy chlorzoxazone d2	10 mM in DMSO	5 µM	0.05 µM
(+/-) hydroxybupropion d6	0.382 in ACN	0.191 µM	1.91 nM
(+/-) 4-hydroxymephenytoin d3	10 mM in DMSO	5 µM	0.05 µM
Dextrorphan d3	0.384 mM in MeOH	0.192 µM	1.92 nM
7-hydroxy coumarin-D5 sulfate potassium salt	10 mM in DMSO	5 µM	0.05 µM

Table 5.3 List of 22 genes evaluated in this study.

Gene Symbol	Protein Abbreviation	Main Function	Forward Primer (5' – 3')	Reverse Primer (5' – 3')	Efficiency (%)
18sRNA	18s rRNA	Ribosome	CGCCGCTAGAGGTGAAATTC	TTGGCAAATGCTTTCGCTC	107.5
CYP1A2	CYP1A2	Phase I Enzyme	CTTCGGACAGCACTTCCCTG	AGGGTTAGGCAGGTAGCGAA	103.9
CYP2C9	CYP2C9	Phase I Enzyme	TCCCTGACTTCTGTGCTACATG	ACTGGAGTGGTGTCAAGGTTC	113.9
CYP2E1	CYP2E1	Phase I Enzyme	TTGAAGCCTCTCGTTGACCC	CGTGGTGGGATACAGCCAA	109.9
CYP3A4	CYP3A4	Phase I Enzyme	TCACAAACCGGAGGCCTTTT	TGGTGAAGGTTGGAGACAGC	100.4
CYP8B1	CYP8B1	Phase I Enzyme	TGCACATGGACCCTGACATC	GTGTCAGGGTCCACCAACTC	91.9
SULT2A1	SULT2A1	Phase II Enzyme	TGAGGAGCTGAAACAGGACAC	AAGTCTTCAGCTTGGGCCAC	106.6
UGT2B4	UGT2B4	Phase II Enzyme	ACACATGAAGGCCAAGGGAG	GAACCAGGTGAGGTCGTGG	94.3
AHR	AhR	Transcription Factor	CTTCCAAGCGGCATAGAGAC	AGTTATCCTGGCCTCCGTTT	101.5
NR1I3	CaR	Transcription Factor	TGATCAGCTGCAAGAGGAGA	AGGCCTAGCAACTTCGCATA	102.6
NR1I2	PxR	Transcription Factor	CCAGGACATACACCCCTTTG	CTACCTGTGATGCCGAACAA	104.3
ABCB1	P-gp	Efflux Pump	GCCAAAGCCAAAATATCAGC	TTCCAATGTGTTCGGCATTA	93.6
ABCC2	MRP2	Transporter (Excretion)	TGAGCAAGTTTGAAACGCACAT	AGCTCTTCTCCTGCCGTCTCT	99.6
ABCC3	MRP3	Transporter (Excretion)	GTCCGCAGAATGGACTTGAT	TCACCACTTGGGGATCATTT	108.5
ABCG2	BCRP	Transporter (Excretion)	TGCAACATGTACTGGCGAAGA	TCTTCCACAAGCCCCAGG	101.5
SLOC1B1	OATP1B1	Transporter (Uptake)	GCCCAAGAGATGATGCTTGT	ATTGAGTGGAAACCCAGTGC	97.3
SLCO2B1	OATP2B1	Transporter (Uptake)	TGATTGGCTATGGGGCTATC	CATATCCTCAGGGCTGGTGT	106.5
SLC10A1	NTCP	Transporter (Uptake)	GGGACATGAACCTCAGCATT	CGTTTGGATTTGAGGACGAT	101.4
SLC22A1	OCT1	Transporter (Uptake)	TAATGGACCACATCGCTCAA	AGCCCCTGATAGAGCACAGA	104.5
ALB	Albumin	Globular Protein	TGAGCAGCTTGGAGAGTACA	GTTCAGGACCACGGATAGAT	124.1
KRT19	CK-19	Biliary-like/Progenitor Cell Marker	TTTGAGACGGAACAGGCTCT	AATCCACCTCCACACTGACC	100.8
TJP1	ZO-1	Tight-Junction	CGAGTTGCAATGGTTAACGGA	TCAGGATCAGGACGACTTACTGG	106.9

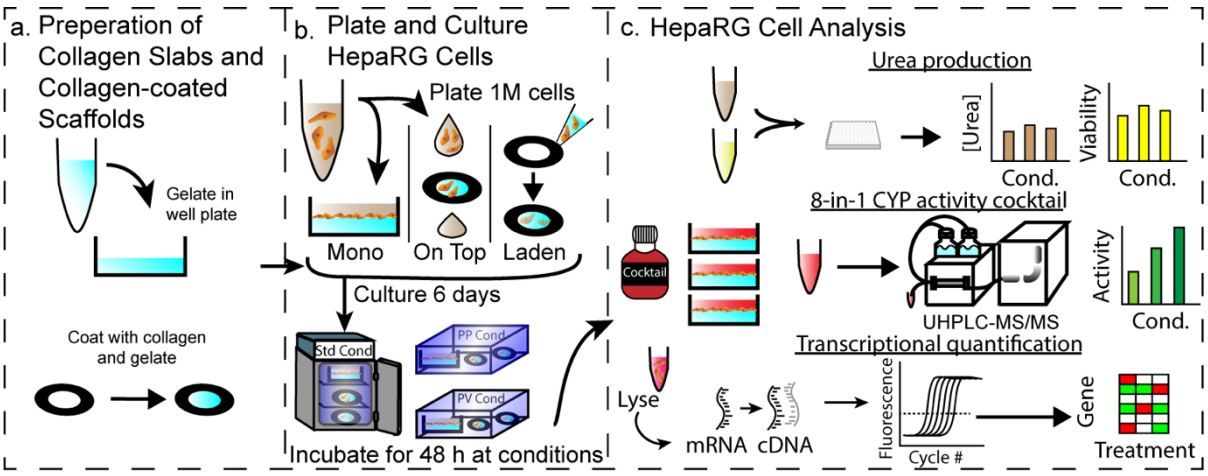

Figure 5.1. Experimental workflow comparing the responses of HepaRG cells exposed to different culture conditions where cells were maintained as monolayer on collagen I slabs. (a) Collagen slabs (2 mg/mL) coated the bottoms of a 12-well plate and collagen-laden paper scaffolds gelate overnight. (b) The HepaRG cells were seeded onto the collagen slabs, on top of paper scaffold and into the paper scaffolds with cell-laden collagen. They were incubated for six days under standard culture conditions (20% O_2, 5% CO_2, and 37 ºC) before being placed in at the experimental conditions for 48 h: standard (20% O_2, 5% CO_2), periportal (11% O_2, 5% CO_2) or perivenous (5% O_2, 5% CO_2, +Wnt). (c) Finally, cell health was evaluated by quantifying urea secretion using a colorimetric assay, CYP activity was quantified with LC-MS/MS, and transcriptional regulation was determined with RT-qPCR.

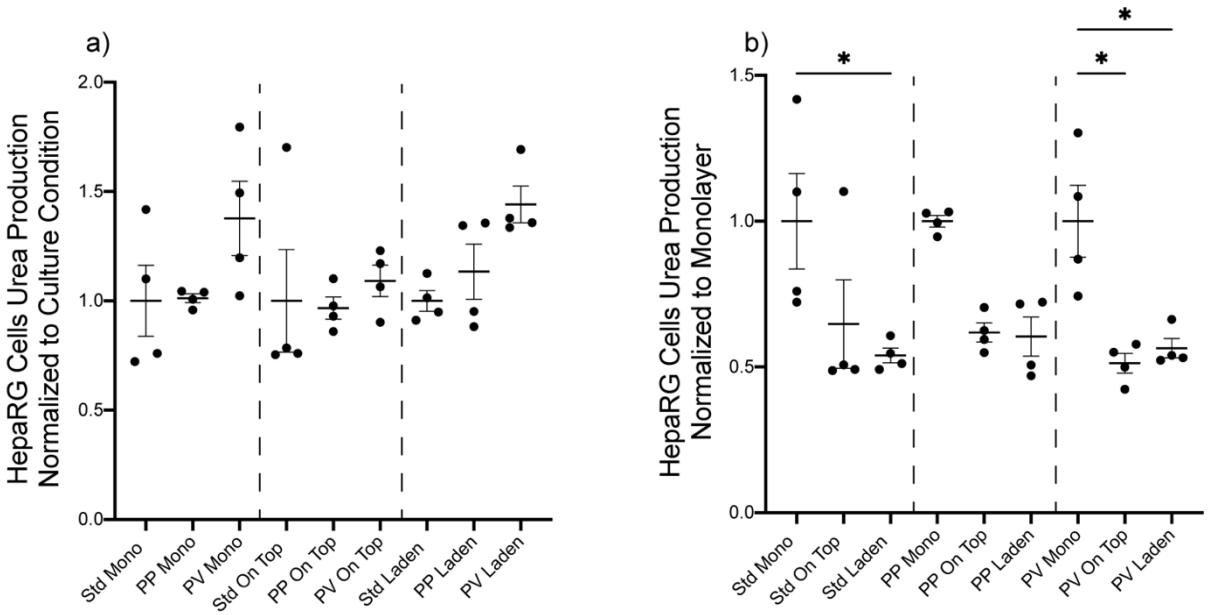

Figure 5.2. Assessment of HepaRG urea secretion after 48 hours in experimental conditions. Urea secretion of the HepaRG cells quantified with a colorimetric assay (Bioassay Systems). (a) Urea secretion was normalized to the standard (Std) condition to assess changes in microenvironmental culture conditions. (b) Urea secretion was normalized to the monolayers to assess changes in culture method. Data points represent the individual technical replicates pooled from two biological replicates; the mean was plotted with error bars representing the SEM. Significant difference was measured with a one-way ANOVA analysis. Std- standard conditions, PP- periportal conditions, PV- perivenous conditions, Mono- HepaRGs cultured as a monolayer on a collagen slab, On Top- HepaRGs cultured on top of a collagen-laden paper scaffold, Laden- HepaRGs cultured in the paper scaffold with cell-laden collagen.

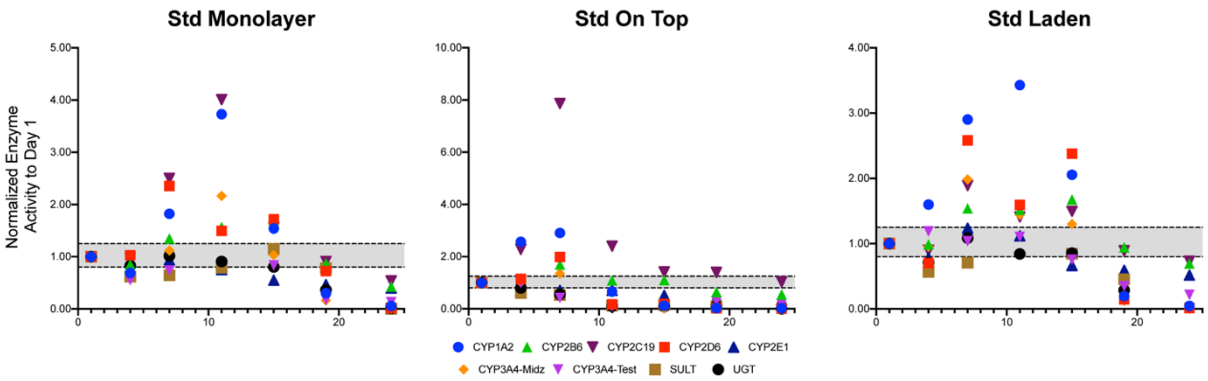

Figure 5.3. HepaRG cells were cultured on a collagen slab, on top of the paper scaffold, and within the paper scaffold at standard culture conditions for 24 days. CYP activity was measured with the 8-in-1 CYP cocktail every 4 days and activity was normalized to day 1 measurements. Dotted black lines represent 1.25- and 0.8-fold change, those associated with a significant difference in activity. Data points represent one biological replicate.

Table 5.4 Summary of maximal increase in drug metabolizing enzyme activity and day it was observed. a

	Monolayer		On Top		Laden	
	Day	Max Activity (Fold Change)	Day	Max Activity (Fold Change)	Day	Max Activity (Fold Change)
CYP1A2	11	3.73	7	2.91	11	3.43
CYP2B6	11	1.57	7	1.70	15	1.68
CYP2C19	11	4.01	7	7.86	7	1.89
CYP2D6	7	2.35	7	1.99	15	2.38
CYP2E1	--	N/A	--	N/A	7	1.24
CYP3A4- Midz	11	2.16	7	1.35	7	1.98
CYP3A4- Test	11	1.49	--	N/A	11	1.10
SULT	7	1.02	--	N/A	--	N/A
UGT	15	1.15	--	N/A	7	1.09

[a] --/ N/A indicates no increase in enzyme activity was observed over the 24 days.

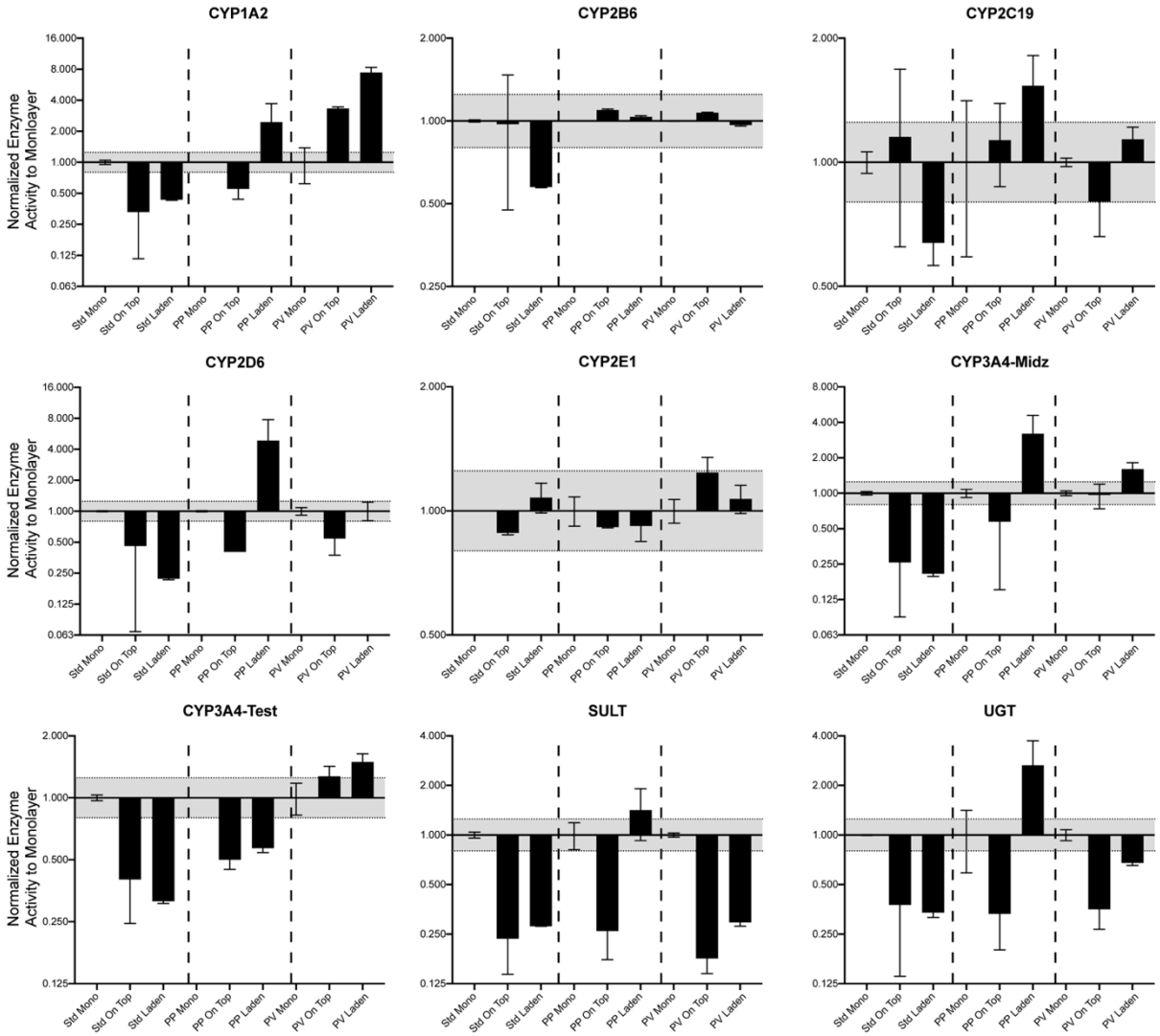

Figure 5.4. Metabolic enzyme activity of HepaRG cells cultured for 6 days followed by 48 hours at standard, PP or PV conditions. Enzyme activity was normalized to the average monolayer activity for each CYP within each cultured microenvironmental condition. Dotted black lines represent 1.25- and 0.8-fold change, those associated with a significant difference in activity. Bars represent the average ± SEM, from 2 biological replicates.

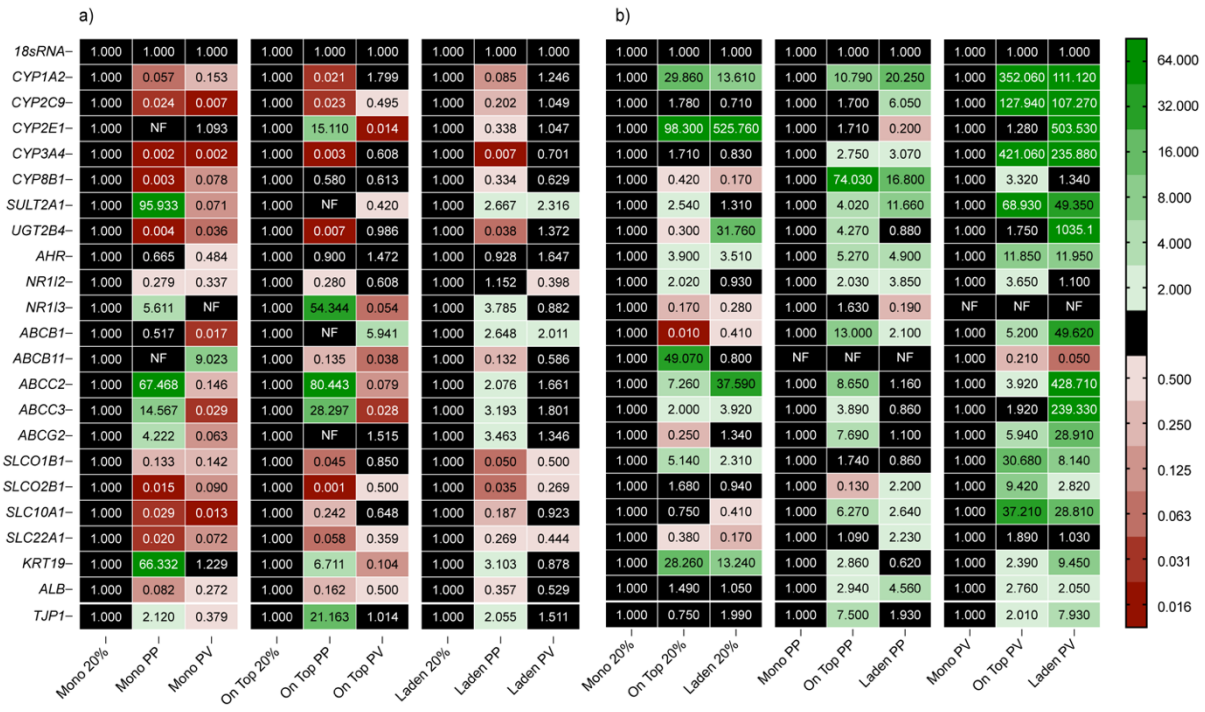

Figure 5.5. Transcript-level regulation of HepaRG cells cultured for 6 days followed by 48 hours at standard, PP or PV conditions was measured and compared. Transcript level analysis of phase I enzymes, phase II enzymes, nuclear receptors, transport enzymes and hepatocyte markers were compared to the monolayer culture format within each microenvironmental condition(a) and the standard culture condition within each culture format (b). Each value is the average of at least three technical replicates, collected from two biological replicates. A fold-change >2 indicates a significant increase in expression; <0.50 indicates a significant decrease. The numerical labels represent the average fold change using the ΔΔCt method. NF indicates no transcript was quantified.

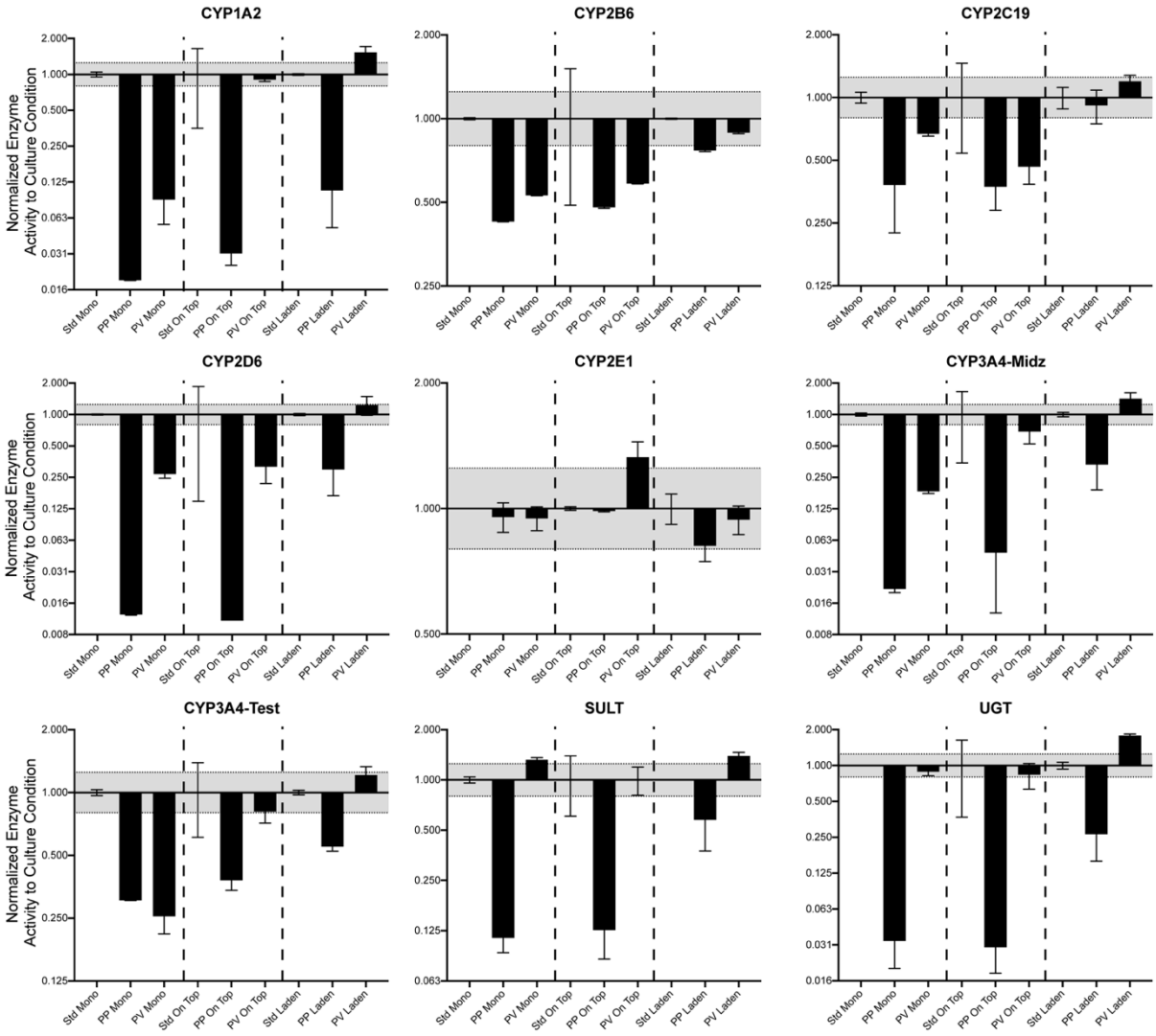

Figure 5.6. Metabolic enzyme activity of HepaRG cells cultured for 6 days followed by 48 hours at standard, PP or PV conditions. Enzyme activity was normalized to the average standard condition activity for each CYP within each cultured format. Dotted black lines represent 1.25- and 0.8-fold change, those associated with a significant difference in activity. Bars represent the average ± SEM, from 2 biological replicates.

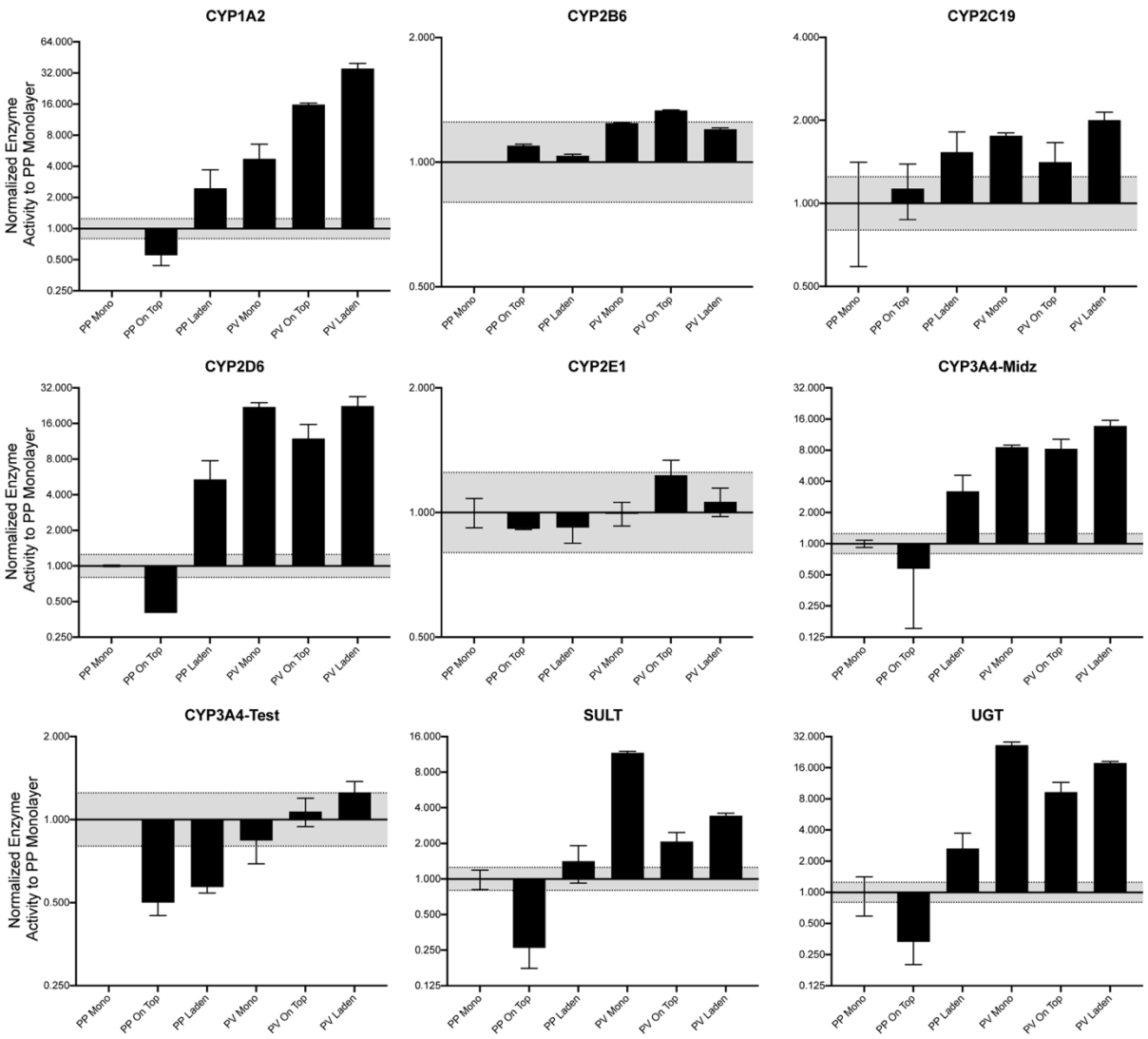

Figure 5.7. Metabolic enzyme activity of HepaRG cells cultured for 6 days followed by 48 hours at PP or PV conditions. (a) Enzyme activity was normalized to the average PP condition, monolayer format for each CYP within each cultured microenvironmental condition. The standard condition was excluded to focus on changes between the PP and PV conditioned cells. Dotted black lines represent 1.25- and 0.8-fold change, those associated with a significant difference in activity. Bars represent the average ± SEM, from 2 biological replicates.

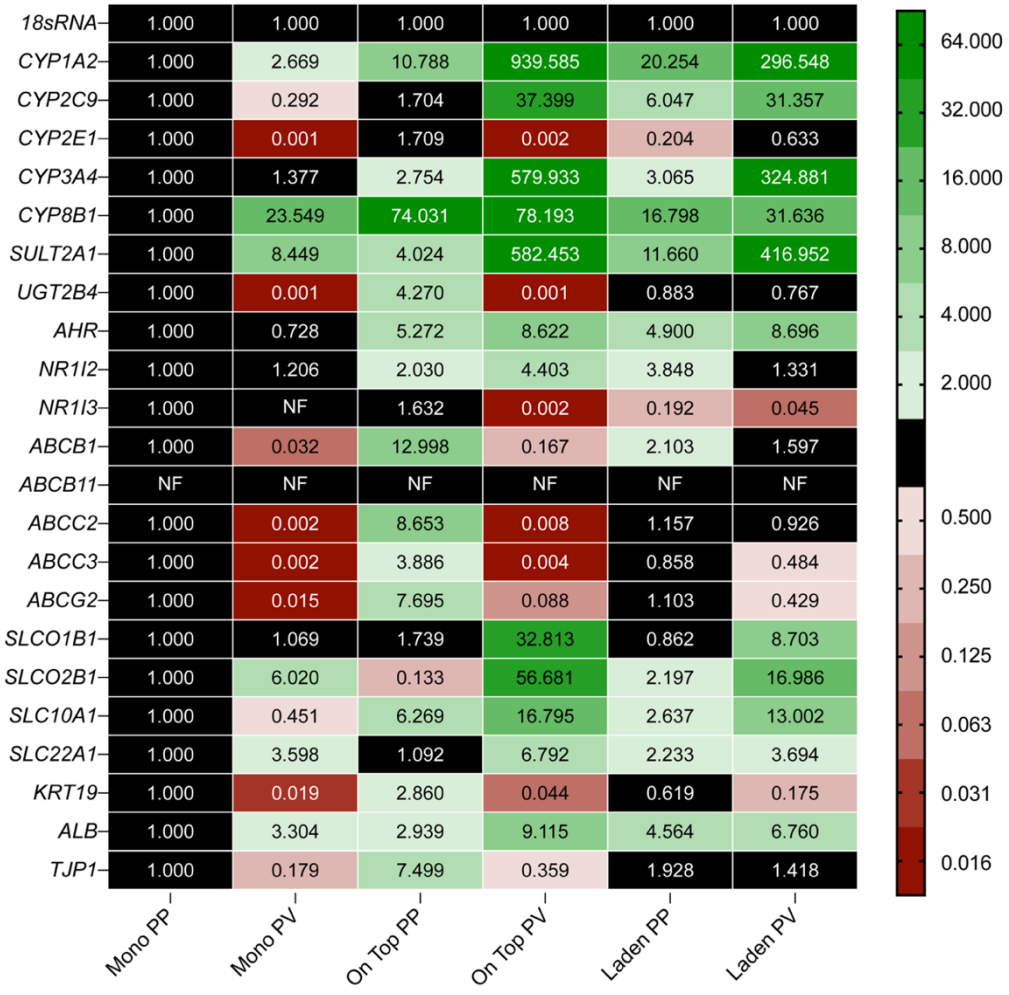

Figure 5.8. Transcript-level regulation of HepaRG cells cultured for 6 days followed by 48 hours at PP or PV conditions was measured and compared. Transcript level analysis of phase I enzymes, phase II enzymes, nuclear receptors, transport enzymes and hepatocyte markers were compared to the PP condition, monolayer culture format. The standard condition was excluded to focus on changes between the PP and PV conditioned cells. Each value is the average of at least three technical replicates, collected from two biological replicates. A fold-change >2 indicates a significant increase in expression; <0.50 indicates a significant decrease. The numerical labels represent the average fold change using the ΔΔCt method. NF indicates no transcript was quantified.

REFERENCES

(1) Kenna, J. G.; Uetrecht, J. Do In Vitro Assays Predict Drug Candidate Idiosyncratic Drug-Induced Liver Injury Risk? *Drug Metab. Dispos.* **2018**, *46* (11), 1658–1669. https://doi.org/10.1124/dmd.118.082719.

(2) Parasrampuria, D. A.; Benet, L. Z.; Sharma, A. Why Drugs Fail in Late Stages of Development: Case Study Analyses from the Last Decade and Recommendations. *AAPS J.* **2018**, *20* (46). https://doi.org/10.1208/s12248-018-0204-y.

(3) Kietzmann, T. Liver Zonation in Health and Disease: Hypoxia and Hypoxia-Inducible Transcription Factors as Concert Masters. *Int. J. Mol. Sci.* **2019**, *20* (9). https://doi.org/10.3390/ijms20092347.

(4) Godoy, P.; Hewitt, N. J.; Albrecht, U.; Andersen, M. E.; Ansari, N.; Bhattacharya, S.; Bode, J. G.; Bolleyn, J.; Borner, C.; Böttger, J.; Braeuning, A.; Budinsky, R. A.; Burkhardt, B.; Cameron, N. R.; Camussi, G.; Cho, C. S.; Choi, Y. J.; Craig Rowlands, J.; Dahmen, U.; Damm, G.; Dirsch, O.; Donato, M. T.; Dong, J.; Dooley, S.; Drasdo, D.; Eakins, R.; Ferreira, K. S.; Fonsato, V.; Fraczek, J.; Gebhardt, R.; Gibson, A.; Glanemann, M.; Goldring, C. E. P. P.; Gómez-Lechón, M. J.; Groothuis, G. M. M. M.; Gustavsson, L.; Guyot, C.; Hallifax, D.; Hammad, S.; Hayward, A.; Häussinger, D.; Hellerbrand, C.; Hewitt, P.; Hoehme, S.; Holzhütter, H. G.; Houston, J. B.; Hrach, J.; Ito, K.; Jaeschke, H.; Keitel, V.; Kelm, J. M.; Kevin Park, B.; Kordes, C.; Kullak-Ublick, G. A.; Lecluyse, E. L.; Lu, P.; Luebke-Wheeler, J.; Lutz, A.; Maltman, D. J.; Matz-Soja, M.; McMullen, P.; Merfort, I.; Messner, S.; Meyer, C.; Mwinyi, J.; Naisbitt, D. J.; Nussler, A. K.; Olinga, P.; Pampaloni, F.; Pi, J.; Pluta, L.; Przyborski, S. A.; Ramachandran, A.; Rogiers, V.; Rowe, C.; Schelcher, C.; Schmich, K.; Schwarz, M.; Singh, B.; Stelzer, E. H. K. K.; Stieger, B.; Stöber, R.; Sugiyama, Y.; Tetta, C.; Thasler, W. E.; Vanhaecke, T.; Vinken, M.; Weiss, T. S.; Widera, A.; Woods, C. G.; Xu, J. J.; Yarborough, K. M.; Hengstler, J. G. Recent Advances in 2D and 3D in Vitro Systems Using Primary Hepatocytes, Alternative Hepatocyte Sources and Non-Parenchymal Liver Cells and Their Use in Investigating Mechanisms of Hepatotoxicity, Cell Signaling and ADME. *Arch. Toxicol.* **2013**, *87* (8), 1315–1530. https://doi.org/10.1007/s00204-013-1078-5.

(5) Cramer, S. M.; Larson, T. S.; Lockett, M. R.; Hill, C.; States, U.; Hill, C.; Hill, C.; States, U. Next Generation of 3D Tissue Models. **2020**, *91* (17), 10916–10926. https://doi.org/10.1021/acs.analchem.9b02102.Tissue.

(6) Kyffin, J. A.; Sharma, P.; Leedale, J.; Colley, H. E.; Murdoch, C.; Mistry, P.; Webb, S. D. Impact of Cell Types and Culture Methods on the Functionality of in Vitro Liver Systems – A Review of Cell Systems for Hepatotoxicity Assessment. *Toxicology in Vitro*. Elsevier Ltd 2018, pp 262–275. https://doi.org/10.1016/j.tiv.2018.01.023.

(7) Dash, A.; Simmers, M. B.; Deering, T. G.; Berry, D. J.; Feaver, R. E.; Hastings, N. E.; Pruett, T. L.; LeCluyse, E. L.; Blackman, B. R.; Wamhoff, B. R. Hemodynamic Flow Improves Rat Hepatocyte Morphology, Function, and Metabolic Activity in Vitro. *Am. J.*

Physiol. - Cell Physiol. **2013**, *304* (11), 1053–1063. https://doi.org/10.1152/ajpcell.00331.2012.

(8) Tibbitt, M. W.; Anseth, K. S. Hydrogels as Extracellular Matrix Mimics for 3D Cell Culture. *Biotechnol. Bioeng.* **2009**, *103* (4), 655–663. https://doi.org/10.1002/bit.22361.

(9) Zhou, Y.; Shen, J. X.; Lauschke, V. M. Comprehensive Evaluation of Organotypic and Microphysiological Liver Models for Prediction of Drug-Induced Liver Injury. *Frontiers in Pharmacology*. Frontiers Media S.A. 2019. https://doi.org/10.3389/fphar.2019.01093.

(10) Gaskell, H.; Sharma, P.; Colley, H. E.; Murdoch, C.; Williams, D. P.; Webb, S. D. Characterization of a Functional C3A Liver Spheroid Model. *Toxicol. Res. (Camb).* **2016**, *5* (4), 1053–1065. https://doi.org/10.1039/c6tx00101g.

(11) Lauschke, V. M.; Hendriks, D. F. G.; Bell, C. C.; Andersson, T. B.; Ingelman-Sundberg, M. Novel 3D Culture Systems for Studies of Human Liver Function and Assessments of the Hepatotoxicity of Drugs and Drug Candidates. *Chem. Res. Toxicol.* **2016**, *29* (12), 1936–1955. https://doi.org/10.1021/acs.chemrestox.6b00150.

(12) Higuchi, Y.; Kawai, K.; Kanaki, T.; Yamazaki, H.; Chesné, C.; Guguen-Guillouzo, C.; Suemizu, H. Functional Polymer-Dependent 3D Culture Accelerates the Differentiation of HepaRG Cells into Mature Hepatocytes. *Hepatol. Res.* **2016**, *46* (10), 1045–1057. https://doi.org/10.1111/hepr.12644.

(13) Cox, C. R.; Lynch, S.; Goldring, C.; Sharma, P. Current Perspective: 3D Spheroid Models Utilizing Human-Based Cells for Investigating Metabolism-Dependent Drug-Induced Liver Injury. *Front. Med. Technol.* **2020**, *2*. https://doi.org/10.3389/fmedt.2020.611913.

(14) Bell, C. C.; Hendriks, D. F. G.; Moro, S. M. L.; Ellis, E.; Walsh, J.; Renblom, A.; Fredriksson Puigvert, L.; Dankers, A. C. A.; Jacobs, F.; Snoeys, J.; Sison-Young, R. L.; Jenkins, R. E.; Nordling, Å.; Mkrtchian, S.; Park, B. K.; Kitteringham, N. R.; Goldring, C. E. P.; Lauschke, V. M.; Ingelman-Sundberg, M. Characterization of Primary Human Hepatocyte Spheroids as a Model System for Drug-Induced Liver Injury, Liver Function and Disease. *Sci. Rep.* **2016**, *6*. https://doi.org/10.1038/srep25187.

(15) Shah, U. K.; Mallia, J. de O.; Singh, N.; Chapman, K. E.; Doak, S. H.; Jenkins, G. J. S. A Three-Dimensional in Vitro HepG2 Cells Liver Spheroid Model for Genotoxicity Studies. *Mutat. Res. - Genet. Toxicol. Environ. Mutagen.* **2018**, *825*, 51–58. https://doi.org/10.1016/j.mrgentox.2017.12.005.

(16) Broutier, L.; Mastrogiovanni, G.; Verstegen, M. M. A.; Francies, H. E.; Gavarró, L. M.; Bradshaw, C. R.; Allen, G. E.; Arnes-Benito, R.; Sidorova, O.; Gaspersz, M. P.; Georgakopoulos, N.; Koo, B. K.; Dietmann, S.; Davies, S. E.; Praseedom, R. K.; Lieshout, R.; IJzermans, J. N. M.; Wigmore, S. J.; Saeb-Parsy, K.; Garnett, M. J.; Van Der Laan, L. J. W.; Huch, M. Human Primary Liver Cancer-Derived Organoid Cultures for Disease Modeling and Drug Screening. *Nat. Med.* **2017**, *23* (12), 1424–1435.

https://doi.org/10.1038/nm.4438.

(17) Hirschhaeuser, F.; Menne, H.; Dittfeld, C.; West, J.; Mueller-Klieser, W.; Kunz-Schughart, L. A. Multicellular Tumor Spheroids: An Underestimated Tool Is Catching up Again. *J. Biotechnol.* **2010**, *148* (1), 3–15. https://doi.org/10.1016/j.jbiotec.2010.01.012.

(18) Derda, R.; Laromaine, A.; Mammoto, A.; Tang, S. K. Y.; Mammoto, T.; Ingber, D. E.; Whitesides, G. M. Paper-Supported 3D Cell Culture for Tissue-Based Bioassays. *Proc. Natl. Acad. Sci. U. S. A.* **2009**, *106* (44), 18457–18462. https://doi.org/10.1073/pnas.0910666106.

(19) Songok, J.; Toivakka, M. Modelling of Capillary-Driven Flow for Closed Paper-Based Microfluidic Channels. *J. Micromechanics Microengineering* **2017**, *27* (6). https://doi.org/10.1088/1361-6439/aa6b40.

(20) Liu, Z.; Hu, J.; Zhao, Y.; Qu, Z.; Xu, F. Experimental and Numerical Studies on Liquid Wicking into Filter Papers for Paper-Based Diagnostics. *Appl. Therm. Eng.* **2015**, *88*, 280–287. https://doi.org/10.1016/j.applthermaleng.2014.09.057.

(21) Chen, Y. H.; Kuo, Z. K.; Cheng, C. M. Paper - a Potential Platform in Pharmaceutical Development. *Trends Biotechnol.* **2015**, *33* (1), 4–9. https://doi.org/10.1016/j.tibtech.2014.11.004.

(22) Lloyd, C. C.; Boyce, M. W.; Lockett, M. R. Paper-Based Invasion Assays for Quantifying Cellular Movement in Three-Dimensional Tissue-like Structures. *Curr. Protoc. Chem. Biol.* **2017**, *9* (2), 75–95. https://doi.org/10.1002/cpch.22.

(23) Kenney, R. M.; Loeser, A.; Whitman, N. A.; Lockett, M. R. Paper-Based Transwell Assays: An Inexpensive Alternative to Study Cellular Invasion. *Analyst* **2019**, *144* (1), 206–211. https://doi.org/10.1039/c8an01157e.

(24) DiProspero, T. J.; Dalrymple, E.; Lockett, M. R. Physiologically Relevant Oxygen Tensions Differentially Regulate Hepatotoxic Responses in HepG2 Cells. *Toxicol. Vitr.* **2021**, *74* (March), 105156. https://doi.org/10.1016/j.tiv.2021.105156.

(25) Dierks, E. A.; Stams, K. R.; Lim, H. K.; Cornelius, G.; Zhang, H.; Ball, S. E. A Method for the Simultaneous Evaluation of the Activities of Seven Major Human Drug-Metabolizing Cytochrome P450s Using an in Vitro Cocktail of Probe Substrates and Fast Gradient Liquid Chromatography Tandem Mass Spectrometry. *Drug Metab. Dispos.* **2001**, *29* (1), 23–29.

(26) Li, G.; Huang, K.; Nikolic, D.; Van Breemen, R. B. High-Throughput Cytochrome P450 Cocktail Inhibition Assay for Assessing Drug-Drug and Drug-Botanical Interactions. *Drug Metab. Dispos.* **2015**, *43* (11), 1670–1678. https://doi.org/10.1124/dmd.115.065987.

(27) Schmittgen, T. D.; Livak, K. J. Analyzing Real-Time PCR Data by the Comparative CT

Method. *Nat. Protoc.* **2008**, *3* (6), 1101–1108. https://doi.org/10.1038/nprot.2008.73.

(28) Janani, G.; Mandal, B. B. Mimicking Physiologically Relevant Hepatocyte Zonation Using Immunomodulatory Silk Liver Extracellular Matrix Scaffolds toward a Bioartificial Liver Platform. *ACS Appl. Mater. Interfaces* **2021**. https://doi.org/10.1021/acsami.1c00719.

(29) Li, J.; Settivari, R. S.; Lebaron, M. J.; Marty, M. S. Functional Comparison of HepaRG Cells and Primary Human Hepatocytes in Sandwich and Spheroid Culture as Repeated-Exposure Models for Hepatotoxicity. *Appl. Vitr. Toxicol.* **2019**, *5* (4), 187–195. https://doi.org/10.1089/aivt.2019.0008.

(30) Jackson, J. P.; Li, L.; Chamberlain, E. D.; Wang, H.; Ferguson, S. S. Contextualizing Hepatocyte Functionality of Cryopreserved HepaRG Cell Cultures. *Drug Metab. Dispos.* **2016**, *44* (9), 1463–1479. https://doi.org/10.1124/dmd.116.069831.

(31) Ramaiahgari, S. C.; Den Braver, M. W.; Herpers, B.; Terpstra, V.; Commandeur, J. N. M.; Van De Water, B.; Price, L. S. A 3D in Vitro Model of Differentiated HepG2 Cell Spheroids with Improved Liver-like Properties for Repeated Dose High-Throughput Toxicity Studies. *Arch. Toxicol.* **2014**, *88* (5), 1083–1095. https://doi.org/10.1007/s00204-014-1215-9.

(32) Higuchi, Y.; Kawai, K.; Yamazaki, H.; Nakamura, M.; Bree, F.; Guguen-Guillouzo, C.; Suemizu, H. The Human Hepatic Cell Line HepaRG as a Possible Cell Source for the Generation of Humanized Liver TK-NOG Mice. *Xenobiotica* **2014**, *44* (2), 146–153. https://doi.org/10.3109/00498254.2013.836257.

(33) Aleksandr, T.; Müsch, A. Hepatocyte Polarity. *Compr Physiol.* **2013**, 243–287. https://doi.org/10.1002/cphy.c120009.Hepatocyte.

(34) Leite, S. B.; Wilk-Zasadna, I.; Zaldivar, J. M.; Airola, E.; Reis-Fernandes, M. A.; Mennecozzi, M.; Guguen-Guillouzo, C.; Chesne, C.; Guillou, C.; Alves, P. M.; Coecke, S. Three-Dimensional HepaRG Model as an Attractive Tool for Toxicity Testing. *Toxicol. Sci.* **2012**, *130* (1), 106–116. https://doi.org/10.1093/toxsci/kfs232.

(35) Schulze, A.; Mills, K.; Weiss, T. S.; Urban, S. Hepatocyte Polarization Is Essential for the Productive Entry of the Hepatitis B Virus. *Hepatology* **2012**, *55* (2), 373–383. https://doi.org/10.1002/hep.24707.

(36) Török, G.; Erdei, Z.; Lilienberg, J.; Apáti, Á.; Homolya, L. The Importance of Transporters and Cell Polarization for the Evaluation of Human Stem Cell-Derived Hepatic Cells. *PLoS One* **2020**, *15* (1), 1–22. https://doi.org/10.1371/journal.pone.0227751.

(37) Ramaiahgari, S. C.; Waidyanatha, S.; Dixon, D.; DeVito, M. J.; Paules, R. S.; Ferguson, S. S. Three-Dimensional (3D) HepaRG Spheroid Model with Physiologically Relevant

Xenobiotic Metabolism Competence and Hepatocyte Functionality for Liver Toxicity Screening. *Toxicol. Sci.* **2017**, *159* (1), 124–136. https://doi.org/10.1093/toxsci/kfx122.

(38) Hernández-Gutiérrez, L.; Camacho-Carranza, R.; Hernández-Ojeda, S. L.; Govezensky, T.; Olguín-Reyes, S. R.; Espinosa-Aguirre, J. J. Reduction in CYP1A1 and 2B2 Activity at Low Oxygen Tension. *Toxicol. Lett.* **2020**, *330*, 90–95. https://doi.org/10.1016/j.toxlet.2020.05.006.

APPENDIX A: IMAGES OF HEPG2 IN PAPER SCAFFOLDS

HepG2 cells were cultured in 3D paper-scaffolds and images to assess distribution of cells. Representative images are shown.

Methods

Cell laden paper scaffolds (large and small) were cultured under standard conditions for 48 h. 40,000 cells were placed on a 1.5 glass coverslip and cultured for 48 h under standard conditions. Cells were fixed with 3.2% paraformaldehyde, permeabilized with 0.5% trition-X. Cell nuclei were stained with DRAQ5 (1, 5-bis{[2-(di-methylamino)ethyl]amino}-4, 8-dihydroxyanthracene-9, 10-dione) and actin was stained with phalloidin conjugated to Alexa fluor 488.

Samples were mounted onto glass slides using Prolong Gold mounting solution. For the cells on top of the glass coverslips and small single zone scaffolds, 20 μL of mounting solution was used; for the large single zone scaffolds, 75 μL of mounting solution was used. Fluorescent images (tile and Z-Stacks) were collected on a Zeiss LSM710 spectral confocal laser scanning microscope with a digital AxioCam camera, acquired with Zen 2.3 acquisition software, using 20 and 40x objectives (Plan-apochromat 20x/0.8 M27; Plan-apochromat 40x/0.95 Korr M27). Excitation light was provided by an argon laser. The paper fibers of the scaffold auto fluoresce under blue light so 488/414-474 nm (ex/em) was used to capture the described auto fluoresce. Alexa fluor 488 was imaged using 543 nm excitation and 502-561 nm emission; DRAQ5 was imaged using 633 nm excitation and 642-700 nm emission. The images were collected with pinhole size set to 1 AU for the 633 nm excitation, 642-700 nm emission channel, and pixel sizes set to 0.415 μm unless specified next to specific image.

ImarisViewer software was used to visualize Z-stacks, tile scans, and planar images (XY, XZ, YZ). Videos were captured using the screen capture function of Microsoft power point. Videos of 3D renderings and slice view were captured. A “3D rendering” is a stitching the Z-stack in the X,Y and Z axis while a “slice view” video is each XY image in the Z-stack is cycled through.

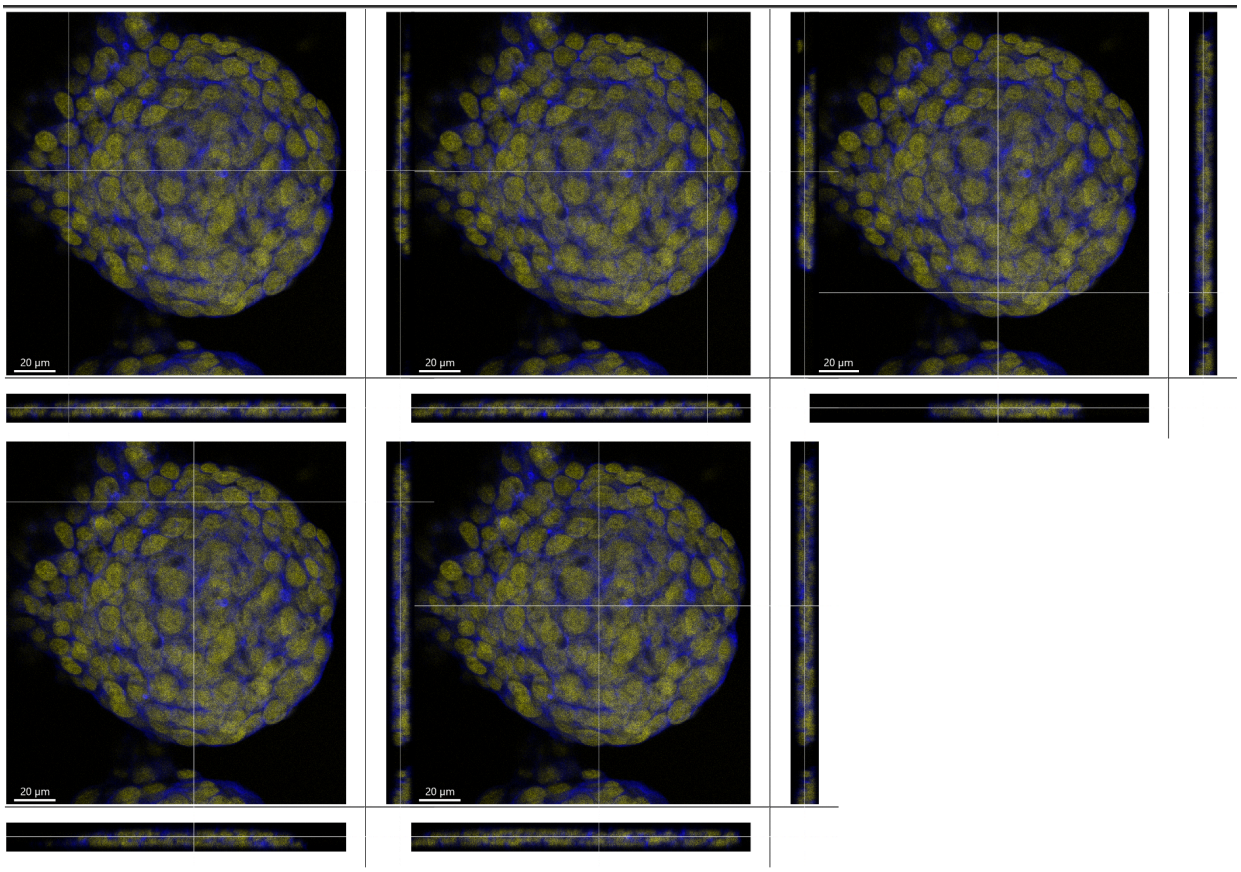

Figure A.1 Planar projection of HepG2 cells on a glass coverslip. Images were collected as a Z-stack (0.3 µm slice, 13.5 µm range) using a Zeiss LSM710 spectral confocal laser and 40x objective. Voxel size is 0.173x 0.173x 0.300 µm. Yellow is nuclei, Blue is f-actin. Scale bar is 20 µm.

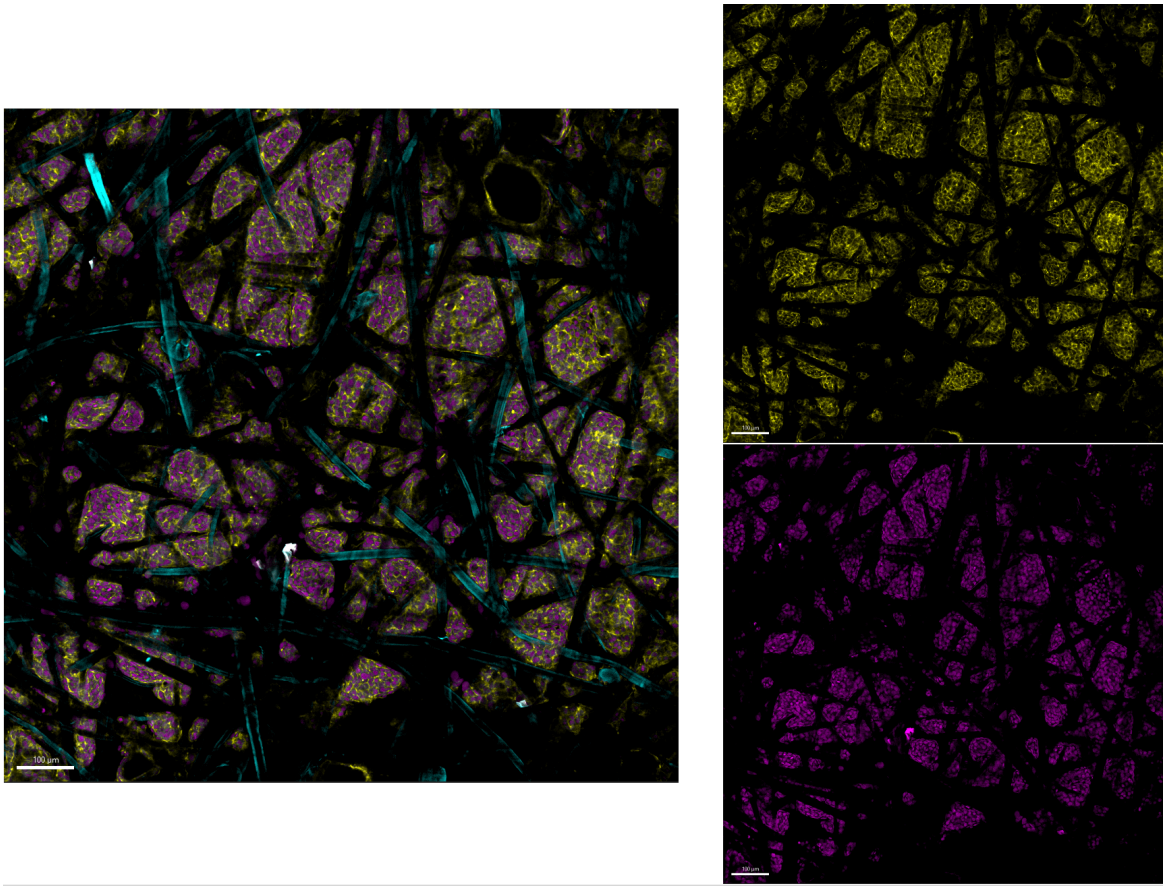

Figure A.2 Snapshot of HepG2 cells in a paper-scaffold. Images were collected as a 3x3 tile scan (1185 x 1185 µm) using a Zeiss LSM710 spectral confocal laser and 20x objective. Pixel size is 0.415x 0.415 µm. Magenta is nuclei, blue is f-actin, and turquoise are paper fibers (autofluorescence). Scale bar is 100 µm.

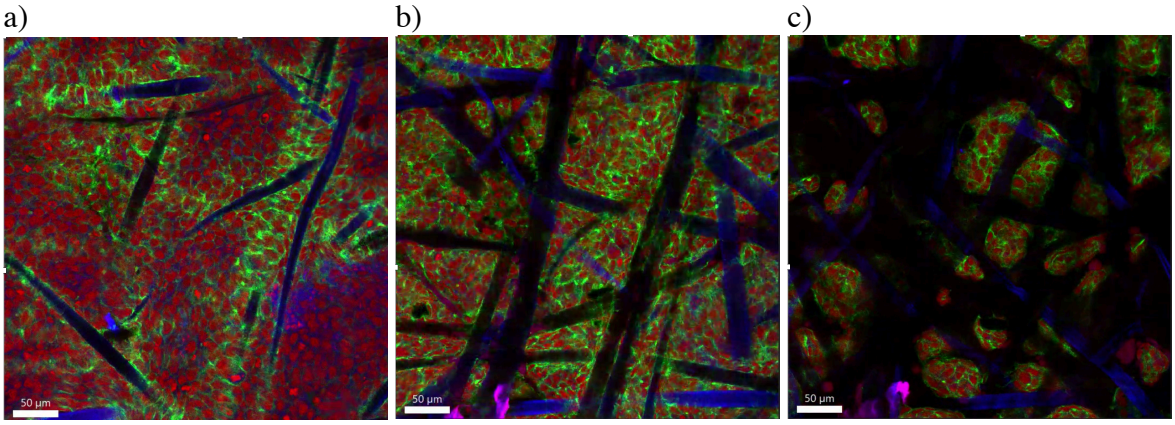

Figure A.3 Snapshots of HepG2 cells in a paper-scaffold at different Z-axes. HepG2 cells were seeded on one side of the scaffold (a) and imaged deeper into the 40 µm scaffold thickness. The middle region (b) and deeper region (c). Images were collected as a Z-stack (0.5 µm slice, 37 µm range) using a Zeiss LSM710 spectral confocal laser and 20x objective. Voxel size is 0..415x 0.415x 0.500 µm. Red is nuclei, green is f-actin and blue is paper-fibers. Scale bar is 50 µm.

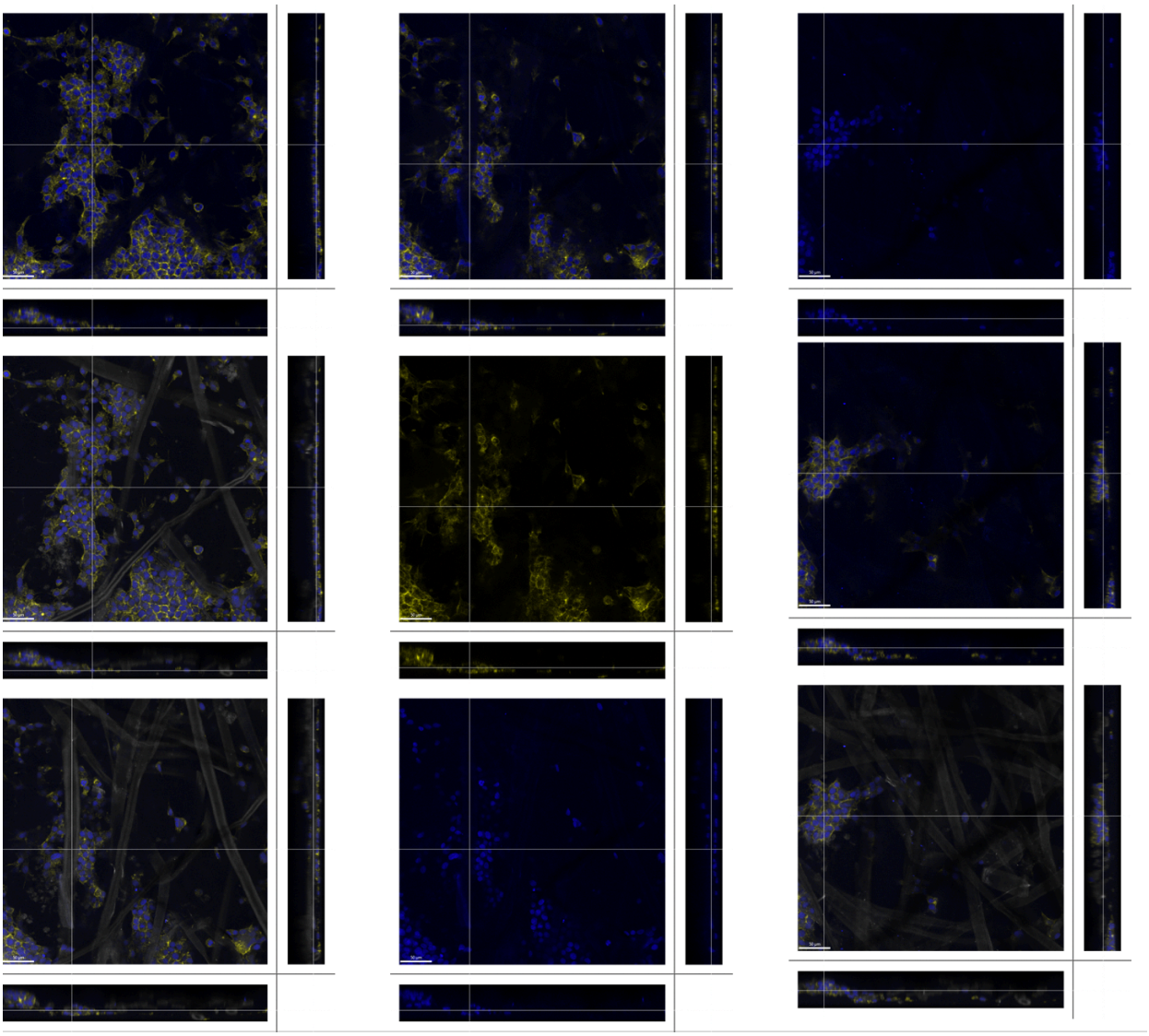

Figure A.4 Planar projection of HepG2 cells in a paper-scaffold. Images were collected as a Z-stack (0.8 µm slice, 75 µm range) using a Zeiss LSM710 spectral confocal laser and 20x objective. Voxel size is 0.450x 0.450x 0.800 µm. Blue is nuclei, yellow is f-actin and grey is paper fibers. Scale bar is 50 µm.

APPENDIX B: CHAPTER 2 CALCULATIONS OF OXYGEN AT THE SURFACE OF CELLS AT THE BOTTOM OF THE WELL PLATE

SI Equation sheet 1:
The following equations to calculate oxygen delivery to the surface of cells was described by Al-Ani et al. [29]

Calculating the moles of oxygen delivered to the surface of the cell per second (Units mol/s*cm^2):

$$Maximum\ deliverable\ oxygen = \frac{Diffusion\ Coefficient\ of\ Oxygen\ in\ Medium}{(Media\ Depth\ in\ cm) * 1000} * Surface\ oxygen\ tension$$

Cellular oxygen requirement (mol/s*cm^2):

$$Cellular\ oxygen\ requirements = (Oxygen\ Consumption * Cell\ Density) * 10^{-18}$$

Oxygen concentration at liquid surface (mol/L):

$$Oxygen\ at\ liquid\ suface = (1 - \%CO_2 - 0.06) * Atmospheric\ Pressure * \%O_2 * (\frac{O_2\ Solubility\ in\ media}{0.209})$$

Oxygen concentration at cell surface (mol/L):

$$Oxygen\ at\ cell\ surface = (O_2\ at\ liquid\ surface) * (1 - (\frac{Cell\ Oxygen\ Requirements}{Deliverable\ O_2}))$$

Constants:

Molar percent CO_2	5.0%
Atmospheric pressure	1.00 atm
Media Depth (cm)	0.361 (100 uL media in a 96 well plate)
Oxygen consumptionrate (amol/cell*s)	34 (https://doi.org/10.1007/s10544-008-9254-8)
Cell Density (cell/ cm^2)	125,000
Diffusion constant (cm^2/s)	2.86 x 10^{-5}
Oxygen Solubility at 20.9% (mol/L)	2.00 x 10^{-4}

At 20% O_2:

$$Oxygen\ at\ liquid\ suface = (1 - 0.05 - 0.06) * 1\ atm * 0.209\ O_2 * (\frac{2.86 \times 10^{-5}\ \frac{mol}{L}}{0.209})$$

$$Oxygen\ at\ liquid\ suface = \mathbf{1.78 \times 10^{-4}\ \frac{mol}{L}}$$

$$Cellular\ oxygen\ requirements = \left(34\ \frac{amol}{cell * s} * 125{,}000\ \frac{cell}{cm^2}\right) * 10^{-18}$$

$$Cellular\ oxygen\ requirements = \mathbf{4.25\ x\ 10^{-12}\ \frac{mol}{cm^2 * s}}$$

$$Maximum\ deliverable\ oxygen = \frac{2.86 \times 10^{-5}\frac{cm^2}{s}}{(0.361\ cm) * 1000} * 1.78 \times 10^{-4}\frac{mol}{L}$$

$$Maximum\ deliverable\ oxygen = \mathbf{1.41 \times 10^{-11}\frac{mol}{cm^2 * s}}$$

$$Oxygen\ at\ cell\ surface = \left(1.78 \times 10^{-4}\frac{mol}{L}\right) * (1 - (\frac{4.25\ x\ 10^{-12}\frac{mol}{cm^2 * s}}{1.41 \times 10^{-11}\frac{mol}{cm^2 * s}})$$

$$Oxygen\ at\ cell\ surface = \left(\mathbf{1.24 \times 10^{-4}\frac{mol}{L}}\right)$$

At 8% O_2:

$$Oxygen\ at\ liquid\ suface = (1 - 0.05 - 0.06) * 1\ atm * 0.209\ O_2 * (\frac{2.86 \times 10^{-5}\frac{mol}{L}}{0.209})$$

$$Oxygen\ at\ liquid\ suface = \mathbf{6.81 \times 10^{-5}\frac{mol}{L}}$$

$$Cellular\ oxygen\ requirements = \left(34\frac{amol}{cell * s} * 125{,}000\frac{cell}{cm^2}\right) *\ 10^{-18}$$

$$Cellular\ oxygen\ requirements = \mathbf{4.25\ x\ 10^{-12}\frac{mol}{cm^2 * s}}$$

$$Maximum\ deliverable\ oxygen = \frac{2.86 \times 10^{-5}\frac{cm^2}{s}}{(0.361\ cm) * 1000} * 6.81 \times 10^{-5}\frac{mol}{L}$$

$$Maximum\ deliverable\ oxygen = \mathbf{5.40 \times 10^{-12}\frac{mol}{cm^2 * s}}$$

$$Oxygen\ at\ cell\ surface = \left(2.56 \times 10^{-5}\frac{mol}{L}\right) * (1 - (\frac{4.25\ x\ 10^{-12}\frac{mol}{cm^2 * s}}{5.40 \times 10^{-12}\frac{mol}{cm^2 * s}})$$

$$Oxygen\ at\ cell\ surface = \left(\mathbf{1.45 \times 10^{-5}\frac{mol}{L}}\right)$$

At 3% O_2:

$$Oxygen\ at\ liquid\ suface = (1 - 0.05 - 0.06) * 1\ atm * 0.209\ O_2 * (\frac{2.86 \times 10^{-5}\frac{mol}{L}}{0.209})$$

$$Oxygen\ at\ liquid\ suface = \mathbf{2.56 \times 10^{-5}\ \frac{mol}{L}}$$

$$Cellular\ oxygen\ requirements = \left(34\ \frac{amol}{cell * s} * 125{,}000\ \frac{cell}{cm^2}\right) *\ 10^{-18}$$

$$Cellular\ oxygen\ requirements = \mathbf{4.25\ x\ 10^{-12}\ \frac{mol}{cm^2 * s}}$$

$$Maximum\ deliverable\ oxygen = \frac{2.86 \times 10^{-5}\ \frac{cm^2}{s}}{(0.361\ cm) * 1000} * 2.56 \times 10^{-5}\ \frac{mol}{L}$$

$$Maximum\ deliverable\ oxygen = \mathbf{2.02 \times 10^{-12}\ \frac{mol}{cm^2 * s}}$$

$$Oxygen\ at\ cell\ surface = (O_2\ at\ liquid\ surface) * (1 - (\frac{Cell\ Oxygen\ Requirements}{Deliverable\ O_2})$$

$$Oxygen\ at\ cell\ surface = \left(2.56 \times 10^{-5}\ \frac{mol}{L}\right) * (1 - (\frac{4.25\ x\ 10^{-12}\ \frac{mol}{cm^2 * s}}{2.02 \times 10^{-12}\ \frac{mol}{cm^2 * s}})$$

$$Oxygen\ at\ cell\ surface = \left(\mathbf{-2.81 \times 10^{-5}\ \frac{mol}{L}}\right)$$

** This means there is ~50% oxygen deficiency for the cells